Morphotectonics and paleoseismology of the western Potwar Plateau and the Kalabagh Fault (Sub-Himalayas, Pakistan)

from the Faculty of Georesources and Materials Engineering of the RWTH Aachen University

to obtain the academic degree of

Doctor of Natural Sciences

approved thesis

submitted by

Wahid Abbas, M.Sc.

From Gujrat, Pakistan

Advisors: Univ.-Prof. Dr. rer. nat. Klaus Reicherter

Prof. Dr. Manfred Frechen

Date of the oral examination: 26.11.2021

dedicated to my grandparents

grandfather Noor Hussain (1919-2002)

and

grandmother Sakina Bibi (1925-2016)

Abstract

The Sub-Himalayas in Pakistan are laterally categorized by the Kalabagh and the Jhelum Faults, bounding the Kohat and Potwar Plateaus and the Hazara Kashmir Syntaxis. The Hazara Kashmir syntaxis separates structurally and morphologically the eastern and the western Sub-Himalayas in Kashmir. The eastern Potwar Plateau and the Hazara Kashmir syntaxis have yielded recent seismicity (e.g., M_w=7.6,2005 and M_w=5.6,2019). Also, the Kohat Plateau has revealed a M_w=6 (1992) earthquake. These earthquakes designate the Kohat Plateau, the eastern Potwar Plateau and the Hazara Kashmir syntaxis as seismically active areas. Moreover, InSAR and GPS data from previous studies reveal uplift and aseismic displacements in the Salt Range, western Potwar Plateau and along the Kalabagh Fault. These anomalies suggest the area is tectonically active, that governs the landform development. This PhD thesis aims at studying the paleoseismology and neotectonics in the Sub-Himalayas with emphasis on the Kalabagh Fault, that delineates the western Potwar Plateau.

The morphometric indices are evaluated in the Hazara Kashmir Syntaxis, Pir Panjal Ranges, Potwar Plateau-Salt Range, Kohat Plateau-Surghar Range and along the Kurram Fault. The landscape development in these areas is influenced by the softer lithologies of the Tertiary sediments, that are rapidly erodible and exhibit degraded morphology even for younger drainage basins. The analysis has established a comparative relation among the watersheds of these areas, denoting the landforms are differentially affected by tectonic deformations. The morphometric indices from the landforms in the Hazara Kashmir Syntaxis, Pir Panjal Ranges, Potwar Plateau-Salt Range, Kohat Plateau-Surghar Range and the western flank of the Bannu Basin reveal moderate to high tectonic activity index.

Deformation history and paleoearthquakes are studied along the Kalabagh Fault using morphotectonics and paleoseismic investigations, supported by the luminescence dating of the deformed sediments. For older sediments, pIRIR luminescence dating method was applied on K-feldspar. The quartz OSL dating was employed for younger (Holocene) sediments. This study finds the tectonic deformation and seismicity that occurred during middle-late Pleistocene and Holocene. The dextral Kalabagh Fault exhibits an en-echelon zone that has formed in the overlapping area between the segments of the fault. The stepover of the en-echelon faults, that had initiated the landform development between the Thathi and Zaluch sections, had a first surface expression ~ 0.5 Ma ago. A push-up block in this en-echelon zone has formed during the past ~ 0.5 Ma. Ongoing tectonic deformations have started developing the landform since ~220 ka at Larkakki, ~140 ka at Ghundi and ~190 ka at Khairabad. This diachronous deformation has initially created meandering in the north to south flowing Indus River in the Mianwali Reentrant. Further uplifting of the push-up block has caused

a tectonic tilt, diverting the course of the Indus River westward during past ~140 ka at a displacement rate of ~12-15 cm/a.

The right lateral displacement in the en-echelon zone of the Kalabagh Fault exhibits morphotectonic features that include stream deflections, offsets in Quaternary sediments, pressure ridges in the foreland, displaced alluvial fans, uplifted sediments at fan apex and a piggyback basin, back tilting in the fan sediments and pebbles that are fractured and displaced. Subsurface scanning from the ground penetrating radar (GPR) and investigations from the trenches, outcrops and streams reveal splays of the Kalabagh Fault has disrupted the late Quaternary sediments during seismic events. Luminescence ages determined from these deformed sediments suggest diachronous Holocene seismicity along the Kalabagh Fault. The recurrence interval of ~10 ± 2 ka on average is calculated based on the ages of the tectonically uplifted Pleistocene sediments and youngest earthquakes at Khairabad, that has disrupted the Holocene sediments. The latest earthquakes at Khairabad in early Holocene (~ 9 ka), and during ~ 1 ka at Ghundi denote these sections of the Kalabagh Fault as tectonically active, whereas foreland is exerting stress that may lead to major seismicity at these locations. Moreover, morphometric analysis and landforms in the eastern Salt Range, Pir Panjal Ranges, Hazara Kashmir syntaxis and the Kurram Fault exhibit results that may support paleoseismic evidences in these parts of the study area.

Kurzfassung

Der Sub-Himalaya in Pakistan wird seitlich durch die Kalabagh-Verwerfung und die Jhelum-Verwerfung gegliedert, die die Grenzen zwischen dem Kohat-Plateau, dem Potwar-Plateau und der Hazara-Kashmir-Syntaxis bilden. Die Hazara-Kaschmir-Syntaxis trennt sowohl strukturell als auch morphologisch den östlichen und den westlichen Sub-Himalaya im Kaschmir. Das östliche Potwar-Plateau und die Hazara-Kashmir-Syntaxis waren in letzter Zeit seismisch aktiv (z.B., Mw=7,6, 2005 und Mw=5,6, 2019). Auf dem Kohat-Plateau gab es 1992 außerdem ein Erdbeben der Stärke Mw=6. Diese Erdbeben weisen das Kohat-Plateau, das östliche Potwar-Plateau und die Hazara-Kashmir-Syntaxis als seismisch aktive Gebiete aus. Darüber hinaus zeigen InSAR- und GPS-Daten aus früheren Studien Hebungen und aseismische Verschiebungen in der Salt Range, dem westlichen Potwar-Plateau und entlang der Kalabagh-Verwerfung. Diese Anomalien deuten ebenfalls darauf hin, dass das Gebiet tektonisch aktiv ist und die Entwicklung der Morphologie beinflusst. Ziel dieser Doktorarbeit war es, die Paläoseismologie und Neotektonik im Sub-Himalaya zu untersuchen mit Schwerpunkt auf der Kalabagh-Verwerfung, die das westliche Potwar-Plateau begrenzt.

Die morphometrischen Indizes der Hazara-Kaschmir-Syntaxis, Pir-Panjal-Gebiet, im Potwar-Plateau-Salzgebirge und im Kohat-Plateau-Surghar-Gebiet und entlang der Kurram-Verwerfung wurden bestimmt und ausgewertet. Die Landschaftsentwicklung in diesen Gebieten wird durch die weicheren Lithologien der tertiären Sedimente beeinflusst, die leicht erodierbar sind und selbst in jüngeren Einzugsgebieten eine degradierte Morphologie aufweisen. Die Beziehung zwischen den Wassereinzugsgebieten dieser Gebiete zeigt, dass die Morphologie des Gebietes in unterschiedlichem Maße von den tektonischen Verformungen betroffen sind. Die morphometrischen Indizes der Hazara-Kaschmir-Syntaxis, Pir-Panjal-Gebiet, im Potwar-Plateau-Salzgebirge, im Kohat-Plateau-Surghar-Gebiet und an der Westflanke des Bannu-Beckens zeigen einen mäßigen bis hohen tektonischen Aktivitätsindex.

Die Deformationsgeschichte und die Paläoerdbeben entlang der Kalabagh-Verwerfung wurden mittels morphotektonischer und paläoseismischer Untersuchungen studiert und durch Lumineszenzdatierungen der deformierten Sedimente zeitlich eingeordnet. Bei älteren Sedimenten wurde die pIRIR-Lumineszenz-Datierungsmethode mittels Kalium-Feldspat angewandt. Für jüngere (holozäne) Sedimente wurden Quarz-OSL-Datierungen verwendet. Diese Studie zeigt die tektonischen Deformationen und die Seismizität, die während des mittleren bis späten Pleistozäns und Holozäns auftraten. Die dextrale Kalabagh-Verwerfung weist eine En-Echelon-Zone auf, die sich im Überschneidungsbereich zwischen den Segmenten der Verwerfung gebildet hat. Die Überschiebung der En-Echelon-Verwerfungen zwischen den Abschnitten Thathi und Zaluch wurde vor etwa 0,5 Ma

erstmals an der Oberfläche sichtbar. Ein Push-up-Block in dieser En-Echelon-Zone hat die Morphologie in den letzten ~ 0,5 Ma maßgeblich geformt. Andauernde tektonische Deformationen haben die Landschaft seit ~220 ka in Larkakki, ~140 ka in Ghundi und ~190 ka in Khairabad geformt. Diese diachrone Deformation hat zunächst zu einer Mäanderbildung des von Norden nach Süden fließenden Indus im Mianwali Reentrant geführt. Die weitere Hebung des Push-up-Blocks hat eine tektonische Neigung verursacht, die den Flusslauf des Indus in den letzten ~140 ka mit einer Versatzrate von ~12-15 cm/a nach Westen ablenkt.

Die dextrale Blattverschiebung in der En-Echelon-Zone der Kalabagh-Verwerfung weist morphotektonische Merkmale auf, zu denen Flussablenkungen, Verschiebungen in quartären Sedimenten, Druckrücken im Vorland, verschobene Schwemmfächer, angehobene Sedimente an der Fächerspitze und im Piggy-Back Becken, Rückrotationen der Fächersedimente, sowie Gerölle, die zerbrochen und verschoben sind, gehören. Die Untersuchung des Untergrunds mit Bodenradar (GPR) und die Untersuchungen der aufgeschlossenen Gräben, Aufschlüsse und Bäche zeigen, dass die Kalabagh-Verwerfung die spätquartären Sedimente bei seismischen Ereignissen deformiert hat. Die aus diesen deformierten Sedimenten ermittelten Lumineszenzalter lassen auf eine diachrone holozäne Seismizität entlang der Kalabagh-Verwerfung schließen. Das Wiederholungsintervall von durchschnittlich ~10 ± 2 ka wurde auf der Grundlage des Alters der tektonisch angehobenen pleistozänen Sedimente und der jüngsten Erdbeben in Khairabad berechnet, die die holozänen Sedimente deformiert haben. Die jüngsten Erdbeben in Khairabad im frühen Holozän (~ 9 ka) und während ~ 1 ka in Ghundi weisen diese Abschnitte der Kalabagh-Verwerfung als tektonisch aktiv aus, und in das Vorland Spannungen transferieren, die an diesen Stellen zu starker Seismizität führen können. Darüber hinaus zeigen morphometrische Analysen in der östlichen Salt Range, der Hazara-Kashmir-Syntaxis, der Pir-Panjal-Gebiet und der Kurram-Verwerfung die paläoseismische Bewegungen in diesen Teilen des Untersuchungsgebiets unterstützen.

Acknowledgments

First, I would like to thank Prof. Dr. Klaus Reicherter for his supervision, guidance, support and motivation during my PhD. I am also grateful to Prof. Dr. Manfred Frechen from LIAG (Leibniz Institute for applied Geophysics, Hannover) for his technical and scientific support for luminescence dating.

I am also obliged to Dr. Sajid Ali, Dr. Junjie Zhang (LIAG) and Dr. Sumiko Tsukamoto (LIAG) for their support and valuable comments on methodologies and write up. I would also like to acknowledge:

- Higher Education Commission (HEC) of Pakistan and Deutscher Akademischer Austaushdienst (DAAD) for their financial and management support for my PhD.
- Mr. Aun Zahoor (Geological Survey of Pakistan) and Mr. Farooq Sultan (Mines and Minerals Department, Punjab, Pakistan) for their technical support.
- Dr. Christoph Grützner (Friedrich-Schiller-Universität Jena) for his support during this study.
- My colleagues including Dr. Peter Biermanns, Dr. Christopher Weismüller, Mr. Aram Fathian Baneh, Dr. Jorien van der Wal and Mr. Rashid Haider for their discussions, comments and help.
- Dr. Jochen Hürtgen, Ms. Lisa Feist, Ms. Sara Pena Castellnou, Mr. Farkhod Hakimov for their day-to-day support.
- Ms. Evelyn Bützler for her administrative support.
- LIAG scientific and technical team for their assistance including Dr. Astrid Techmer, Ms. Gwynlyn Buchanen, Mr. Frank Oppermann, Mr. Karsten Vollmer, Ms. Neda Rahimzadeh, Mr. Marcus Richter, Ms. Petra Posimowski, Ms. Sabine Mogwitz and Ms. Sonja Riemenschneider.

Apart from all scientific and technical acknowledgements, I would like to importantly mention my parents: Muhammad Abbas (father) and Safia Abbas (mother) for making me able to approach this position. My wife Faiza Khalid, my son Abdul Ahad and my daughter Muntaha Noor for supporting me to complete my PhD and bearing the hardships to spend their days in my absence in Pakistan. I am also thankful to my siblings and their families for all their love and best wishes.

Table of Contents

List of figures

Chapter 1

Chapter 2

Chapter 3

Chapter 4

Chapter 5

Appendices

List of tables

Chapter 2

Chapter 3

Chapter 5

Appendices

1. Introduction

The dynamics and effects of earthquakes are important to explain their relevance with the modern infrastructure. The designs of the sustainable mega projects and urban development are largely dependent on the seismic behavior and future risks, for which prediction of future earthquakes is important. Moreover, processing and interpretation of satellite imageries is widely used nowadays to observe the aseismic displacements of the earth crust. Whereas analogue models of large geological features are used to simulate solid earth processes. These modern scientific methods are unable to predict the timing of an earthquake. For this purpose, paleoearthquakes are used to infer the seismic history and probable future earthquakes, using the earthquake recurrence interval as a parameter (McCalpin and Nelson, 2009; Mozafari et al., 2019). A fault may exhibit longer earthquake recurrence interval that may go beyond available earthquake archives. Therefore, the area under observation may not necessarily have the historical earthquake data of the nearby faults.

The earthquake catalogs are available since a) human civilization records and b) availability of the seismic instruments. These criteria cover the time span of up to few hundreds or few thousands of years, e.g. Indus civilization is as old as c.2600-1900 BC (Mohser, 2017). Therefore, active faults with an earthquake recurrence interval of ~ 5 ka or more are not covered by this time span. Furthermore, ancient civilizations were not equally distributed and documented in different parts of the Earth. Consequently, historical data alone is insufficient to describe the timing of the paleoearthquakes.

Modern scientific approaches elaborate the (pre-)historic earthquakes including their location, timing and size, termed as Paleoseismology (McCalpin and Nelson, 2009). The sediments deformed by these earthquakes has formed different geologic structures and landforms, that are studied using the morphometric analysis, sub surface geophysical data, high-resolution surface models, outcrop geology and trench investigation across the faults. The chronology of the deformed sediments defines the timing of these deformations. Several dating techniques are used nowadays for this purpose such as cosmogenic radionuclide dating, radiocarbon dating and luminescence dating (Ivo et al., 2000; Mozafari et al., 2019; Sohbati et al., 2012). Using a specific dating method usually depends on the dating range and material used for that technique. e.g., all sediments may not contain charcoal for radiocarbon dating. Integration of the geological observations with the chronology of the sediments yields deformation and seismic history of a fault. A geologic section may show deformations reflecting several paleoseismic episodes along a fault. The chronology of these deformations indicates the earthquake recurrence interval and youngest seismic event.

Modern scientific methods record present-day aseismic displacement rates using global positioning system (GPS) and Interferometric synthetic aperture radar (InSAR). The latter is also used to mark

seismic displacements. Results from the GPS and InSAR observations are helpful to choose the active faults to study their neotectonics. Moreover, morphotectonics has emerged as a technique to study the surface morphology evolved due to tectonic deformations that are recent in the geologic time. These morphological features and their changing patterns mark the active tectonic behavior of the faults. This thesis is based on the morphotectonics and paleoseismology of the Sub-Himalayas in Pakistan. These observations are supported by the luminescence dating of the sediments that are deformed by the tectonic deformations and paleoearthquakes.

1.1 Motivation and project relevance

The Sub-Himalayas in Pakistan are bounded in the South by the Salt Range and the Trans Indus Ranges (Fig. 2.2). The Trans Indus Ranges include the Surghar Range, Khisor Range and the Marwat Range. These mountain ranges are uplifted along the Main Frontal Thrust (MFT), that is segmented by the strike slip faults. These faults have formed offsets among these mountain ranges. The Kalabagh Fault (KBF) is one of the largest transform faults in the study area that causes an offset of ~ 70 km between the Salt Range and the Surghar Range. The fault is considered active based on the InSAR data and magnetic polarity of the sedimentary rocks deposited until ~0.4 Ma (Chen and Khan, 2010; Johnson et al., 1979; Keller et al., 1977; Khan, 1983; McDougall and Khan, 1990; Yeats et al., 1984). No recent or historical earthquakes of large magnitude are reported along the fault. Whereas the proposed site for the Kalabagh dam is located near the Kalabagh Fault Zone. The tectonic geomorphology and its connection with the structural deformations along the Kalabagh Fault have not been investigated in detail from the paleoseismic aspect. Therefore, paleoseismicity and active tectonics of the fault is important to estimate the future risks.

The Hazara-Kashmir Syntaxis (HKS) forms an antiformal tectonic bend that separates the Sub-Himalayas in Pakistan from the eastern Himalayas (Baig et al., 2010). The sinistral Jhelum Fault (JF) on the western flank of the HKS delineates the eastern margin of the Salt Range. It is also active and exhibits several recent earthquakes (Fig. 2.2). The active nature of the Sub-Himalaya has developed landforms that reveal variable morphology. Therefore, morphometric Indices are important to study the active tectonics of the Sub-Himalayas in Pakistan. The Jhelum Fault is close to the Mangla Dam that further enhance the importance of the active tectonics in this part.

The morphometric indices in the Sub-Himalayas are calculated in this study that are further supported by the paleoseismology. The paleoseismic investigations along the Kalabagh Fault are validated by

dating the deformed sediments along the fault. Moreover, sediment correlation and luminescence dating is utilized to find the diversion history and diversion rates of the Indus River.

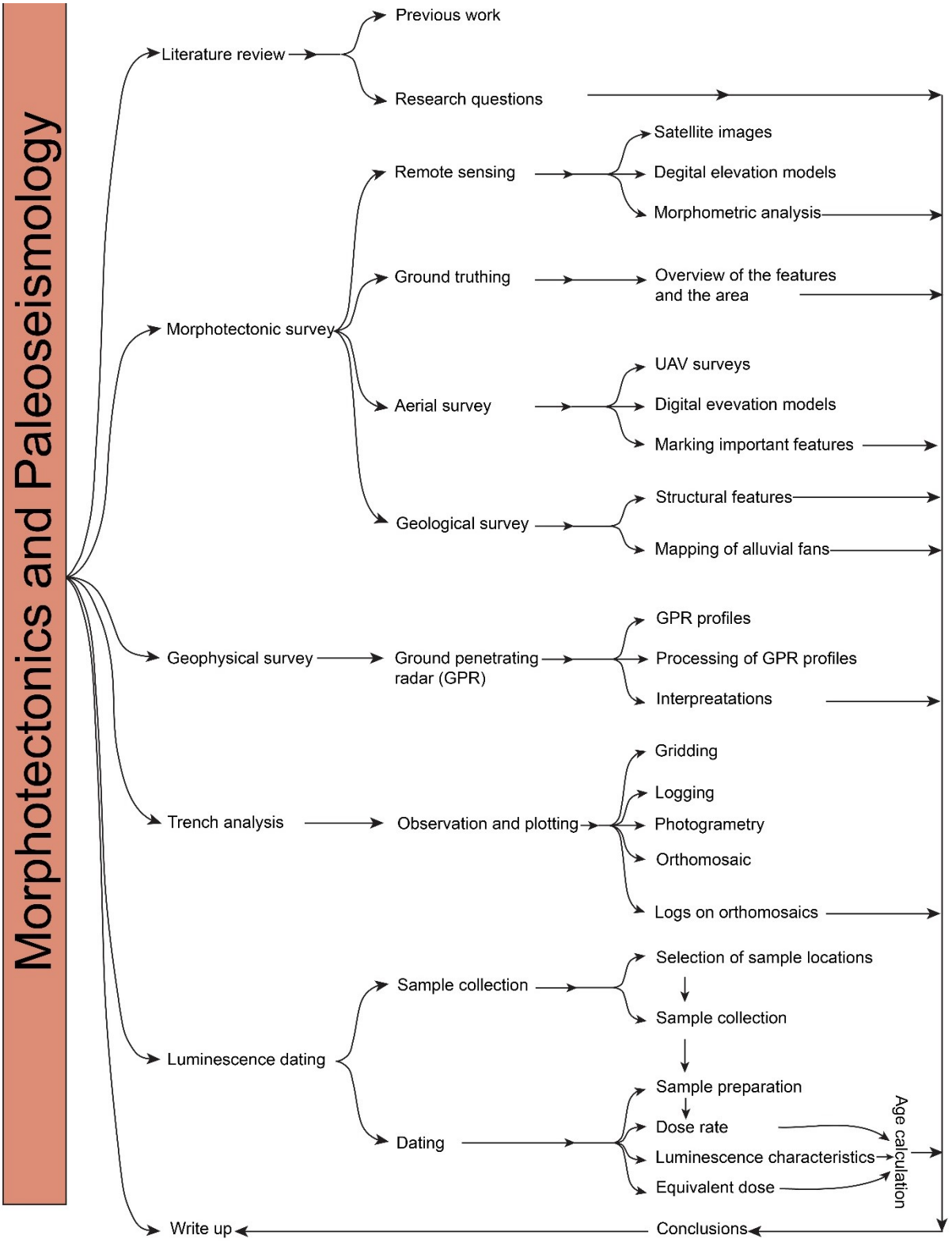

Fig. 1.1 Flow chart illustrates the approaches and methods adopted to study the morphotectonic features and investigating the paleoseismic behavior of the study area.

1.2 Objectives and approaches

The focus of this research was to determine the active tectonics based on the paleoseismology and morphotectonics of the Sub-Himalayas in Pakistan with special emphasis on the Kalabagh Fault and the western Potwar Plateau. A multi-dimensional approach (Fig. 1.1) was used including Remote sensing, outcrop geology, geophysics and chronology data to fulfill following objectives.

I. Active tectonic behavior using morphometric indices
II. Studying the tectonic geomorphology along the Kalabagh Fault zone.
III. Deformation and seismic history of the active Kalabagh Fault
IV. Chronology and sequence of landform development of the Kalabagh Fault Zone (KBFZ)
V. Application of luminescence dating methods to determine the chronology of the sediments from the mountain front.
VI. Timing and diversion rates of the Indus River in the Mianwali Reentrant

1.3 Materials and methods

This study is carried out by integrating the aerial images, surface, subsurface and chronology data. For this purpose, satellite data from SRTM 30 m, ALOS 30 m and Google Earth imagery were used for calculation of the morphometric indices and aerial reconnaissance. After selection of the area with active tectonic features, field excursion was carried out for aerial surveys using unmanned aerial vehicle (UAV). Structure from motion (SFM) technique was used to make high resolution digital elevation models from UAV data followed by field mapping of the morphotectonic features. Ground penetrating radar (GPR) was used to scan the subsurface geologic structures along the morphotectonic features. Outcrops and trenches across the morphotectonic features were logged. Samples were collected from the sediments that are deformed by the earthquakes and tectonic uplifts. These samples were utilized for infrared stimulated luminescence (IRSL) and optically stimulated luminescence (OSL) dating. Fig. 1.1 shows workflow for collection, processing and interpretation of the research data. Detailed methodology is described in the relevant sections of the following chapters.

1.4 Thesis Outline

This thesis consists of chapters that are Published, submitted or are intended to be published in peer reviewed Journals. Partial overlapping and repetition of text, context and figures is hence likely and inevitable. Chapters following the first Introductory chapter include:

Chapter 2 This Chapter briefly describes broader tectonic classification of the Himalayas with details of the tectonic elements of the Sub-Himalayas in Pakistan. Stratigraphic variations among different tectonic elements of the Sub-Himalayas are also documented in this chapter.

Chapter 3 This chapter presents results and analysis from the morphometric indices of the mountain ranges along the Himalayan front and frontal foreland basins (Potwar Basin and Kohat Basin uplifted as Potwar Plateau and Kohat Plateau respectively). Morphometric Indices were applied on the SRTM 30 m digital elevation models to analyze the active behavior in different parts of the study area, and relative active tectonic index was calculated.

Chapter 4 This chapter is a slightly modified version of a published article and presents the evidences of seismic deformations along the Kalabagh Fault and their contribution towards the landform development. Evidences for the westward diversion of the Indus River are also presented.

Chapter 5 This chapter is a slightly modified version of an article in press and presents results from the luminescence dating of the paleoseismic features presented in Chapter 4. This chapter describes the late Pleistocene-Holocene deformation and seismic history of the Kalabagh Fault. Moreover, diversion rates of the Indus River are also calculated and presented in this chapter.

Chapter 6 This chapter includes integrated synthesis and conclusion from the preceding chapters and outlook of the research.

2. Structural and stratigraphic controls in the Sub-Himalayas

2.1 Overview and relevance

This chapter describes major tectonic elements that classify Himalayas into constituent zones. Details of the tectonic and structural components of the Sub-Himalayas of Pakistan are also discussed in this chapter. The structural variations are marked by the stratigraphic changes and therefore enhance the importance of stratigraphy. For example, the Kohat Plateau (KP) and the Potwar Plateau (PP) are frontal foreland basins that are uplifted along the Himalayan frontal ramp in Pakistan (Fig. 2.2). Both basins exhibit different Eocene stratigraphy. The Eocene evaporite zone of the Kohat Plateau that causes development of the duplex structures, is absent in the Potwar Plateau (Gee, 1980; Ghani et al., 2018). Stratigraphic contact of the older rocks with the younger rocks is used to mark faults that are also discussed in Chapter 4 and 5. Considering the importance of stratigraphy, later part of this chapter includes brief stratigraphic descriptions and lithological variations of the rock units in different parts of the study area.

2.2 Tectonic framework

The Himalayan orogeny has developed along various thrusts after collision between the Indian and the Eurasian plates. These thrusts categorize the Himalayas into various tectonic elements (Fig. 2.1) that exhibit different lithological, metamorphic and stratigraphic characteristics (Gansser, 1964; Le Fort, 1975, Dipietro and Pogue, 2004). Major subdivisions from the South to the North include the Sub-Himalayas, Lesser Himalaya, Higher Himalaya, Suture zone and the Tibetan Himalaya. Geology of the western most Himalayas differ from the central and the eastern Himalayas such as the fossiliferous Tibetan Himalayas is less evident in the West (Gansser, 1964).

2.2.1 Suture zone

The Suture zone is located in the North of the Himalayas (Fig. 2.1) and has two constituents: 1) Shyok suture (SS) in the North and 2) Indus-Tsangpo suture (ITS) in the South (Petterson, 2010). Former makes thrusted contact with the Karakoram and later marks the northern margin of the Higher Himalayan Crystallines (HHC) also termed as the Greater Himalayas. In the North of the Indus-Tsangpo suture, the intra oceanic Kohistan-Ladakh island arc (KLIA) and Eurasian plate lithologies of the Lhasa-Karakoram block are situated (Henderson et al., 2011; Honegger et al., 1982; Searle et al., 1999). The Kohistan-Ladakh island arc is dissected by the Nanga Parbat-Haramosh (NPHS) Syntaxis (Petterson,

2010). In the eastern Himalayas, Trans Himalayan Batholiths mark the northern end of the suture zone (Fig. 2.1).

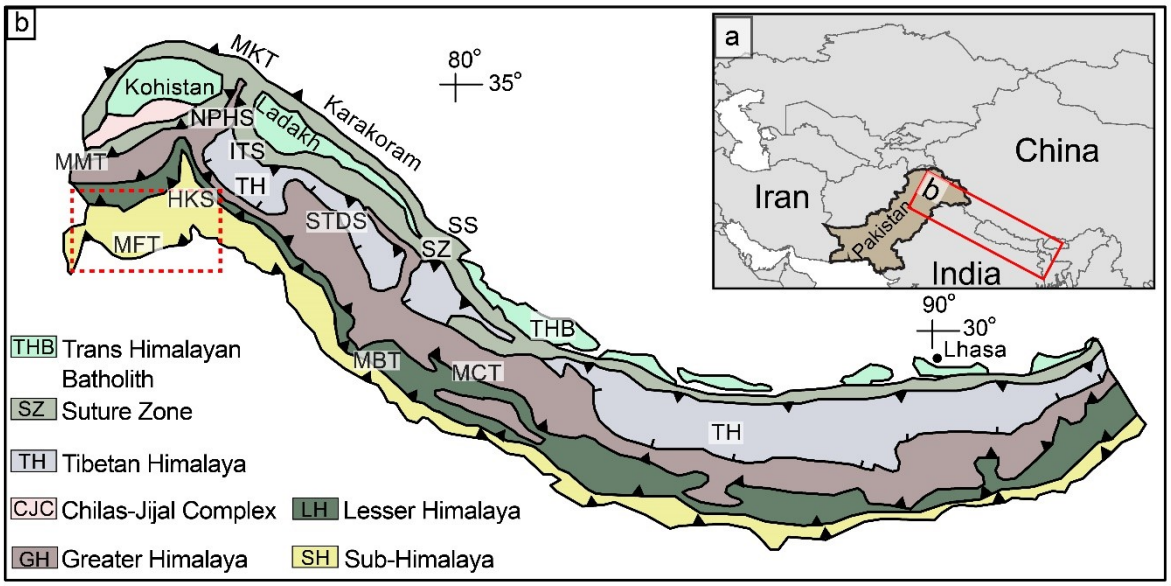

Fig. 2.1 (a) Geographical location of the Himalayas, (b) Map shows tectonic elements of the Himalayas (modified after Ali et al., 2018; Honegger et al., 1982; Searle and Treloar, 2019). GH=Greater Himalaya or Higher Himalayan Crystalline Zone, HKS=Hazara-Kashmir Syntaxis, ITS=Indus-Tsangpo Suture, MBT=Main Boundary Thrust, MCT=Main Central Thrust, MFT=Main Frontal Thrust, MKT=Main Karakoram Thrust, MMT=Main Mantle Thrust, NPHS=Nanga Parbat Haramosh Syntaxis, SS=Shyok Suture, STDS=South Tibetan Detachment System, TH=Tibetan Himalaya, THB=Trans Himalayan Batholith.

2.2.2 Tibetan Himalaya

The western most Himalayas are differentiated from the central and the eastern Himalayas (Fig. 2.1) due to the absence of the Tibetan Himalayas (Gansser, 1964). These Himalayas represent Paleozoic-Eocene Tibetan sedimentary series in the South of the Indus-Tsangpo Suture, marking the pre India-Eurasia collision sediments on the northern passive margin of the Indian Plate (Gaetani and Garzanti, 1991; Henderson et al., 2011). The South Tibetan Detachment System (STDS) in the south of the Tibetan Himalayas is a large extensional fault system that differentiates it from the Higher Himalayan Crystallines (HHC) on the basis of metamorphism (Dipietro and Pogue, 2004; Henderson et al., 2011).

2.2.3 Higher Himalaya

The Higher Himalaya or Greater Himalaya or Higher Himalayan Crystalline (HHC) is characterized by high grade metamorphic rocks that make a thrusted contact with metasediments of the Lesser Himalayas along the Main Central Thrust (Kazmi and Jan, 1997). Delineation of the Main Central Thrust (MCT) as the southern margin of the Higher Himalayas (Fig. 2.1) has been controversial (Dipietro and Pogue, 2004). Chaudhry and Ghazanfar (1990) has marked the MCT in the NW Himalaya and correlated the HHC in this area and further in the East.

2.2.4 Lesser Himalaya

The northern boundary of the Lesser or Lower Himalaya in the NW Himalayas is marked by the Main Central Thrust (Chaudhry and Ghazanfar, 1990). The Lesser Himalaya are bounded in the South (Fig. 2.1) by the Main Boundary Thrust (Gansser, 1964; Dipietro and Pogue, 2004; Ahsan and Chaudhry, 2008). In the northwestern (NW) Himalayas in Pakistan, this zone consists of Precambrian to late Paleozoic metasediments, Paleozoic sedimentary and volcanic rocks (Kazmi and Jan, 1997).

2.2.5 Sub-Himalayas

The southernmost part of the Himalayas is classified as the Sub-Himalayas (Gansser, 1964; Le Fort, 1975; Dipietro and Pogue, 2004). The Main Boundary Thrust (MBT) marks its northern margin based on the red Neogene molasse deposits to the South of the Main Boundary Thrust (Ahsan and Chaudhry, 2008). These molasse sediments were deposited in the frontal foreland basins, the Kohat Basin (KB) and the Potwar Basin (PB). The Sub-Himalayas in Pakistan include the Kohat Plateau (KP), Potwar Plateau (PP), Bannu Basin (BB), Salt Range (SR) and the Trans Indus Ranges (Fig. 2.2). The Kohat Plateau and the Potwar Plateau contain frontal foreland sediments of the Himalayas in the Kohat and the Potwar basins respectively. The Potwar Plateau is thrusted southwards forming a frontal ramp along the Salt Range Thrust (SRT) in the Salt Range. The Precambrian strata is thrusted above the synorogenic Quaternary Alluvium (QAL) along the Salt Range Thrust (Yeats et al., 1984). The Salt Range thrust is considered as an equivalent of the Main Frontal Thrust (MFT) of the eastern Himalayas (Dipietro and Pogue, 2004). In the West, the Kohat Plateau and the Surghar Range (SGR) are uplifted along the Main Frontal Thrust (Ahmad et al., 1999; Ali et al., 2014). Furthermore, the Hazara-Kashmir Syntaxis (HKS) differentiates the structures of the Sub-Himalayas of Pakistan (Fig. 2.1) from the eastern Himalayas (Baker et al., 1988; Ghani et al., 2018). The Jhelum sinistral strike slip fault marks the eastern termination of the Sub-Himalayas in Pakistan classifying the zone as the Potwar Plateau (Fig. 2.2). The Kohat Plateau is differentiated from the western Potwar Plateau based on the structural and stratigraphic variations (Abbasi and McElroy, 1991). The late Miocene-Pleistocene Siwalik group of sediments (TSK) were deposited in the Kohat and Potwar frontal foreland basins of the sub-Himalayas, later uplifted and has formed the Kohat Plateau and the Potwar Plateau (Ahsan and Chaudhry, 2008; Gansser, 1964; Gee, 1980; Johnson et al., 1986b). Keeping into account the relevance, the Sub-Himalayas and its integral tectonic elements are discussed in the following paragraphs.

Potwar Plateau and Salt Range

The Salt Range Thrust (SRT) separates the Potwar Plateau from the Punjab Plain. This thrust forms the Salt Range along the Himalayan front (Jaumé and Lillie, 1988). While MBT marks the northern margin of the Potwar Plateau (Fig. 2.2) and the Sub-Himalayas (Ahsan and Chaudhry, 2008; Jaumé and Lillie, 1988). The eastern Salt Range is characterized by the fault blocks bounded by thrusts and back thrusts (Baker et al., 1988; Johnson et al., 1986a). The boundaries of the Salt Range are marked by the sinistral Jhelum Fault (JF) in the East (Fig. 2.2) and the dextral Kalabagh fault (KBF) in the West (Abir et al., 2015; Butler et al., 1987; Jaumé and Lillie, 1988). The Siwalik sediments (TSK) cover most part of the Potwar Plateau that is further discussed in the stratigraphy section.

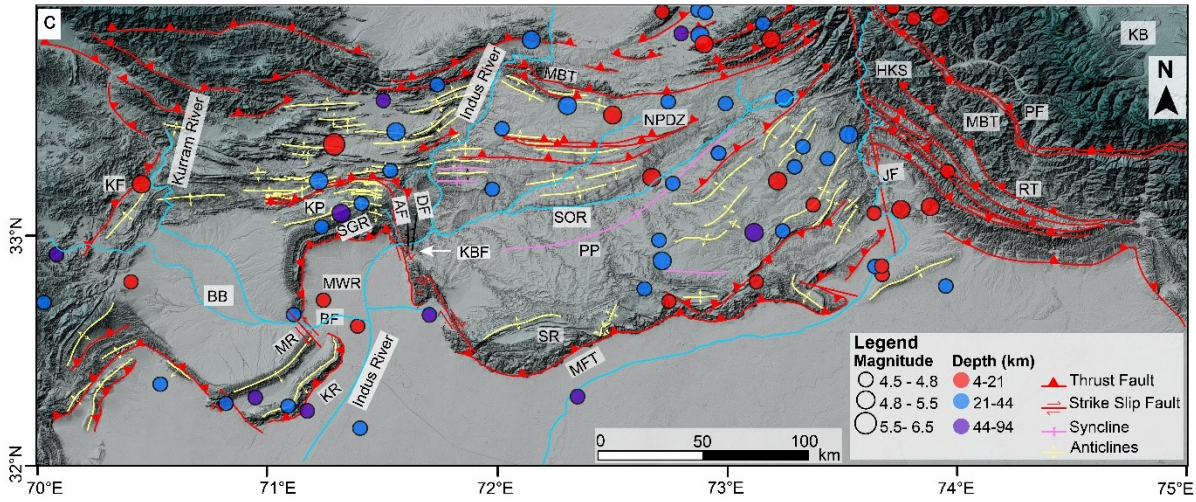

Fig. 2.2 Integrated tectonic map of the Sub-Himalayas showing main structural features and tectonic subdivisions on hillshade image, (modified after Abbas et. al. 2022; Abir et al., 2017; Alam, 2008; Ali, 2010; Kazmi and Rana, 1982) based on digital elevation models (DEM) from the ALOS 30m and Global Imagery of ArcGIS. Circles show instrumental seismicity (USGS Earthquake catalogue, 2019). AF=Ainwan Fault, BB=Bannu Basin, BF=Bannu Fault, DF=Dinghot Fault, FR=Frontal Ramp, JF=Jhelum Fault, KBF=Kalabagh Fault, KP=Kohat Plateau, KR=Khisor Range, LR=Lateral Ramp, MBT=Main Boundary Thrust, MFT=Main Frontal Thrust, MR=Marwat Range, MWR=Mianwali Reentrant, NPDZ=North Potwar Deformed Zone, PP=Potwar Plateau, SR=Salt Range, SGR=Surghar Range, TR=Tank Reentrant.

The Salt Range in the South and in the West of the Potwar Plateau is considered as the museum of geology for its characteristic exposures that reveal stratigraphy from Precambrian to Quaternary age. The Khewra gorge, Nammal gorge and the Karoli section are examples of these exposures. The Potwar Plateau is divided by the Soan syncline into the northern and the southern Potwar Plateau. Former is characterized by fold and thrust belts (Fig. 2.2) and termed as the North Potwar Deformed Zone (NPDZ), whereas, later is less deformed slab in the South that thrusts southwards (Alam, 2008; Baker et al., 1988). Mechanics of the southern Potwar Plateau are controlled by salt tectonics and reveal a combination of compressional and extensional faults.

Kohat Plateau and Surghar Range

The Kohat Plateau is differentiated from the Potwar Plateau in the East by the Kalabagh Fault (Abbasi and McElroy, 1991). The Surghar Range along the Main Frontal Thrust is less emergent as compared to the Salt Range, differentiating the Kohat Plateau from the Potwar Plateau along the Kalabagh Fault (Baker et al., 1988). Thus, stratigraphy of the Kohat Plateau is mostly exhibited by the Miocene rocks with a narrow belt of the Mesozoic strata (Crawford, 1974; Gee, 1980). The Kohat Plateau exhibits duplex structures formed by double decollement, with floor thrust above the basement rocks and the roof thrust along the Paleocene and older strata (Ghani et al., 2018).

Kalabagh Fault

The Kalabagh Fault is a dextral strike slip fault that marks tectonic boundary between the Kohat Plateau and the Potwar Plateau with ~ 70 km of lateral offset between the Salt Range and the Surghar Range (Fig. 2.2). The Kalabagh Fault has formed landforms through its extent from the range bound fault to lateral ramp (details in Chapters 4 and 5). The KBF mainly exhibit 2 segments. The southern segment strikes N35°W starting from the western termination of the Salt Range and bounds the eastern part of NW striking fold and thrust system in the western Potwar Plateau. This segment is characterized by a big lake that is connected with the foreland by a deeply incised stream in the Nammal gorge. In 1913 A.D., a storage dam was constructed at the lake outlet, termed as the Nammal Dam and the lake is called the Nammal lake. This segment of the Kalabagh Fault is termed as the Nammal Ridge in the following text.

The northern segment makes nearly ten kilometers wide fault stepover at Ghundi. This segment bounds the NW striking fold and thrust system of the lateral ramp in the West. In this area it demarcates boundary between the Potwar Plateau and the Mianwali Reentrant (MWR). The range front in this area exhibits alluvial fans of variable diameter and thickness (Chapter 4). The streams deflections in the stepover zone reveal right lateral kinematics of the Kalabagh Fault. The landforms of the Kalabagh Fault Zone (KBFZ) disappear in the North of the Khairabad section and reappear near the Indus River (Fig. 2.2). This part of the fault zone is termed as the Khairabad-Ghundi (KG) section in the following text.

In the North of the Indus River, along the Chisal Algad stream, the northern segment of the KBF is bounded by the Potwar Plateau and the Kohat Plateau. The vertical contact between the Precambrian Salt Range formation (PCSR) against the Siwaliks (TSK) indicate N15°W striking Kalabagh Fault in the Chisal Algad (CA) stream (Fig. 2.3). Therefore, this segment is termed as the northern segment or

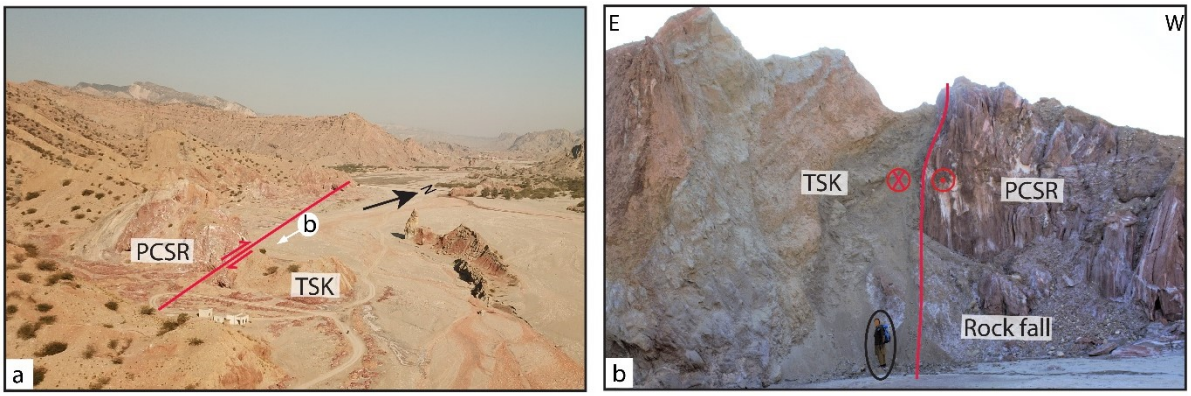

Fig. 2. 3 (a) The Kalabagh Fault marked along the Chisal Algad stream, (b) The Precambrian Salt Range Formation (PCSR) makes a vertical contact with the Tertiary-Quaternary Siwaliks Rocks (32°58'45.28''N, 71°34'41.77''E). Location of (b) is marked on (a).

Chisal Algad segment (Chen and Khan, 2010; McDougall and Khan, 1990). The Ainwan and Dinghot faults in the East of this segment are considered as active offshoots of the main Kalabagh Fault (Chen and Khan, 2010; Khan et al., 2012). In the further North, the Kalabagh Fault bends towards the West parallel to the North dipping thrusts in the Kohat Plateau (McDougall and Khan, 1990). Previous work, history and active tectonics of the Kalabagh Fault is discussed in detail in the following chapters.

Trans Indus Ranges

Mountain ranges in the West of the Indus River (IR) are termed as the Trans Indus Ranges (TIR). These include the Surghar Range (SGR), Khisor Range (KR) and Marwat Range (MR). The Surghar Range in the South of the Kohat Plateau (Fig.2.2) makes a tectonic bend that creates a divide between the Bannu Basin (BB) and the Mianwali Reentrant. The morphological expressions indicate that the Surghar Range is separated from the Khisor Range and Marwat Range by the Bannu Fault (BF). Apart from the structural dissimilarities, Trans Indus Ranges are differentiated from the Salt Range due to the Precambrian, Paleozoic and Tertiary stratigraphic variations (Ali, 2010).

2.3 Stratigraphic framework

The Sub-Himalayan Ranges in Pakistan reveal diverse stratigraphy from Precambrian to Quaternary age. The stratigraphic variations differentiate this Himalayan segment from the Lesser Himalayas (Ahmad, 2009; Ahsan and Chaudhry, 2008; Gee, 1980). The stratigraphic sequences are exposed along the thrusts, gorges and streams. e.g., Nammal gorge, Zaluch and Khewra gorge (Fig. 2.4). The stratigraphic nomenclature is adopted to name these units (Shah, 1977a). Moreover, the Kohat and Potwar frontal foreland basins exhibit stratigraphic variations. e.g., Eocene limestones in the Potwar Plateau and evaporites in the Kohat Plateau. The lithological dissimilarities within the same unit or chronological resemblances in different units classify the stratigraphy into members and groups

respectively (Kadri, 1995; Shah, 1977a). Brief description of the stratigraphic units in the western Sub-Himalayas is discussed in the following section. While their ages are summarized in Table 2.1.

2.3.1 Precambrian

Salt Range Formation

The Salt Range Formation consists of evaporites that had caused frontal slab of the Potwar Plateau to thrust along the decollement (Jaumé and Lillie, 1988). Asrarullah, 1967 classified this unit into following three constituent members (Shah, 1977b)

a) *Sahwal Marl member* at the bottom consists of bright to dull red marl with intercalations of Gypsum, Dolomite and salt
b) *Bhandar Kas Gypsum member* in the middle showing massive gypsum with intercalated dolomite and clay
c) *Bahadur Khel Salt member* on the top reveals ferruginous red marl with thick seams of salt.

The Salt Range Formation (PCSR) is exposed mainly in the eastern part of the Salt Range, with exposures at some localities in the western part and along the Kalabagh Fault (Figs. 2.4, 2.5 and 4.2) The unit is also drilled in the Punjab plain at Karampur well where the formation is drilled up to the base (Kadri, 1995; Shah, 1977b). In the Kohat Plateau, that exhibits duplex structures, the Salt Range Formation is not witnessed (Kadri, 1995).

2.3.2 Paleozoic

2.3.2.1 Cambrian

Jhelum Group

The Cambrian rocks in the Sub-Himalayas of Pakistan are variably exposed in the Salt Range and the Khisor Range, whereas they are absent in the Kalabagh Fault Zone and the Surghar Range (Gee, 1980; Shah, 1977a). The stratigraphic units termed as the Jhelum Group consist of the following rock units:

The Khewra sandstone is composed of purple sandstones with shale intercalations. It exhibits syn-depositional (laminations, ripple marks, cross stratifications) and post depositional (load casts, pseudo nodules, ball and pillow, flame structures, mud cracks and rain prints) sedimentary structures (Saqib et al., 2009). The Kalabagh Fault Zone and the Surghar Range lack the Khewra Sandstone contrasting with the Salt Range and the Khisor Range due to erosion prior to the Permian deposition (Ali, 2010).

The Kussak Formation consists of greenish gray, glauconitic, micaceous sandstone and siltstone (Shah, 1977a). The unit is reported in the eastern and the central Salt Range and the Khisor Range (Ali, 2010; Pervaiz et al., 2017).

The Jutana Formation exhibit thick bedded to massive sandy dolomite and dolomitic sandstones with intercalated shale (Kazmi and Rana, 1982). The unit exhibits sedimentary features including ripple marks, cross-bedding, slump bedding and stylolites (Khan et al., 1977; Khan and Shah, 2019). Additionally, it also shows precursors of the original limestone in dolostone including micaliths, ooids, pisolites intra-clasts, glauconite and foraminiferal assemblages (Khan and Shah, 2019). The Jutana Formation is exposed in the eastern and the central Salt Range (Gee, 1980).

The Baghanwala Formation is composed of red shale and clay, intercalated with flaggy sandstone of variegated colors (Shah, 1977a). Apart from the diagnostic pseudomorphic casts, the formation consists of stratification, cross-bedding, ripple marks, fossil mud cracks and burrows (Khan and Khan, 1979; Shah, 1977a). The stratigraphic unit is exposed in the Eastern Salt Range (Gee, 1980; Khan and Khan, 1979).

The Khisor Formation is composed of gypsum, dolomite, shale and sandstone facies and considered as an equivalent of the Baghanwala Formation due to same stratigraphic position (Alam, 2008; Ali, 2010; Shah, 1977a). The Khisor Formation is only exposed in the Khisor Range (Shah, 1977a).

2.3.2.2 Permian

The Upper Indus basin of Pakistan show an unconformity missing the Ordovician-Carboniferous strata. Therefore, the Cambrian rocks are directly overlain by the Permian stratigraphy (Gee, 1980; Shah, 1977a). The Permian rocks of the Upper Indus Basin are classified into the Nilawahan Group and the Zaluch Group (Shah, 1977a). Formations of these groups are reported in the outcrops and well logs in the Potwar Plateau-Salt Range and the Kohat Plateau-Trans Indus Ranges. The Stratigraphy of these Permian groups is as follows.

Nilawahan Group

The Permian Nilawahan group (PNG) is variably exposed in the Salt Range and the Khisor Range. The friable lithologies of this group are exposed at places along the degraded mountain front of the lateral ramp along the Kalabagh Fault. The Nilawahan Group is also exposed in the Salt Range (Fig. 2.5), and consists of the following early Permian rock units:

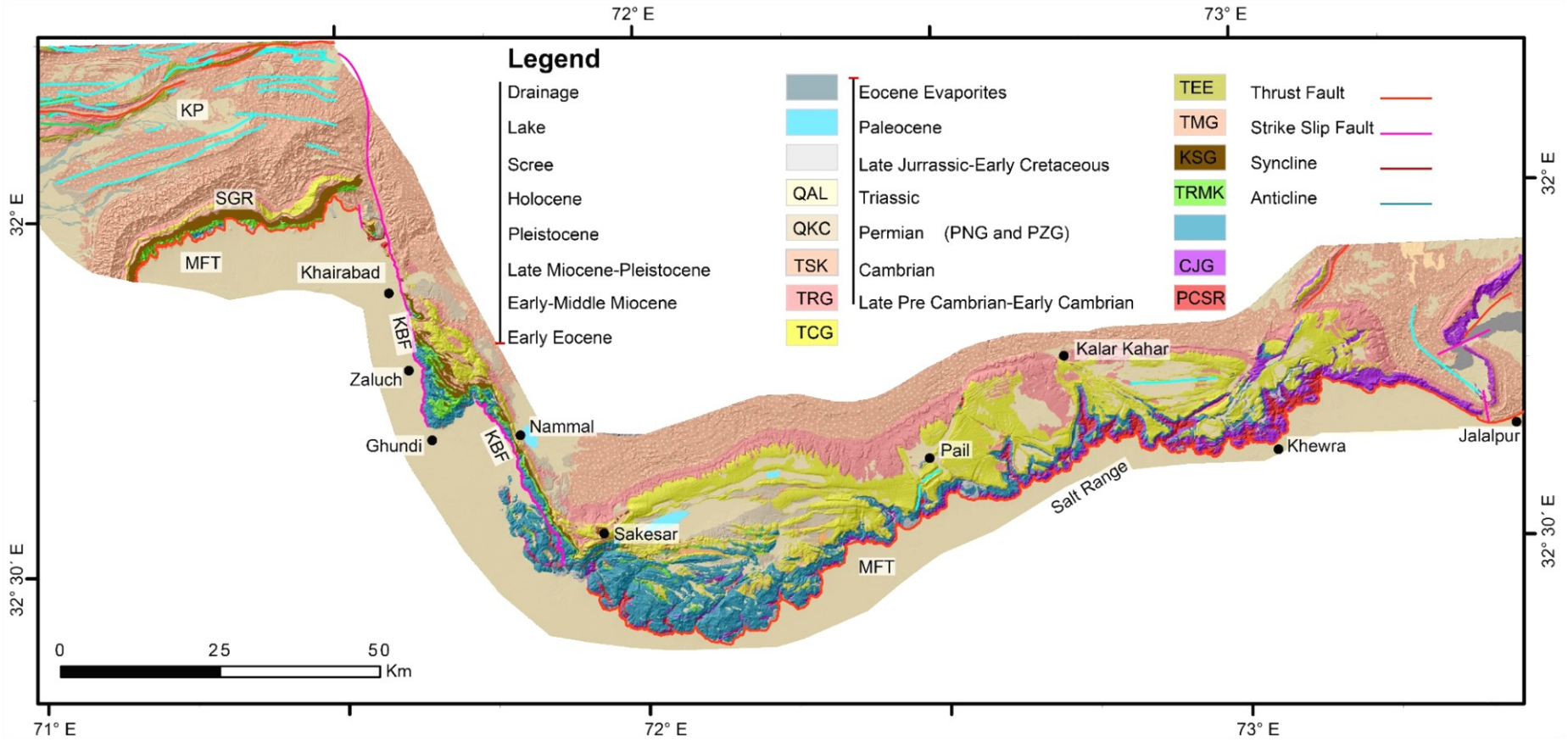

Fig. 2.4 Geological map of the Salt Range, Surghar Range and the southern Kohat Plateau, showing distribution of stratigraphic groups in the study area (modified after Dawar et al., 2009; Gee, 1980; Meissner et al., 1974). PCSR=Salt Range Formation (Precambrian), CJG=Jhelum Group (Cambrian), PNG=Nilawahan Group (Early Permian), PZG=Zaluch Group (Late Permian), TRMK=Musa Khel Group (Triassic), KSG=Surghar Group (Jurassic-Cretaceous), TMG=Makarwal Group (Tertiary), TEE=Eocene Evaporites (Tertiary), TCG=Chharat Group (Tertiary), TRG=Rawalpindi Group (Tertiary), TSK=Siwalik Group (Tertiary), QKC=Kalabagh Conglomerates (Quaternary), QAL=Alluvium (Quaternary), SC=Scree (Recent). Abbreviations: KBF=Kalabagh Fault, KP=Kohat Plateau, MFT=Main Frontal Thrust, SGR=Surghar Range.

Table 2.1 Stratigraphic table of the Potwar Plateau-Salt Range and Kohat Plateau-Surghar Range after Kadri (1997). F.=Formation, G.=Group, Lst. =Limestone, Sst. = Sandstone

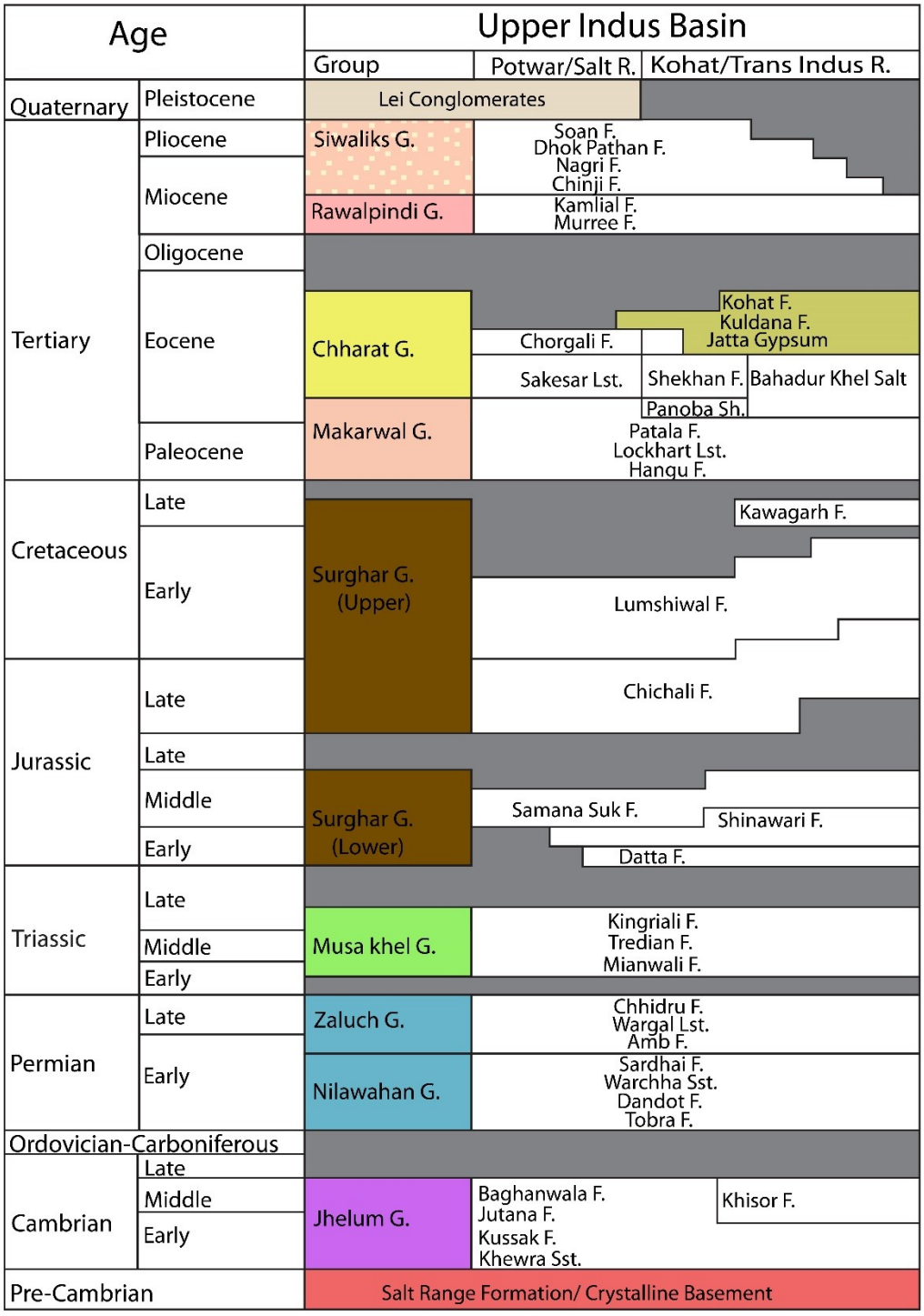

The Tobra Formation shows tillite facies in the eastern Salt Range, fresh water facies of siltstone and shale in the central Salt Range and diamictite sandstone and boulder bed facies in the western Salt Range and the Khisor Range (Shah, 1977a). The Tobra Formation was accumulated in different types of depositional settings including glacial, glaciofluvial to estuarine and marine conditions (Ghauri et al., 1977; Jan and Stephenson, 2011).

The Dandot Formation is composed of the alternating layers of sandstone, claystone, splintery shale and occasional thin pebbly beds. The unit is well developed in the eastern Salt Range and thins out towards the West and absent in the Khisor Range (Ghazi et al., 2012; Jan et al., 2009; Kadri, 1995; Shah, 1977a). The Dandot Formation exhibit flaser, lenticular and wavy bedding and ripple cross laminations (Ghazi et al., 2012; Jan et al., 2016). It is sandwiched between the older Tobra Formation of the glaciofluvial setting and the younger Warchha Sandstone of the fluvial environment leading to mark end of the glaciation period (Jan et al., 2016). Whereas, marginal to shallow marine environment is suggested for the Dandot Formation (Ghazi et al., 2012; Jan et al., 2016).

The Warchha Sandstone shows repeated fining upward depositional cycles of cross-bedded sandstone, bioturbated siltstone and shale. Additionally, it contains ripple forms, ripple stratification, channels, flute casts, load casts, desiccation cracks, rain imprints and cone in cone structures (Ghazi and Mountney, 2009). The formation is exposed in the Salt Range including the Kalabagh Fault Zone along the lateral ramp and the Khisor Range (Ghazi and Mountney, 2009; Jan et al., 2009; Shah, 1977a).

The Sardhai Formation is composed of bluish to greenish grey claystone with minor sand, shale and carbonaceous clays containing copper, Jarosite, chert and gypsum. It show facies variation from lavender color clays in the Salt Range to black shales and brownish argillaceous limestone in the Khisor Range (Shah, 1977a).The Sardhai Formation is exposed variably in the eastern and the western Salt Range and the Khisor Range (Jan et al., 2009).

Zaluch Group

The name Zaluch group comes from the Zaluch stream flowing through the Kalabagh Fault stepover zone. The Permian Zaluch Group (PZG) represents rocks from early-late Permian age. The brecciated limestones of the Zaluch group are thrusted out at places along the Kalabagh Fault (Figs. 2.4 and 4.2). The stratigraphic units that form the Zaluch group are absent in the eastern and most of the central Salt Range (Gee, 1980). It is dominantly composed of carbonate platform deposits with some sandstone at the basal part towards the East (Mertmann, 2003). The group consists of the following formations:

The Amb Formation is composed of sandy limestone, sandstone and shale (Mertmann, 2003; Sadiq et al., 2016; Shah, 1977a). Highly sheared limestone found at Khairabad and Larkakki belongs to the Permian Amb Formation (Fig. 2.4 and 4.2). It is absent in the Surghar Range. While exposures are also reported in the Khisor Range (Shah, 1977a).

The Wargal Limestone is fossiliferous limestone with dolomite and basal sandy limestone (Shah, 1977a). Apart from the Nammal Gorge and Zaluch, it is exposed at various locations along the Kalabagh Fault and the Main Frontal Thrust (Gee, 1980). Additionally, Wargal Limestone and the overlying Chhidru Formation are also exposed in the Surghar Range and the Marwat Range (Shah, 1977a).

The Chhidru Formation is mostly exposed along with the Wargal Limestone. It is mainly composed of limestone with basal shale, top Sandy limestone or calcareous sandstone beds and phosphatic nodules (Ahmad et al., 2015; Shah, 1977a).

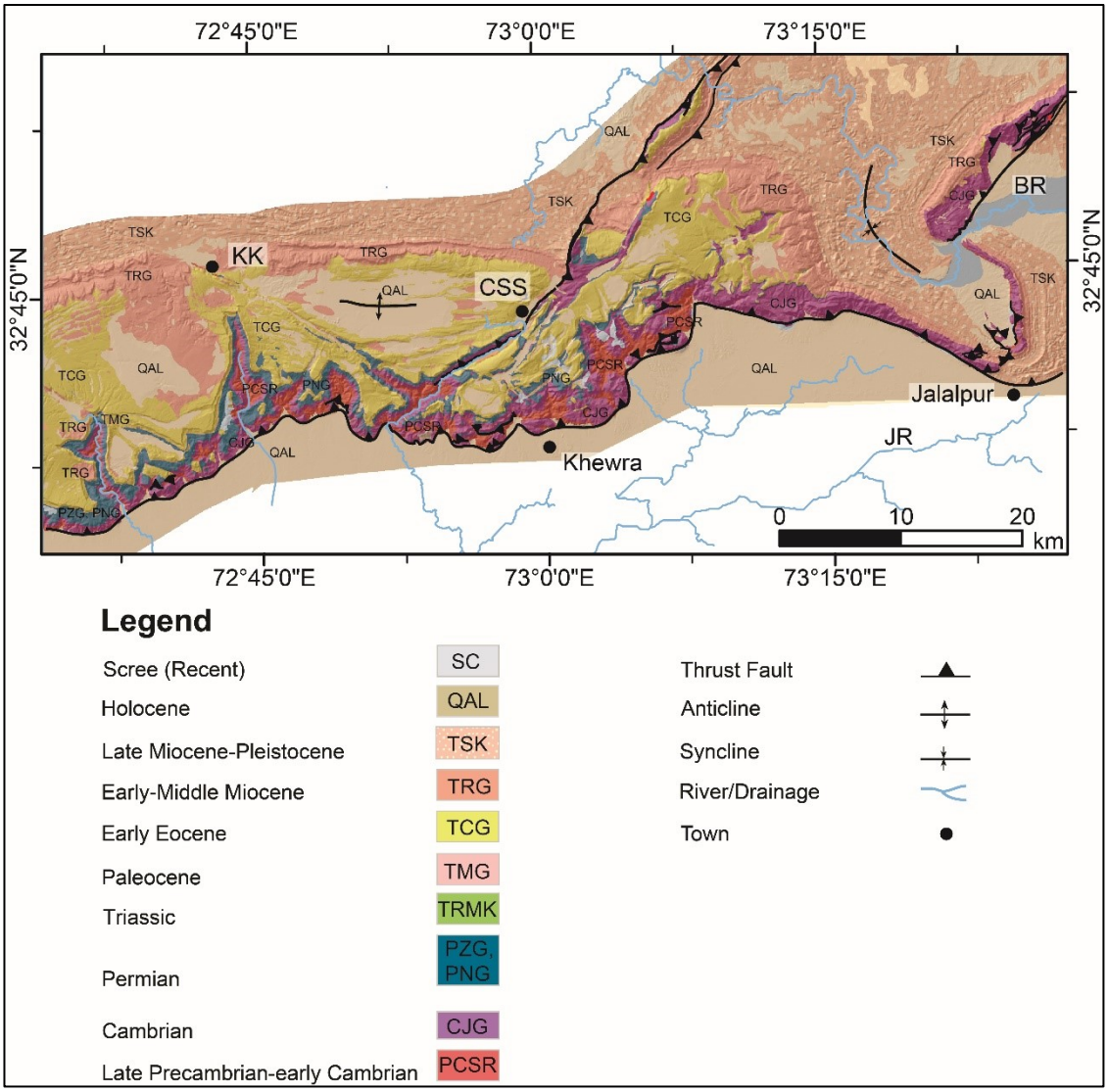

Fig. 2.5 Geological map of the eastern and the central Salt Range (modified after Gee, 1980). Stratigraphy: PCSR=Salt Range Formation (Precambrian), PNG=Nilawahan Group (Early Permian), PZG=Zaluch Group (Late Permian), TRMK=Musa Khel Group (Triassic), KSG=Surghar Group (Jurassic-Cretaceous), TMG=Makarwal Group (Tertiary), TEE=Eocene Evaporites (Tertiary), TCG=Chharat Group (Tertiary), TRG=Rawalpindi Group (Tertiary), TSK=Siwalik Group (Tertiary), QKC=Kalabagh Conglomerates (Quaternary), QAL=Alluvium (Quaternary), SC=Scree (Recent), Abbreviations: BR=Bunhar River, CA=Chisal Algad, IR=Indus River, JR=Jhelum River, KBF=Kalabagh Fault, KP=Kohat Plateau, SF-Surghar Fault, TN=Takht-e-Nasarati

2.3.3 Mesozoic

2.3.3.1 Triassic

Musa Khel Group

The Musa Khel group of the Triassic age is exposed in the western Salt Range, Trans Indus Ranges and additionally in the Kala Chitta Range (Fatmi, 1977). It is best exposed in the western Salt Range and eroded by the pre-Paleocene uplift in the East (Gee, 1980; Kazmi and Jan, 1997). The group consists of following units:

The Mianwali Formation marks the onset of the Triassic and comprises of dolomites, limestone, shale and siltstone (Fatmi, 1977; Iqbal et al., 2013). The unit is exposed in the western Salt Range and the lateral ramp along the Kalabagh Fault (Gee, 1980).

The Tredian Formation is composed of sandstone, shale and dolomite (Fatmi, 1977; Iqbal et al., 2013). Contrasting to other group members, this unit is not present in the Kala Chitta Range (Fatmi, 1977), whereas it is exposed in other parts of the Sub-Himalayas.

The Kingriali Formation shows massive dolomite and dolomitic limestone as dominant lithologies with shale and marl in the upper part (Fatmi, 1977).

Surghar Group (Early to Middle Jurassic)

The Surghar Group of early-middle Jurassic, also termed as Broach Group, is exposed in the Salt Range, Trans Indus Ranges including Samana Range, Kala Chitta Range and Hazara Ranges (Abbasi et al., 2011; Fatmi, 1977; Fatmi and Hölder, 1975; Gee, 1980; Nizami and Sheikh, 2009; Zaidi et al., 2013). The lower Surghar Group comprises of the following rock units.

The Data Formation is the oldest Mesozoic rock unit that contains the sediments of the continental origin (Fatmi, 1977; Zaidi et al., 2013). It exhibits mainly sandstone with associated siltstone, shale, mudstone, carbonaceous clays and coal stringers (Abbasi et al., 2011; Ahmad et al., 2020; Fatmi, 1977; Iqbal et al., 2015; Zaidi et al., 2013). The unit is exposed along the Kalabagh Fault, western Potwar Plateau and thins out towards the eastern Salt Range (Gee, 1980; Iqbal et al., 2015).

The Shinawari Formation consists of the mixed limestone, sandstone, shale, nodular marl, siltstone and mudstone units with the association of laterite and coal layers (Ahmad et al., 2020; Ahmed et al.,

1997; Ali et al., 2019; Fatmi, 1977; Fatmi and Hölder, 1975). Its exposure along the Kalabagh Fault is inversely reported (Ahmed et al., 1997; Gee, 1980).

The *Samana Suk Formation* is mainly oolitic limestone with some marl and shale at various levels. It also shows addition of dolomite and dolomitic limestone in the Kohat Plateau and Hazara area, whereas, the unit is absent in the eastern Salt Range (Fatmi, 1977; Nizami and Sheikh, 2009).

Surghar Group (Late Jurassic to Cretaceous)

The upper Surghar group is also present in the Salt Range, Trans Indus Ranges and Hazara area. The top of this group marks the boundary between the Cretaceous and Tertiary (K-T boundary), that differentiate it from mountain ranges from Hazara, Kala Chitta, Kohat and other areas where the Kawagarh Formation lies on the top of Cretaceous (Fatmi, 1977; Gee, 1980). This group includes following units:

The Chichali Formation is phosphorite bearing rock of late Jurassic-early Cretaceous age. Which is classified by the glauconite bearing sandstone and shale that contains phosphate nodules and belemnites (Fatmi, 1977; Hallam and Maynard, 1987).

The Lumshiwal Formation exhibits massive sandstone with silty, sandy, glauconitic shales at the base and carbonaceous material at the upper part. Lithologic characteristics designate mostly continental origin in Trans Indus Ranges and marine environment towards the North, northeast and northwest (Fatmi, 1977).

The Kawagarh Formation is mainly limestone with variation of facies between Hazara and Kohat areas. Associated compositions contain coarser lithologies on the top including dolomitic limestone and dolomitic sandstone with some silt, shale intercalations (Chaudhry et al., 1992; Fatmi, 1977). The depositional chronology of the Kawagarh Formation matches with initial collision between India and Eurasia making it important (Chaudhry et al., 1992). In the Sub-Himalayas, the unit is not reported in areas that constitute the Salt Range and the Trans Indus Ranges (Fatmi, 1977; Gee, 1980).

2.3.4 Cenozoic

Cheema et al. (1977) and Gee (1980) reported rocks from Paleocene-Pliocene in the Sub-Himalayas. Lithological descriptions of these rocks are briefly described here.

2.3.4.1 Paleocene

Makarwal Group

The Paleocene Makarwal Group (TMG) of the Kohat and the Potwar basins make disconformable contact with the older rocks marking the K-T boundary (Fatmi, 1977). The Paleocene succession of the Sub-Himalayas are constituted by the following stratigraphic units:

The Hangu Formation is sandstone bearing rock unit with laterite and bauxite layers at the base. It also contains few limestone nodules and coal at some localities (Fatmi, 1977; Wardlaw et al., 2007). The basal Layer marks the onset of Paleocene over Paleozoic or Mesozoic strata (Cheema et al., 1977; Wardlaw et al., 2007).

The Lockhart Limestone is predominantly nodular-bedded, fossiliferous limestone and limy siltstone with some shale and marl intercalations at places (Cheema et al., 1977; Wardlaw et al., 2007). The unit is deposited and exposed or drilled in most of the Sub-Himalayas and Hazara area in Pakistan (Awais et al., 2019; Khan et al., 2018; Sameeni et al., 2013; Wardlaw et al., 2007).

The Patala Formation is also widely spread in the Sub-Himalayas with dominantly shale of variegated colors and subordinate calcareous and argillaceous lithologies with some coal seems (Cheema et al., 1977; Wardlaw et al., 2007). The unit is exposed in the Salt Range at the base of the cliff forming Eocene limestones.

2.3.4.2 Eocene

The Eocene succession of the PP shows a major difference from the Kohat Plateau. The cliff forming limestone formations of the Potwar Plateau differentiate it from the evaporites that cause to form duplex structures in the Kohat Plateau (Cheema et al., 1977; Ghani et al., 2018; Kadri, 1995). Eocene stratigraphy of the Potwar Plateau and the Kohat Plateau is as under:

Chharat Group (Potwar)

The Chharat Group in the Salt Range and the Potwar Plateau make cliffs after gentle slopes of the shales of the Patala Formation. The Group consists of the following constituent units:

The Nammal Formation is exposed as cliffs in the Salt Range and the Surghar Range exhibiting fossiliferous limestone with shale and marl intercalations (Cheema et al., 1977; Shehzad et al., 2018). It is overlain by the *Sakesar Limestone* with variable fauna and wavy-nodular bedded, cherty limestone (Cheema et al., 1977; Wardlaw et al., 2007). Both of these units are not recognized as separable map

units and considered as equivalent to the limestone dominant unit termed as the *Margalla Hill Limestone* in the northern Potwar Plateau, parts of the Kohat Plateau and Hazara Area (Wardlaw et al., 2007).

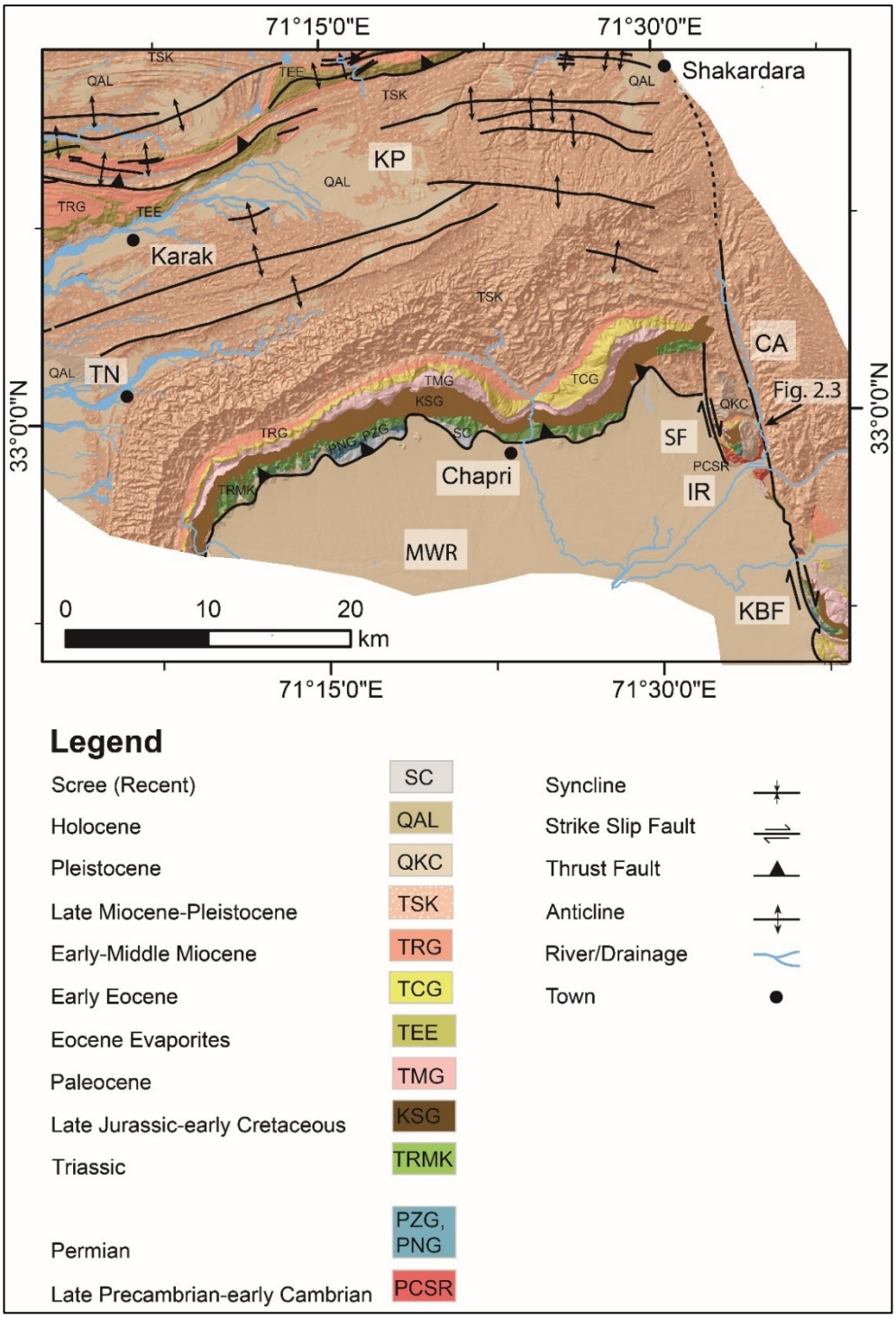

Fig. 2.6 Map shows stratigraphy of the southern KP and the northern part of the KBF (modified after Dawar et al., 2009; Gee, 1980; Meissner et al., 1974). Stratigraphy: PCSR=Salt Range Formation (Precambrian), PNG=Nilawahan Group (Early Permian), PZG=Zaluch Group (Late Permian), TRMK=Musa Khel Group (Triassic), KSG=Surghar Group (Jurassic-Cretaceous), TMG=Makarwal Group (Tertiary), TEE=Eocene Evaporites (Tertiary), TCG=Chharat Group (Tertiary), TRG=Rawalpindi Group (Tertiary), TSK=Siwalik Group (Tertiary), QKC=Kalabagh Conglomerates (Quaternary), QAL=Alluvium (Quaternary), SC=Scree (Recent), Abbreviations: CA=Chisal Algad, IR=Indus River, KBF=Kalabagh Fault, KP=Kohat Plateau, SF-Surghar Fault, TN=Takht-e-Nasarati

The Chorgali Formation is composed of limestone and dolomitic limestone with interbedded shale (Awais et al., 2020; Cheema et al., 1977; Kazmi and Abbasi, 2008a). The unit is distributed in the Salt Range, Kala Chitta Range, Khair-e-Murat Range, eastern Kohat Plateau and the Hazara area (Awais et al., 2020; Cheema et al., 1977).

Chharat Group (Kohat)

The Chharat group of the Kohat Plateau (Fig. 2.6) consists of stratigraphy correlative with the Potwar Plateau with addition of the evaporites (Awais et al., 2020; Cheema et al., 1977; Kadri, 1995; Shah, 2009). Following formations are included in the Chharat Group of the Kohat Plateau:

The Panoba shale is a shale dominant rock unit with occasional bands of sandstone (Cheema et al., 1977). This unit is a facies change from limestone (two third part of Sakesar Limestone) in the South to shale (Panoba Shale) in the North (Meissner et al., 1974).

The Shekhan Formation is a limestone dominant unit with gypsiferous shale beds (Cheema et al., 1977; Meissner et al., 1974). It is correlated with the upper parts of the Sakesar Limestone and Margalla Hill Limestone (Kadri, 1995; Meissner et al., 1974). The Shekhan Formation is restricted to Kohat Area (Cheema et al., 1977).

The Bahadur Khel Salt is equivalent to the Shekhan Formation indicating widespread but short lived regression (Ahmad et al., 2011; Cheema et al., 1977; Kadri, 1995). This salt zone is the reason of double decollement under the Kohat Plateau and overlain by *the Jatta Gypsum* (Cheema et al., 1977; Ghani, 2019; Kadri, 1995).

The Kuldana Formation is distributed in the Hazara, Kala Chitta Ranges, Kohat Plateau and parts of the Potwar Plateau with dominant shale and claystone, limestone, marl and occasional sandstone (Cheema et al., 1977; Warwick and Wardlaw, 2007).

The Kohat Formation is reported in the Kohat Plateau, northern Potwar Plateau and the Kala Chitta Range and consists of shale and limestone in the lower parts with subordinate shale in the middle part (Cheema et al., 1977; Yaseen and Munir, 2007).

2.3.4.3 Miocene

Rawalpindi Group (Early Miocene)

After a late Eocene-Oligocene unconformity in the Upper Indus Basin of Pakistan, the Rawalpindi Group (TRG) marks the early Miocene stratigraphy (Abbasi, 1991; Cheema et al., 1977; Kadri, 1995).

The Rawalpindi group is reported in most of the Sub-Himalayas in Pakistan including the Hazara-Kashmir syntaxis (Bossart and Ottiger, 1989; Cheema et al., 1977).

The group consists of the following units:

The Murree Formation is described as reddish, brownish or purple sandstone with intraformational conglomerates and shale (Bossart and Ottiger, 1989; Cheema et al., 1977). This previously considered as fluvially derived unit is interpreted to be deposited under very shallow, tidally influenced environment and marks the onset of the molasse sediments of the Tertiary Siwaliks Group (TSK) in the Sub-Himalayas (Bossart and Ottiger, 1989; Qureshi and Tanoli, 1992).

The Kamlial Formation exhibits dominance of cross-bedded sandstone with spheroidal weathering, siltstone and intraformational conglomerates with heavy minerals including tourmaline and epidote (Abbasi, 1991; Abbasi and Khan, 1990; Cheema et al., 1977; Ullah et al., 2006).

Siwaliks (Late Miocene-Pleistocene)

The molasse succession is reworked from the rising Himalayas and deposited in the frontal foreland basin of the entire Himalayas (Gansser, 1964; Zia et al., 2018). Following constituent formations are reported in the Potwar Plateau and the Kohat Plateau in Pakistan, named as Tertiary Siwaliks Group (TSK) hereinafter. While parts of the succession are also reported in some areas of the Lower Indus Basin (Cheema et al., 1977; Kadri, 1995). The Siwaliks Group (TSK) represent the Neogene-Quaternary late orogenic sedimentation in response to Himalayan uplift (Barndt et al., 1978).

The Chinji Formation consists of red clay with subordinate soft sandstone exhibiting cross-bedding, which is overlain by the Nagri Formation consisting of clay as secondary lithology and predominantly massive, cross-bedded, bluish grey to red sandstone showing salt and pepper pattern (Cheema et al., 1977; Kadri, 1995). Both of these units also contain conglomerate horizons (Abbasi et al., 2017; Cheema et al., 1977; Zia et al., 2018).

The Dhok Pathan Formation is composed of the cyclic sandstone, silt and clay. The sandstone is moderately cemented, soft, cross-bedded and thinner than the Nagri Formation, while clay is reddish but lighter than older Siwalik sediments (Cheema et al., 1977; Opdyke et al., 1982).

The Soan Formation is composed of sandstone, siltstone, clay and conglomerates with variable dominance of different lithologies (Bilal et al., 2017; Cheema et al., 1977). The conglomerates are derived from Paleocene-Miocene rocks (Bilal et al., 2017).

2.3.4.4 Quaternary

The Quaternary sediments of the sub Himalayas consists of Lei conglomerates and Alluvium (Cheema et al., 1977; Gee, 1980). Conglomerates are derived from Eocene limestones, igneous and metamorphic rocks (Cheema et al., 1977; McDougall, 1989a). The conglomerates from the uplifted Eocene limestones constitute the Pleistocene *Kalabagh Conglomerates (QKC).* Base of these deposits mark the onset of the tectonic uplift along the Kalabagh Fault (Gee, 1980; McDougall, 1989a).

The late Pleistocene-Holocene *Quaternary alluvium (QAL)* is deposited on the alluvial fans, alluvial plains and lakes along the mountain front and hinterland (Gee, 1980). These sediments show variable lithology and include silt, sand, clay and conglomerate intercalations.

These stratigraphic units and subsequent stratigraphic groups are used to describe the geological context and tectonic processes in the following chapters.

3. Morphological variations among the active zones in the Sub Himalayas of Pakistan: comparative analysis from morphometric indicators

Abstract

The western part of the sub-Himalayas in Pakistan is separated from the eastern part by the Hazara-Kashmir Terrain. The Himalayan Frontal Thrust in the West of the Hazara-Kashmir Terrain is segmented along the strike slip Kalabagh Fault, Jhelum Fault and the Bannu Fault. These segments along with the Hazara-Kashmir Terrain has formed the mountain ranges in Kashmir, Salt Range and Trans Indus Ranges. Differential seismic and aseismic displacement rates along the faults have caused tectonic uplifts that has formed the landscapes at variable scales. The faults and associated mountain ranges are also mutually dissimilar in terms of uplift rates, rock strength and geomorphology. This study is carried out to evaluate and compare relative variations among the morphometric indicators of the tectonically active areas in the western Sub-Himalayas in Pakistan. For this purpose, mountain front sinuosity *(S_{mf})*, hypsometric integral *(HI)*, stream length gradient index *(SL index)*, bifurcation ratio *(R_b)* of streams, basin elongation ratio *(E_b)* and basin asymmetry factor *(A_f)* are computed, and relative active tectonic index *(I_{at})* is calculated. Watersheds on different fault segments have variable active tectonic index. Morphometric indicators are influenced by lithological variations between the soft lithologies and high strength rocks. Watersheds close to the faults yield Class-1 active tectonic index, whereas other parts of the study area indicate Class-2 tectonic activity index.

Keywords: Morphometric indices; Active tectonics; Sub-Himalayas; Main Frontal Thrust; Salt Range; Hazara-Kashmir syntaxis, Pakistan

3.1 Introduction

Deformations in tectonically active zones form landscapes that are distributed based on the intensity of deformations such as tectonic uplifts and erosion rates. Interplay between tectonic landforms and fluvial processes design the surface morphology (W. B. Bull, 2007; Burbank and Anderson, 2001; Keller and Pinter, 2002). Therefore, landscape analysis of active tectonic zones and studies of drainage networks are helpful to underline the active tectonic processes (Gaidzik and Ramírez-Herrera, 2017). Parameters that are used to evaluate the neotectonics of active faults are termed as geomorphic indicators or geomorphic indices. Geomorphic indices have been established and verified in different areas to quantify the scales of active tectonic deformations (e.g. Strahler, 1952; Bull and Mcfadden, 1977; Keller and Pinter, 2002; Bull, 2007a, Ntokos et al., 2016). Geomorphic or morphometric indices

are computed from surface morphology of mountain fronts and mountain ranges along active faults. In the modern science, introduction of computer-based modelling using satellite data have improved the accuracy and reduced the timing for the geomorphic analysis (e.g. Mahmood and Gloaguen, 2012; Gao et al., 2016; Ntokos et al., 2016; Gaidzik and Ramírez-Herrera, 2017). Although modern geodetic measurement techniques are contributing towards the recent tectonic activities, at longer time scales (>10 ka), erosion becomes increasingly important due to enough time for interaction between tectonic deformation and erosional processes(Burbank and Anderson, 2001). Tectonic deformations can be resulted from seismic and aseismic (episodic and continuous) displacements. The intermediate time scale deformations (~10-400 ka) cover all type of displacements and tectonic geomorphology can be used to cumulatively quantify the landform response towards such displacements (Burbank and Anderson, 2001).

The Sub-Himalayas are the southernmost tectonic element of the Himalayan orogeny (Fig. 3.1). The hairpin shaped antiformal Hazara-Kashmir Syntaxis (HKS) and the Pir Panjal Ranges in the South constitute the Hazara-Kashmir Terrain (Tahirkheli, 2005). The westernmost Sub-Himalayas are laterally separated from the eastern part by the Hazara-Kashmir Terrain (HKT) in Pakistan(Kazmi and Jan, 1997). The broader structures in the West of the HKT are differentiated from the narrow, high angle cross sectional taper in the East (Baker et al., 1988). The Salt Range and the Trans Indus Mountain Ranges make the frontal ramp of the Himalayan orogeny in the West of the HKT. The area between the HKT and Trans Indus Ranges is called the Potwar Plateau (Fig. 3.1). The HKT, eastern Potwar Plateau and parts of the Trans Indus Ranges exhibit more frequent seismicity than the western Potwar Plateau (Fig. 3.1c). The InSAR analysis from the western Potwar Plateau yield aseismic displacement and uplift rates (Abir et al., 2015; Ahmad Abir, 2012; Chen and Khan, 2010). Whereas InSAR analysis is not yet carried out for most of the Sub-Himalayas in Pakistan. Few morphometric studies have been carried out to assess the extent of tectonic deformations in the western Himalayas (Ahmad et al., 2018; Mahmood et al., 2012; Qureshi and Khan, 2020). These studies are either from the north or southwest of the Sub-Himalayas or only discuss few morphometric parameters. The Sub-Himalayas exhibit seismically more active to aseismically active fault zones, such as the Kalabagh Fault Zone with aseismic deformations and earthquake recurrence interval that may reach up to ~ 10 ka (Abbas et al., 2022). Whereas most of the landscapes of the Kalabagh Fault zone have emerged during past ~0.5 Ma (Abbas et al., 2022; McDougall, 1989b). The neotectonics of the Sub-Himalayas of Pakistan (up to Hazara-Kashmir Terrain) therefore need to be evaluated for intermediate time scale landscapes (~10ka- 400ka) as suggested by Burbank and Anderson (2001).

In this study, we have computed morphometric indices using digital elevation models (DEMs) from shuttle radar topography mission (SRTM) to quantify and compare the active behavior of the western Sub-Himalayas including the HKT. As erosional processes largely depend on strength of the rocks that can lead to faster or slower erosion rates (Burbank and Anderson, 2001), therefore values of morphometric indices can be sometimes comparative rather than absolute. A single morphometric indicator is therefore not useful, and we need an integrated approach to analyze scale of tectonic activity. The morphotectonic parameters from the mountain fronts and mountain ranges, including mountain front sinuosity (S_{mf}), stream length gradient (SL) index, asymmetry factor (A_f), bifurcation ratio (R_b), basin elongation ratio (R_e) and hypsometric integral (HI), are used to estimate the active tectonics of rising mountains (W. B. Bull, 2007; Hack, 1973; Keller and Pinter, 2002; Strahler, 1952). To estimate the comparative variation of tectonic activity among adjacent areas with different lithological and structural controls, relative active tectonic index (I_{at}) was also computed using the active tectonic class of each morphometric indicator.

3.2 Study Area

3.2.1 Tectonic framework

The western Himalayas in Pakistan exhibit complex tectonic settings consisting of tectonic elements that are discussed in Chapter 2. The Sub-Himalayas are the southernmost tectonic element of the Himalayan orogeny. The Hazara-Kashmir Syntaxis (HKS) is a hairpin shaped tectonic zone (Fig. 3.1b) that distinguish the westernmost Sub-Himalayas of Pakistan from the eastern Sub-Himalayas (Kazmi and Jan, 1997). The HKS is formed by the left lateral strike slip movement along the Jhelum Fault, which displaces the mega thrust sheets bounded by the Main Boundary Thrust, the Panjal Thrust (Fig. 3.1c) and the Balakot Bagh Fault (Baig et al., 2010; Sana and Kumar Nath, 2016). The northern HKS is comprised of tight structures, whereas the southern HKS exhibit open structures (Baig et al., 2010). The HKS and associated mountain ranges in the South are referred as the Hazara-Kashmir Terrain (Tahirkheli, 2005). The thrust sheets in the Hazara-Kashmir Terrain (HKT) have tectonically uplifted the Pir Panjal ranges with high relief landscapes. Moreover, a stack of thrust faults is truncated by the sinistral Jhelum Fault (Fig. 3.1c) at the western flank of the HKS (Baig et al., 2010). The Panjal Thrust and the Main Boundary Thrust are parallel to subparallel faults that strike EW in the East and turns NS in the eastern flank of the HKS and make a loop to the southwest near the apex of the HKS (Baig et al., 2010; Sana and Kumar Nath, 2016; Tahirkheli, 2005). The main Boundary Thrust strikes SW-NE at the western limb of the HKS (Fig. 3.1b) and then turns EW marking the northern boundary of the Sub-Himalayas (Baig et al., 2010). The Panjal Thrust is formed at the base of Precambrian rocks, whereas, Mesozoic and older rocks are juxtaposed against the Oligocene-Miocene Murree Formation along the

Main Boundary Thrust (Kazmi and Abbasi, 2008b; Tahirkheli, 2005). Therefore, the Main Boundary Thrust is also named as the Murree Thrust in this area (Kazmi and Abbasi, 2008b; Sana and Kumar Nath, 2016).

The Sub-Himalayas are characterized in the South by the segmented Main frontal Thrust (MFT). The Salt Range and the Surghar Range has started to crop-out ~ 2 Ma ago along the MFT (Baker et al., 1988; Jaumé and Lillie, 1988; McDougall and Khan, 1990). These mountain ranges mark the southern boundaries of the Potwar Plateau and the Kohat Plateau (Fig. 3.1). The Kohat Plateau is marked in the East by the sinistral Jhelum Fault and in the West by the dextral Kalabagh Fault. The Pir Panjal Ranges in the southern part of the HKT are located to the East of the Potwar Plateau. Furthermore, the arcuate Surghar Range to the West of the Kalabagh Fault forms a ramp in the South of the Kohat Plateau and in the East of the Bannu Basin. The Bannu Basin is further marked in the southeast by an overturned anticlinal structure known as the Marwat Range.

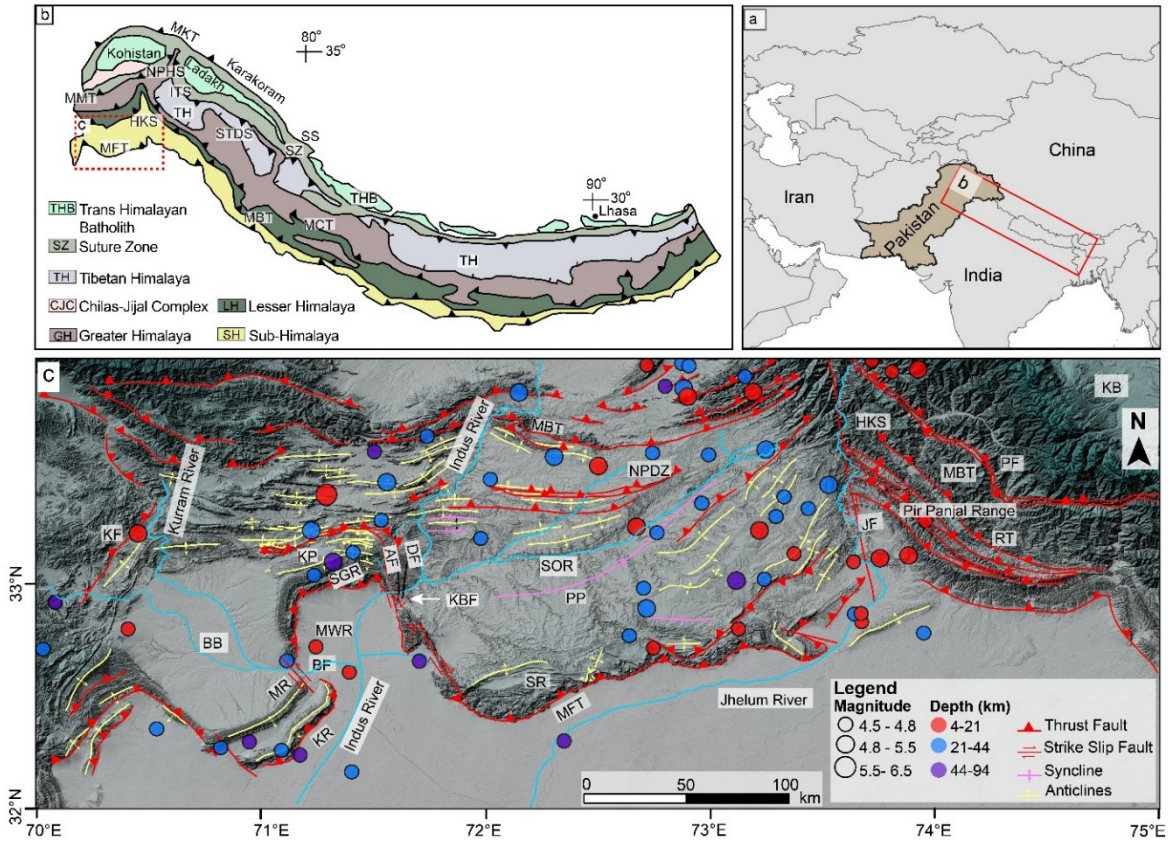

Fig. 3.1 (a) Geographical location of the Himalayas, (b) Map shows tectonic elements of the Himalayas (modified after Ali et al., 2018; Honegger et al., 1982; Searle and Treloar, 2019), (c) Integrated tectonic map of the Sub-Himalayas showing main structural features and tectonic subdivisions on hillshade image, (modified after Abir et al., 2017; Alam, 2008; Ali, 2010; Kazmi and Rana, 1982) based on digital elevation models (DEMs) from the ALOS 30m and Global Imagery of ArcGIS. Circles show instrumental seismicity (USGS Earthquake catalogue, 2019). AF=Ainwan Fault, BB=Bannu Basin, BF=Bannu Fault, DF=Dinghot Fault, HKS=Hazara-Kashmir Syntaxis, ITS=Indus-Tsangpo Suture, JF=Jhelum Fault, KBF=Kalabagh Fault, KF=Kurram Fault, KP=Kohat Plateau, KR=Khisor Range, LR=Lateral Ramp, MBT=Main Boundary Thrust, MFT=Main Frontal Thrust, MKT=Main Karakoram Thrust, MMT=Main Mantle Thrust, MR=Marwat Range, MWR=Mianwali Reentrant, NPDZ=North Potwar Deformed Zone, NPHS=Nanga Parbat Haramosh Syntaxis, PF=Panjal Fault, PP=Potwar Plateau, RT=Reasi Thrust, SGR=Surghar Range, SOR=Soan River, SR=Salt Range, SS=Shyok Suture, STDS=South Tibetan Detachment System, TR=Tank Reentrant.

3.2.2 Stratigraphy

The Sub-Himalayas contain Precambrian to Tertiary sedimentary sequence. The thickest part of sedimentary cover comprises of the Tertiary molasse sediments, that are derived from the rising Himalayas. These sediments are grouped into the Miocene Rawalpindi Group (TRG) and the late Miocene-Pleistocene Siwaliks Group (Gee, 1980). These two groups spatially cover most part of the study area and are subjected to erosion due to their soft and fragile nature (Gansser, 1964). The erosive nature of the Tertiary sediments had resulted in bad land topography and had created watersheds with degraded morphotectonic characters.

The Salt Range, Surghar Range and the Khisor Range exhibit stratigraphic units that range from Precambrian to Holocene. The Eocene limestones mark the ridge lines, whereas easily erodible molasse sediments of the Siwaliks Group (TSK) cover most of the hinterland of these mountain ranges. The axial zone of the HKS is mostly covered by the Murree Formation of the Tertiary Rawalpindi Group (Kazmi and Jan, 1997). The Murree Formation is characterized as reddish, brownish or purple sandstone with intraformational conglomerates and shale (Bossart and Ottiger, 1989; Cheema et al., 1977). The Precambrian-Neogene sedimentary, volcanic, metamorphic and granitic rocks are exposed in the West of the HKS zone (Calkins et al., 1975; Kazmi and Abbasi, 2008b). Apart from the Kohat Plateau and the Potwar Plateau, the TSK is also exposed at the SW part of the HKT (Bakr and Jackson, 1964). The mountain fronts in the study area exhibit limestones and sandstones. Overall, the HKT and mountain fronts comprise of rocks with more strength as compared with the fragile sediments of the Kohat and Potwar Plateaus.

3.2.3 Neotectonics

Seismicity is unequally distributed in the study area; however, the eastern part of the study area (Fig. 3.1) is relatively more active due to active faults in the HKT (Fig. 3.1b). The faults in the HKT yield shallow focus earthquakes reaching up to Mw ≥ 6. The 2005 Kashmir earthquake (Mw = 7.6) and 2019 Mirpur earthquake (Mw = 5.8) are recent examples of active tectonics in the HKT (Baig et al., 2010; Muhammad et al., 2020; Sana and Kumar Nath, 2016). Apart from these major seismic events, shallow to medium focus earthquakes (up to ~45 km depth) are also common in the HKT and eastern part of the Potwar Plateau (Fig. 3.1c). The western Potwar Plateau seems to be seismically less active (Fig. 3.1c),however, it is uplifting at a rate of 10 mm/a (Abir et al., 2015; Cortés-Aranda et al., 2017). Whereas Jouanne et al., (2014) measured 5 mm/a displacement rate in the central segment of the Salt Range. The InSAR analysis reveals ~3.7-7.7 mm/a displacement rates in different segments of the Kalabagh Fault, measured as an average between 1992 and 1999 (Chen and Khan, 2010). The Himalayan Frontal Zone in the southwest is uplifting on average at a rate of 5-9 mm/a (Qureshi and

Khan, 2020)Apart from the aseismic displacements in the western Potwar Plateau and the Kalabagh Fault, various earthquakes are observed in the Kohat Plateau (Fig. 3.1) including a rare Mw=6 earthquake (Satyabala et al., 2012). In the West of the Bannu Basin, Kurram Fault also yields an earthquake with Mw > 5 (Fig. 3.1c).

3.2.4 Morphology

The rising topography and subsequent erosion have sculptured various landforms in the HKT, the Salt Range and the Trans Indus Ranges (Surghar Range, Khisor Range, Marwat Range). Morphology of the HKT is more emergent as compared with other parts of the study area. The HKT yields higher reliefs controlled by the stacked and imbricated thrust faults. The mountain fronts, drainage divides and river profiles in the study area exhibit variable morphological extents. The complex structures in the HKT and various compressional structures in the Potwar Plateau, Kohat Plateau and the mountain ranges surrounding the Bannu Basin are transected by the streams and rivers (Fig. 3.2). The longitudinal profiles along these drainages exhibit knick points along the prominent faults. The Indus River in the Potwar Plateau crosses the fold and thrust belts and the Kalabagh Fault. The Jhelum River that is flowing through the HKT (Fig. 3.1c), is deflected while crossing the stack of faults. The Soan River in the Potwar Platea runs parallel to the strike of the fold and thrust belts and gets less importance for river profile measurements. Furthermore, the Kurram River also crosses the mountain ranges and enters the Bannu Basin from the North (Fig. 3.1).

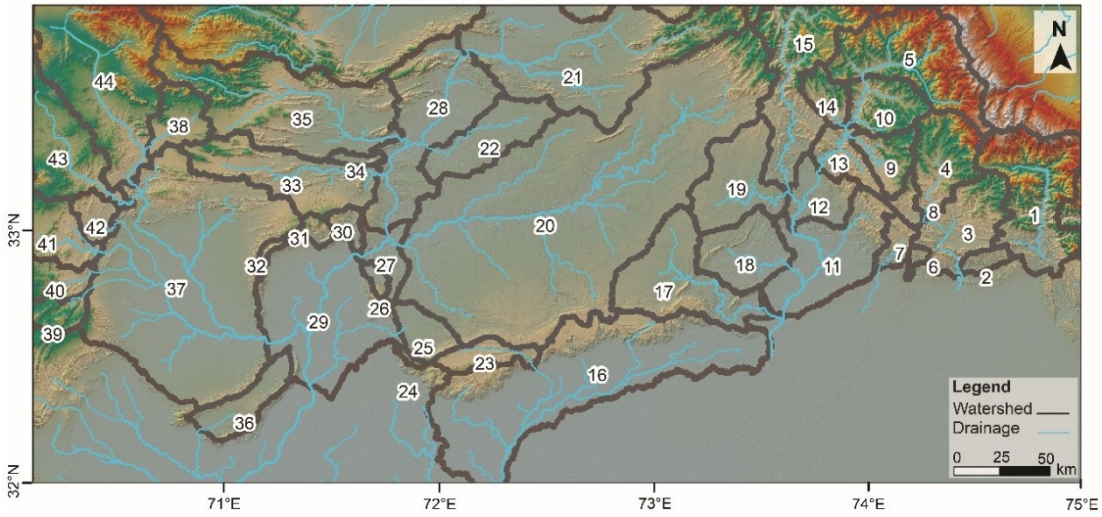

Fig. 3.2 Watersheds extracted from the drainage networks using SRTM 30 m DEMs of the HKT, and the Sub-Himalayas in Pakistan.

3.3 Methodology

The morphometric analysis was executed using the digital elevation models (DEMs) from the Shuttle Radar Topographic Mission (SRTM). Eight tiles of SRTM 30 m resolution between 32°-34° N and 70°-74°E were processed using the ArcGIS v. 10.5.1. Overall, 44 watersheds were delineated from these

DEMs (Fig. 2). The data yields watersheds at variable scales. The watersheds situated in the areas with high seismic activity, displacement and uplift rates and prominent morphological features, such as less sinuous mountain fronts, triangular facets and river profiles, were shortlisted for further investigations. ArcGIS v.10.5.1 was utilized with relevant built-in tools on the DEMs, to measure different parameters for morphometric analysis. Details of the morphometric parameters are discussed in the following paragraphs.

3.3.1 Mountain front sinuosity (S_{mf})

The S_{mf} defines the balance between the erosional factors that tend to deform the straight mountain fronts, formed by the uplift along active faults making a fault scarp, into a sinuous one (W. B. Bull, 2007; Keller and Pinter, 2002). The ratio of length of the sinuous mountain front *(L_{mf})* and straight distance between the end points *(L_s)* yields the S_{mf} *(Fig. 3.3)* and this relation is expressed as follows:

$$S_{mf} = \frac{L_{mf}}{L_s}$$

Bull (2007) and Keller and Pinter (2002) defined the faults exhibiting S_{mf} ~1.0-1.5 as active, 1.5-3 as moderately active and 3.0 or more as inactive.

3.3.2 Hypsometric analysis

The hypsometric curve defines the distribution of elevation across an area of land (Keller and Pinter, 2002; Strahler, 1952). The hypsometric analysis was carried out for various contours of watersheds and hypsometric curves were generated using the area and elevation, as suggested by Strahler (1952). Fig. 3.4 illustrates the procedure to calculate the proportion of area and elevation above the selected contour, with respect to total area and elevation of the watershed, using following equations after Strahler (1952);

$$Proportion\ of\ area = x = \frac{a}{A} \qquad (1)$$

$$Proportion\ of\ elevation = y = \frac{h}{H} \qquad (2)$$

where “a” is area of individual contour, “A” is total area of the watershed, “h” is height of the watershed above the selected contour, “H” is the elevation difference between the highest and the lowest contours of the watershed. The x and y values were used to make the hypsometric curves (Fig. 3.4). Strahler (1952) also defined the area under the hypsometric curve in the graph as Hypsometric integral (HI), describing the portion of the total volume of the watershed that is not eroded. Keller and Pinter (2002) suggested a simplified equation for calculation of HI as follows:

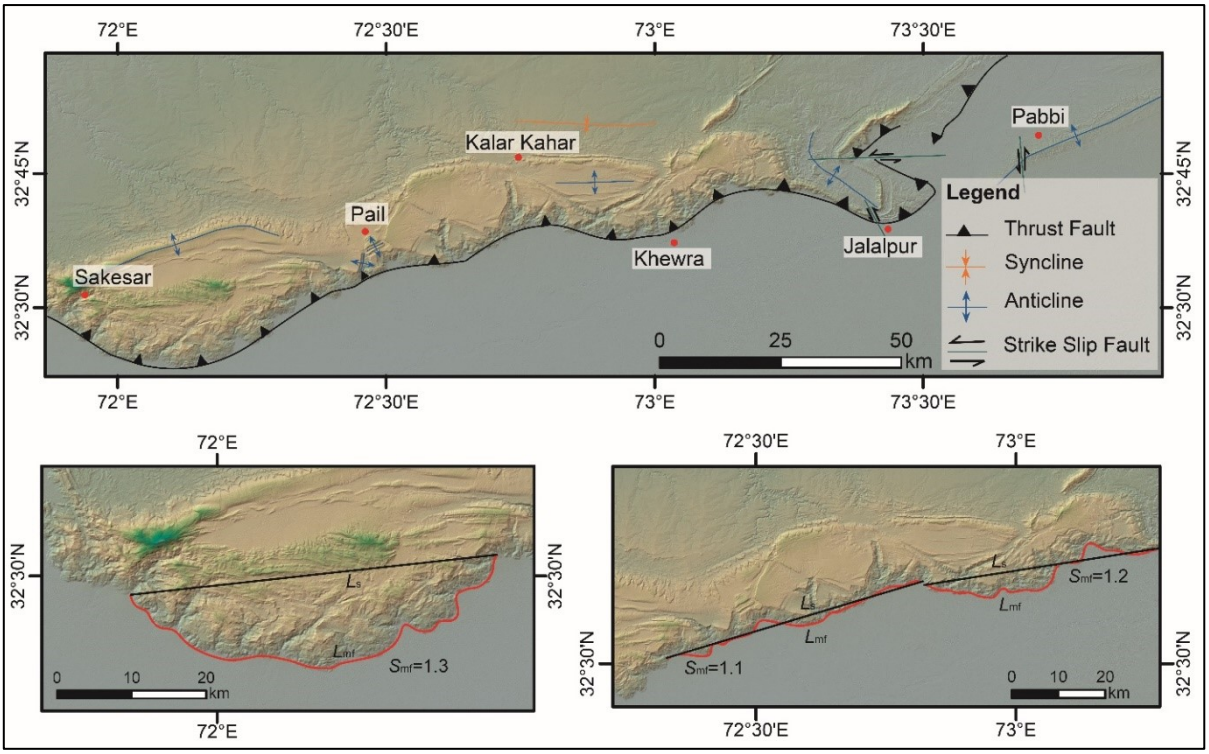

Fig. 3.3 Mountain front marked on the hillshade from SRTM 30 m along the Main Frontal Thrust in the Salt Range. Length of the mountain front (L_{mf}) and straight length (L_s) between the two points was used for calculation of the mountain front sinuosity (S_{mf}).

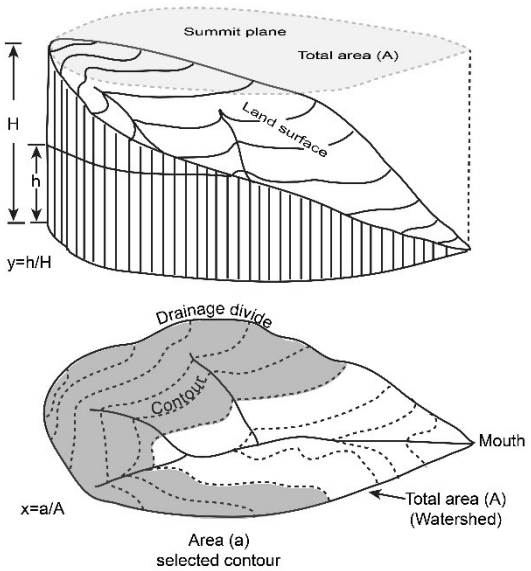

Fig. 3.4 Illustrates the area and height calculations for hypsometric curves after Strahler (1952).

$$HI = \frac{Mean\ elevation - Minimum\ elevation}{Maximum\ elevation - Minimum\ elevation} \qquad (3)$$

In this study, the hypsometric analysis was carried out in ArcGIS v. 10.5.1 and graphs were made in Microsoft Excel using the data exported from ArcGIS. HI was computed using equation 3 and results were compared with Strahler's equation for 11 watersheds. The HI values designate the stages of

landscape evolution as youth, through maturity, to old age, with the HI values of 0.6, between 0.35 and 0.6, and less than 0.35, respectively (Luo et al., 2018; Strahler, 1952).

3.3.3 Stream length gradient index (SL index)

A longitudinal river profile exhibit gradient variations in individual segments. These variations are caused by the changes in geological settings like faulting (Troiani et al., 2014 and references therein). The stream length gradient index (SL index) is an indicator of tectonic uplift and erosion, used to evaluate relative intensity of active tectonics (Gao et al., 2016; Hack, 1973; Keller and Pinter, 2002). The SL index along six rivers/streams including the Indus River and the Jhelum river were calculated after Hack (1973) as follows:

$$SL = (\frac{dH}{dL})L \qquad (4)$$

Where "*dH*" is change in elevation, "*dL*" is change in length of a segment and "*L*" is the total length of the stream in the watershed. The SL index was calculated in gradient meters. SL index <200 indicates weak tectonics activity, whereas 200<SL index>400 shows moderate and SL>400 marks high tectonic activity (Wang and He, 2020 and references therein).

3.3.4 Elongation ratio (R_e)

The shape of the watershed or drainage basin is measured as the Elongation Ratio *(R_e),* that is the ratio of the diameter of a circle with same area as that of the basin, and maximum length of the basin (Biswas et al., 2014; Sharma et al., 2018; Wilson et al., 2012). The ratio is expressed as follows:

$$R_e = \frac{2\sqrt{\frac{A_b}{\pi}}}{l_b} \qquad (5)$$

where "R_e" is elongation ratio, "A_b" is area of basin or watershed, "l_b" is maximum length of the basin. The basin shape may be circular (R_e > 0.9), oval (R_e = 0.9-0.8), and elongated (R_e < 0.7) for a basin or watershed (Wilson et al., 2012). R_e values vary from 0.6-1.0 in different geologic and climate settings, with a high relief and steep ground slope values yield R_e ~0.6-0.8 (Strahler, 1964).

3.3.5 Bifurcation ratio (R_b)

Bifurcation ratio (R_b) is calculated as the ratio of the number of streams of a given order to the number of streams in the next higher order (Schumm, 1956). Active tectonics features like fault scarp initiate formation of new stream branches of lower order, making the ratio higher. Therefore, R_b indicates influence of tectonic deformations causing development of stream networks. Basins with R_b ~3-5

reveals that the geologic structures has not distorted the basin (Dar et al., 2014), while higher values indicate structural deformations. A basin may exhibit variable R_b for different stream orders within a drainage basin or watershed.

3.3.6 Basin Asymmetry factor (A_f)

Tectonic tilting that is transverse to the trunk stream is caused by the active tectonics of the basin or watershed making the basin geometry asymmetric (Keller and Pinter, 2002). Due to this tectonic tilt, area on either side of the stream is not equal. The percentage of the area on the right side of the stream, while looking downstream, with respect to the total area of the basin gives the asymmetry factor (A_f). This can be expressed as follows:

$$A_f = \left(\frac{A_r}{A_t}\right) \times 100 \qquad (6)$$

where *"A_f" is* asymmetry factor, *"A_r"* is area on the right side of the stream, *"A_t"* is total area of the basin or watershed. For a tectonically inactive basin the stream will flow in the mid of the basin or watershed, making the A_f = 50. Deviation of A_f from central value of 50 indicates tectonic tilt. The A_f > 50 reveals uplift on the right side of the stream, and A_f < 50 is resulted from the uplift on the left side (looking in the downstream direction), diverting the stream away from the center of the basin.

Table 3.1 Sinuosity of the mountain fronts in the study area.

S_{mf} No.	Geological section	Length of mountain front (L_{mf}) (km)	Straight length (L_s) (km)	Mountain front sinuosity (S_{mf})
S_{mf1}	Pir Panjal	95.6	84.2	1.1
S_{mf2}	Jhelum	15.9	14.7	1.1
S_{mf3}	West Jhelum	36.6	30.7	1.2
S_{mf4}	Jalalpur	12.7	12.3	1.0
S_{mf5}	West of Jalalpur	49.3	41.9	1.2
S_{mf6}	Central Salt Range	54.6	48.5	1.1
S_{mf7}	Western Salt Range	53.1	41.8	1.3
S_{mf8}	Kalabagh Fault (South)	21.7	18.6	1.2
S_{mf9}	Kalabagh Fault (North)	23.4	20.5	1.1
S_{mf10}	Surghar Range (South Verging)	46.6	33.7	1.4
S_{mf11}	Surghar Range (East verging)	35.8	32.9	1.1
S_{mf12}	Khisor Range	62.3	51.2	1.2
S_{mf13}	Marwat Range	54.7	48.8	1.1
S_{mf14}	Bannu Basin (North)	43.4	41.7	1.0
S_{mf15}	Bannu Basin (West)	23.1	21.7	1.1

3.3.7 Relative Active tectonic index (I_{at})

Morphotectonic parameters may yield different levels of tectonic activity, such as a transpressional fault along a river may not exhibit high tectonic activity using A_f and R_b indexes. Moreover, a river may rapidly erode the steeper slopes at knick points while the drainage basin is tectonically active. To avoid this, various active tectonic parameters are computed, and an active tectonic class is assigned. For each morphometric index strong, moderate and week tectonic activities are termed as Class 1, Class

2 and Class 3 respectively. A relative active tectonic index (I_{at}) was then calculated by averaging these active tectonic classes (El Hamdouni et al., 2008; Ntokos et al., 2016; Sharma et al., 2018). However, while averaging the tectonic classes, we average either strong and moderate activity or moderate and weak activity. Therefore, in this study we have classified $I_{at} < 1.5$ as tectonically active, $1.5 < I_{at} > 3$ as moderately active and $I_{at} > 3$ as tectonically least active.

3.3.8 Morphotectonic features

Surface morphology, deflection patterns and structural offsets were marked using satellite images of Google Earth Pro and hillshade images created from SRTM 30 m DEMs (Fig. 3.1). Stream deflections follow the kinematics of the strike slip faults. Deflections in the Jhelum River were used to mark the Jhelum Fault. Offsets in mountain fronts and escarpment faces were used to marks faults and folds in Fig. 3.1. Moreover, morphotectonic features like triangular facets and straight mountain fronts helped to mark the active segments of the faults.

3.4 Results

This section presents the data of morphometric indices from the HKT and parts of the Sub-Himalayas in Pakistan. These parameters are computed from the 44 watersheds that were delineated based on the drainage networks, landforms of mountain ranges, and river profiles. Later part of this section presents the data for relative active tectonic index (I_{at}).

3.4.1 Mountain front sinuosity (S_{mf})

The mountain fronts in the HKT, Salt Range, Surghar Range, Khisor Range (KR), Marwat Range (MR) and the Bannu Basin (BB) are measured to calculate sinuosity index as shown in Table 1. The mountain fronts in these mountain ranges are segmented by faults and arcuate mountain fronts (MFT in Fig. 3.1). These segments exhibit straight mountain fronts with S_{mf} *ranging* between 1-1.4 (Table 3.1). Results indicate that the western Potwar Plateau, and the South verging segment of the Surghar Range are less active as compared with other mountain fronts in the study area. However, this arcuate morphology is not erosional, rather these mountain fronts are tectonically bent.

3.4.2 Hypsometric analysis

DEMs of the 44 watersheds were extracted to calculate area and elevation values for hypsometric analysis. Hypsometric curves were constructed to estimate the elevation distribution within the drainage basins. Table 3.2 shows the hypsometric integrals (HI) that represent the proportion of each basin that is not eroded. A larger HI reveals a relatively younger stage of landform evolution. The HI were calculated after Strahler (1952) and Keller and Pinter (2002) to make a comparison, that has revealed nearly same values (Table 3.2). The HI yields values between ~0.14 and 0.52 in different parts of the study area (Table 3.2 and Fig. 3.5). The watersheds with relatively large HI belong to the mountain ranges that are adjacent to the faults (Fig. 3.1, 3.2 and 3.7) in the HKT, western Salt Range-Potwar Plateau, Surghar Range, and the western flank of the Bannu Basin. e.g. WS-23 with HI=0.49 is located in the western Salt Range-Potwar Plateau block that is uplifting at a rate of 10 mm/a along the Main Frontal Thrust (Abir et al., 2015). The largest HI is measured to the West of the Bannu Basin in WS-39 (HI=0.52). Moreover, watersheds along the mountain fronts exhibit a smaller HI value such as WS-11 has HI=0.14. WS-20 that contains rapidly eroding Siwalik sediments, also exhibit smaller HI (0.14).

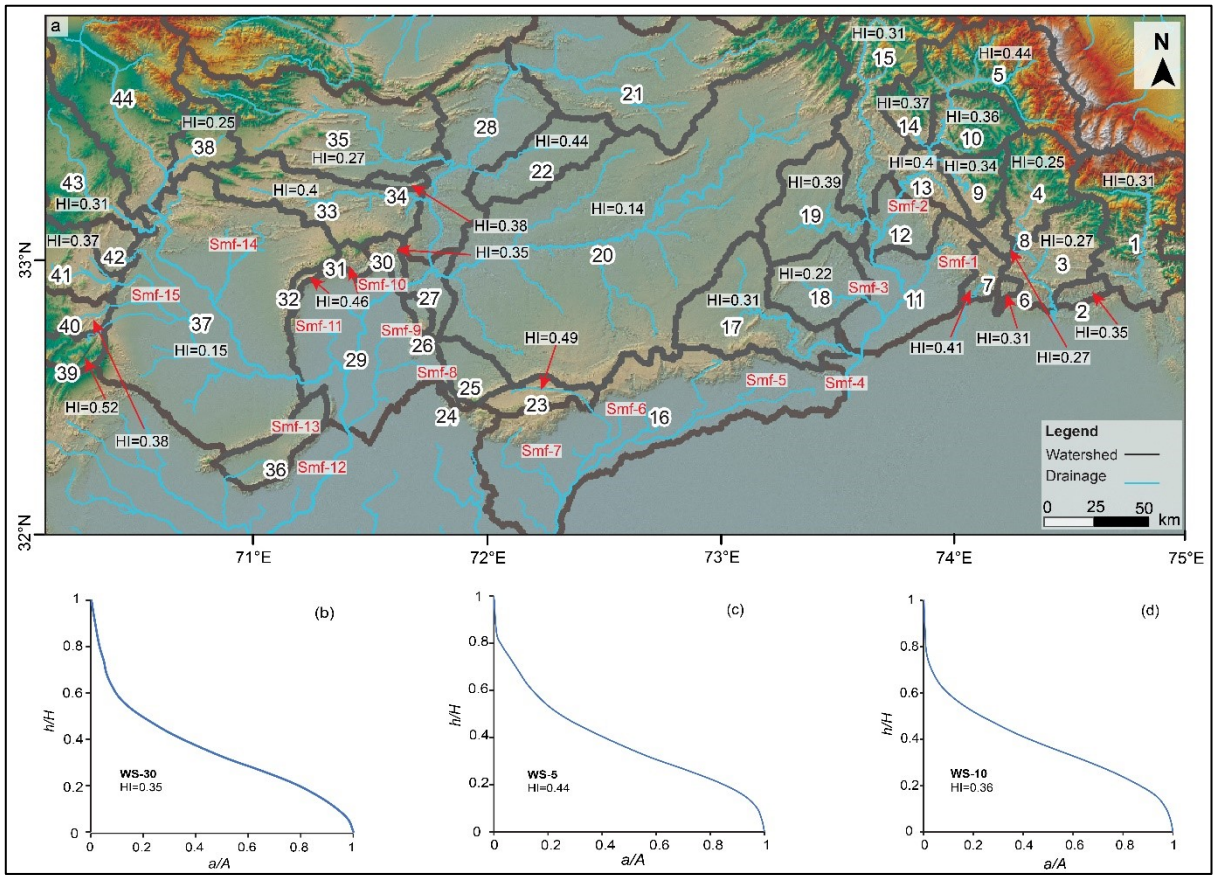

Fig. 3.5 (a) Map showing HI of individual drainage basin. Locations of mountain from segments, where S_{mf} was calculated and presented in Table 1, are also marked. (b,c,d) hypsometric curves and HI form WS-30, WS-5 and WS-10

3.4.3 SL index

The rivers and streams in the HKT, Salt Range, Potwar Plateau and the western Bannu Basin cross various faults (Fig. 3.7). The longitudinal profiles of water drainages that have incised the Jhelum Fault, Main Frontal Thrust, Kurram Fault and compressional structures in the northern Potwar Plateau were used to measure the stream length gradient index (SL index). Results of the stream length gradient analysis are presented in Fig. 3.7. The Indus River in the northern Potwar Plateau transect the less compacted Tertiary Siwalik sediments and older bed rocks exposed along the fold and thrust belts. The SL index does not exhibit much tectonic activity along the Indus River's longitudinal profile, as the values are below 60 gradient-meter. A stream in the western Potwar Plateau (WS-23), that crosses the Main Frontal Thrust, exhibits an SL index more than 1000 gradient-meter. Streams that cross the Jhelum Fault and thrust stacks in the southern HKT exhibit moderate to strong tectonic activity, yielding the SL index values greater than 400 gradient-meter. This part of the study area exhibit Miocene and older rocks that are more compact than the Siwaliks. The Jhelum River that shows deflected patterns along the Jhelum Fault. Whereas the stream that crosses the Jhelum Fault near Mangla dam reservoir (Fig. 3.7), exhibit greater SL index that indicate moderate to high tectonic activity. Furthermore, the Kurram Fault also exhibit moderate tectonic activity making a steeper river profile in the West of the Bannu Basin.

3.4.4 Elongation ratio (Re)

Basin elongation ratio was calculated for 14 drainage basins in the study area (Table 3.3 and Fig. 3.8). The R_e values shown in Table 3.3 reveal most of the watersheds are elongated with R_e values ~ 0.56-0.77 that indicate high relief and steep slopes (Strahler, 1964). Moreover, the watershed with soft lithologies exhibit values less than 0.6. e.g., WS-20 and WS-28. Whereas watersheds that are aligned along the river/stream with high erosion rates or piggyback basins also yield R_e<0.6 as evident from WS-15 and WS-23. The watershed along the Kalabagh Fault and the Kurram Fault also show high relief.

3.4.5 Bifurcation ratio (Rb)

The ratio between two consecutive stream orders indicates tectonic activity with a larger bifurcation ratio (R_b). Results presented in Table 3.3 are plotted in Fig. 3.6 and 3.8. Weighted average of bifurcation ratio suggested by Schumm (1956) accounts for all stream orders. In this study we have calculated R_b of consecutive streams to specify a stream order resulted from the structural deformations.

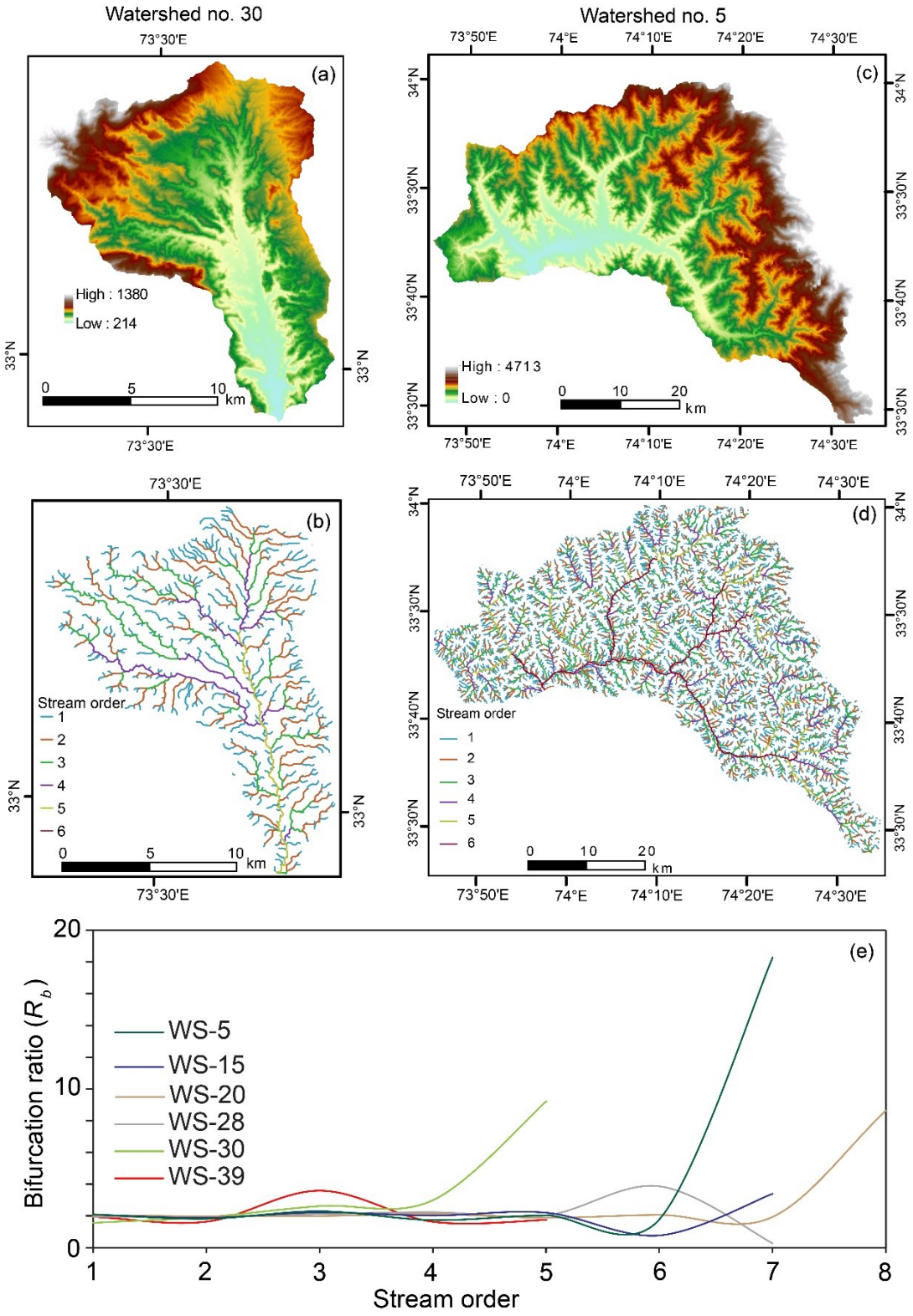

Fig. 3.6 (a,c) Shows DEMs from WS-30 and WS-5, (b, d) streams and stream orders extracted from 3.6a and 3.6c, (e) graph shows variations of bifurcation ratios between consecutive stream orders in 6 watersheds.

Results indicate lager R_b for higher stream orders along the Soan River of the Potwar Plateau in WS-20. This R_b is revealed by softer lithologies of the Siwaliks along the Soan River that erode rapidly and form bad land topography. Whereas the WS-5 and WS-30 that are located to the East of the Jhelum

Fault and along the Kalabagh Fault, respectively, yield high R_b values along the highest stream orders (Table 3.3). Smaller R_b values have a comparative relation within a watershed and are plotted in Fig. 3.6e, indicating the larger R_b values dominate in higher stream orders.

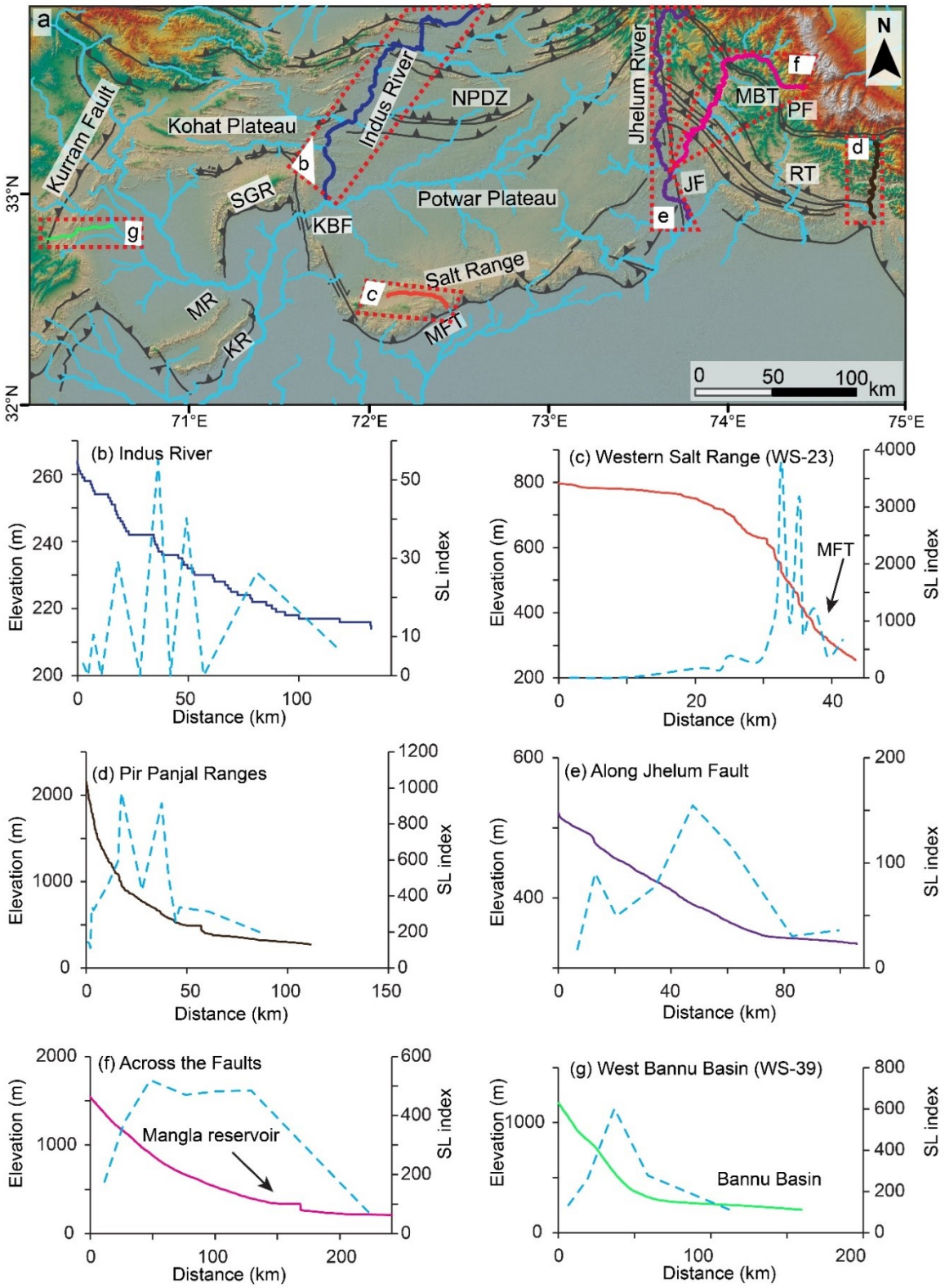

Fig. 3.7 (a)Map shows location of streams where SL index is calculated, (b-g) SL index of the streams and rivers in the Hazara-Kashmir Terrain, Salt Range, Potwar Plateau and Bannu Basin.

Table 3.2 Hypsometric integral of the watersheds in the Hazara-Kashmir Terrain and Sub-Himalayas in Pakistan.

Watershed ID	Minimum elevation (m)	Maximum elevation (m)	Mean elevation (m)	HI Keller and Pinter (2002)	HI Strahler (1952)	Watershed ID	Minimum elevation (m)	Maximum elevation (m)	Mean elevation (m)	HI Keller and Pinter (2002)	HI Strahler (1952)
1	316	4637	1668	0.31	0.32	23	254	1388	813	0.49	
2	280	1183	596	0.35		24	278	1456	626	0.30	
3	265	2349	836	0.27	0.28	25	311	1520	499	0.16	
4	545	3876	1377	0.25	0.26	26	224	1036	450	0.28	
5	235	4713	2186	0.44	0.38	27	195	2257	364	0.08	
6	328	1114	573	0.31	0.32	28	209	1530	438	0.17	0.18
7	304	1113	636	0.41		29	178	1303	273	0.08	
8	535	1698	855	0.27		30	214	1380	605	0.35	0.35
9	540	2100	1068	0.34		31	314	1443	831	0.46	
10	530	2272	1159	0.36	0.38	32	350	1374	826	0.46	
11	203	1303	358	0.14		33	243	1495	739	0.40	
12	241	1315	440	0.18	0.18	34	240	817	457	0.38	
13	337	1313	724	0.40		35	266	2722	920	0.27	
14	532	2163	1140	0.37		36	219	1365	488	0.23	
15	170	3403	1186	0.31	0.31	37	214	1929	478	0.15	
16	153	1147	318	0.17	0.17	38	725	2459	1152	0.25	
17	213	1102	493	0.31		39	656	2068	1391	0.52	
18	220	964	381	0.22		40	540	1918	1066	0.38	
19	264	872	502	0.39		41	520	1674	944	0.37	
20	214	2274	501	0.14	0.14	42	473	1523	724	0.24	
21	245	2646	567	0.13		43	554	2514	1171	0.31	
22	236	640	398	0.40		44	566	4522	1622	0.27	

3.4.6 Basin asymmetry (A_f)

Basin asymmetry factor (A_f) was calculated for the watersheds situated in the areas that are topographically more emergent, and results are presented in Table 3.3. As the basin without any tectonic tilt would have a A_f=50, values presented in the table indicate the level of tectonic tilt and level of variation among different watersheds in the study area. Deviation from the reference value of 50 indicates relative magnitude of tilt, while positive or negative variations mark the direction of the tilting. A_f values reveal higher levels of basin tilting in the HKT in the WS-5, WS-9 and WS-10. Whereas WS-15 in the same area exhibit lesser tilt as this is situated along the sinistral JF with come compressional component. Same is the case with the WS-28 that is along the Indus River. The drainage in the Potwar Plateau exhibit A_f = 38 in the WS-20, that can again be regarded to the rapid erosion rates. Moreover, the stream along the Kalabagh Fault and across the Kurram Fault (KF) to the West of the Bannu Basin exhibit R_e values of 65 and 75, respectively.

3.4.7 Morphotectonic features

Investigations from the remote sensing data reveals variations in morphology in the study area, controlled by tectonic deformations along the thrust, reverse and strike slip faults. The HKT has uplifted mountains along the Jhelum Fault and other imbricate faults (Baig et al., 2010). These mountain ranges show high relief and are transected by the streams and rivers. These mountain ranges along with the eastern Salt Range and to the West of the Bannu Basin exhibit triangular facets at the mountain fronts along the faults (Figs. 3.9 and 3.10). The triangular facets in the western flank of the Bannu Basin yield overlapping alluvial fans that form alluvial plain at the mountain front. Deflections of the rivers and streams in the fault zones of the Jhelum Fault and the Kalabagh Fault define the strike slip kinematics of these faults. The decollement along the main Frontal Thrust exhibit degraded fault scarp. Stream deflection, pressure ridges, Quaternary deformations and offsets are observed along the Kalabagh Fault and discussed in Chapter 4.

3.4.8 Relative active tectonic Index (Iat)

Active tectonic classes from morphometric indices were used to compute an average as tectonic activity index. Watersheds with 3 or more morphometric indices were utilized for estimation of relative active tectonic index (I_{at}) and results are given in Table 3.4. The I_{at} *and* I_{at} classes indicate that most of the study area is moderately active. Whereas parts of the HKT, western Potwar Plateau and western Bannu Basin reveal Class 1 tectonic activity in the WS-5, WS-10, WS-23, WS-30, WS-39 and WS-40.

3.5 Discussion

3.5.1 Morphometric analysis

This section presents the interpretations made from the morphometric analysis of the study area with variable tectonic characteristics. Therefore, this study makes a comparison of different morphometric indices that may reveal variable tectonic activity classes in a drainage basin. It is observed from the results that morphometric indices are helpful in I_{at} estimations. However, different factors may affect the drainage basin morphology and include the tectonic activity, lithological controls and density and orientation of structures surrounding the drainage basins. Watersheds with smaller HI may yield higher R_b values (WS-20), due to rapid erosion and badland topography. Furthermore, R_e, A_f and SL index may have contrasting results along the strike slip faults, such as R_e along the Jhelum Fault in WS-15 indicates high tectonic activity whereas SL index and A_f reveal low tectonic activity (Table 3.4).

Moreover, these 3 morphometric indices exhibit high tectonic activity in WS-5, that is aligned at oblique angle to the Jhelum Fault and exhibit triangular facets along the thrust stack to the East of the Jhelum Fault (Table 3.4, Figs. 3.8 and 3.10). WS-30 along the Kalabagh fault exhibit more tectonic activity as compared with WS-15 that is along the Jhelum Fault (Table 3.4 and Fig. 3.2), where later is along the active channel of the Jhelum River and have more erosion than uplifts. Therefore, we need to apply a set of morphometric parameters on drainage basins to reach a conclusion.

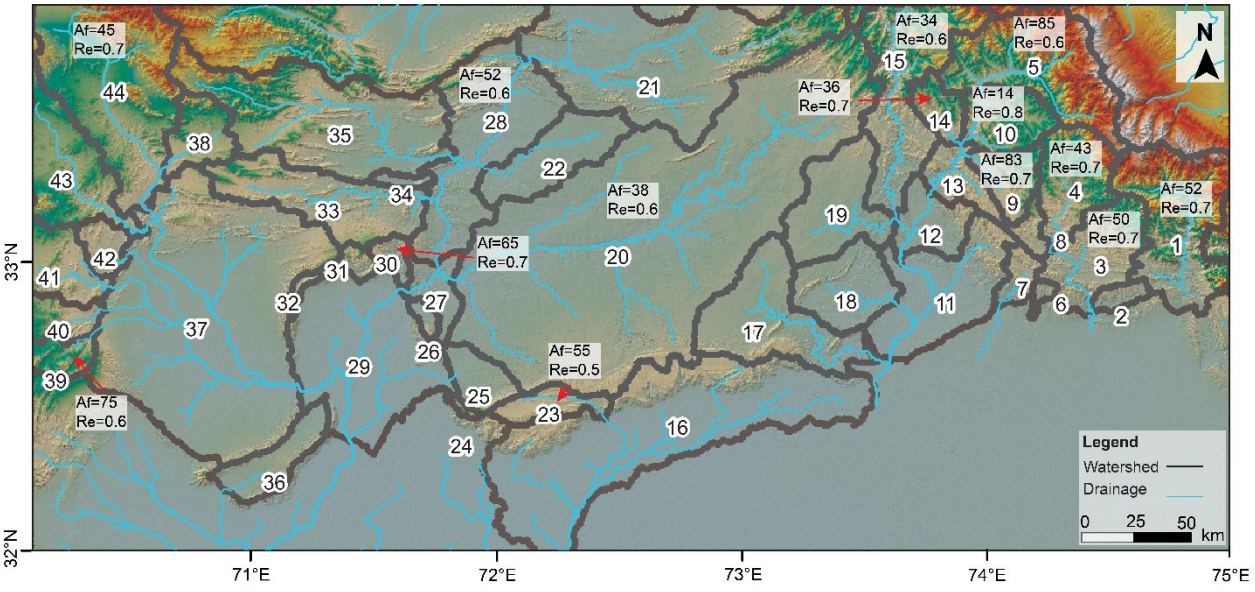

Fig. 3.8 Relative variation of elongation ratio (Re) and asymmetry factor (A_f) between consecutive stream orders.

Table 3.3 Basin elongation ratio (R_e), asymmetry factor (A_f) and bifurcation ratio (R_b) of the watersheds in areas with higher possibility of tectonic activity.

Watershed no.	Location	A_r (km^2)	A_t (km^2)	L_b (Km)	R_e	A_f	R_b							
							Stream order							
							1	2	3	4	5	6	7	8
							1/2	2/3	3/4	4/5	5/6	6/7	7/8	8/9
1		1050	2021	71	0.72	52								
3		560	1117	53	0.72	50								
4		447	1033	51	0.71	43								
5	(WS-1 to WS-15) Hazara-Kashmir syntaxis in the East	1760	2058	83	0.62	85	2.1	1.8	2.3	1.7	2.0	1.8	18.3	
9	of the Jhelum Fault	429	515	35	0.74	83								
10		106	750	40	0.77	14								
14		133	369	31	0.70	36								
15		674	1983	91	0.56	34	2.1	1.9	2.2	2.0	2.2	0.8	3.4	
20	Potwar Plateau (PP)	4209	11113	203	0.59	38	2.0	2.0	2.0	2.1	1.9	2.1	1.9	8.6
23	Western Potwar Plateau	234	427	48	0.48	55								
28	Northern PP	1289	2466	98	0.57	52	2.0	2.0	2.1	2.2	2.0	3.9	0.3	
30	Chisal Algad, Kalabagh Fault	119	187	22	0.70	65	1.6	1.9	2.6	3.0	9.2			
39	Kurram Fault in the West of Bannu Basin	382	386	35	0.63	75	1.9	1.6	3.6	1.6	1.7			
44	NW of Bannu Basin	1530	3409	101	0.65	45								

A_r= Area of watershed in the right side of the stream while looking downstream
A_t= Total area of watershed
L_b= Maximum length of the basin or watershed

Table 3.4 Active tectonic Index (I_{at}) and active tectonic classes of watersheds where 3 or more morphometric indices were calculated.

Drainage basin no.	Tectonic activity class of						I_{at}	I_{at} class
	Smf	HI index	SL index	Rb	Af	Re		
1		3	1		3	2	2.3	2
3		3			3	2	2.7	2
4		3			3	2	2.7	2
5		2		1	1	1	1.3	1
9		3			2	2	2.3	2
10		2	1		1	2	1.5	1
14		2			3	1	2.0	2
15		3	3	2	3	1	2.4	2
20		3		1	3	1	2.0	2
23	1	2	1	1	3	1	1.5	1
28		3	3	2	3	1	2.4	2
29	1	3					2.0	2
30	1	2		1	2	1	1.4	1
36	1	3					2.0	2
37	1	3					2.0	2
39	1	2	1	2	2	1	1.5	1
40	1	2					1.0	1
44		3			3	1	2.3	2

As discussed in the section 3.2, the HKT, eastern Potwar Plateau, Kohat Plateau and Kurram Fault exhibit seismicity (Fig. 3.1), whereas, the western Potwar Plateau and the Kalabagh Fault are facing aseismic displacements and uplifts (Abir et al., 2015; Chen and Khan, 2010). Results from the morphometric analysis are coherent with those instrumental findings. As the watersheds to the East of Jhelum Fault (WS-5 and WS-10), western Potwar Plateau-Salt Range (WS-23), Kalabagh Fault (WS-30) and the Kurram fault (WS-39 and WS-40) yield high tectonic activity class in I_{at} index (Table 3.4).

Fig. 3.9 (a) Triangular facets in the late Quaternary sediments in the eastern Salt Range. (b) TSK sediments are juxtaposed against the late Quaternary sediments.

The study area contains the molasse sediments from early Miocene in the HKT, late Miocene to Pleistocene in the Kohat Plateau and the Potwar Plateau. Lithologies in the HKT are more compact as compared to the softer lithologies of the Kohat Plateau and the Potwar Plateaus. The mountain fronts and ridges exhibit more consolidated and resistant Paleozoic to Cenozoic rocks. The hypsometric analysis in the study area exhibits moderate to low tectonic activity (Table 3.2). Even the watersheds that show active tectonics in instrumental data indicate smaller HI. The smaller HI values imply one of the following hypotheses: i) the area under observation is not affected by young tectonic activity, ii)

rapid erosion of the molasse sediments denote the relatively younger watersheds as tectonically mature to older drainage basins and iii) due to strike slip displacement, no considerable uplift occurred. The WS-5 (HI=0.44, I_{at}=Class 1) and WS-15 (HI=0.31, I_{at}=Class 1) are in the seismically active parts of the HKT (Fig. 3.1), whereas WS-30 (HI=0.35, I_{at}=Class 1) is along the dextral Kalabagh Fault that yield aseismic displacements between ~3.7-7.7 mm/a instead of instrumental seismicity (Chen and Khan, 2010). Moreover, WS-23 in the western Potwar Plateau (HI=0.49, I_{at}=Class 1) is uplifting at a rate of 10 mm/a. The western flank of the Bannu Basin is also seismically active (HI=0.52, I_{at}=Class 1). The dissimilarities in HI and I_{at} in these watersheds are denoted to lithological controls because of resistant lithologies in the more emergent HKT (HI=0.44 in WS-5) and western flank of the Bannu Basin (HI=0.52) as compared with the Kalabagh Fault Zone (HI=0.49 in WS-23). Therefore, the second hypothesis is more valid than the first, as the study area is facing tectonic uplifts and displacements and should exhibit youth stages of mountain uplifts. The WS-30 and WS-5 also seem to fulfill the third hypothesis. The morphometric analysis yield result that are coherent with the lithological variations. Lithological controls are also evident in the SL index. The Indus River that crosses fold and thrust belts in the North Potwar does not show tectonic activity from the SL index, whereas the stream across the faults in other parts of the study area show moderate to high tectonic activity (Fig. 3.7). Therefore, instead of applying the absolute values of specific morphometric indicator(s), relative tectonic index is more useful that accounts for combined outcome of various morphometric parameters to have more impact of the morphometric analysis.

Straight mountain fronts in the study area are indicators of young morphologies. Triangular facets in segments of the mountain fronts implies active tectonics of the Reasi Thrust, Main Frontal Thrust and western flank of the Bannu Basin (Figs. 3.9 and 3.10). Deposition of thick alluvial plain sediments and triangular facets to the West of the Bannu Basin implies simultaneous tectonic uplift and erosion of the mountains (Fig. 3.10). InSAR analysis in this part of the study area can establish better understanding of the tectonic activity. Morphotectonic indicators and relative tectonic activity of the mountain ranges is separately discussed as follows.

3.5.2 Hazara-Kashmir Terrain (HKT)

The SL index in the HKT exhibit strong tectonic activity (WS-01) in a stream across the structural orientations (Fig. 3.7). The same parameter along the Jhelum Fault in the Jhelum River (WS-15) implies a weak tectonic activity due to strike slip displacement and strong tectonic activity where the stream crosses the thrust stack in WS-5 and WS-10 (Fig. 3.7). Active tectonic index *(I_{at})* of the southern HKT classify the mountain ranges in this part of the study area as tectonically moderate to highly active. WS-5 and WS-10 where the highest bifurcation ratio is observed in this study, is tectonically most active part of the study area and reveal triangular facets. Furthermore, WS-05 that has a relatively

higher HI (0.44), exhibits a greater tectonic tilt (A_f=86) causing a SW diversion of the trunk stream, implying an uplift in the NE. Whereas, R_e=0.62 and R_b=18.3 also indicate that the WS-05 is influenced by tectonic activity. I_{at} of WS-05 is also comparable with that of WS-10 (Table 3.4). It can be inferred from the morphometric indices of the HKT that the area is under active deformation. This deformation is controlled by the thrust stack in the HKS zone and vertical component of the transpressional Jhelum Fault. Whereas the strike slip component of the Jhelum Fault has a little influence on the landform development.

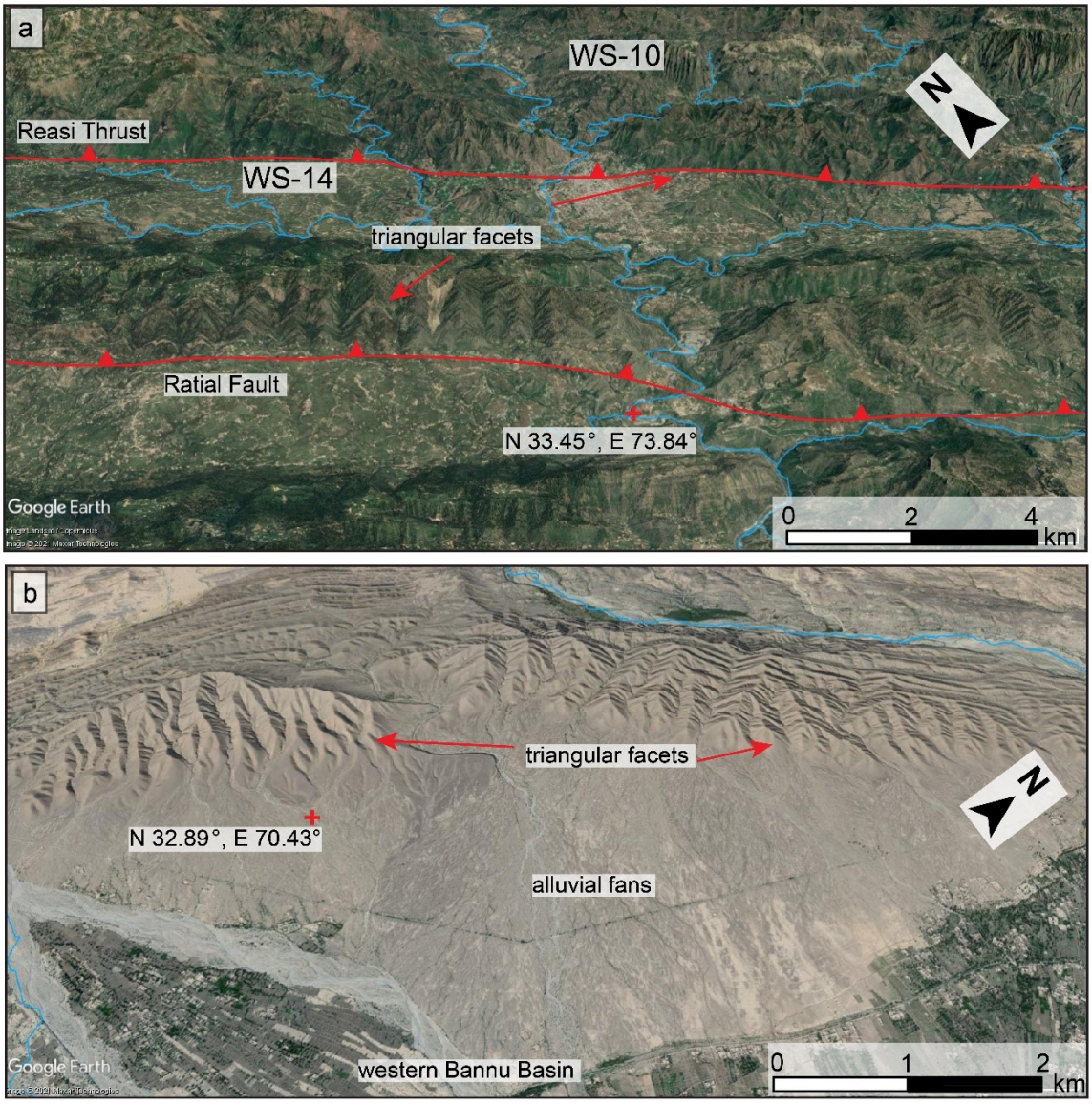

Fig. 3.10 Triangular facets in the active mountain fronts in the (a) southern Hazara-Kashmir Terrain, and (b) western flank of the Bannu Basin.

3.5.3 Salt Range-Potwar Plateau

The HI in the Salt Range-Potwar Plateau reveal variable results and are mainly dependent on the soft lithologies of the Siwalik sediments. The WS-20, with bad land topography exhibited by the Siwalik

sediments, reveals the lowest calculated HI (0.14) in the study area and a large bifurcation ration in the high order streams. i.e., R_b=*8.6 (Table 3.4)*. Whereas, WS-19 and WS-23 exhibit relatively greater HI values, implying more uplift in the northern Potwar Plateau and the western Salt Range, respectively. A relatively greater HI (WS-23=0.49) in the western Salt Range is comparable with the 10 mm/a uplift rate calculated by Abir et al. (2015). The SL index from a stream across the Main Frontal Thrust in WS-23 (SL= 3785), that has incised down the Eocene limestones (Fig. 4.2), indicates strong tectonic activity (Fig. 3.7). The WS-23 is a lake formed in a piggyback basin where R_e and A_f does not reveal a strong tectonic activity. I_{at} from longitudinal profile of the Indus River in the North Potwar Plateau does not show noticeable relief, while the SL index (Fig. 3.7) shows weak tectonic activity (SL<100), probably due to higher erosion rates coupled with Class 2 of I_{at} (Table 3.4, WS-28). The morphometric analysis implies the results are coherent with the instrumental data, as the western Potwar Plateau (and Salt Range) exhibit stronger tectonic activity. More instrumental seismicity and triangular facets at the mountain front designate the eastern Salt Range as the tectonically active zone.

3.5.4 Kalabagh Fault Zone

The Kalabagh fault forms a ramp against the Mianwali Reentrant (MWR) in the western Potwar Plateau (Fig. 3.1). The S_{mf} shows active mountain front along this ramp. Other morphometric indices are applied to WS-30, where the northern segment of the Kalabagh Fault is a range bound fault. WS-30 reveals a mature stage from the HI (0.35), where soft lithologies of the Siwaliks are eroded along the strike slip Kalabagh Fault. As the watershed is along the strike slip fault, that may not necessarily have a compressional component, the mature to old HI cannot describe the tectonic influence independently. The R_e=0.7 and R_b=9.2 indicates high relief and tectonic effects. Morphotectonic features observed along the Kalabagh Fault are discussed in Chapters 4 and 5, that designate it as an active fault with high earthquake recurrence intervals. Assuming the strike slip faults may have lesser vertical displacement as compared with normal and reverse faults, these faults may exhibit poor tectonic activity when evaluated using single morphometric indicator and an integrated value from I_{at} validate the importance of using multiple morphometric indicators together denoting the class-1 I_{at}.

3.5.5 Western flank of the Bannu Basin

Morphometric indices from the WS-39 indicates stronger tectonic activity along the Kurram Fault and the western flank of the Bannu Basin. The SL index (Fig. 3.7), A_f and R_e (Table 3.3) of the WS-39 implies the watershed is influenced by the tectonic deformations. R_b of the 3rd and 4th order streams is slightly greater. The HI=0.52 (Table 3.2) of the WS-39 is measured as the largest in the study area. Moreover, the Kurram Fault has also exhibited instrumental seismicity (Fig. 3.1). The instrumental data and Class

1 of the I_{at} imply that the Kurram Fault and associated mountain ranges in the western flank of the Bannu Basin are tectonically active.

3.6 Conclusions

The absolute values of the morphometric indices of the tectonically active zones may not always comply with the stratigraphic and tectonic context of the area under observation. A morphometric indicator sometimes does not explain the tectonic activity independently, rather an integrated approach is required to get reliable results. A comparative relation needs to be established using the active tectonic index (I_{at}) by integrating the morphometric indices of a drainage basin. Strong tectonic activity is evident from landform configurations in the HK, western Potwar Plateau and the Kurram Fault, that is also confirmed by the instrumental data in previous studies. The morphotectonic indicators in the Salt Range denote the Main Frontal Thrust as tectonically active fault. Active tectonics of the Kalabagh Fault measured from instrumental data is confirmed by the Class-1 I_{at} in the Kalabagh Fault Zone.

4. Seismicity and landform development of the dextral Kalabagh Fault Zone, Pakistan: Implications from morphotectonics and paleoseismology

Abbas, W., Ali, S., Reicherter, K., 2021. Seismicity and landform development of the dextral Kalabagh Fault Zone, Pakistan: Implications from morphotectonics and paleoseismology. Tectonophysics. DOI: 10.1016/j.tecto.2021.229182

Abstract

The Kalabagh Fault Zone in the western Sub-Himalayas is a dextral strike slip fault zone that exhibits a push-up block in the stepover zone of the two fault segments. The inception of the push-up block occurred along the restraining faults that form two morphotectonic bends along the mountain front at Zaluch and in the South of Thathi. The landform was further developed by en-echelon fold and thrust sequence up to Khairabad in the North and Ghundi village in the South. The aseismically moving fault zone has experienced earthquakes during late Quaternary forming surface expressions in the West of the push-up block at Khairabad, Larkakki and Ghundi. The Khairabad and Ghundi sections are the active tectonic fronts of the stepover zone. Displacements caused by these seismic activities has deformed Quaternary sediments creating stream deflections, surface ruptures, pressure ridges, uplifted sediments at the mountain front, foreland ridges and an uplifted alluvial fan. Offsets in the late Quaternary sediments indicate that the Kalabagh Fault is active and seismic events of $M_w \geq 6$ has formed these ground effects. Furthermore, stratigraphic correlations of fluvial sediments indicate that the Indus River has been flowing in the NS direction along the northern segment of the Kalabagh Fault. Uplift of the push-up block in the Kalabagh Fault Zone and subsequent deposition of the alluvial fans has caused westward diversion of the Indus River.

Key words: Morphotectonics; Paleoseismology; Tectonic landscape evolution; GPR; Kalabagh fault; Pakistan

4.1 Introduction

Active faults have been studied with reference to recent seismicity, historic and prehistoric earthquakes. For this purpose, instrumental seismicity and historical seismic catalogs have been utilized. Global positioning system (GPS) and interferometric synthetic aperture radar (InSAR) have been used to evaluate the fault activity by recording the real time displacements (Chen and Khan, 2010; Jouanne et al., 2014; Lisa et al., 2007). Whereas historical and prehistoric earthquakes are not well documented for most of the active faults. Which can be due to two possibilities: either poor documentation/investigation of these seismic events or episodic/continuous fault creep during the

inter-seismic period. This aseismic creep may have enhanced the earthquake recurrence interval, limit the maximum earthquake magnitude on a particular fault segment or prevent the occurrence of earthquakes (Barnhart, 2017). Such faults may not be activated during the span of available earthquake records. For these type of faults, morphotectonic and paleoseismic techniques are used to study active tectonics, historic and prehistoric earthquakes and their contribution towards the landform development (W. Bull, 2007; Demanet et al., 2001; Gourabi and Yamani, 2011; Grützner et al., 2012; Keller and Rockwell, 1984; Mason and Reicherter, 2017). Morphotectonics of the active regions utilize landform assemblages and landscape evolution in response to recent tectonic activity (W. Bull, 2007; Doornkamp, 1986; Keller and Rockwell, 1984). Whereas, paleoseismic investigations are carried out by exploring prehistoric seismic deformations in Quaternary sediments (Keller and Rockwell, 1984; McCalpin and Nelson, 2009).

The Kalabagh Fault Zone (KBFZ) is an active dextral fault zone in the western Sub-Himalayas in Pakistan (Chen and Khan, 2010). The KBFZ delineate the tectonic boundary between the Potwar Plateau (PP) in the East and the Kohat Plateau (KP) in the West (Fig. 4.1). McDougall and Khan (1990) have estimated average displacement rate of ~7-10 mm/a along the KBFZ near the Indus River during past ~2 Ma. Whereas Chen and Khan (2010) have calculated variable aseismic displacement rates in different segments of the KBFZ using InSAR data. The instrumental seismicity in the KBFZ is not significant (Fig. 4.1b), whereas the area lacks historical seismic record. Therefore, the KBFZ is considered as an aseismically active fault due to absence of known earthquakes during late Quaternary. Lack of earthquake record may also be denoted to long earthquake recurrence intervals (Barnhart, 2017), causing lack of seismic activity along the KBFZ. Therefore, morphotectonics and paleoseismic evidences along the KBFZ can help to find historic/prehistoric earthquakes during late Quaternary, leading to deduce whether the landforms in the KBFZ has contributions from the seismic uplifts. Morphotectonic and paleoseismic observations combined with the geologic evidences can therefore be employed to infer deformation mechanisms and landform development in the KBFZ.

The KBFZ to the North of the Indus River has faced major deformation during the past ~0.5 Ma that has created landforms, diverting the course of the Indus River towards the East (McDougall, 1989b). McDougall (1989) has suggested a north-south flow of the IR before this tectonically induced diversion. The Indus River in the West of the KBFZ (Fig. 4.1) make an east-west to north-south turn, shifting the river up to ~18 km from the KBFZ. Hypothesizing the north-south flow of the Indus River near the KBFZ before the landform was developed, it is possible that the river may have undergone westward diversion caused by the tectonically uplifted landforms in the KBFZ and deposition of the thick alluvial fans. Correlations between the sediments of the paleo Indus River and fluvial sediments along the KBFZ can be used to confirm this hypothesis.

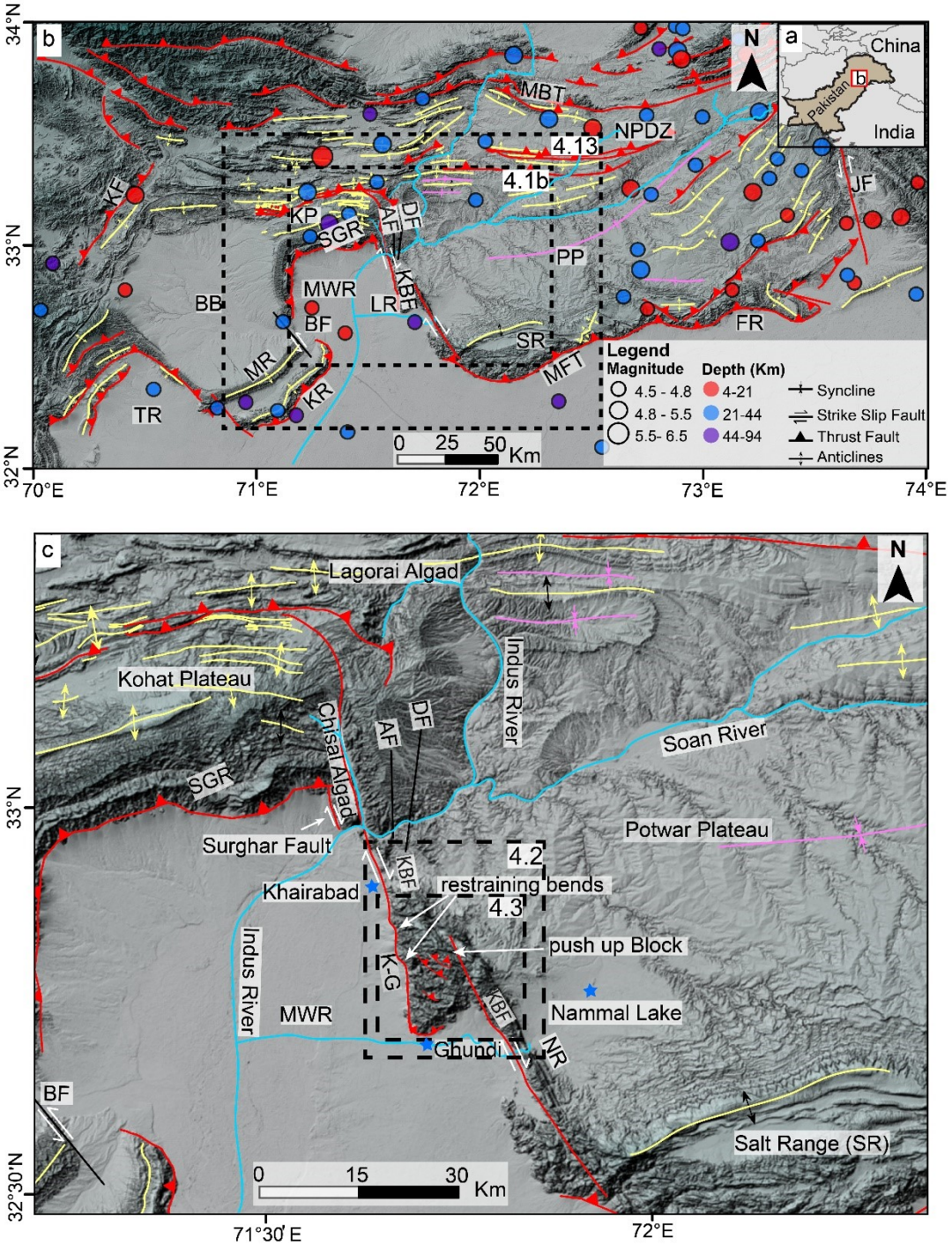

Fig. 4.1(a) Geographical location of the Sub-Himalayas in Pakistan. (b) Integrated tectonic map of the Sub-Himalayas shows main structural features and tectonic subdivisions marked on the hillshade image (modified after Abir et al., 2017; Alam, 2008; Ali, 2010; Kazmi and Rana, 1982) based on digital elevation models (DEM) from the ALOS 30 m and Global Imagery of ArcGIS. Circles show instrumental seismicity (USGS Earthquake catalog, 2019). (c) Map shows major features along the Kalabagh fault. AF=Ainwan Fault, BB=Bannu Basin, BF=Bannu Fault, DF=Dinghot Fault, FR=Frontal Ramp, JF=Jhelum Fault, KBF=Kalabagh Fault, KP=Kohat Plateau, KR=Khisor Range, LR=Lateral Ramp, MBT=Main Boundary Thrust, MFT=Main Frontal Thrust, MR=Marwat Range, MWR=Mianwali Reentrant, NPDZ=North Potwar Deformed Zone, NR=Nammal Ridge, PP=Potwar Plateau, SR=Salt Range, SGR=Surghar Range, TR=Tank Reentrant.

This study was aimed at: (i) evaluating the landforms that are resulted by the active tectonics (ii) assessment of seismic behavior of the KBFZ in the absence of historical seismic catalogs and instrumental seismicity, (iii) establishing a mechanism of the landform development of the KBFZ and

(iii) investigating the westward migration of the Indus River. Therefore, morphotectonic evidences were collected from the digital elevation models (DEMs) and structure from motion (SFM) techniques. The areas with active tectonic geomorphology were further investigated by integrating the shallow subsurface geophysical data from ground penetrating radar (GPR), paleoseismic trenches, morphology of alluvial fans and stratigraphic correlations. These investigations were carried out at the mountain front and alluvial fans so that seismically induced displacements and morphotectonic features may be explored in most recent sediments close to the main strand of the Kalabagh Fault (KBF). Results from these studies were used to determine seismic behavior of the KBF and landform development in the Kalabagh Fault Zone (KBFZ). Sedimentary correlations from the mountain front were carried out to infer the source of sediment influx. Such sedimentary comparisons coupled with the characteristics of the alluvial fans have led to establish the mechanism of the Westward diversion of the Indus River during the landform development in the KBFZ.

4.2 Study area

4.2.1 Tectonic framework

The Sub-Himalayas (SH) are marked by the Main Boundary Thrust (MBT) in the North and the Main Frontal Thrust (MFT) in the South (Fig. 4.1b). The Potwar Plateau (PP) and the Kohat Plateau (KP) constitute the western Sub-Himalayas in Pakistan. The Potwar Plateau is bounded by a frontal ramp (FR) along the South-verging Main Frontal Thrust (MFT) in the Salt Range (SR). While the Surghar Range (SGR) is formed along the Main Frontal Thrust in the South of the Kohat Plateau. Inception of the Salt Range and the Surghar Range was initiated ~1.9-2.1 Ma (Baker et al., 1988; Jaumé and Lillie, 1988; McDougall and Khan, 1990). The Salt Range and the Surghar Range exhibit a lateral offset of ~ 70 km (Fig. 4.1) along the Kalabagh Fault (KBF). As the kinematics of the KBF are also governed by the splay faults and fault stepover, therefore, the fault zone is collectively termed as the Kalabagh Fault Zone (KBFZ), whereas the main strand of the fault is termed as the Kalabagh Fault (KBF) hereinafter. The KBFZ starts in the South from the western termination of the Salt Range (SR) and extends up to the North of the Indus River along the Chisal Algad stream (Fig. 4.1c), and turns to the West parallel to the North dipping thrusts in the Kohat Plateau (McDougall and Khan, 1990). The fault is broadly classified into two segments: The southern segment strikes N35°W between the western termination of the SR and the Ghundi stepover and forms the Nammal Ridge (NR). Whereas the northern segment strikes N15°W starting from Ghundi and extends up to the North of the Indus River (Fig. 4.1c). The latter segment in the Chisal Algad stream is a range bound fault that is surrounded by the Surghar Range-Kohat Plateau in the West and the Potwar Plateau in the East (Fig. 4.1c). The NNW striking Surghar Fault is situated to the West of the KBF and the NE trending Ainwan (AF) and Dinghot (DF) splay faults

are situated to the East of the Chisal Algad stream (Chen and Khan, 2010; Gee, 1980; Khan et al., 2012). McDougall (1989) designated the Chisal Algad (CA) and the Lagorai Algad (LA) streams as the paleo Indus River using sedimentary correlations between channel sediments and chronology of the top of the Miocene-Pleistocene Siwalik group of sediments (TSK), i.e. 0.4-0.7 Ma (Johnson et al., 1979; Khan, 1983; McDougall, 1989b; Yeats et al., 1984). A thrust fault between the Chisal Algad and the Lagorai Algad had produced landforms, hindering the flow of the Indus River during ~0.5-0.1 Ma, the Indus River then adopted the present-day channel (McDougall, 1989).

The overlapping zone of the two fault segments form a stepover at Ghundi exhibiting NW striking fold and thrust sequence with some extensional faults between Ghundi and Khairabad (Fig. 4.2). The fault zone in this part is termed as stepover zone in the following text. The frontal part of the KBFZ between Khairabad and Ghundi is termed as the Khairabad-Ghundi (KG) section hereinafter. The fault stepover exhibits a maximum width of ~10 km at Ghundi and decreases northward, where it reaches minimum horizontal and vertical thickness between Khairabad and the Indus River (Fig. 4.1c). The KBFZ in the KG section and the Nammal Ridge forms a ramp that is developed along the transpressional KBFZ and termed as the lateral ramp (LR). The western Potwar Plateau is uplifted against the Mianwali Reentrant along the Lateral Ramp. The Nammal Ridge exhibits sedimentary units with thrusts and back thrusts, that are steeply dipping compared with the stepover zone. Due to the evaporite bearing Precambrian Salt Range Formation (PCSR) in the subsurface, the KBFZ also exhibit extensional faults (Fig. 4.2). Whereas, these evaporites are not well preserved in the subsurface to the West of the KBFZ (Khan et al., 2012).

4.2.2 Stratigraphy

The KBFZ exhibit diverse stratigraphy ranging from Precambrian to late Quaternary. The foreland represents the Quaternary sediments in the study area (Gee, 1980). The Precambrian Salt Range Formation (PCSR) is thrusted against the Quaternary Alluvium (QAL) at various locations along the mountain front of the lateral ramp (Fig. 4.2). While the Cambrian formations are missing in most of the study area except the western termination of the Salt Range. The sedimentary units from Permian to Quaternary are exposed along the KG section (Fig. 4.2). The limestones of the late Permian Zaluch Group (PZG) are thrusted and sheared along the mountain front. Late Miocene to Pleistocene molasse sediments jointly termed as the Tertiary Siwaliks Group (TSK) or Siwaliks are present in the East and the northwest of the KBFZ (Gee, 1980). The Pleistocene Kalabagh Conglomerates (QKC) that are underlain by the Siwaliks (Fig. 4.2), consist of sediments that were eroded and transported from the rising mountains and deposited in the adjacent foothills along the KBFZ (McDougall and Khan, 1990). The QKC sediments consist of the clasts of the lower Tertiary limestones (McDougall, 1989 and

reference therein), whereas base of the QKC marks the termination of the Siwaliks' deposition and the onset of uplift of the Siwalik and pre-Siwalik rocks along the KBFZ. Alluvial fans are developed in the West of the KG section (Fig. 4.2 and 4.3) and are composed of Quaternary sediments (Gee, 1980).

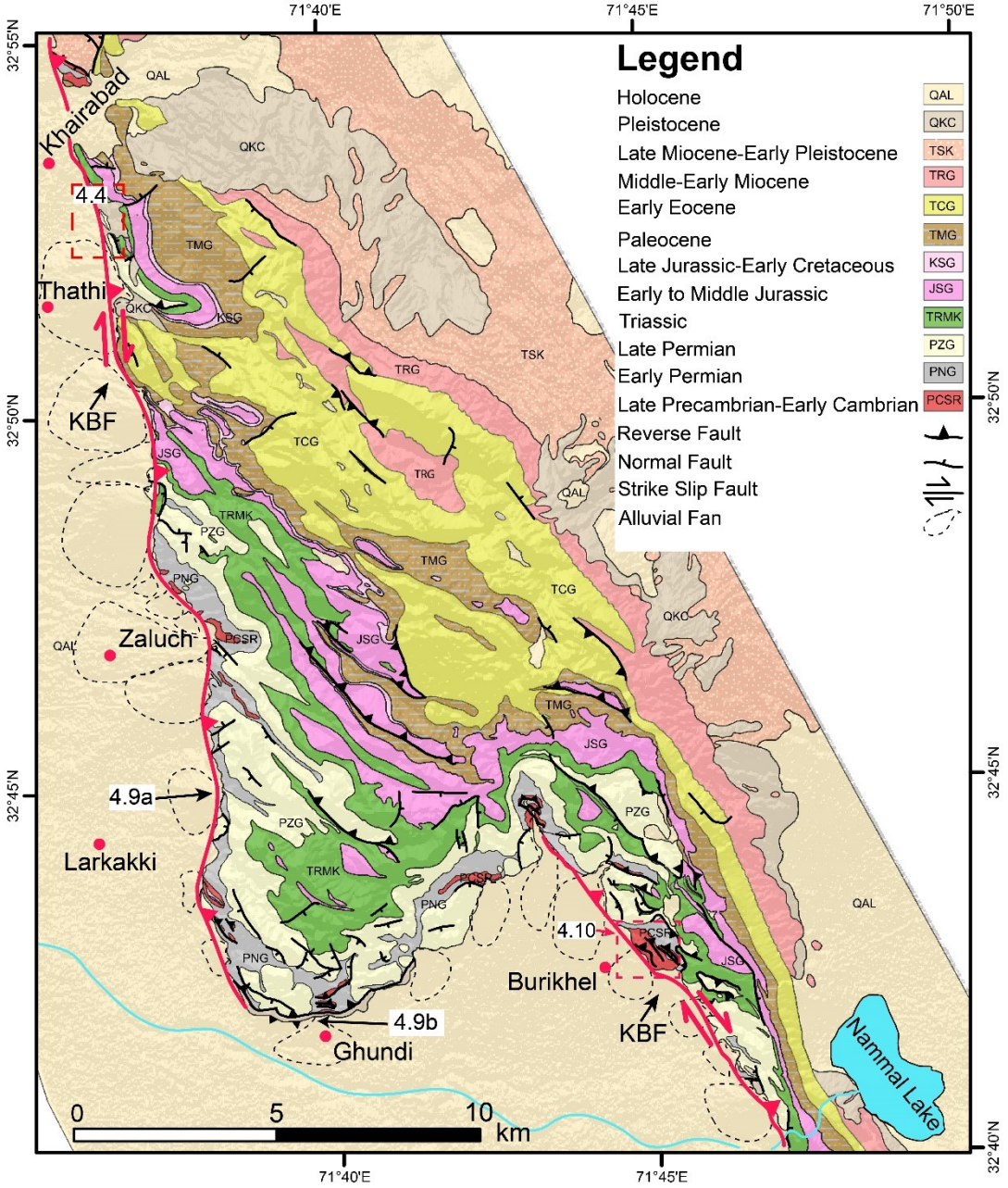

Fig. 4.2 Geological map of the study area marked in Fig. 4.1c (after Gee, 1980). PCSR=Salt Range Formation (Precambrian), PNG=Nilawahan Group (Early Permian), PZJ=Zaluch Group (Late Permian), TRMK=Musa Khel Group (Triassic), JSG=Surghar Group (Jurassic), KSG=Surghar Group (Cretaceous), TMG=Makarwal Group, TCG=Chharat Group (Late Miocene to Pleistocene), TRG=Rawalpindi Group (Tertiary), TSK=Siwalik Group (Tertiary), QKC=Kalabagh Conglomerates (Quaternary), QAL=Alluvium (Quaternary)

The TSK represent molasse sediments reworked from the rising Himalayas (Gansser, 1964). Landform development along folds and thrusts has terminated the deposition of the TSK in the Sub-Himalayas. The upper depositional boundary of the TSK thus predate the major deformations in the Salt Range and the Potwar Plateau (Johnson et al., 1979; Mirza, 1980; Yeats et al., 1984). The age of the top of

the TSK in the eastern Salt Range is ~0.7-0.4 Ma (Johnson et al., 1979; Yeats et al., 1984) and ~0.5 Ma or even younger in the West of the KBFZ (Khan, 1983; McDougall, 1989b). Whereas chronology of the TSK is not determined in the western Salt Range. Diachronous lithological boundaries of the TSK are getting younger westward across the KBFZ (McDougall and Khan, 1990). The TSK-QKC contact is chronological indicator of the onset of deformation along the KBFZ. This stratigraphic contact coupled with structural and sedimentary correlations in the Chisal Algad and the Lagorai Algad stream indicate a tectonically induced eastward diversion of the Indus River during ~0.5-0.1 Ma (McDougall, 1989b).

4.2.3 Neotectonics

The historical record of earthquakes is not available along the KBFZ, this phenomena is possible due to long earthquake recurrence intervals or lack of seismic displacements in aseismically moving faults or even non-existence of earthquakes for an inactive fault (Barnhart, 2017). Whereas the USGS earthquake catalog for the past 65 years reveal very few seismic events with M_w=4.5 and above (Fig. 4.1b), having a focal depth ~73 km in the South of Ghundi. This low magnitude earthquake has relatively deeper focal depth, as compared to the shallow focus earthquakes in the eastern Potwar Plateau and the southern Kohat Plateau (Fig. 4.1b).

The right lateral displacement along the KBFZ occurred at a rate of ~7-10 mm/a during past ~2 Ma near the Indus River (McDougall and Khan, 1990), creating the landforms along the KBFZ. Moreover, the InSAR analysis from one interferogram (Nov 1992 and April 1999) indicates the KBFZ is moving with a maximum displacement rate to the East of the Chisal Algad section (Fig. 4.1c), located in the North of the Indus River (Chen and Khan, 2010). It reveals a slip rate of 5.3 mm/a along the main KBF and 6.6 and 5.4 mm/a along the Ainwan (AF) and Dinghot (DF) splay faults, respectively. Chen and Khan (2010) have also mentioned line of sight (LOS) displacement rate of 5.7 and 3.7 in the KG section and the Nammal Ridge, respectively. Displacement rates of Chen and Khan (2010) are lower than McDougall and Khan (1990) possibly because later represent average of seismic and aseismic displacements. Furthermore, GPS measurements along the southern segment of the KBFZ do not show significant displacement between 2006 and 2012, indicating the displacement along the fault is episodic (Jouanne et al., 2014). The western Potwar Plateau that is bounded in the West by the KBFZ reveals an uplift rate of 10 mm/a from the InSAR analysis (Abir et al., 2015).

4.3 Methodology

An integrated approach was applied based on the remote sensing data, structure from motion (SFM) data, outcrop geology, geophysical data and geological data from trenches. Initially, remote sensing data was utilized to outline the morphological features that can be indicative of active tectonics.

Locations including Khairabad, Larkakki, Ghundi, Burikhel, Nammal and alluvial fans were shortlisted to conduct unmanned aerial vehicle (UAV) surveys and to collect SFM data. High resolution UAV images and DEMs were employed to delineate morphotectonic features and alluvial fan channels. The outcrop geology and channels on the alluvial fans were investigated near these morphotectonic features. The Khairabad section was found to be more promising for paleoseismic features and better accessibility. Therefore, geophysical data was recorded using GPR near these morphotectonic features at Khairabad followed by paleoseismic trench investigation. Whereas outcrop geology was utilized to study the paleoseismicity and landform development at Larkakki, Ghundi and Burikhel. Tools and parameters adopted during this study are elaborated as follows:

4.3.1 Remote sensing data

Remote sensing data was utilized for reconnaissance and selection of locations for morphotectonic and paleoseismic investigations. Eight tiles (70°E-74°E, 32°N-34°N) from ALOS 30 m DEMs were acquired and processed using ArcGIS v-10.5.1 to create hillshade image of the study area (Fig. 4.1). The hillshade image helped to explore structural features e.g., regional offsets, anticlines and synclines apart from previously published literature, morphotectonic features such as mountain front sinuosity and wind gaps etc. Moreover, the Google Earth Imagery was used for initial reconnaissance of the alluvial fans, escarpments, and stream patterns (Fig. 4.3).

4.3.2 Structure from motion

Structure from motion (SFM) technique was employed to create high resolution digital elevation models (DEMs) along the mountain front of the KBFZ. For this, unmanned aerial vehicle (UAV) was used to photograph the morphotectonic features near the main strand of the KBF. An average overlap of 60% with vertical view at an altitude of 80 m from the foothills was used during photogrammetry. Agisoft Metashape software was used to produce DEMs for Khairabad, Larkakki and Burikhel. Whereas the alluvial fans and the lobate area of Ghundi were aerially photographed. DEMs and aerial photographs were used to visualize and delineate the morphotectonic features in the KBFZ and stream patterns of the alluvial fans in the foreland. The SFM was also employed to create the orthomosaic images of the trenches, outcrops and walls of the stream channels.

4.3.3 Outcrop geology

The exposed sedimentary rocks at the mountain front of the lateral ramp of the KBFZ, deformed quaternary sediments, alluvial fans and walls of stream channels near the apex of the alluvial fans were checked for any offsets, folded sediments and fractured pebbles etc. Sedimentary layers were also correlated, and cross cutting relationship was established. Such outcrop characteristics from

Khairabad, Larkakki, Ghundi and Burikhel were used as paleoseismic indicators that also helped in describing the landform development of the KBFZ.

4.3.4 Ground penetrating radar

Ground penetrating radar (GPR) is a widely used tool for geophysical investigation of shallow subsurface structures (Grützner et al., 2012; Koster et al., 2011; Schneiderwind et al., 2016; Thomas et al., 2017). Considering the thick QAL sediments at the mountain front, a deeper geophysical investigation was preferred to include the deformed bedrock in the sub surface, so that splays of the KBF may be mapped. Therefore, a GSSI-Sir 3000 GPR with a 100 MHz antenna was used to scan shallow subsurface geology in the Khairabad section. GPR profiles were processed using the ReflexW v-7.0 software for 2D analysis and presentation of the subsurface features (Sandmeier, 2012). Processing tools included: i) static correction to move start time up to arrival of the first signal, ii) a standard background removal, iii) energy decay, iv) Bandpassbutterworth 1d filter (min. ≥ 50 and max. ≤ 200) and v) topographic correction based on the ALOS 30 m DEM. Individual profiles were manually traced after processing. The interpretations were based on the variable depth of reflectors, variation of sedimentary packages, offset in reflectors and correlation with surface features (Fig. 4.6).

4.3.5 Paleoseismic trenches

The main strand of the KBF exhibits limestones and sandstones that belong to Tertiary or older formations and cannot be excavated for paleoseismic trenching. The deformed QKC and QAL sediments adjacent to the main strand of the KBF may reveal most recent seismic displacements along the splays of the main KBF. Therefore, based on the morphotectonic features and outcrop geology, paleoseismic investigations were carried out at Khairabad. Six paleoseismic trenches near the main strand of the KBF were studied (Fig. 4.4). Trench 1,2 and 3 were perpendicular to the main strand of the KBF and Trench 4 was at oblique angle to study lateral extension of the faults in trench 1. Whereas trench 5 was excavated at an oblique angle to the KBF to look for the lateral compression in the KBF blocks. Moreover, trench 6 was excavated in the hinter side of the main KBF in a bid to find splay faults. The walls of the trenches were photographed with 60% overlap and orthomosaic images were constructed using Agisoft Metashape software. Trenches were logged using 1 m grid scale and later digitized over the orthomosaic images (Fig. 4.7 and 4.8). Stratigraphic correlations, offsets in the

Quaternary sediments, characteristics of displaced pebbles, cross cutting relationship of the deformed sediments were established.

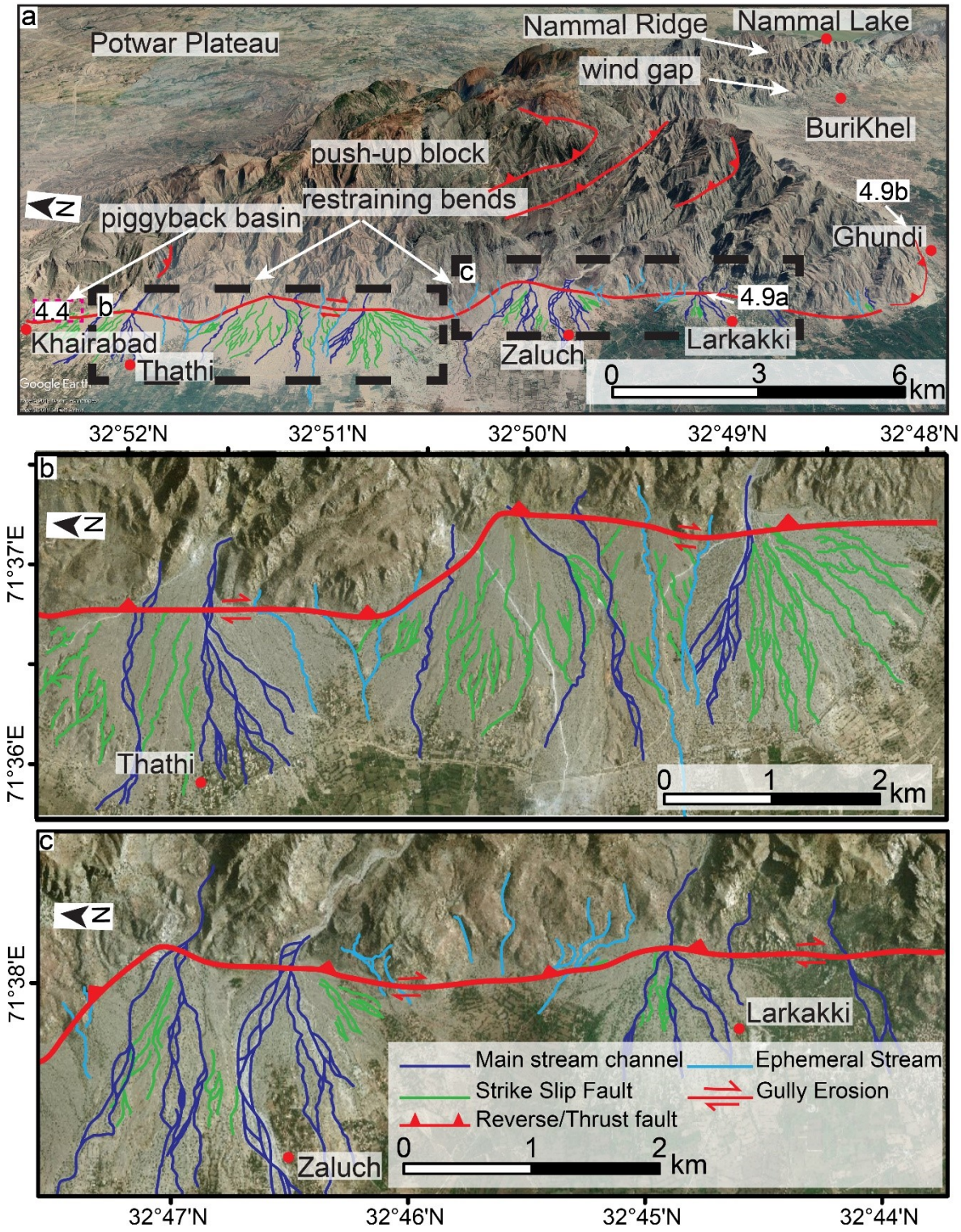

Fig. 4.3(a) Google earth image showing a mountain range and adjacent alluvial fans of the Khairabad-Ghundi section. Channels are marked on the alluvial fans based on the field observations and the Google Earth and ArcMap Global Imageries. (b and c) show zoomed in drainage patterns on alluvial fans.

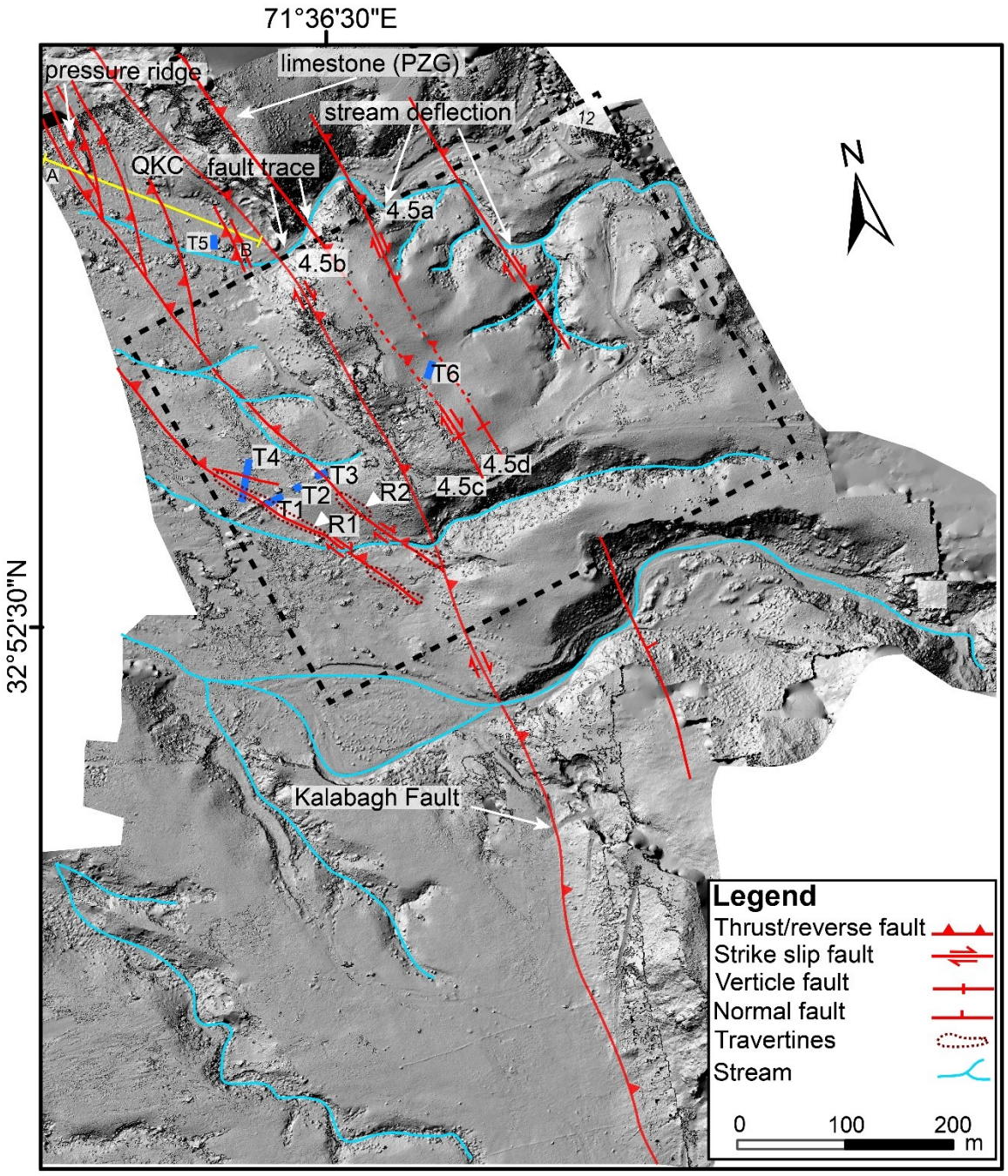

Fig. 4.4 Digital elevation model of 10.7 cm resolution in the South of Khairabad village (Fig. 4.2 and 4.3) showing geomorphic features. AB=Location of the GPR profile in Fig 4.6. T1-T6=Locations of trenches, R1-R2=Ruptures along latest earthquakes, 5(a-d)=Locations of the features shown in Fig. 4.5

4.3.6 Alluvial fans and outcrops

The morphology of the alluvial fans in the West of the KBFZ was investigated in terms of fan size, geometry, stream patterns, fan displacements and maturation of gully erosions on the alluvial fans (Fig. 4.3). Google Earth pro satellite imagery, UAV surveys and field mapping were used as a tool to establish a relationship between the characteristics of the alluvial fans and the landform development of the KBFZ. The outcrops at the mountain front in the West of the KBFZ and walls of the incised

channels on the alluvial fans were also checked for paleoseismic features including pebble alignments, stratigraphic correlations and offsets (Fig. 4.5 and 4.9). Moreover, these outcrops and streams were also photographed to create orthomosaic images. Lithological and structural features were logged and later digitized over these images (Fig. 4.9a).

4.4 Results

4.4.1 Morphotectonics of the Kalabagh Fault Zone

In this section, we present the results achieved from the remote sensing data, SFM, field surveys including outcrop geology and alluvial fan mapping, paleoseismic trench investigation and stratigraphic correlations. The morphology for the KBFZ is presented, followed by observations from the Khairabad, Larkakki, Ghundi and Burikhel sections.

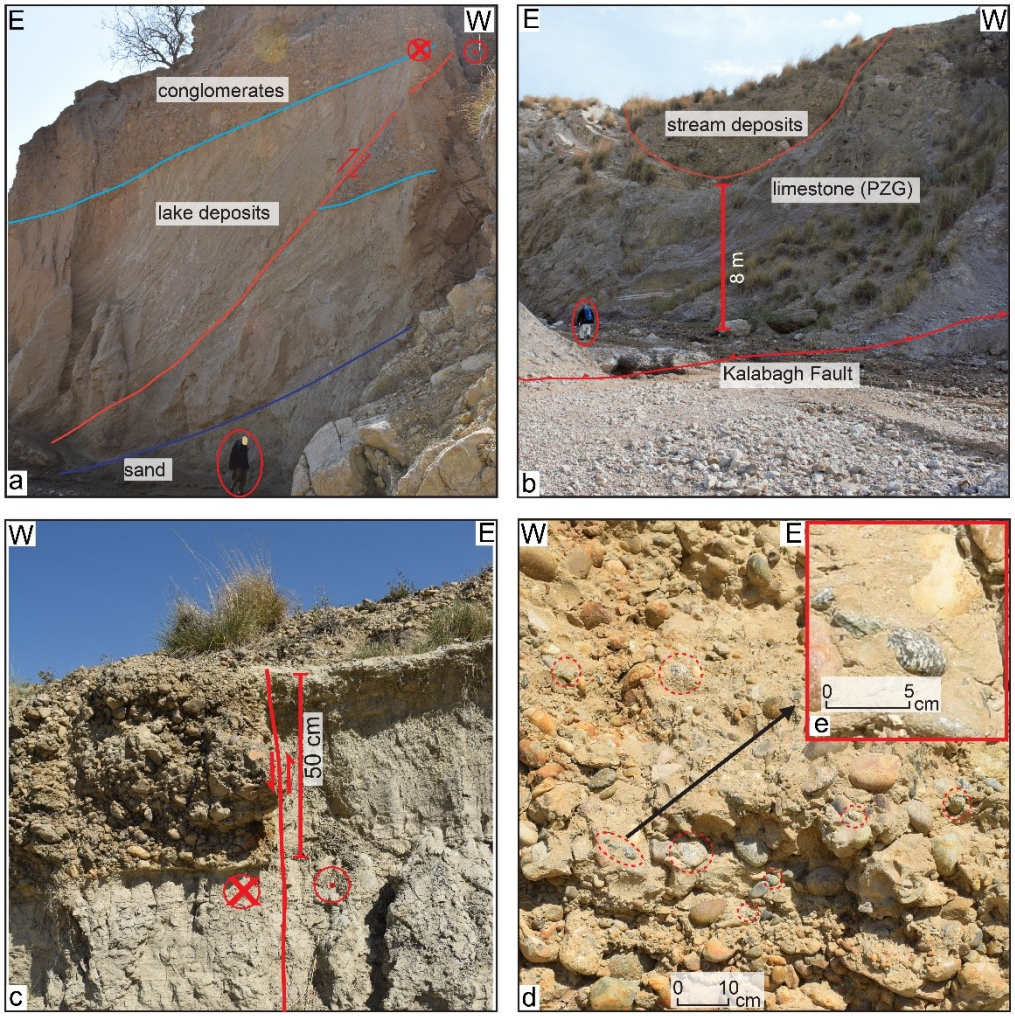

Fig. 4.5 (a) Reverse movement in the Quaternary sediments (32.8773138°N, 71.6112138°E). (b) paleo channel filled with gravels and uplifted 8 m from the current stream base level (32.87713°N, 71.610608°E). (c) lake deposits faulted against the conglomerate layer (32.8750805°N, 71.611566°E). (d) showing well rounded diorite pebbles (32.875145°N, 71.61186°E) originating from the North and resemble with the pebbles of the Chisal Algad stream.

The mountain front in the KG section reveals two morphotectonic bends near Thathi and Zaluch, aligned with the thrust faults in the KBFZ (Fig. 4.1c and 4.3a). These thrust faults are the restraining faults between the two segments of the KBFZ, creating a left stepover that is characteristic for contractional bend of a dextral fault (Campagna and Levandowski, 1991). The older sedimentary rocks are uplifted and exposed along the NW-SE striking en-echelon fault and fold sequence in the stepover zone of the KBFZ (Fig. 4.2), forming a push-up block.

Twelve alluvial fans of variable radius and thickness are identified in the foreland of the KG section in the West of the push-up block (Fig. 4.2 and 4.3). The fan radius is measured as distance between the toe and the apex of each fan. Whereas fan thickness at the mountain front is calculated as surface elevation difference between the toe and the fan apex. Mountain front between the two restraining faults exhibit alluvial fans that are ~80-90 m in thickness and ~1.8-2 km in radius (Figs. 4.2 and 4.3). Whereas the Thathi alluvial fan is 65 m thick and 1.8 km in radius. Fan sizes decrease in the South of Zaluch and up to Ghundi, exhibit ~2.1-0.7 km radius and ~35-18 m thickness. Stream channels are mapped on the alluvial fans. The feeder streams extend up to medial and distal places on each fan. The gullies on the alluvial fans start from the toe and extend towards the apex of the fan (Fig. 4.3). It is observed that the gullies on the larger alluvial fans are mature compared to the smaller fans. Furthermore, sediments of the larger alluvial fans are more consolidated compared with smaller fans due to earlier deposition and calcification, making them relatively mature. The feeder streams of these fans have deeply incised into high relief mountains of the push-up block. Moreover, the foreland in the West of the Nammal Ridge (NR) is covered with the gravels, and alluvial fans are poorly distinguished.

4.4.1.1 Khairabad section

The Khairabad section exhibits linear mountain front. The limestones of the Paleozoic Zaluch Group (PZG) are exposed along the main strand of the KBF (Fig. 4.2). These highly sheared limestones dip in the NE direction and kinematics of the fault are not distinguished from outcrop. The morphological expressions across the stream near the main strand of the KBF mark the fault traces (Fig. 4.4). A stream channel filled with the QKC sediments is identified along the KBF (Fig. 4.5b). This paleo channel is uplifted ~8 m along the KBF with respect to the foreland. The high-resolution (10.7 cm) DEM from the Khairabad section, created using SFM technique, exhibit a headward eroding and a deflected stream near the main KBF (Fig. 4.4). The stream deflections reveal right lateral displacements. These streams have incised into the sediments of the eastern block of the KBF. Stratigraphy of this block contain QKC at the surface, underlain by the lake sediments, that are further underlain by the fluvial sand deposits (Fig. 4.5a). These sediments are transpressively faulted along a stream deflection (Fig. 4.4 and 4.5a).

Furthermore, these sediments are also faulted along the headward eroding stream (Fig. 4.4 and 4.5c). These faults in the East of the KBF exhibit vertical offsets of ~50-100 cm (Fig. 4.5). Stratigraphic correlations reveal these sediments dip in the NE direction. Conglomerates close to the fault in Fig. 4.5c are fractured and contain well rounded diorite pebbles (Fig. 4.5d). These pebbles are also observed in the Chisal Algad stream, considered as an old channel of the Indus River (McDougall, 1989b). The diorite pebbles are deposited with the fluvial sands, resembling those underlain by the lake sediments in Fig. 4.5a.

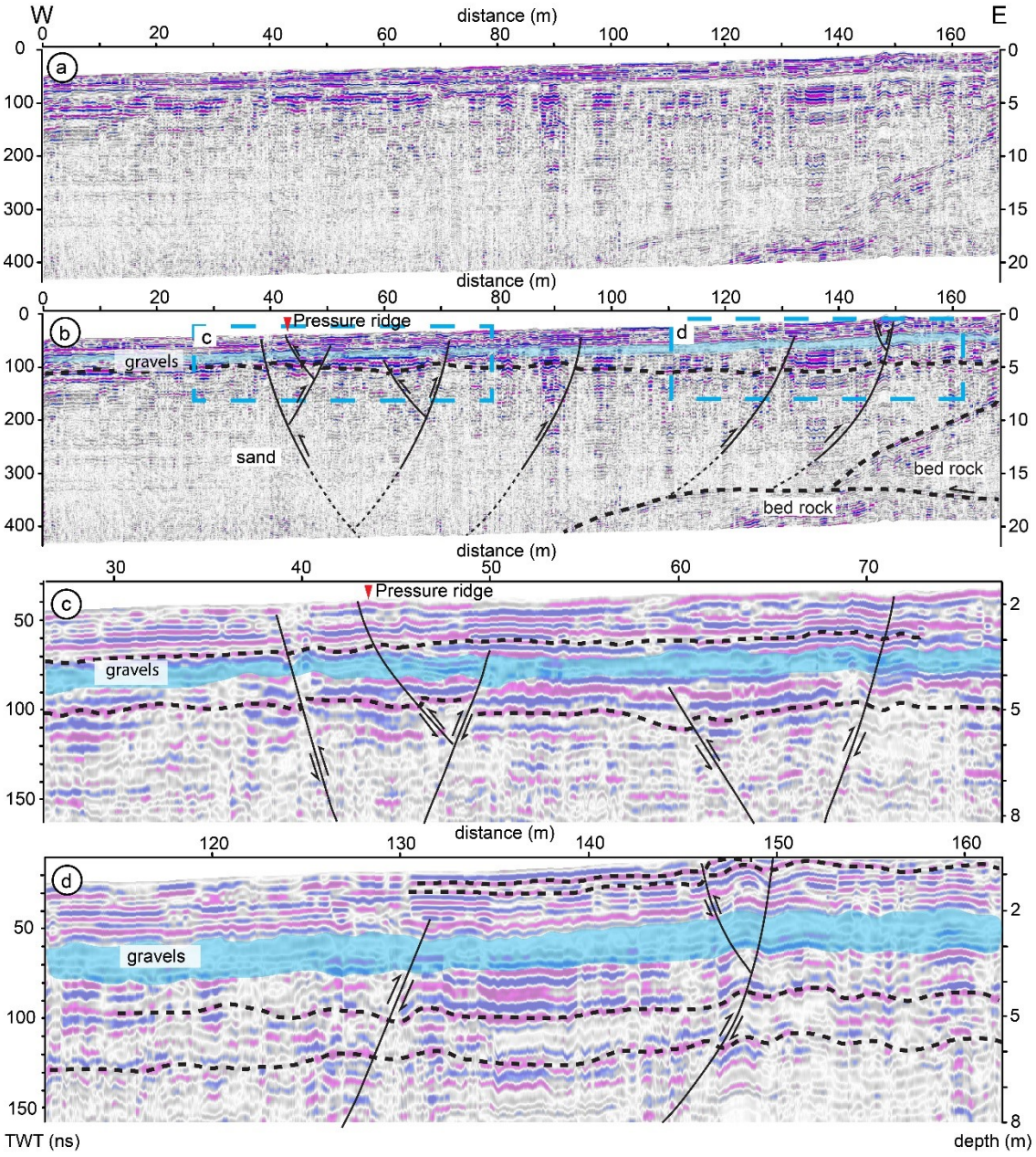

Fig. 4.6 Shows the GPR profile along the line marked in Fig. 4.4. The cross-section view of the bed rock overlain by the Quaternary sediments is represented in two-way time (TWT) in nanoseconds (ns) and depth (m). Dotted lines mark deformed reflectors.

The foreland at Khairabad consists of the QKC and QAL sediments. The mountain front is characterized by a pressure ridge parallel to the KBF (Fig. 4.4). Two surface ruptures (R1 and R2) are present near the KBF, each ~ 200 m in length (Fig. 4.4). These fault ruptures have disrupted Quaternary sediments, starting in the southeast near the main strand of the KBF and blinding in the northwest. The R1 has an offset of 30 cm, while that of the R2 is up to 80 cm. The surface ruptures contain travertine deposits at the surface and in the interstitial spaces between conglomerates.

GPR data near the fault ruptures exhibit poor quality. Whereas GPR data was also acquired along a track with least surface gravels and less topographic variation, at an oblique angle to the KBF and the pressure ridge (Fig. 4.4 and 4.6). The GPR data was later utilized to check for lateral extension of the R1 and R2, offsets and subsurface structural configurations in the Quaternary sediments in paleoseismic trenches. The GPR profile reveals the thrusted bedrock (Fig. 4.6b). Whereas an east dipping fault at 39 m horizontal distance is also identified in Quaternary sediments. Moreover, five West dipping reverse faults join this East dipping synthetic fault, making a flower structure (Fig. 4.6b). These faults are steeply dipping near the surface and gentler in the depth. Shallow synthetic faults that join these antithetic faults in the flower structure are also marked at 43 m and 146 m. The pressure ridge across the GPR profile is situated above a pop-up structure at 44 m horizontal distance scale (Fig. 4.6c). A deformed gravel layer is identified at ~2-4 m depth. Stream water at the mountain front is percolated through these gravels, causing the disappearance of surface runoff in the foreland. Apart from the bedrock identified in the GPR data, the faults marked on the GPR profile have deformed the Quaternary sediments including the QKC and QAL.

Trench investigations are used to correlate the interpretations from the GPR and its lateral extension towards the surface ruptures. Six paleoseismic trenches were logged near the KBF. Trenches 1,2 and 3 (T1, T2 and T3) were perpendicular to the KBF and the surface ruptures. The limestone of PZG is thrusted in the SW direction. Therefore, Trench 4 was aligned in NE-SW direction to check for the Quaternary offsets caused by the NE-SW stress, and lateral extension of the faults in T1. Moreover, the stream close to the GPR profile in Fig. 4.4 consists of loose sand and gravels. Trench-5 (T5) was excavated perpendicular to the GPR profile to check for lateral compressions caused by strike slip movement. The trenching conditions were not favorable near the stream. Therefore, T5 was confined to 5 m length and 2 m depth. Trench-6 (T6) was excavated to check paleoseismic offsets in the hinterland.

Trench log from T1 reveals an East dipping fault, synthetic with the KBF, along the R1 at 8 m distance (left-right in Fig. 4.7b). The units-3 and 5 reveal a 30 cm offset along this fault. The units-2 and 6 are not correlated between both blocks of the fault due to the lateral offset. These dip slip and strike slip

displacements imply transpressional kinematics for this fault. The travertines are deposited along the fault plane, in the interstitial spaces of sediments and cover the fault trace (Unit 5 in Fig. 4.7b). This fault along R1 has a lateral extension in T4 in the NW and blinds into the subsurface. This fault is beyond the GPR profile in Fig. 4.6. The units-2 and 3 are folded and back tilted, also deforming the unit-4. These units exhibit two blind reverse faults at 2 m and 5 m distance. The sediments along these faults exhibit offsets of ~ 30 cm. Whereas, a fault with 5 cm offset reaches up to the surface at 2 m.

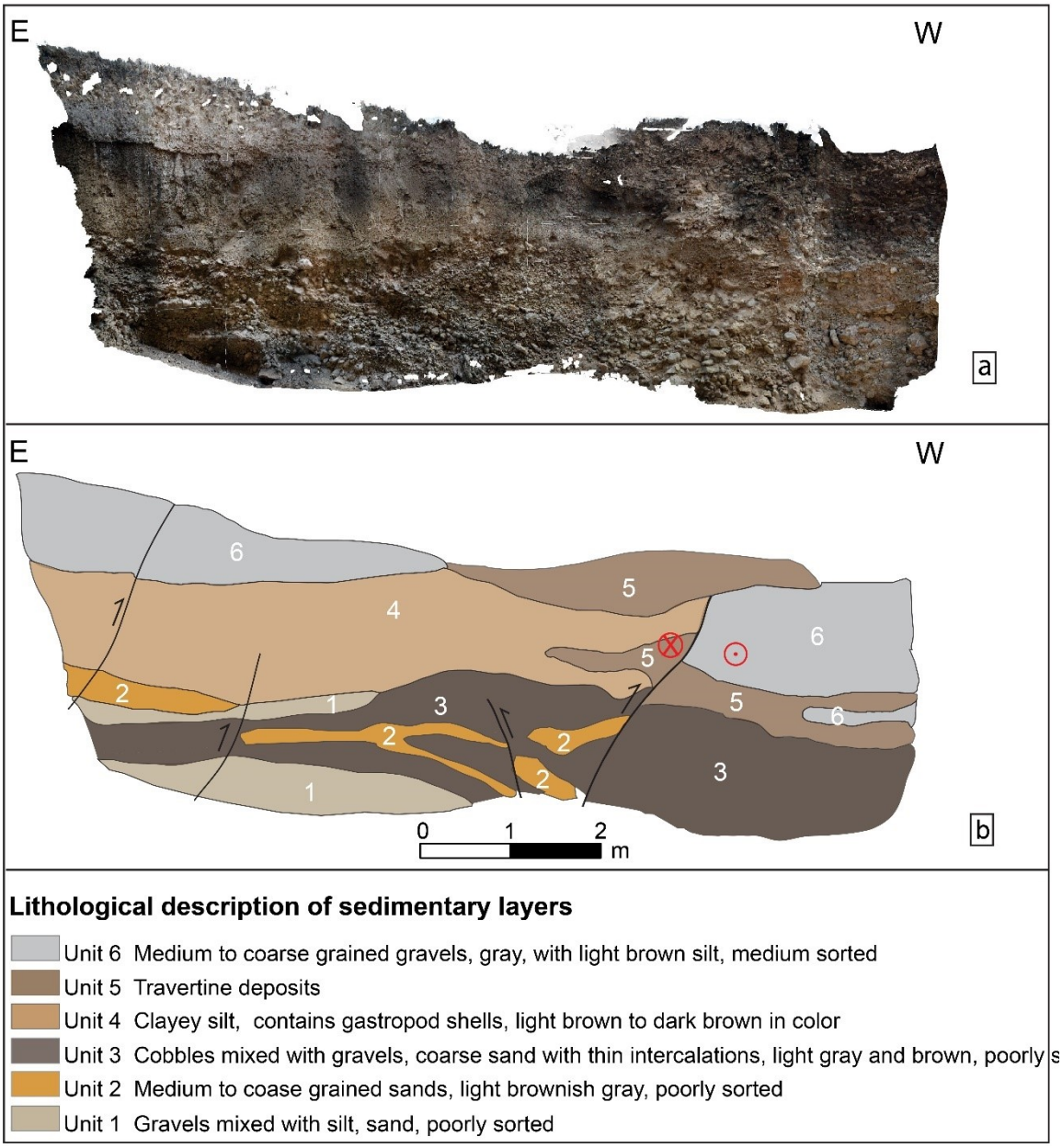

Fig. 4.7 (a) orthomosaic image of the southern wall of trench T1 (b) trench log from Fig. 4.7a, marks lithological and structural variations in T1.

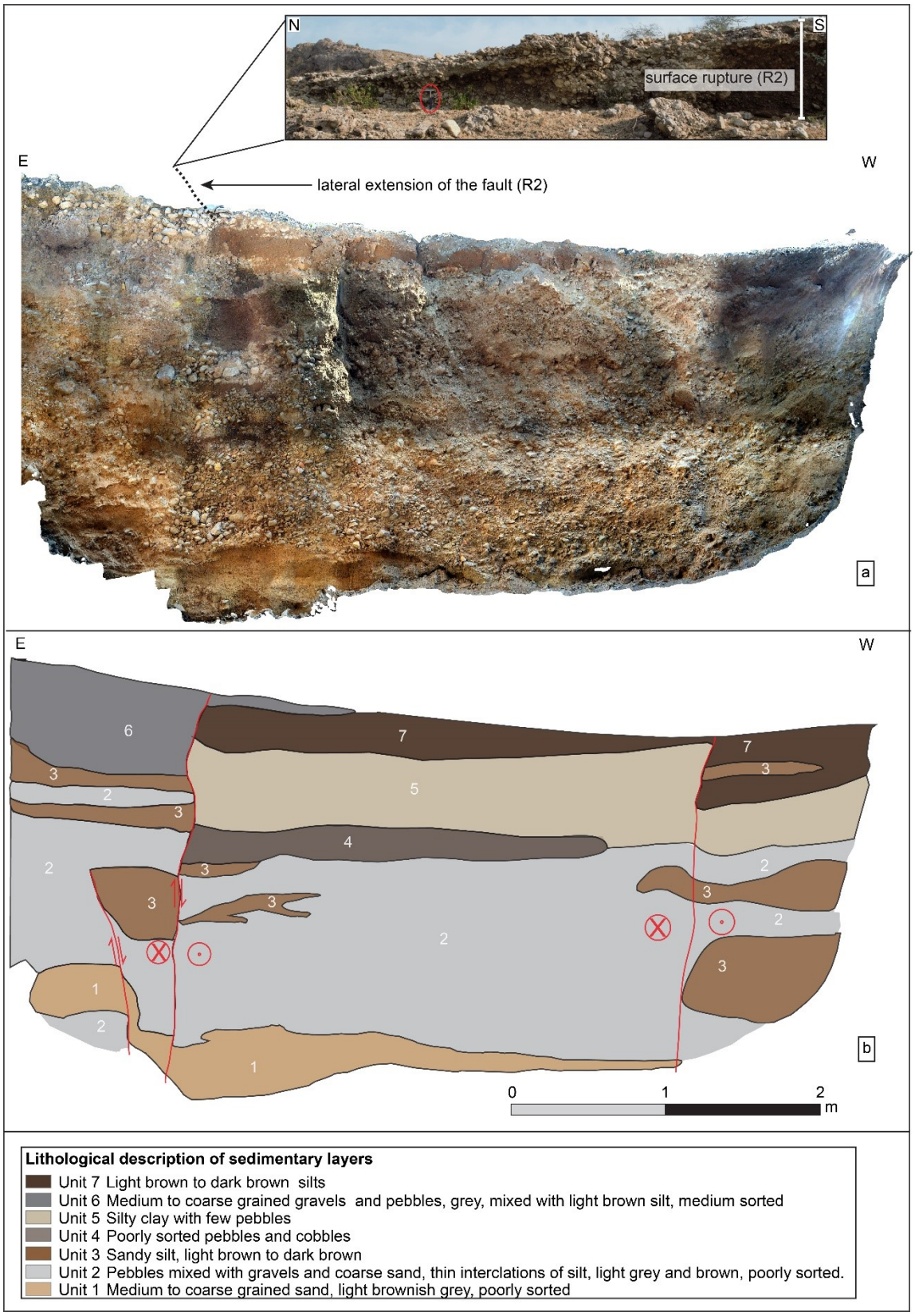

Fig. 4.8 (a) orthomosaic image of the southern wall of trench T3, (b) log from the southern wall of trench 3 indicates variation of sediments across the faults. The eastern Part of the trench wall is across the surface rupture shown in the inset image and marked in the Fig.4.4.

Trench 3 (T3) is also perpendicular to the KBF (Fig. 4.4) across the R2 (Fig. 4.8). This trench is 5.5 m long and 2.5 m deep and exhibit disrupted layers at three places. A fault is located at 1.3 m (left to right in Fig 4.8), forming R2. The R2 strikes NW-SE and blinds in the NW. The unit-7 in T3 forms an alluvial wedge on the footwall of the reverse fault. Sedimentary layers on either side of this fault does not match, whereas, offset in the unit-3 indicates a reverse slip component associated with the R2. These evidences imply transpressional kinematics for this fault. The fault plane of R2 consists of pebbles that are fractured and filled with calcite, whereas the travertine deposits are not considerably witnessed in T3. A blind fault in the East imbricates with this fault along R2. Another fault is identified in the West at 4.5 m, exhibiting weak correlation of the sedimentary units on either side of the fault (unit-3 and 5), implying a strike slip displacement. Moreover, the unit 3 that crosses this fault at 1 m depth, does not reveal considerable dip slip component. This implies that the offset in the unit-5 also lack dip slip component and variations in this sedimentary unit across the fault are only influenced by the strike slip displacement.

Trench 4 (T4) was excavated to record foreland compression against the NE dipping PZG rocks. This trench was aligned at an oblique angle to the main KBF and T1. Trench investigations reveal extension of the fault along R1 and associated travertine deposition in T4. The fault further blinds in the NW. Another offset in T4 is identified in the East and marked in Fig. 4.4. Trench 2 (T2) that is topographically higher than T1, does not show any lateral extension of this fault. Furthermore, trench 5 (T5) is aligned perpendicular to the GPR profile in Fig. 4.6. Lateral compression in the blocks of the strike slip movement is recorded by a flexure with 20 cm vertical displacement in the Quaternary sediments. This flexure strikes perpendicular to the structures in the GPR profile, implying a southward moving block in the East of the West-verging reverse fault in Fig. 4.6b, indicating right lateral transpressive kinematics for this fault. Moreover, Trench 6 (T6) marked on the Fig. 4.4 was excavated to record the hinterland deformations. This trench is 10 m long and 3 m deep, located in the East of the main strand of the KBF, near the highly sheared PZG limestone. The faults marked in the East of the KBF in Fig. 4.4 does not cross T6 and are laterally extended based on the evidences from the adjoining streams. T6 exhibit sheared diorite gravels resembling those in the Fig. 4.5d. Shearing in the pebbles implies post depositional deformation in the hinterland.

4.4.1.2 Larkakki section

The Larkakki section is situated in the South of the restraining faults at Zaluch (Fig. 4.2 and 4.3). The mountain front at this section exhibits the sandstones of the Permian Nilawahan Group (PNG) and limestones of the PZG. The limestone at the frontal part is sheared and dips in the NE direction. An alluvial fan is developed at Larkakki with a radius of 1 km. The mountain front at the apex of the alluvial

fan exhibits a terrace. Here, the Quaternary sediments are uplifted ~15 m from the apex of the alluvial fan. Alluvial fan sediments are also deformed at proximal distance from the apex. Fig. 4.9a shows outcrop from the incised channel on the alluvial fan at Larkakki. Pebble alignment and sedimentary contacts reveal folding in the sediments. Back tilting is evident at 2.5 m (Left to right in Fig. 4.9a). A west dipping fault, antithetic to the KBF, is identified at 1 m that does not extend up to the surface. Alluvial fans in the South of Zaluch are smaller in size and sediments are less consolidated.

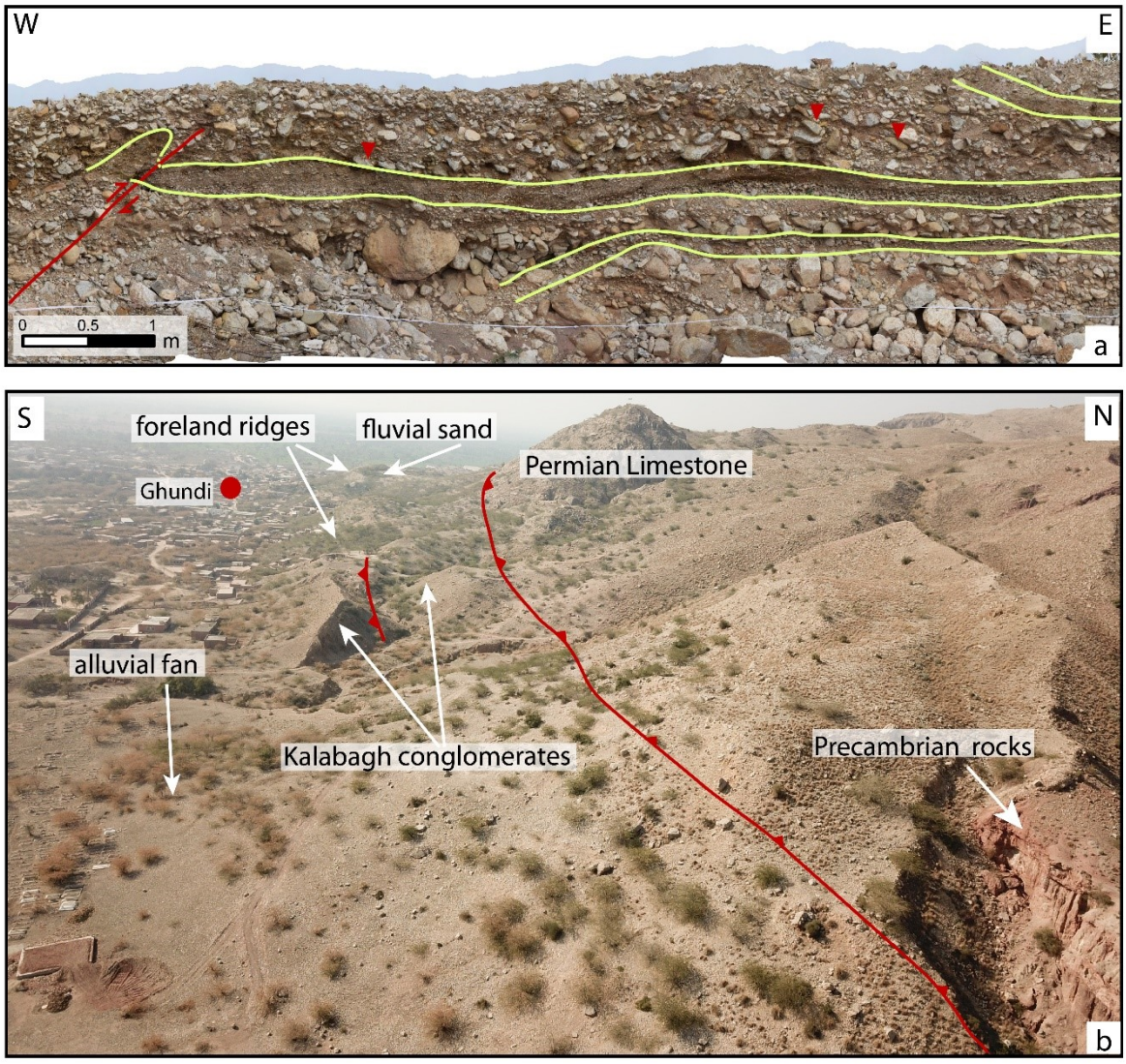

Fig. 4.9 a) Sediment deformation along a channel on the Larkakki alluvial fan marked on Fig. 4.2 and 4.3. (b) Southern flank of the push up block at the Ghundi stepover. Precambrian rocks are juxtaposed against the Quaternary deposits at the mountain front. Deformation in the Quaternary sediments is marked by the fault and ridges that also extend across the alluvial fan.

4.4.1.3 Ghundi Section

The Ghundi section is located at the lobate area of the ~10 km wide fault stepover (Fig. 4.1, 4.2 and 4.3), also termed as the Ghundi lobe. The KBFZ is marked by the PZG rocks (Fig. 4.9b) and Precambrian evaporites (PCSR), thrusted against the Quaternary sediments in the East of Ghundi. The foreland at

the Ghundi lobe exhibits foreland ridges trending in the NS direction in the West of the Ghundi lobe and extend in the EW direction to the South of the stepover zone (Fig. 4.9b). These ridges consist of the QKC sediments at the surface underlain by fluvial sands. These sands are identical to those of the Khairabad section. We define the ridges at the Ghundi lobe as folded and antithetically faulted sediments from the foreland (Fig. 4.9b). A ridge crosses apex of an alluvial fan at Ghundi. The alluvial fan is degraded exhibiting bad land topography. A Mw=4.6 earthquake was recorded in the South of this section in 1993 A. D. (Fig. 4.1b).

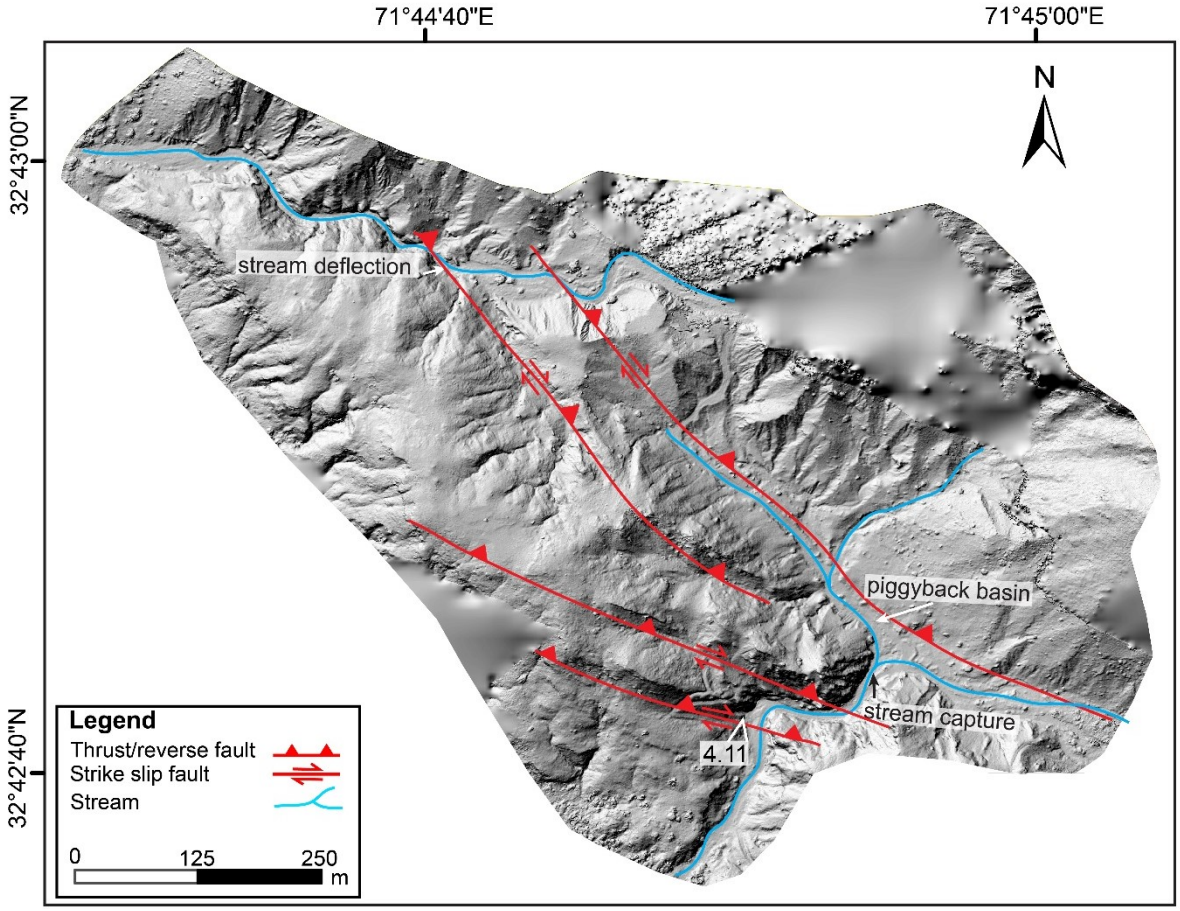

Fig. 4.10 Digital elevation model from Burikhel village along the Nammal Ridge (Fig. 4.2). Shows repeated thrusting that created a small piggyback basin which was captured by a stream. The streams are deflected in left stepping patterns.

4.4.1.4 Nammal Ridge

The KBFZ in the southern segment yields a ridge, termed as the Nammal Ridge (NR), that has separated the Potwar Plateau (Fig. 4.1b) from the Mianwali Reentrant (MWR). The Nammal Ridge exhibits thrusted and back thrusted rocks along the KBFZ (Fig. 4.2). A stream has incised down the sedimentary rocks and the Nammal lake in the Potwar Plateau with the Mianwali Reentrant. The Nammal lake peripheries consist of Quaternary sediments, that are uplifted and consolidated, implying deposition at the very initial stages of the ridge uplift. At Burikhel village, repeated faulting has cropped out the PCSR rocks in the KBFZ (Fig. 4.10 and 4.11). This faulting has formed a small and elongated piggyback

basin between these reverse faults, filled with fine grained sediments from the nearby provenance. A stream has created a wind gap by connecting the piggyback basin with the foreland. The stream is later deflected by the right lateral faulting (Fig. 4.10). The Precambrian sediments are juxtaposed against the Quaternary sediments along the southernmost fault (Fig. 4.10 and 4.11a). This fault exhibits fractured pebbles embedded in the marlstone of Precambrian. These pebbles are disrupted at an angle of N35°W (Fig. 4.11b and 4.11c). Displacement in the pebbles suggest right lateral kinematics for the fault.

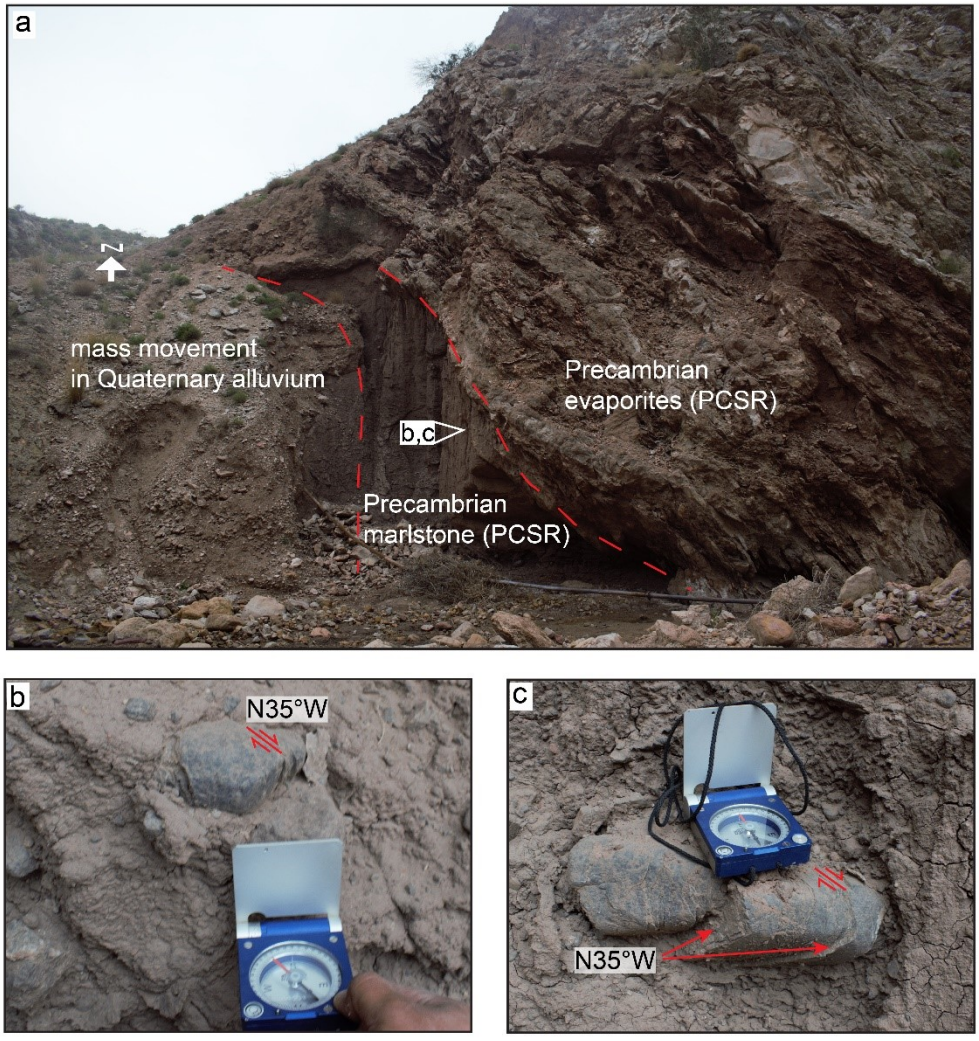

Fig. 4.11 (a) The Precambrian Salt Range Formation thrusting out at Burikhel (Fig. 4.2 and 4.11). (b and c) show fractured pebbles that represent the kinematics of the Kalabagh Fault along the Nammal Ridge.

4.5 Discussion

In this section, evidences regarding the paleoseismicity, active tectonics and subsequent landform development in the KBFZ are discussed. Moreover, arguments about the westward diversion of the Indus River are established. Interpretations are also integrated to present the schematic block diagram for the Khairabad section (Fig. 4.12) and landform development model of the KBFZ (Fig. 4.13).

Offsets in sedimentary layers that extend into deeper subsurface are related to seismic displacements along the faults. Whereas these offsets are younger than the sedimentary layer itself. Here, the QKC and QAL are described in the literature as late Pleistocene and Holocene sediments, respectively (e.g. Gee, 1980). Therefore, any distortions in the QKC and QAL are considered post depositional and younger than these sediments. Sedimentary layer offsets, uplifted channel sediments, deflected streams, fault ruptures and a pressure ridge have deformed the Quaternary sediments at the Khairabad section. These features are distributed in the piedmont and frontal part of the KBFZ.

The fault along R2 in T3 strikes NW-SE, aligned with the East dipping fault to the West of the pressure ridge (Fig. 4.6b). The strike and kinematics of both faults inferred from T3 and GPR profile implies that the fault in GPR profile is a lateral extension of R2 and regarded as a single synthetic fault, an offshoot of the KBF (Fig. 4.12). This KBF offshoot is steeper near the surface and gentler in the depth where it imbricates with the main strand of the KBF. Similarly, the fault along R1 that is identified in T1, extends in the NW in T4 and strikes NW-SE (Fig. 4.4). This transpressive fault blinds in the NW and is interpreted to continue beyond the extent of the GPR profile in Fig. 4.6. Deposition of travertines along R1 indicate that the fault is deep and facilitates upward migration of water from calcite provenance. Therefore, the fault along R1 is interpreted as another offshoot of the KBF. Undisturbed travertine deposits have cross cutting relationship with the R1, indicating their youngness as compared to the earthquake that has formed the R1. Since then, the fault has not been activated. Whereas the West dipping faults identified in T1, T3 and GPR profile join the KBF offshoots. These faults combined with the back tilted sedimentary layers are resulted from the foreland stress on the offshoots of the KBF. These ~5-30 cm vertical displacements can be shallow aseismic adjustments to accommodate foreland stress. The faulted bedrock in Fig. 4.6b is also disrupted along the offshoots of the main strand of the KBF.

The stream deflections (Fig. 4.4) follow the right lateral kinematics of the transpressive fault in the East of the KBF (Fig. 4.5a), implying these faults as eastern offshoots of the KBF. These streams have incised down the late Pleistocene-Holocene sediments (Gee, 1980) followed by the right lateral displacements, forming stream deflections. The faults marked along the fault trace (Fig. 4.4) and disrupted sediments (Fig. 4.5a) are aligned along the faults identified in headward eroding stream (Fig. 4.4 and 4.5c). Similar to R1 and R2, these offshoot faults get steeper towards the South, and form flower structure with the KBF.

The sedimentary layer offsets identified in the late Pleistocene-Holocene sediments in the Khairabad section are linked with the transpressive seismic displacements along the KBF. These offsets exhibit vertical displacements of ~50-100 cm in one seismic event (Fig. 4.5a and 4.5c). This implies the uplift of the stream channel up to 8 meters is caused by ~12 ± 4 seismic events, that formed a surface

rupture. Therefore, late Pleistocene-Holocene ages of these deformed sediments indicate that the KBF and its offshoots have been seismically activated nearly 10 times during the late Pleistocene. The above discussion coupled with the LOS displacement rates by Chen and Khan (2010) imply that the Khairabad section is seismically active with a long earthquake recurrence interval due to aseismic creep, as suggested by Barnhart (2017).

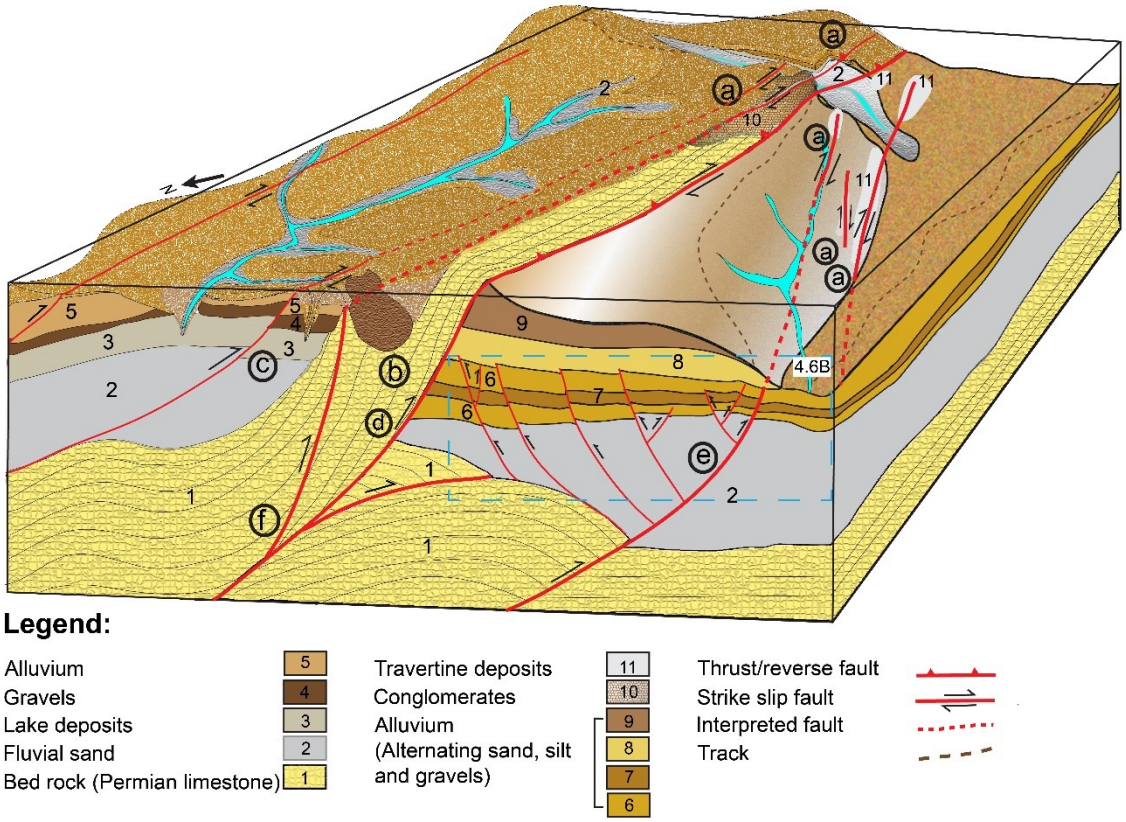

Fig. 4.12 Integrated schematic model of the Khairabad section made from DEM, GPR data, surface geology and trench logs. (a) surface expressions of the youngest faults, (b) uplifted stream, (c) fault that has disrupted the late Quaternary sediments deposited in the piggyback basin, (d) the Kalabagh fault (KBF), (e-f) offshoots of the Kalabagh fault.

The KBFZ at Larkakki section is tectonically less active. The uplifted sediments belong to alluvial fan deposits that has been uplifted during seismic displacements along the KBF. However, there are no other evidences that may support recent/Holocene seismicity. Like the Khairabad section antithetic displacements and back tilted sediments at the Larkakki alluvial fan indicate strain development resulted from the foreland stress against the KBFZ (Fig. 4.9a). Therefore, the KBFZ at Larkakki is seismically less active, however, foreland stress can cause seismicity and subsequent deformation on the alluvial fans.

Deformations in QKC and QAL sediments in the foreland ridges at Ghundi indicate head on collision between the KBFZ and the foreland is under active stress accumulation. These ridges coupled with the degraded alluvial fan surface imply seismic uplift at the apex of the fan along a back thrust, followed by the diverted course of feeder stream and ultimate degradation of the fan surface. A recent M_w=4.5

earthquake in the south of this stepover zone also indicate release of energy, accumulated by foreland compression. Furthermore, the thrusted PCSR sediment at Burikhel, juxtaposed against the QAL sediments, contain fractured pebbles designating the right lateral transpressive kinematics of the fault. Deposition of fine-grained sediments in the piggyback basin was followed by the stream capture. Later seismic displacements have formed right lateral deflections in this stream. The QAL sediments from the piggyback basin predate the incision and deflection of this stream. It is therefore concluded that the KBF has been activated during Holocene or late Pleistocene.

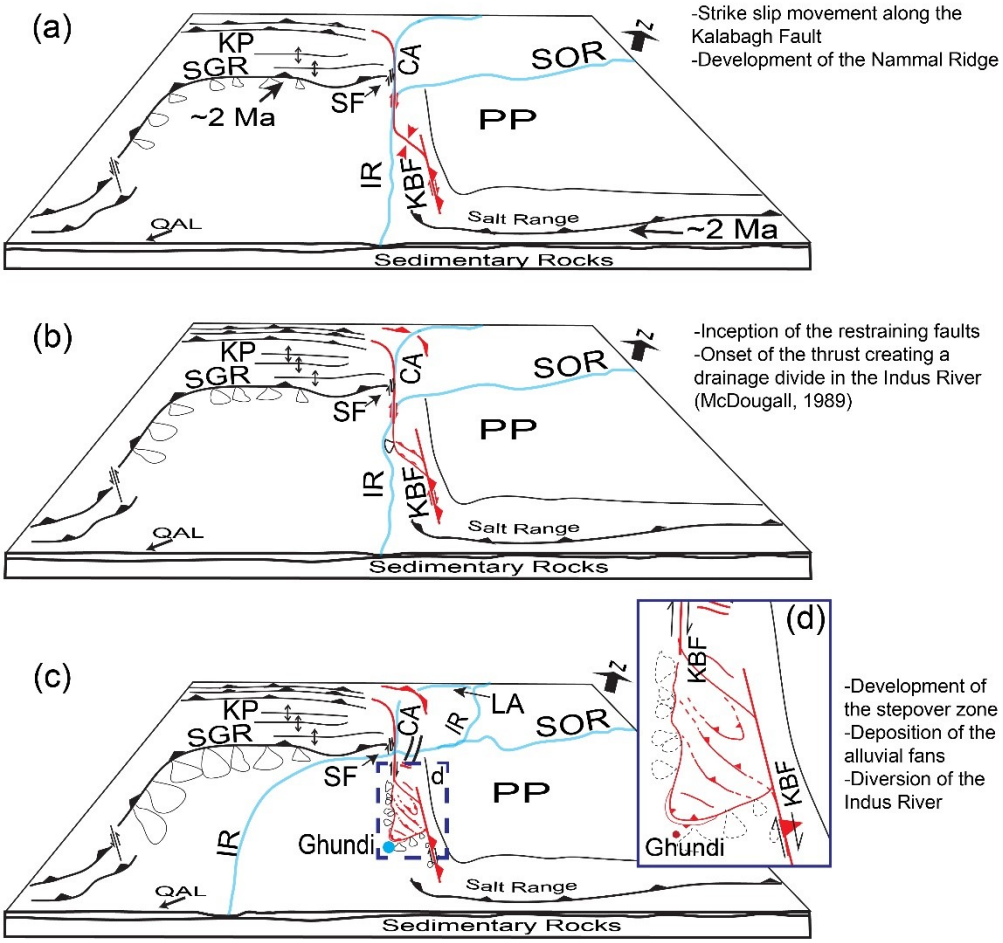

Fig. 4.13 Schematic model of the Kalabagh Fault. (a) shows two segments of the Kalabagh fault before the development of the fault stepover. While the Indus River was flowing in N-S direction. The Main Frontal Thrust has emerged at ~2 Ma giving rise to the Potwar Plateau and the Kohat Plateau. (b) Inception of restraining faults (c) development of the stepover zone along with the westward migration of the Indus River. The Eastward migration of the Indus River from the Chisal Algad and the Lagorai-Algad streams is marked after McDougall, (1989). (d) shows zoomed in image of the stepover zone. CA=Chisal Algad, IR=Indus River, KBF=Kalabagh Fault, KP=Kohat Plateau, LA=Lagorai Algad, PP=Potwar Plateau, QAL=Quaternary alluvium, SF=Surghar Fault, SOR=Soan River

Fault segments in the KBFZ has revealed earthquakes that cause surface ruptures with vertical displacements up to 1 m. Such type of surface expression is formed by the seismic events of M_w=5.5-6 (Lettis et al., 1997; Michetti et al., 2000; Vittori et al., 2000; Wells and Coppersmith, 1994). Whereas,

surface ruptures with 1 m vertical displacement may be resulted from much bigger seismic event (Vittori et al., 2000). Therefore, the seismic events at Khairabad, Ghundi and Burikhel had M_w=6 or more.

The landform development of the stepover zone is described based on the alluvial fan characteristics, geometry and active tectonic features of the KBFZ. The size of an alluvial fan may depend upon various factors including catchment area, uplift and ultimate incision rates and age of the fan. Only the size of the alluvial fans in the West of the KBFZ cannot define the age of these fans. Deeply incised streams in high relief mountains indicate more uplift and sediment influx between the restraining faults, forming larger alluvial fans. Moreover, consolidation level of the sediments on these alluvial fans is an indicator of the earlier deposition, compared with the unconsolidated alluvial fans in the South. The active fan development on these fans was terminated before the adjacent alluvial fans as the gully erosion on these fans is relatively mature. Therefore, alluvial fans formed in the West of the mountain front between the two restraining faults of the KBFZ, are chronologically older from the adjacent fans. Hence, the inception of stepover zone of the KBFZ occurred from a left stepover between the two restraining faults. This stepover was later developed in the North towards Khairabad and in the South towards Ghundi, that are the active tectonic fronts of the stepover and exhibit active morphotectonics discussed earlier.

The Indus River sediments are used by McDougall (1989) as the key indicator of the paleo channel of the river. The Soan River (SOR) and the IR are the source of sediment influx in the study area. Whereas transportation and deposition of the well-rounded diorite pebbles is only possible from the Karakoram and Kohistan ranges in the North Pakistan, from where the Indus River flows. The presence of the diorite pebbles in the Khairabad section is indicative of the provenance identical to that of the paleo Indus River channel in the Chisal-Algad stream (Fig. 4.1 and 4.5d). This is also unlikely that the diorite pebbles are originated from the ridge in the North of the Khairabad section because the pebbles are well rounded and far derived. Hence, these pebbles were deposited before the uplift of the ridge in the North. Resemblance of fluvial sands at Khairabad and Ghundi also imply the deposition under the fluvial environment. We infer from these evidences that the Indus River has been flowing from the North to the South along the KBF before the landform was developed in the stepover zone (Fig. 4.13). Chronology of these Indus River sediments need to be investigated to date the landform development of the stepover zone and diversion of the Indus River. However, ~0.5 Ma age for the top of TSK and deposition of the QKC sediments over TSK in the East and West of the KBFZ (Fig. 4.2) implies the inception of the KBFZ stepover is synchronous with the termination of the TSK deposition. Therefore, the westward diversion of the Indus River is also synchronous with the eastward shift of the Indus

River in the North. Mechanism of the diversion of the IR is illustrated in fig. 4.13. The inception of the stepover along the restraining bends formed the first surface expression of the stepover and initiated the deposition of the alluvial fans in the West of the KBFZ, thus creating a meander in the Indus River (Fig. 4.13 b). In the subsequent phases, the landform of the stepover zone evolved in the North and the South of the restraining faults, forming more alluvial fans in the West (Fig. 4.13c). This uplift of the stepover zone and deposition of thick alluvial fans has diverted the Indus River towards the West to develop the equilibrium in the Mianwali Reentrant.

4.6 Conclusions

Morphology, outcrop geology and shallow sub-surface structures were investigated to delineate the evolution and neotectonics of the KBFZ. The KBF is a segmented fault that has formed a stepover zone between the restraining faults of the two segments. The stepover zone was further developed towards the North and the South. The landform development in the stepover zone and subsequent alluvial fan deposition has diverted the Indus River towards the West. The Khairabad and the Ghundi sections are the active tectonic fronts of the KBFZ stepover. Late Quaternary offsets along the KBF are denoted to seismic events with $M_w \geq 6$. The foreland is exerting stress on the KBFZ that may cause earthquakes, forming surface ruptures. The earthquake recurrence interval at Khairabad is estimated to reach ~10 ka or more due to release of energy during aseismic creep. The head on collision and lesser aseismic displacements suggest more seismic vulnerability at Ghundi.

Acknowledgments

We would like to thank the Higher Education Commission of Pakistan and the German Academic Exchange Service (DAAD) for the financial and management support for this research. We are also grateful for the field cooperation by Farooq Sultan from the Mines and Minerals department, Punjab, Pakistan. While discussions and comments from Rashid Haider, RWTH Aachen University, were also helpful in interpretations.

5. Pleistocene-Holocene deformation and seismic history of the Kalabagh Fault in Pakistan using OSL and post-IR IRSL dating

Abbas, W., Zhang, J., Tsukamoto, S., Ali, S., Frechen, M., Reicherter, K., (202). Pleistocene-Holocene deformation history of the Kalabagh Fault in Pakistan using OSL and post-IR IRSL dating. Quaternary International.

Abstract

The Kalabagh Fault forms a lateral offset in the Main Frontal Thrust in the Sub-Himalayan area of Pakistan, forming a push-up block within the stepover zone of its segments. Deformed sediments along the frontal part of this push-up block have cross cutting relations with morphotectonic and paleoseismic features. These sediments are dated using luminescence dating methods. The post-infrared infrared stimulated luminescence (post-IR IRSL) of K-feldspar was used for samples representing these sedimentary units. For stratigraphically younger sediments with partially-bleached pIRIR signal, optically stimulated luminescence (OSL) of quartz was applied with the minimum age model (MAM). These ages are used to illustrate the timing of development of the push-up block, the westward diversion of the Indus River and Holocene earthquakes along the Kalabagh Fault (KBF). The deformed sediments from the mountain front at Larkakki are older than those of Khairabad and Ghundi. These age estimates are consistent with the chronological order of the tectonic deformations in the stepover zone of the Kalabagh Fault. Age estimates and correlation of the sedimentary units suggest the emergence of the push-up block in the stepover zone during the past ~ 0.5 Ma. Active faulting and development of the ramp along the Kalabagh Fault has diverted the course of the Indus River towards the west at a displacement rate of 12-15 cm/a during last ~140 ka. Luminescence data indicate Holocene timing for the earthquakes along the Kalabagh Fault, which are diachronous and suggest differential movements along the segments of the fault. The earthquake recurrence interval at Khairabad is about 10 ± 2 ka on average. The younger earthquakes at the foreland in the south of the stepover indicate seismically active zone.

Keywords: OSL; Post-IR IRSL dating; Active faults; Earthquakes; Strike slip fault; Kalabagh fault

5.1 Introduction

Historic and pre-historic earthquakes have been studied to establish the seismic behavior of faults (James P. McCalpin, 2009; Quittmeyer and Jacob, 1979; Van Balen et al., 2019). The available earthquake catalogues, that mainly depend on historical and instrumental data, may only span up to few hundreds of years, whereas the faults with long earthquake recurrence intervals may not be activated during this period (Abbas et al., 2022). Therefore, instrumental and historical earthquake

records are sometimes not helpful to investigate faults with longer earthquake recurrence intervals. The timing and slip rate of paleoearthquakes are recoverable beyond the range of historical archives and can be used to infer the probable future earthquakes (J.P. McCalpin, 2009; Mozafari et al., 2019). Chronology of paleoearthquakes is needed to cover the complete seismic cycle for estimation of the recurrence intervals of surface rupturing earthquakes along a fault. Multiple paleoseismic approaches have been used to identify (pre-)historical earthquakes (McCalpin and Nelson, 2009 and references therein). The ages of seismically deformed sediments are determined nowadays to illustrate the timing of the paleoseismic events and deformation history of faults (e.g. Fattahi et al., 2006; Kagan et al., 2018; Mozafari et al., 2019). For this purpose, multiple dating methods are adopted including radiocarbon dating, cosmogenic nuclide dating and luminescence dating (e.g. Ivo et al., 2000; Mozafari et al., 2019; Sohbati et al., 2012). Moreover, strike slip faults have visible geomorphic expressions and long records of seismicity (McCalpin et al., 2009). The chronology of those seismic events thus leads to infer the deformation history of the faults, earthquake recurrence intervals and timing of the latest seismicity.

The Kalabagh Fault (KBF) is a dextral strike slip fault in Pakistan (Fig. 5.1c) that exhibit morphotectonic and paleoseismic features (Abbas et al., 2022). The instrumental seismic records (between 1953 and 2019 A.D.) do not show any considerable earthquake (Fig. 5.1c) along the KBF (USGS earthquake catalogue, 2019). Abbas et al. (2022) have identified paleoearthquakes that have deformed Quaternary sediments at the mountain front along the KBF and alluvial fans. The ages of these seismically deformed sediments are indicators of the timing of the earthquakes. The Quaternary sediments are underlain by the Siwalik Group (TSK) of sediments in the study area. The TSK were deposited from the late Tertiary until ~0.4 Ma (Gee, 1980; Johnson et al., 1979; Keller et al., 1977; Khan, 1983; Yeats et al., 1984). The chronology of the sediments younger than the TSK was not investigated to date. This indicates a research gap that needs to be filled with a reliable chronology for the seismically deformed sediments that are younger than the TSK. Moreover, the Indus River was flowing in the north-south direction until the landform development in the KBF stepover zone have shifted the Indus River ~15-18 km westward from the KBF (Abbas et al., 2022). The Indus River sediments are uplifted and deformed at Khairabad and Ghundi. The chronology of these sediments thus illustrates the history of the deformation along the KBF and timing of the north-south flow of the Indus River near the KBF. This also allows deducing the rate of the westward migration of the Indus River.

This study is carried out to determine the ages of the deformed Quaternary sediments using optically stimulated luminescence (OSL) and post infrared-infrared (pIRIR) dating methods. These ages combined with geological evidences from Abbas et al., (2022) and stratigraphic correlations are used

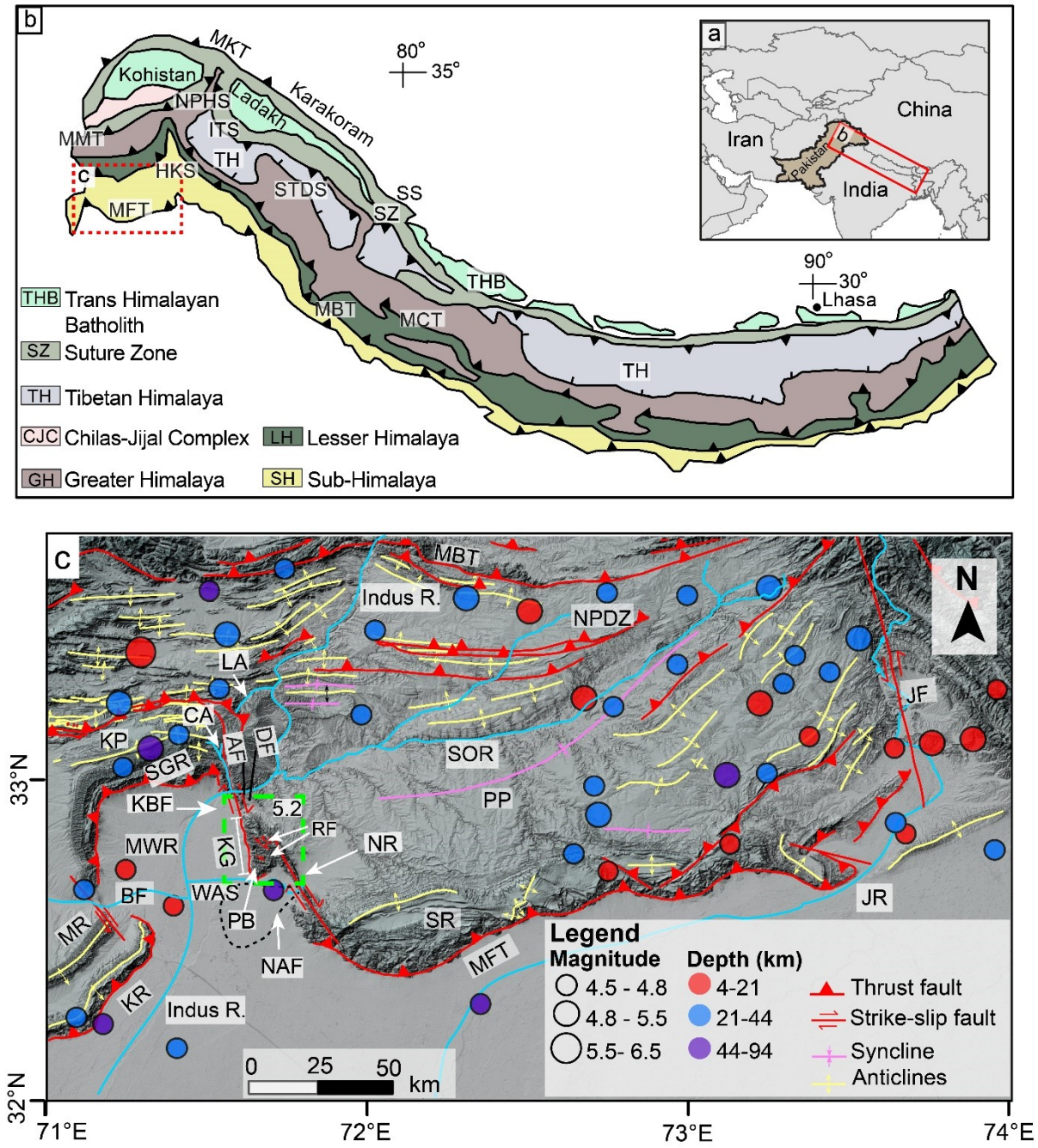

Fig. 5.1 (a) Geographic location of the study area, (b) location of the Potwar Plateau in the Himalayan framework (modified after Ali et al., 2018; Searle and Treloar, 2019), *(c) tectonic map of the study area showing the main structural features along the KBF (modified after Abbas et al. (2022), Abir et al., 2017; Alam, 2008; Ali, 2010; Kazmi and Rana, 1982) based on digital elevation models from ALOS 30 m and satellite imagery of ArcGIS. Instrumental seismicity (between 1953 and 2019 A.D.) is plotted to show depth and magnitudes of earthquakes (USGS earthquake catalogue, 2019). The rectangle marks the extent of the map in Fig. 5.2. AF=Ainwan Fault, BF=Bannu Fault, CA=Chisal Algad, DF=Dinghot Fault, KBF=Kalabagh Fault, HKS=Hazara Kashmir Syntaxis, Indus R.=Indus River, ITS=Indus-Tsangpo Suture, JF=Jhelum Fault, JR=Jhelum River, KP=Kohat Plateau, KR=Khisor Range, KBF=Kalabagh Fault, KG=Khairabad-Ghundi Section, LA=Lagorai Algad, LR=Lateral Ramp, MBT=Main Boundary Thrust, MCT=Main Central Thrust, MFT=Main Frontal Thrust, MKT=Main Karakoram Thrust, MMT=Main Mantle Thrust, MR=Marwat Range, NPDZ=North Potwar Deformed Zone, NPHS=Nanga Parbat Haramosh Syntaxis, NAF=Nammal Alluvial Fan, NR=Nammal Ridge, PB=Push-up Block, RF=Restraining Fault, SR=Salt Range, SGR=Surghar Range, SOR=Soan River, SS=Shyok Suture, STDS=South Tibetan De, MWR=Mianwali Reentrant, SS=Shyok Suture, TH=Tibetan Himalaya, SGR=Surghar Range, WAS=Wahi Stream.*

to determine the timing of: (a) landform development of the push-up block in the stepover zone of the KBF, (b) the latest earthquakes with surface ruptures and (c) the tectonically induced westward diversion of the Indus River. Thirteen samples were collected from the sediments across the surface ruptures, uplifted sediments at the mountain front and displaced sediments at the apex of the alluvial fans. These samples represent Paleoseismic and morphotectonic features identified by Abbas et al. (2022), from Khairabad, Larkakki, Ghundi and Burikhel (Fig.5.2).

5.2 Study area

The Main Frontal Thrust (MFT) in the Sub-Himalayas of Pakistan shows a right lateral offset of ~70 km between the Salt Range and the Surghar Range, marked by the transpressional Kalabagh Fault (KBF). The KBF extends from south to north (Fig. 5.1c) between the western termination of the Salt Range up to the eastern margin of the Kohat Plateau (KP), where it turns westwards, parallel to the north dipping faults in the Kohat Plateau (McDougall and Khan, 1990). The KBF marks the tectonic boundary between the Potwar Plateau-Salt Range block in the east, the Kohat Plateau-Surghar Range block and the Mianwali Reentrant in the west (Fig. 5.1c).

The KBF exhibit strike of N15°W in the northern segment and N35°W in the southern segment along the Nammal Ridge. The overlapping zone of the two segments form a fault stepover along two restraining faults that was later developed as a push-up block (Abbas et al., 2022).The frontal part of this push-up block is termed as the Khairabad-Ghundi (KG) section hereinafter (Fig. 5.1c). As the KBF exhibit segments and a stepover zone, it is collectively termed as the Kalabagh Fault Zone (KBFZ). The main strand of the fault is termed as the KBF in the text. The KBF along the northern segment is a range bound fault along the Chisal Algad stream (Fig. 5.1c). The Chisal Algad and the Lagorai Algad streams are older channels of the Indus River that were abandoned during ~ 0.5-0.1 Ma and the river adopted a new channel in the east (McDougall, 1989b). The frontal part along the KBF exhibit paleoearthquakes and various morphotectonic features that illustrate landform development in the push-up block and associated westward migration of the Indus River (Abbas et al., 2022). Those paleoseismic features are located at Khairabad, Larkakki, Ghundi and Burikhel. Abbas et al. (2022) described central part of the KG section have emerged earlier than the Khairabad and Ghundi sections, that is justified by more compacted and more consolidated alluvial fan sediments in the central part of the KG section.

The stratigraphic variations along the KBF help to delineate the fault. In the Chisal Algad stream, evaporites from the Precambrian rocks are juxtaposed against the Tertiary-Pleistocene rocks (TSK). Whereas the outcrops on the frontal part of the KG section and the Nammal Ridge are mainly characterized by the Permian sandstones (PNG), limestones (PZG) and Precambrian evaporites at

some places that are in contact with the QKC and QAL sediments (Fig. 5.2) of Quaternary age (Gee, 1980). The QKC are mainly composed of limestone pebbles originated from the uplifting rock units of the KBFZ and differ from the Indus River conglomerates of igneous origin (McDougall, 1989b; McDougall and Khan, 1990). The QKC and the Indus River conglomerates are time equivalent and are jointly termed as the QKC and contain pebbles, sand lenses and silt. Furthermore, the QAL forms alluvial fans in the foreland area and consists of silt and associated sand and gravels.

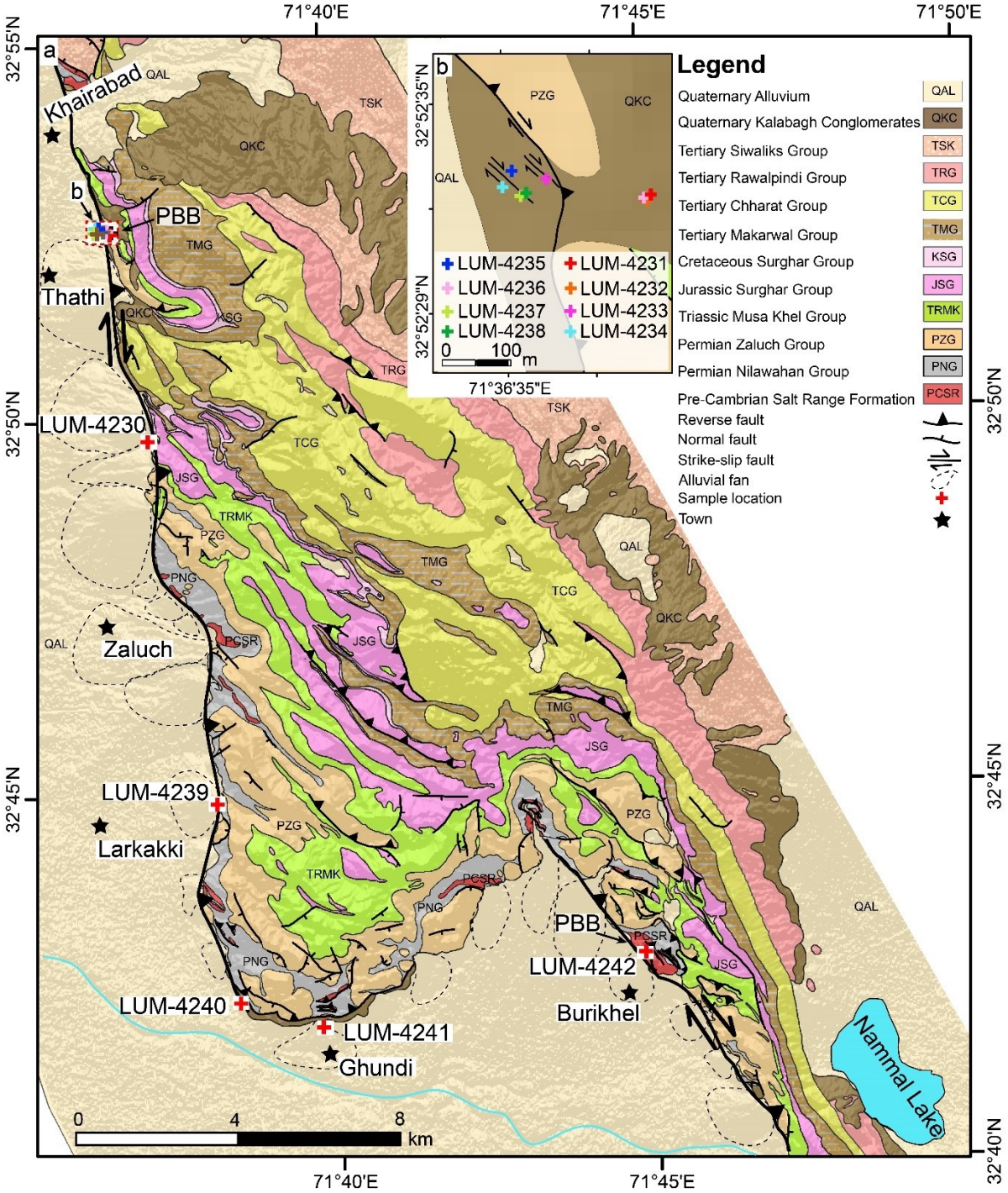

Fig. 5. 2 (a) Geological map of the study area (modified after Abbas et al., 2022 and Gee, 1980)with locations of the luminescence samples, (b) locations of the luminescence samples at Khairabad. PBB=Piggyback basin,

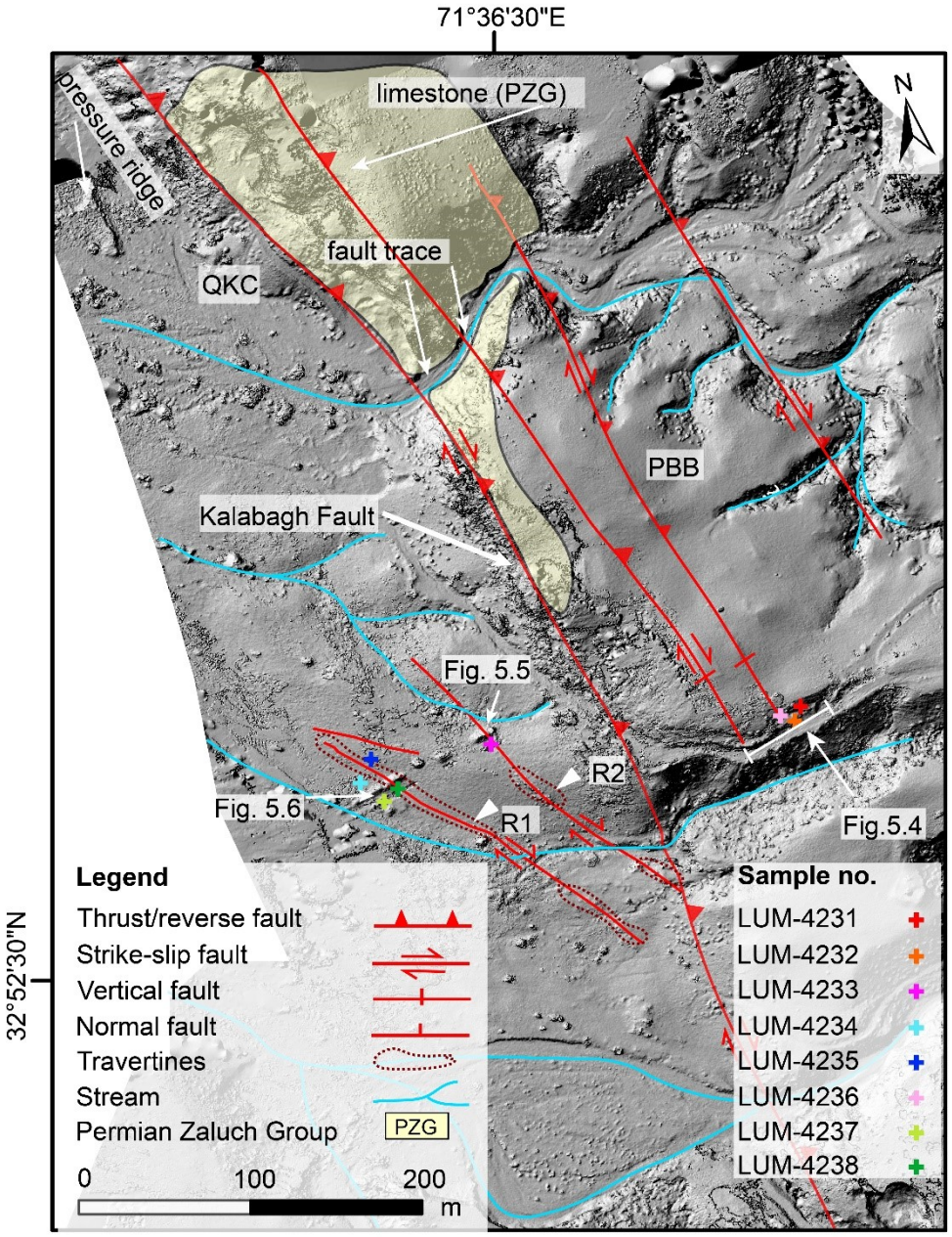

Fig. 5.3 High resolution DEM showing sample locations with respect to morphotectonic features at the Khairabad section modified after Abbas et al. (2022). QKC=Quaternary Kalabagh Conglomerates, PBB=Piggyback basin, R1 and R2=Surface ruptures

The deformed Siwaliks sediments from Tertiary to Pleistocene (TSK) are indicative of post-depositional deformations in the Potwar Plateau and in the Salt Range (Yeats et al., 1984). The TSK were deposited until ~0.4-0.7 Ma in the eastern Salt Range and 0.5 Ma in the Surghar Range (Johnson et al., 1979; Keller et al., 1977; Khan, 1983; Yeats et al., 1984). No chronological data from the TSK of the western Potwar Plateau and the Salt Range are available to date (Abbas et al., 2022). The TSK and the older sedimentary units (Fig. 5.2) are tectonically uplifted in the KBFZ. These sedimentary units are reworked and deposited at the foothills and constitute the QKC and QAL sediments (McDougall and Khan, 1990). These Quaternary sediments are deformed at various locations by tectonic activity (Abbas et al., 2022). McDougall and Khan (1990) marked the unconformable contact between the TSK and the QKC

as a chronological indicator for the inception of the KBF (McDougall and Khan, 1990). Considering that the timing of deposition for the TSK in the Surghar Range, and in the eastern and western Salt Ranges is synchronous, it can be inferred that the tectonic deformation must be younger than the ~0.5 Ma in the western Potwar Plateau and the KBFZ (Abbas et al., 2022). i.e., it started after deposition of the TSK. This observation is important to decide which dating technique should be used to find the ages of the sediments younger than the TSK.

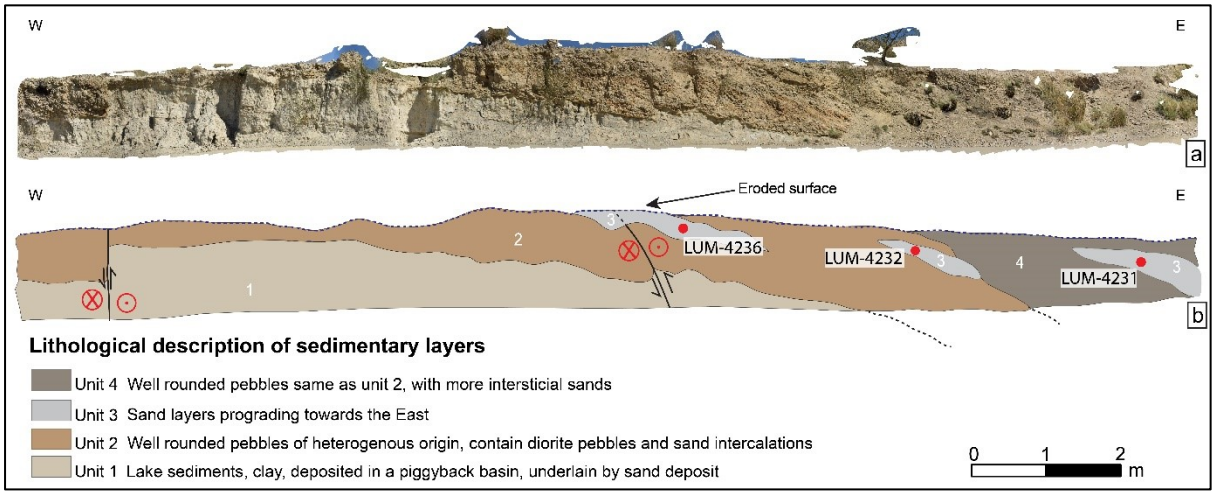

Fig. 5.4 Uplifted and faulted lake sediments of the piggyback basin in the east of the main strand of the KBF (marked on Fig. 5.3). The lake sediments are overlain by the conglomerates consisting of well-rounded diorite pebbles from the Indus River. East dipping sand lenses in these river deposits prograde eastwards. Three samples (LUM-4231, LUM-4232 and LUM-4236) were collected from these sand lenses.

The active tectonics of the KBF have been described based on the instrumental data of less than one hundred years' observations (between 1953 and 2019 A.D.). The KBF has not yielded considerable earthquakes (Fig. 5.1c) as revealed by the instrumental data. i.e., Mw ≥ 4.5 (USGS earthquake catalogue, 2019). Analysis from the InSAR data indicates 6.2 mm/a strike-slip displacement rate in the Chisal Algad stream, 7.7 mm/a along the Ainwan fault (Fig. 5.1) and 6.3 mm/a along the Dinghot fault (Chen and Khan, 2010). McDougall and Khan (1990) have estimated ~7-10 mm/a displacement near the Chisal Algad stream during the past ~2 Ma. The KBF also exhibits 5.7 mm/a line of sight displacement rate along the KG section and 3.7 mm/a along the Nammal Ridge (Chen and Khan, 2010). Furthermore, the western part of the Potwar Plateau and Salt Range is uplifting at a rate of 10 mm/a (Abir et al., 2015). The displacement rates along the KBF decrease southwards along the structural obstructions at the Main Frontal Thrust and the KBF stepover, whereas, higher displacement rates around the Chisal Algad stream are shifting the strain along the splay faults (Chen and Khan, 2010). In their study, Chen and Khan (2020) found that the fault blocks of the KBF and the splay faults are moving in the same direction (southeast) and a fault block outpace the adjacent block resulting in less net displacement. However, InSAR analysis by Chen and Khan (2010) yield more evident, relative line

of sight displacement on the KBF blocks along the KG section and along the Nammal Ridge. Jouanne et al. (2014) suggested that the KBF shows episodic aseismic creep. These studies indicate that the eastern block of the KBF exhibit southward aseismic creep in a caterpillar type of motion, mainly due to the underlying salt layer that is missing in the west of the KBF (Ahmad Abir, 2012).

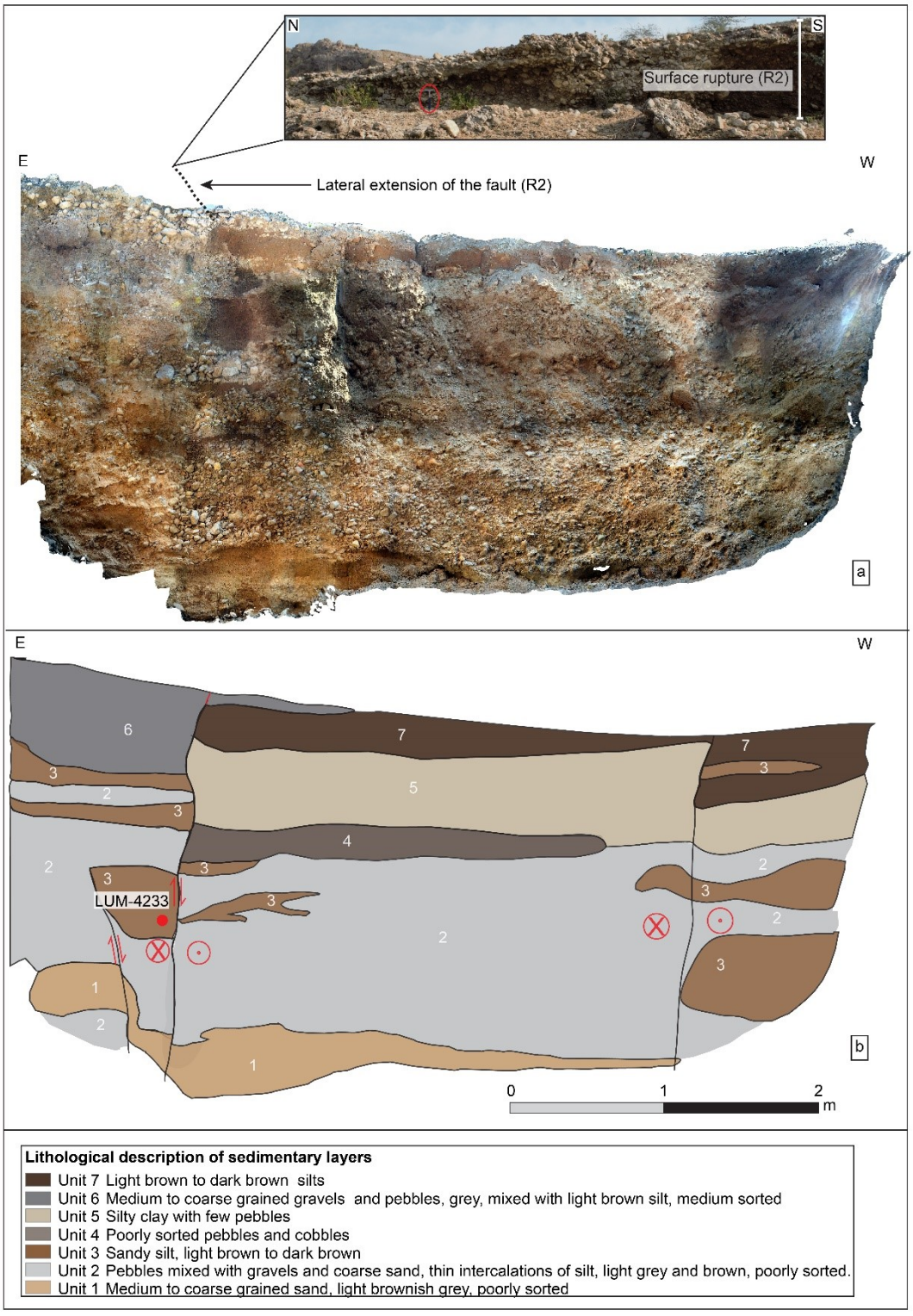

Fig. 5.5 Trench log modified after Abbas et al. (2022), indicates the sediments deformed by the splays of the Kalabagh Fault (marked in Fig.5.3). Luminescence sample (LUM-4233) was collected from the trench that predates the fault rupture.

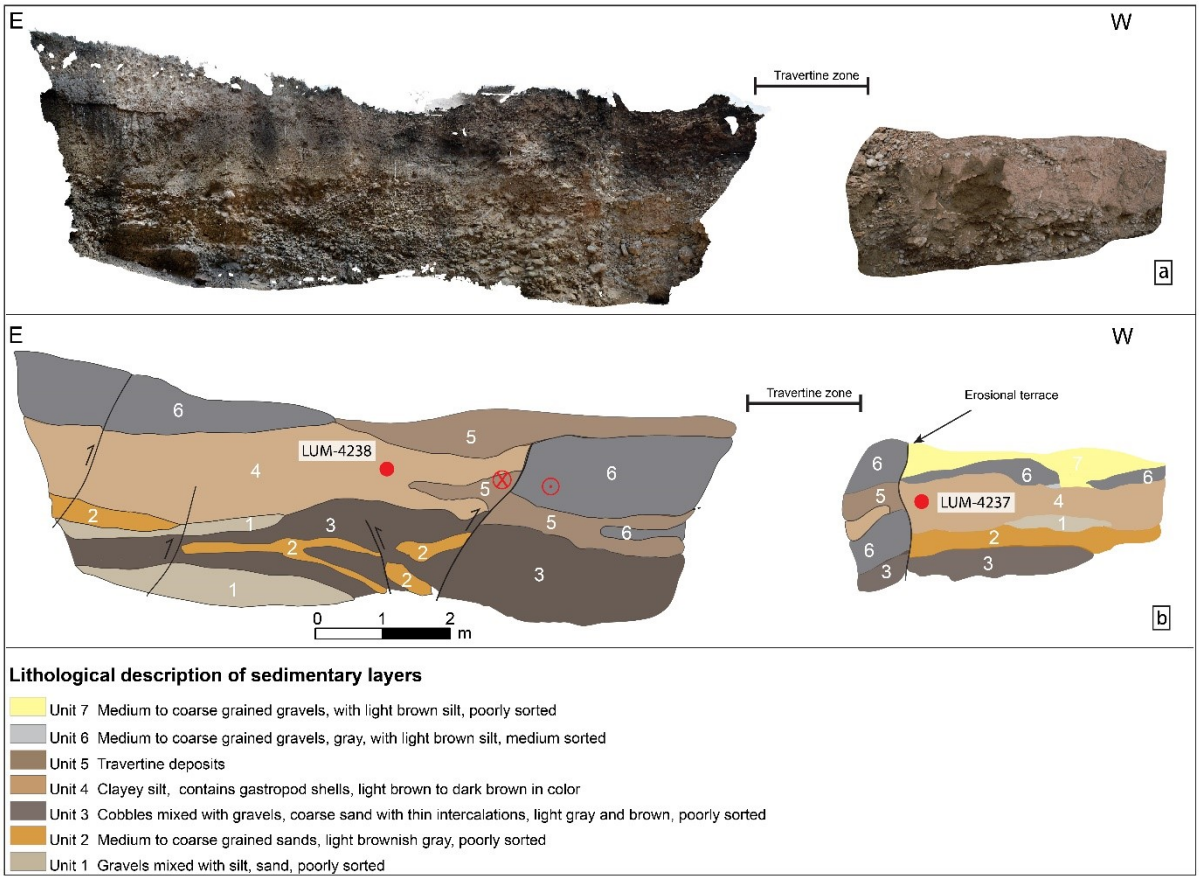

Fig. 5. 6 Trench log modified after Abbas et al. (2022), indicates the sediments deformed by the splays of the Kalabagh Fault (marked in Fig. 5.3). The samples were collected on both sides of the fault zone. LUM-4238 predates the earthquake that created the environmental effect. LUM-4237 postdates the deformation in the travertine bearing fault zone.

Abbas et al. (2022) have used morphotectonics and paleoseismic evidences to underline the contribution of seismic deformations in the landform development of the KBF. Those evidences include fault traces, surface ruptures, displacements at the apex of the alluvial fans, uplifted and deformed Quaternary sediments. At Khairabad, deformed Quaternary sediments along the splays of the KBF (Figs. 5.3, 5.4, 5.5 and 5.6) indicate that several paleoearthquakes have uplifted the sediments up to ~8 meters than the foreland. The environmental effects of paleoearthquakes include ~0.5-1 m of vertical displacements in each seismic event, whereas the ~8 m uplift was possible in 12 ± 4 seismic events (Abbas et al., 2022).The uplifted sediments include lake deposits of a piggyback basin that are overlain by the diorite bearing Indus River sediments (Figs. 5.3 and 5.4) and underlain by the well sorted sand deposits (Abbas et al., 2022). Ages of the sands from the Indus River sediments predate the deformations at the mountain front. Paleoseismic trenches across the strike of the 2 surface ruptures (Figs. 5.3, 5.5 and 5.6) yield the deformed Quaternary sediments in the foreland of the KBF (Abbas et al., 2022). Trench across the strike of the surface rupture (R2) exhibit splays of the KBF (Fig. 5.5). The fault along the R2 extends on the slope in the South of the trench. Structural reconstruction of the scarp at the slope suggests a lateral displacement of ~3-4 m. Those disrupted sediments in the

trenches predate the paleoseismic event along that fault. A fault trace along surface rupture (R1) is covered by undisturbed travertine deposits (Figs. 5.3 and 5.6). In the west, the travertine deposits make up an erosional terrace (Fig. 5.6). Deposition of the unit-4 in the west of this terrace therefore postdates the paleoearthquake that had formed R1 and subsequent deposition of the travertine.

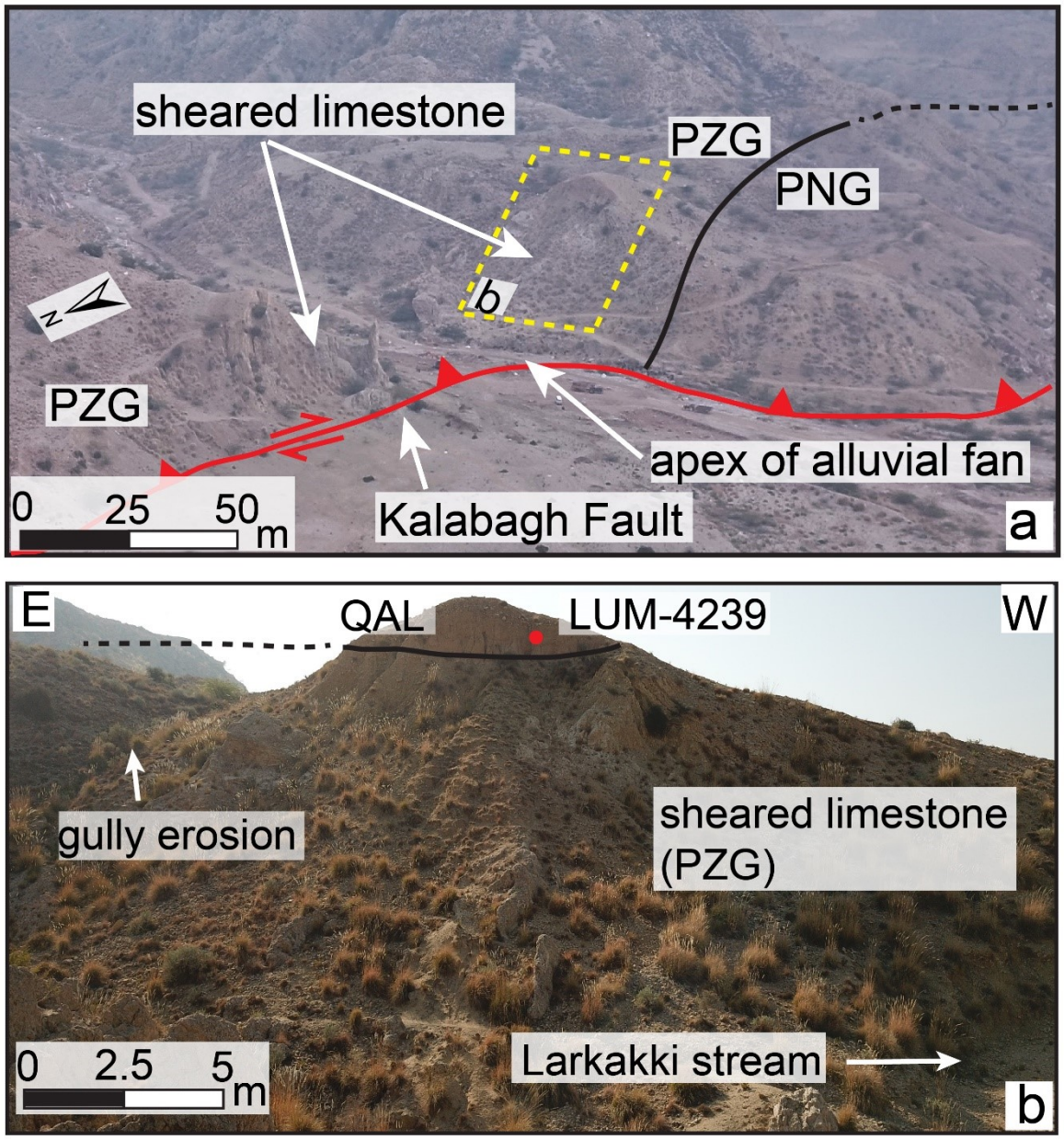

Fig. 5. 7 Uplifted Quaternary sediments along the Kalabagh Fault, at the apex of the Larkakki alluvial fan. LUM-4239 was taken from the uplifted Quaternary Alluvium (QAL) sediments. PNG=Permian Nilawahan Group, PZG=Permian Zaluch Group

At the apex of the Larkakki alluvial fan (Fig. 5.2), sheared limestones of the Permian Zaluch Group (PZG) and uplifted QAL sediments characterize the deformation along the KBF (Fig. 5.7). The QAL sediments represent alluvial fan deposits that are uplifted up to ~15 m at the apex of the alluvial fan. These sediments were deposited at the mountain front in the early phase of uplift of the push-up block in the KBFZ. Further uplift at the mountain front had uplifted this alluvium at the apex of the

alluvial fan. In the south, the Gundi section (Fig. 5.2) exhibits antithetically deformed and uplifted foreland sediments that form ridges (Fig. 5.8). These ridges contain the Indus River sands overlain by the QKC and QAL sediments (Abbas et al., 2022). At the southern face of the stepover zone at Ghundi, antithetically faulted and uplifted ridges have displaced the alluvial fan (Fig. 5.8). Abbas et al. (2022) suggested that the trunk stream was diverted at the apex of this displaced alluvial fan, that was followed by geomorphic degradation of the alluvial fan.

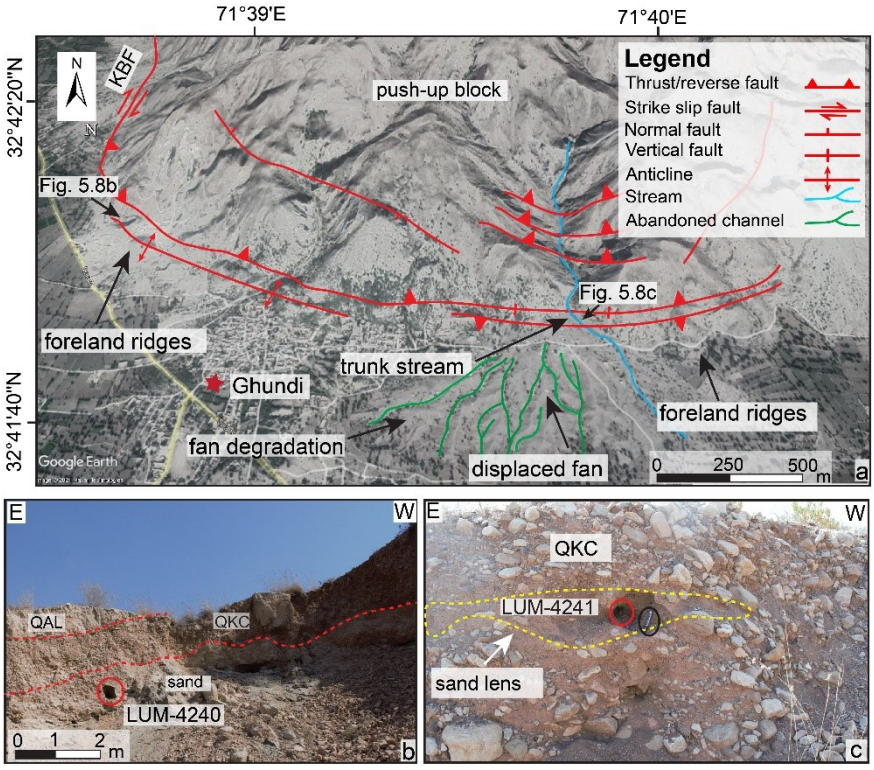

Fig. 5.8 (a) Morphotectonic features at the Ghundi stepover. Locations of samples collected to predate these features are marked as Fig. 5.8 (b and c), (b) back tilted Indus River sediments (LUM-4240) overlain by the Quaternary Kalabagh Conglomerates (QKC) and Quaternary Alluvium (QAL). Back tilting, folding and back thrusting of the sediments form these foreland ridges as marked in Fig. 5.8a, (c) Sample (LUM-4241) was collected from the incised stream near the displaced fan apex. It marks the termination of the alluvial fan development before morphological degradation and stream incision.

The Nammal Ridge is incised by a stream connecting the Potwar Plateau and the Mianwali Reentrant at Nammal Lake. The sediments from the Potwar Plateau are reworked and deposited in the foreland, forming a large alluvial fan (Fig. 5.1c). The morphological development of the Nammal alluvial fan has diverted the Wahi stream northwards. The Nammal alluvial fan and Wahi stream consist of the poorly sorted Nammal Ridge and Potwar Plateau sediments. The Nammal Ridge at Burikhel had formed a small piggyback basin (Fig. 5.9b) that was filled with fine grain sediments reworked from the adjoining mountains (Abbas et al., 2022). Those fine-grained sediments postdate the seismic event that had formed the basin.

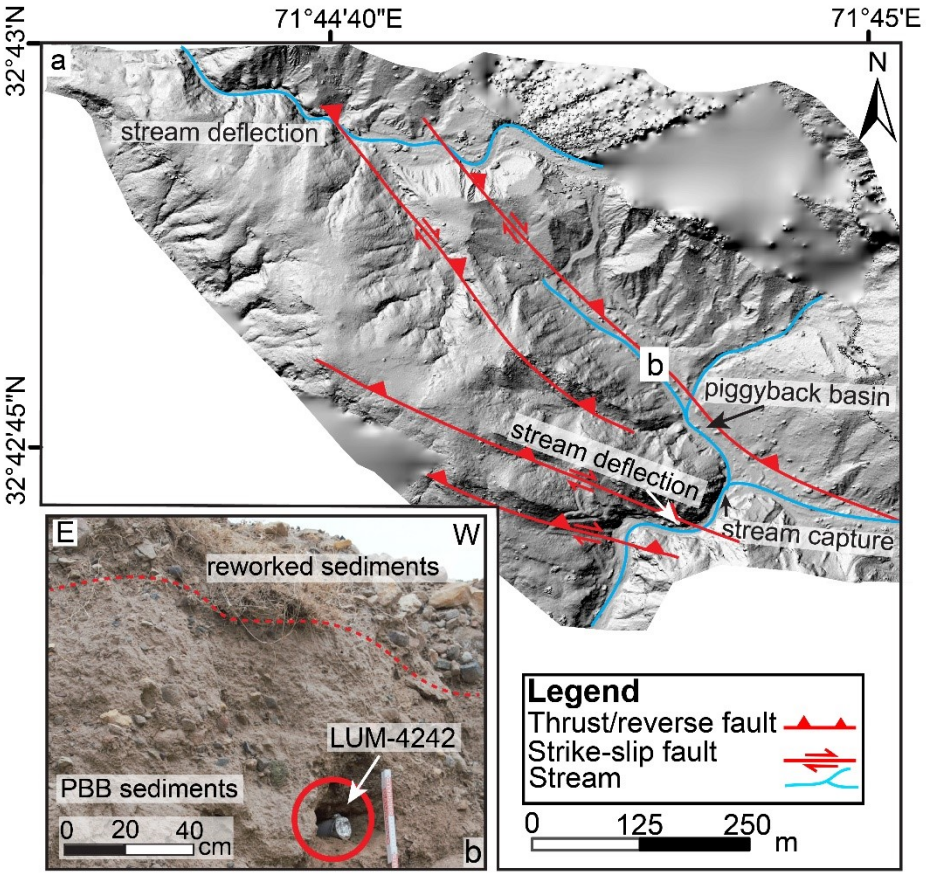

Fig. 5. 9 (a) High resolution DEM of the Burikhel section indicating morphotectonic features along the Kalabagh Fault, modified after Abbas et al. (2022). (b) Luminescence sample (LUM=4242) was collected from the sediments deposited in the piggyback basin that postdates the paleoseismic evet and predates the stream incision at the mountain front.

5.3 Methodology

5. 3.1 Sample locations

Thirteen samples were collected for luminescence dating from the study area (Fig. 5.2). These sample locations were selected close to the morphotectonic and paleoseismic features (Table 5.1). The samples from the sand intercalations in the uplifted conglomerates (Fig. 5.4) were collected. The ages of three samples (LUM-4231, LUM-4232, LUM-4236) were used to estimate the timing of the Indus River flow from the Khairabad section and mechanism of seismic uplifts. LUM-4233 predates the earthquake that has formed R2 (Fig. 5.5). The age of R1 is determined using LUM-4237 and LUM-4238 (Fig. 5.6). Unit-4 was sampled from the east and the west of the travertine zone. LUM-4238 predates the deformation along the R1, whereas LUM-4237 was used to postdate the paleoearthquake. LUM-4234 and LUM-4235 represent the lateral extension of the unit-4 along the R1 (Fig. 5.2 and 5.3) and are correlated with LUM-4237 and LUM-4238 respectively. At the central part of the KG section, the deeply incised feeder streams had reduced the sediment influx earlier than at the other parts of the push-up block. This part of the KG section exhibits morphological and lithological maturity, the alluvial fan development has stopped in this part and streams have incised into the alluvial fans. To check this,

Table 5.1 Field description for the Luminescence samples taken from the Quaternary Kalabagh Conglomerates (QKC) and Quaternary Alluvium (QAL).

Sample	Coordinates	Lithology/Formation	Description of sample and stratigraphic location
LUM-4230	32.82904°N, 71.62064°E	Sandy Silt/ QAL	Youngest sediments deposited on the alluvial fan before the start of incision at the alluvial fan
LUM-4231	32.875145°N, 71.61187°E	Sand/ QKC	Uplifted Indus River deposits from Khairabad associated with the diorite pebbles
LUM-4232	32.875072°N, 71.61179°E	Silty sand/QKC	Uplifted Indus River deposits from Khairabad associated with the diorite pebbles
LUM-4233	32.875295°N, 71.61036°E	Silt/QAL	Trench sample from sediments deformed by the earthquake rupture (R2)
LUM-4234	32.875286°N, 71.6095°E	Silt/QAL	Trench sample from the sediments that postdates the displacement along the earthquake rupture (R1)
LUM-4235	32.875492°N, 71.60965°E	Silt/QAL	Trench sample from the sediments to the west of the fault and predates the displacement along the earthquake rupture (R1).
LUM-4236	32.875094°N, 71.61176°E	Sand/QKC	Uplifted Indus River deposits from Khairabad associated with the diorite pebbles
LUM-4237	32.875172°N, 71.60977°E	Silt/QAL	Trench sample from the sediments that postdates the displacement along the earthquake rupture (R1), parallel to LUM-4234
LUM-4238	32.875199°N, 71.60987°E	Silt/QAL	Trench sample from the sediments to the west of the fault and predates the displacement along the earthquake rupture (R1), correlates with LUM-4235
LUM-4239	32.74805556°N,71.63656°E	Silt/QAL	Uplifted alluvium (QAL) at the Larkakki fan apex predating the uplift along the KBF
LUM-4240	32.70390278°N,71.64158°E	Sand/QKC	Indus River sand from foreland ridges at Ghundi, marks termination of the river deposits and the onset of the diversion of the Indus River
LUM-4241	32.698195°N,71.66356°E	Sand/QKC	Youngest sediments from the displaced and degraded alluvial fan at Ghundi, marking the timing for the displacement and termination of the fan development
LUM-4242	32.71293611°N,71.74821°E	Silt/QAL	Sediments from the piggyback basin at Burikhel. The basin was formed by thrusting along the KBF followed by deposition and stream capture, marking the timing of basin formation during seismic uplift

a sample (LUM-4230) was taken, and it represents the youngest unconsolidated sediments deposited on the alluvial fan before the incision of the alluvial fan started near the apex.

Sample LUM-4239 was taken from the uplifted QAL sediments at Larkakki to estimate the timing of inception of the uplift along the KBF (Fig. 5.7). The Indus River sands at Ghundi, which resemble the sand deposits at Khairabad, were sampled to determine the time when the Indus River was flowing along the KBF, depositing these sands (Fig. 5.8). LUM-4241 was taken from the trunk stream to infer the timing of alluvial fan development, followed by the displacement and subsequent degradation of the alluvial fan. Moreover, the sediments at Burikhel (Fig. 5.9) were sampled from the piggyback basin (LUM-4242) to postdate the paleoseismic event along the KBF (Abbas et al., 2022).

5.3.2 Sample collection

Thirteen samples were collected for luminescence dating from the study area (Fig. 5.2). The outcrop was cleaned to get the sample with original moisture and unexposed to light. Samples were collected in hard, opaque and labelled plastic tubes with a diameter of 5 cm and a length of 20 cm. The two ends of the tubes were covered, and samples were transported to the lab. Material surrounding the tubes was collected in plastic bags for dose rate measurements.

5.3.3 Sample Preparation

The samples were prepared in the dark room under subdued red light. The 150-200 µm grain size fraction was separated after sieving the samples. This fraction was treated with sodium oxalate to disaggregate the grains. HCl and H_2O_2 solutions were used for removal of carbonates and organic matter respectively. The K-feldspar fraction (<2.58 g/cm^3) and the quartz fraction (2.62-2.70 g/cm^3) were separated using the heavy liquid of sodium polytungstate. Quartz grains were etched with 40 % hydrofluoric acid (HF) for 1 hour to remove the alpha ray affected outer part of the grain, as well as any residual feldspar grains. This was followed by HCl treatment to dissolve the fluorides precipitated on the grain surface during the etching process. For K-feldspar grains, no HF etching was performed, and the alpha contribution on dose rate was included when evaluating the environmental dose rate. Small aliquots with 1 mm diameter (containing 10-20 grains) were prepared by mounting the K-feldspar or quartz grains on the stainless-steel discs with silicone oil. These aliquots were used for the equivalent dose (D_e) measurements.

5.3.4 Environmental dose rate

Fifty grams of each dried sample were measured with the gamma spectrometry to obtain the uranium (U), thorium (Th) and potassium (K) concentrations for the external dose rates (Table 5.2). A radon

(^{222}Rn) loss of 20 % was assumed (Olley et al., 1997). The conversion factor of Liritzis et al. (2013) and beta absorption factor of Guérin et al. (2012) were applied. For K-feldspar, the alpha attenuation factor from Brennan et al. (1991) and the *a*-value of 0.09 ± 0.02 from Kreutzer et al. (2014) were applied. Internal K concentration of 12.5 ± 1.0 %, Rb concentration of 400 ± 100 ppm (Huntley and Baril, 1997; Huntley and Hancock, 2001; Zhao and Li, 2005) were used for K-feldspar. Cosmic dose rate was calculated as a function of depth, altitude and coordinates of the individual sample (Prescott and Hutton, 1994). The in-situ water contents of the samples were also measured to adjust the environmental dose absorbed by water (Table 5.2). For samples with a water content higher than 5 %, an error of 5 % is assumed for the water content. The water content from sand samples may have been evaporated due to greater permeability and surface temperatures, changing the natural configuration. Therefore, to adjust the evaporation factor for samples with a water content smaller than 5 %, an error equal to water content is assumed, because the water content cannot be negative.

5.3.5 Equivalent dose measurements

Equivalent dose (D_e) was measured using Risø TL/OSL DA-20 reader. For quartz, blue LEDs (470 ± 30 nm) were used for stimulation and OSL signal was detected though a U-340 filter with a transmitting band peaked in UV (280-380 nm). For K-feldspar, IR LEDs (875 ± 40 nm) were used for stimulation, and the IRSL signal was detected through a filter package of Schott BG-39 and Corning 7-59 filters, which has a transmitting band peaked in blue (320-480 nm). The single aliquot regenerative dose (SAR) protocol was used for both quartz (Murray and Wintle, 2000) and K-feldspar (Buylaert et al., 2009). Table 5.3 shows sequences used for the D_e measurements. For the pIRIR measurements, the K-feldspar was preheated at 250 °C for 60 s, followed by a first IR stimulation at 50 °C for 100 s, and a second IR stimulation ($pIRIR_{225}$ signal) at 225 °C for 200 s. The first 10 s of the decay curve were used as signal, with the last 10 s of the decay curve used as background (Fig. 5.10). For the quartz sample, the preheat was performed at 240 °C for 10 s and the OSL was measured at 125 °C for 40 s. An IR stimulation for 40 s at 125 °C was additionally performed before the OSL measurement at the last cycle of the SAR protocol. The first 0.5 s of the decay curve was used as signal with the last 8 s subtracted as background (Fig. 5.10).

For pIRIR dating of K-feldspar, 3 aliquots from each sample were measured with the full SAR sequence with the largest regenerative dose up to 1950 Gy. The data of the three aliquots were applied to build

Table 5.2 Dose rate determination from the gamma spectrometry.

Sample	Depth (m)	Grain size (μm)	U (ppm)	Th (ppm)	K (%)	Cosmic (Gy/ka)	Water $_{in\ situ}$ (%)	Dose rate (Gy/ka)	
								K-feldspar	quartz
LUM-4230	0.9	150-200	3.2 ± 0.03	19.7 ± 0.08	0.7 ± 0.01	0.18 ± 0.02	0.6 ± 0.6		2.86 ± 0.07
LUM-4231	1.0	150-200	2.3 ± 0.02	12.3 ± 0.09	1.5 ± 0.02	0.18 ± 0.02	0.4 ± 0.4	3.9 ± 0.14	
LUM-4232	1.2	150-200	2.4 ± 0.02	13.3 ± 0.09	1.5 ± 0.02	0.18 ± 0.02	7.4 ± 5	3.67 ± 0.2	
LUM-4233	1.7	150-200	3.3 ± 0.03	14.7 ± 0.10	1.3 ± 0.02	0.16 ± 0.02	7.4 ± 5		2.88 ± 0.13
LUM-4234	1.0	150-200	1.7 ± 0.01	7.8 ± 0.08	2.1 ± 0.02	0.18 ± 0.02	2.5 ± 2.5		3.07 ± 0.11
LUM-4235	1.1	150-200	2.3 ± 0.02	12.3 ± 0.09	1.5 ± 0.02	0.18 ± 0.02	3.4 ± 3.4		2.90 ± 0.11
LUM-4236	1.2	150-200	1.7 ± 0.01	8.4 ± 0.08	1.4 ± 0.02	0.18 ± 0.02	0.4 ± 0.4	3.32 ± 0.13	
LUM-4237	1.0	150-200	3.2 ± 0.03	13.4 ± 0.09	1.2 ± 0.02	0.18 ± 0.02	3.3 ± 3.3		2.81 ± 0.1
LUM-4238	1.1	150-200	3.0 ± 0.02	11.9 ± 0.07	1.1 ± 0.01	0.18 ± 0.02	4.4 ± 4.4		2.51 ± 0.1
LUM-4239	1.0	150-200	2.8 ± 0.02	16.5 ± 0.08	1.5 ± 0.02	0.18 ± 0.02	1.7 ± 1.7	4.22 ± 0.15	
LUM-4240	3.8	150-200	1.5 ± 0.01	7.5 ± 0.08	1.2 ± 0.02	0.12 ± 0.01	0.3 ± 0.3	2.96 ± 0.12	
LUM-4241	0.9	150-200	1.8 ± 0.01	9.0 ± 0.05	1.8 ± 0.01	0.18 ± 0.02	0.9 ± 0.9		2.96 ± 0.08
LUM-4242	0.8	150-200	3.2 ± 0.03	13.7 ± 0.06	1.2 ± 0.01	0.19 ± 0.02	1.8 ± 1.8		2.88 ± 0.08

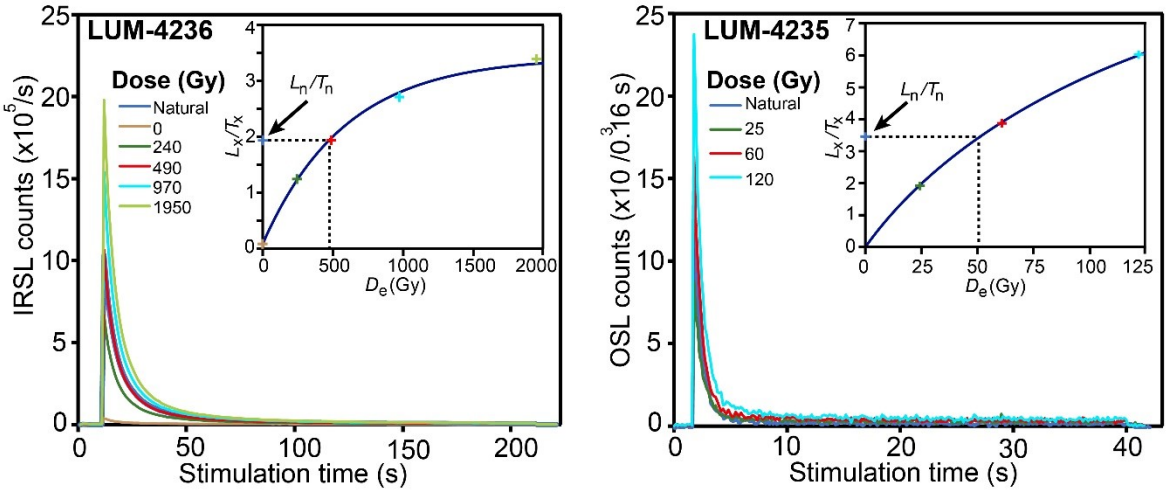

Fig. 5.10 Decay curves and dose response curves (DRC) of LUM-4236 for feldspar and LUM-4235 for quartz. First 10 seconds of the feldspar curve and 0.5 second of the quartz curve were used as signal.

a standard growth curve (SGC) for each individual sample in the R package "numOSL" (Li et al., 2016; Peng et al., 2013). For the other aliquots, only one regenerative dose was employed, which was close to the D_e. The SGC D_e was estimated with the numOSL package (Peng and Li, 2017). As the ages yielded by the K-feldspar samples are old, fading correction procedure of Kars et al. (2008) is performed with the R package 'Luminescence' (Kreutzer et al., 2012). Sensitivity corrected natural signals (L_n/T_n values) were projected on the simulated natural dose response curve to yield the D_e values after fading correction (Fig. 5.14).

For 8 of the 13 samples, the pIRIR D_e values are very scattered with overdispersion larger than 20 % (40-83 %), indicating partial-bleaching. Quartz OSL dating was performed for these 8 samples. A larger number of aliquots (70-80 aliquots) were tested for each sample. Aliquots with the recycling ratio between 0.9-1.1 and recuperation ratio <5% were accepted. Each aliquot with a diameter of 1mm contains 10-20 quartz grains. The probability of light-emitting grains in quartz is usually lower than 5% (Duller et al., 2000), thus the small-aliquot dating can be regarded as single-grain dating. The minimum age model (MAM) was applied to deduce the D_e corresponding to well-bleached grains (Galbraith et al., 1999). For more accurate age determinations, luminescence characteristics were measured, and relevant corrections were applied. These characteristics include fading rate, residual dose, test dose and dose recovery. Detailed descriptions of these characteristics and relevant corrections are as follows.

5.3.6 K-feldspar Luminescence characteristics

5.3.6.1 Fading rate

Compared to the IRSL signal at 50 °C, the biggest advantage of the $pIRIR_{225}$ signal is that the anomalous fading rate of the $pIRIR_{225}$ signal is much smaller (Buylaert et al., 2009; Thomsen et al., 2008). However,

noticeable fading still exists for the $pIRIR_{225}$ signal and fading correction is still needed (Buylaert et al., 2009; Li et al., 2019, 2018; Thomsen et al., 2008). The measurement of fading rate were conducted following the single aliquot regenerative dose (SAR) protocol (Auclair et al., 2003). Nine aliquots were tested for fading rates for each sample. Fig. 5.11a shows the fading rates of nine aliquots from sample LUM4236. The individual g-values varied between 1.29 % and 1.95% per decade, with a mean value of 1.58 ± 0.09 % per decade. The t_c used here was 0.23 hour. After conversion, the mean g_{2d} value of LUM4236 was 1.64 ± 0.09 %/decade (Table 5.4). The g_{2d} values of the five K-feldspar samples were from 1.42 ± 0.08% to 2.14 ± 0.09 %.

Table 5.3 SAR sequence used for measurements of quartz OSL signal after Murray and Wintle, (2000), and K-feldspar pIRIR signal after Buylaert et al. (2009).

Quartz OSL			K-feldspar post-IR IRSL		
Step	Treatment	Observed	Step	Treatment	Observed
1	D_n, Given dose (D_i) [a]		1	D_n, Given dose (D_i) [a]	
2	Preheat at 240 °C for 10 s		2	Preheat at 250°C for 60 s	
3	IR stimulation for 40s at 125°C [b]		3	IR stimulation at 50°C for 100s	
4	Blue stimulation for 40s at 125°C	*Ln, Li*	4	IR stimulation for at 225°C for 200s	*Ln, Li*
5	Test Dose, D_i	*T*d	5	Test Dose, D_i	T_d
6	Cutheat to 220 °C		6	Preheat at 250°C for 60 s	
7	Blue stimulation for 40s at 125°C	T_n, T_i	7	IR stimulation at 50°C for 100s	
8	Blue stimulation for 40s at 260°C		8	IR stimulation at 225°C for 200s	T_n, T_i
9	Return to 1		9	Return to 1	

[a] D_n is for natural signal without irradiation, D_i is for several irradiation doses given to generate growth curve.

[b] IR stimulation conducted before OSL in the last cycle.

5.3.6.2 Residual dose

The $pIRIR_{225}$ signal is more difficult to bleach than the IRSL signal at 50 °C (Buylaert et al., 2011; Thomsen et al., 2008). Even for well-bleached modern samples, a small amount of residual dose can still be measured, which might be a result of thermal transfer during preheating (Buylaert et al., 2011). To measure the residual dose, seven K-feldspar samples were bleached by the Hönle SOL2 solar simulator for 4 hours. Here, a positive relationship is observed between the residual doses and the D_e values (Fig. 5.11b), which has also been widely reported in previous studies (Buylaert et al., 2012; Kars et al., 2014; Li et al., 2020; Murray et al., 2014; Schmidt et al., 2014; Sohbati et al., 2012; Yi et al., 2016). The intercept on the y-axis gives a value of 7.0 ± 1.2 Gy for the $pIRIR_{225}$ signal (Fig. 5.11b). It is interpreted to be the residual dose from a modern sample with D_e of 0 Gy, which represents the

contribution of an un-bleachable component. Following previous studies, we subtracted this intercept dose from all samples (Li et al., 2020; Schmidt et al., 2014; Yi et al., 2016).

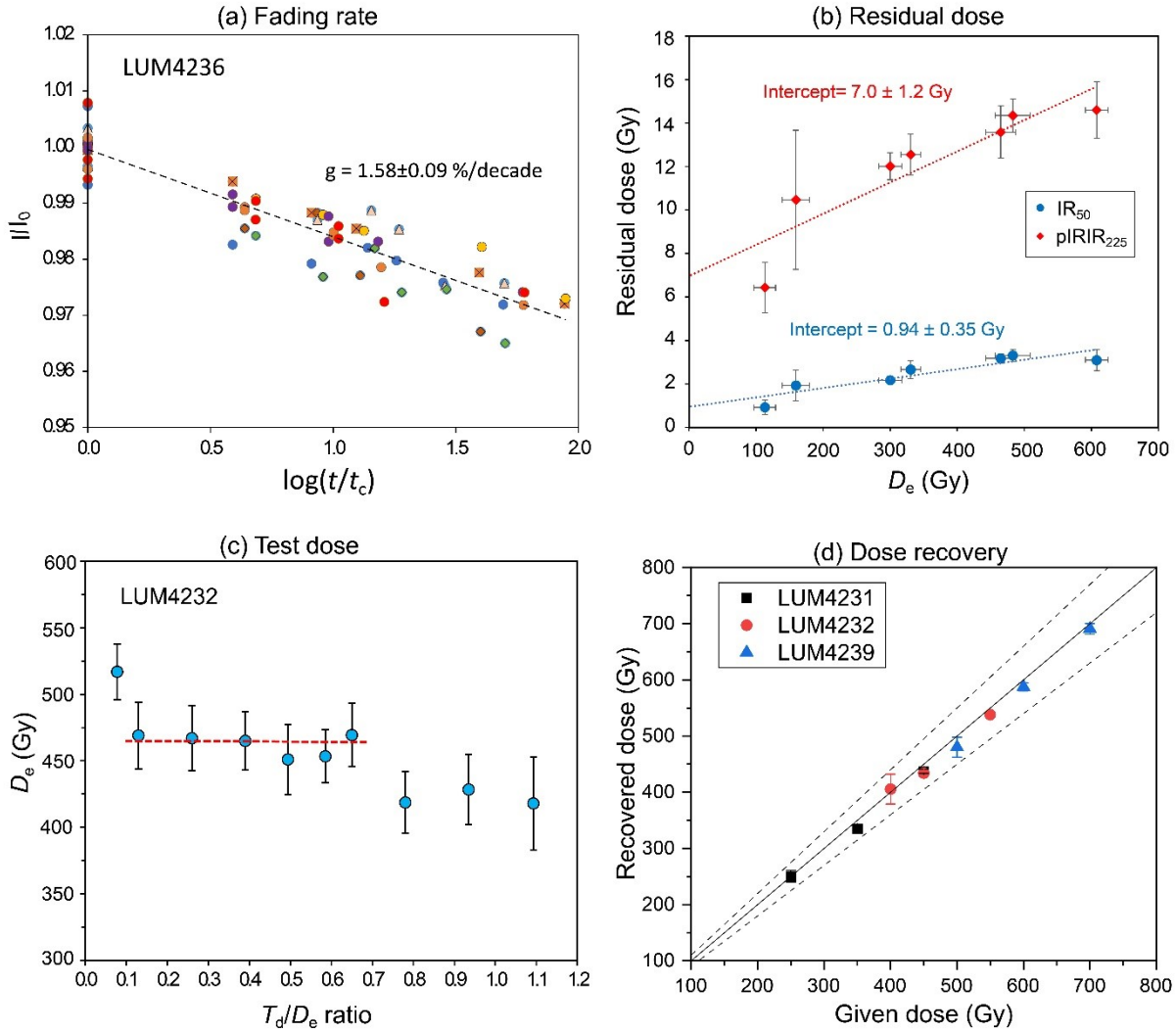

Fig. 5.11 K-feldspar luminescence characteristics. a) The g-values of sample LUM-4236. Nine aliquots were measured with the SAR procedure. Each symbol represents an individual aliquot. b) The residual doses of seven samples after bleaching for 4 hours with Hönle SOL2 solar simulator. Four aliquots were measured for each sample. c) D_e of sample LUM-4232 measured with different T_d/D_e ratios. About 12 aliquots were measured for each group. A D_e plateau was reached when the T_d/D_e ratio was 0.13-0.65. d) Dose recovery tests of three samples with different given doses. 3-4 aliquots were measured for each group. All the recovered doses were within 10 % of the given doses.

5.3.6.3 Size of test dose

For K-feldspar pIRIR signal, it has been reported that the size of the test dose (T_d) has influence on the D_e measurements, as well as the dose recovery ratios (Colarossi et al., 2018; Fu et al., 2015; Nian et al., 2016; Qin and Zhou, 2012; Stevens et al., 2018; Yi et al., 2016). Suitable T_d/D_e ratio has been proposed, such as 15-80 % (Yi et al., 2016), 30-70 % (Stevens et al., 2018). LUM-4232 has a D_e of ~470 Gy, when a T_d of 180 Gy was used. D_e for LUM-4232 was measured using multiple test doses to check the range of the test dose suitable for the D_e measurements. Different test doses ranging from 36 Gy to 508 Gy were applied. These test doses are 8 % to 110 % of the D_e.The D_e showed a plateau when

the T_d is 60-300 Gy, corresponding to a T_d/D_e ratio of 13-65 % (Fig. 5.11c). This indicates the suitable range of T_d/D_e ratio for accurate D_e estimation. As different samples may have different suitable T_d/D_e ranges, the T_d/D_e ratios were kept within a narrow range of 30-60 % for all K-feldspar samples this study.

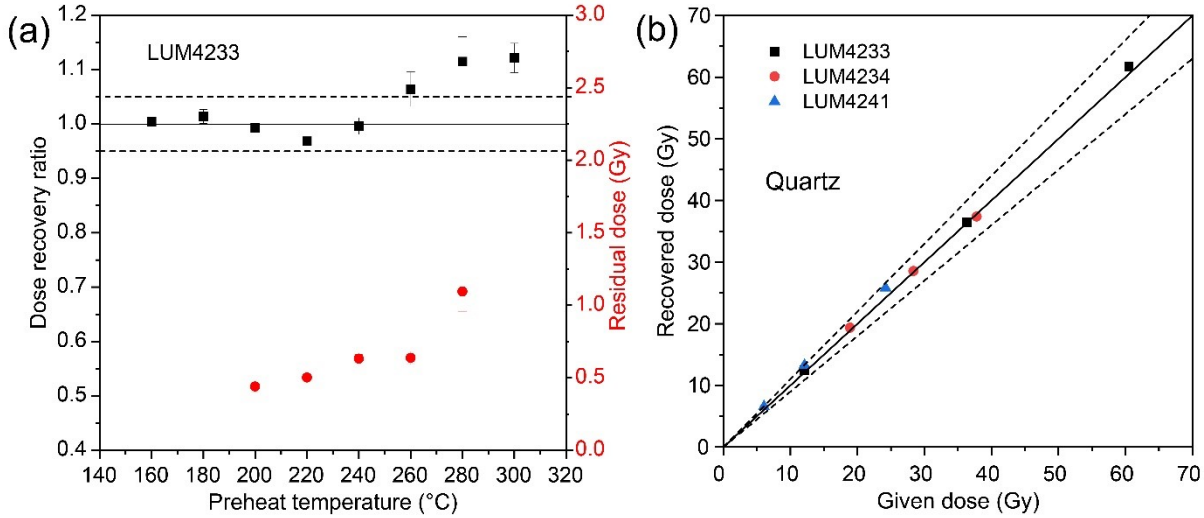

Fig. 5.12 Quartz luminescence characteristics. a) Dose recovery ratios and thermal transferred doses with different preheat temperatures for quartz sample LUM-4233. The bleaching was performed with the Hönle SOL2 solar simulator for 20 minutes. The given dose was 36 Gy. Three aliquots were measured for each group. Dose recovery ratios were within 5 % of unity when the preheat temperature was 160 °C to 240 °C. b) Dose recovery tests for three samples with different given doses. The preheat temperature was fixed at 240 °C. 3-4 aliquots were measured for each group. All the recovered doses were within 10 % of the given doses.

5.3.6.4 Dose recovery tests

Dose recovery tests were performed to check whether the D_e can be measured accurately with the dating protocols (Murray and Wintle, 2000; Wallinga et al., 2000). For dose recovery test, K-feldspar aliquots from three samples (LUM-4231, LUM-4232, LUM-4239) were bleached by the SOL2 for 4 hours and divided into 3 groups for each sample. Different doses, ranging from 250 Gy to 700 Gy, were administered to each group. The given doses were treated as unknown and measured by the SAR protocol. The recovered doses (after residual dose subtraction) of the $pIRIR_{225}$ were within 10% of the given doses (Fig. 5.11d), demonstrating that the SAR protocol applied for K-feldspar was suitable.

5.3.6.5 Quartz Luminescence characteristics

Suitable preheat temperature needs to be determined for quartz OSL dating (Wintle and Murray, 2006). Usually, the D_e is measured with different preheat temperatures to define the suitable preheat temperature range. Due to the partial-bleaching nature of the samples in this study, we performed the dose recovery tests with different preheat temperatures. 24 aliquots of sample LUM-4233 were bleached by the SOL2 solar simulator for 20 min, then given a dose of 36 Gy. The aliquots were divided

into 8 groups with 3 aliquots in each, and the given dose was measured with the SAR protocol with different preheat temperatures ranging from 160 °C to 300 °C. The cutheat temperature was always 20 °C lower than the preheat temperature, except for the preheat temperature of 160 °C, for which a cutheat temperature of 160 °C was used. The dose recovery ratios are plotted against the preheat temperature in Fig. 5.12a. It reveals that the recovery ratios were within 5% of unity when the preheat temperature was between 160 °C and 240 °C. The thermal transferred doses were <0.6 Gy when the preheat temperature was lower than 260 °C. Such a small dose is negligible. Using the fixed preheat temperature of 240 °C, dose recovery tests were further performed on three quartz samples (LUM-4233, LUM-4234, LUM-4241) with different given doses ranging from ~6 Gy to 60 Gy. The recovered doses were all within 10% of the given doses (Fig. 5.12b), which further validated the use of 240 °C as the preheat temperature for D_e measurements. Infrared depletion ratio was always close to 1, revealing that there was no feldspar contamination in the quartz sample.

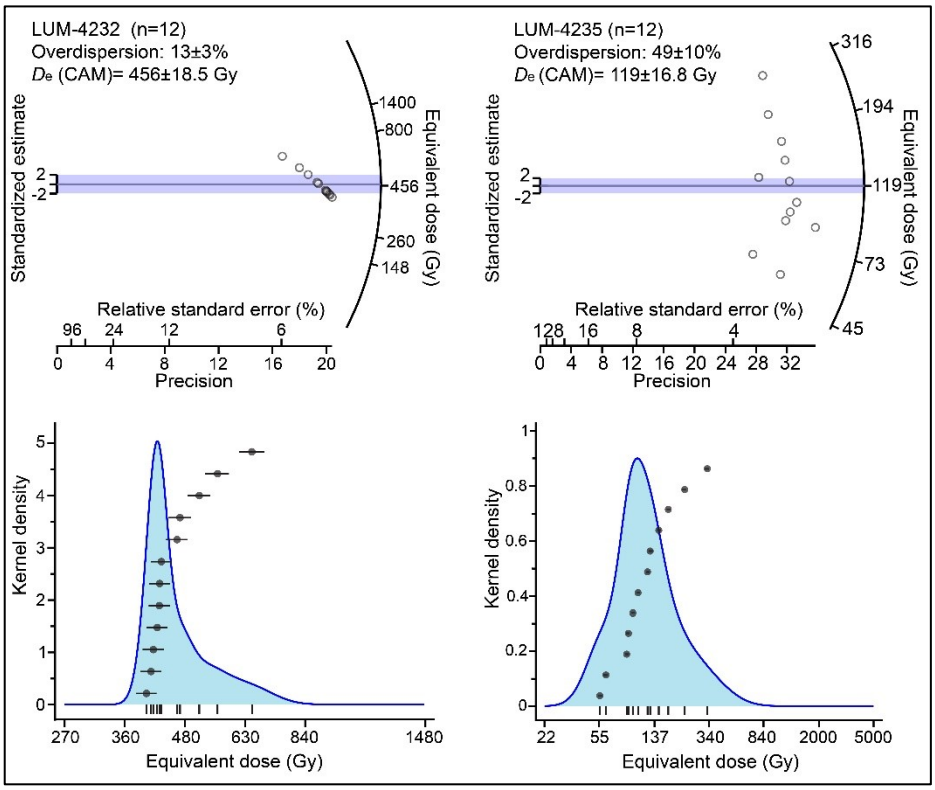

Fig. 5.13 Radial and Kernel density plots of pIRIR$_{225}$ from LUM-4232 and LUM-4235. High overdispersion of the LUM-4235 indicates partial-bleaching of sediments before the deposition and burial. Overdispersion of LUM-4232 indicates well-bleached sediments.

5.4 Results

5.4.1 Equivalent doses (D_e) and ages

5.4.1.1 K-feldspar pIRIR

Equivalent doses and ages are determined from the pIRIR and OSL dating methods and results are presented in Table 5.4. The K-feldspar pIRIR dating was performed for all the 13 samples. The D_e values from 5 samples exhibit small overdispersion (8-19 %). These samples were regarded as well-bleached and the central age model (CAM) was applied for the D_e estimation (Galbraith et al., 1999). Table 5.4 shows the measured D_e values, dose rates, g-values, apparent ages and fading corrected ages of K-feldspar. The well-bleached samples include LUM-4231, LUM-4232, LUM-4236, LUM-4239 and LUM-4240. Samples collected from sands at Khairabad include LUM-4231, LUM-4232 and LUM4236 (Table 5.1, Fig. 5.4). These sediments yield ages of 122 ± 7 ka, 162 ± 13 ka and 190 ± 12 ka respectively. The sand deposits at Ghundi are interpreted to be equivalent of the sands exposed at Khairabad. The sand deposits from the foreland ridges at Ghundi (Fig. 5.8) are also well-bleached and reveal a deposition at 146 ± 8 ka (LUM-4240). The LUM-4239 from Larkakki belongs to the silt deposited and tectonically uplifted at the Larkakki fan apex (Fig. 5.7). Deposition of these sediments occurred at 212 ± 11 ka, i.e., at the initial phase of uplift along the KBF.

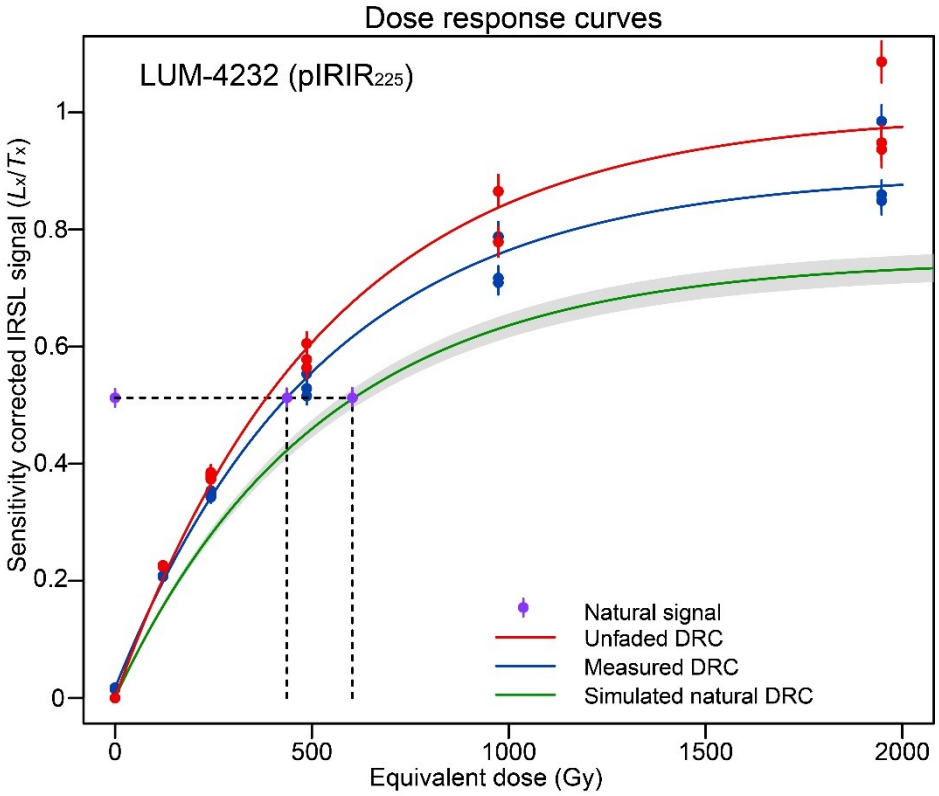

Fig. 5.14 Standard growth curve from LUM-4232 measured in lab, and dose response curve of unfaded signal and simulated natural DRC. Sensitivity corrected natural signal is projected up to the curves for D_e estimation.

5.4.3.2 Quartz OSL

During the pIRIR measurements of K-feldspar, 8 samples show greater overdispersion values in D_e distributions (40-83 %) indicating partial-bleaching of K-feldspar before deposition. As quartz bleaches more quickly than K-feldspar and the lowest pIRIR D_e values also indicate that these sediments are quite younger, therefore, quartz OSL dating was further used to measure the D_e of these 8 samples. The D_e values from quartz also reveal greater overdispersion values and, therefore, quartz grains of these sediments were also partially-bleached before deposition. The minimum age model (MAM) of Galbraith et al. (1999) was applied to get the quartz D_e values used to calculate the ages. The D_e from MAM were calculated using the EXCEL based program after Liang and Forman (2019). The parameter of sigma-b (σ_b) in the MAM model of this program corresponds to the overdispersion of D_e values in the well-bleached samples. 48 aliquots (1 mm) of quartz from LUM-4233 were bleached by the solar simulator and given a dose of 36 Gy, and then measured. The measured D_e values showed an overdispersion of 6 ± 1%. The true overdispersion in well-bleached samples in nature should be larger than this value, due to the dose rate heterogeneity. In this study, the 5 well-bleached samples are beyond quartz dating limit, so the overdispersion of quartz D_e values cannot be deduced from those samples and used as reference. However, the overdispersion of K-feldspar D_e values can provide some constraints. The IRSL signal from K-feldspar grains is much brighter than quartz OSL signal, which would result in smaller uncertainty in counting statistics. The internal K content in K-feldspar would also reduce the effect of heterogeneous micro-dosimetry compared to quartz grains (Guérin et al., 2015; Mayya et al., 2006). Thus, the overdispersion of K-feldspar D_e values should be smaller than quartz D_e values in the well-bleached samples. Apart from the sample LUM-4239 whose overdispersion is 8±2 %, the left 4 well-bleached samples have overdispersion values ranging from 13±3 % to 19±3 % for K-feldspar D_e values. As quartz should have larger overdispersion than K-feldspar, the σ_b was set to 0.2 in the MAM model.

Table 5.4 shows quartz OSL ages calculated using the MAM. Results indicate that these sediments were deposited during the Holocene or at the Pleistocene-Holocene boundary. The quartz OSL ages are discussed here from north to south (Fig. 5.2). The age of LUM-4233 from Khairabad is 12.6 ± 1.4 ka. These sediments have a cross cutting relation with a fault along R2 (Figs. 5.3 and 5.5) and predate the earthquake that had formed the surface rupture. LUM-4235 and LUM-4238 are taken from the east of the R1 and predate the earthquake along R1. The quartz OSL ages of these sediments are nearly similar and reveal a deposition at 11.1 ± 1.3 ka and 11.3 ± 0.9 ka, respectively. The unit-4 in the western part of the trench was deposited after the travertine and formation of the erosional terrace (Fig. 5.6). Therefore, LUM-4234 and LUM-4237 postdate the earthquake along R1. The quartz OSL ages revealed that the sediments were deposited 8.9 ± 0.6 ka and 8.9 ± 1.2 ka ago, respectively. Sample LUM-4230

in the south of Thathi marks the youngest sediments deposited on the alluvial fan, followed by incision of streams on the fan surface. The OSL measurements indicate that the sediments were deposited 2.2 ± 0.3 ka ago. The sediments of the adjoining alluvial fans are more cemented and more compacted than the LUM-4230 sediments. Therefore, LUM-4230 represent the youngest sediments deposited in the central part of the KG section. Moreover, the youngest sediments of the displaced alluvial fan at Ghundi were deposited 1.1 ± 0.2 ka ago, as revealed by the age of LUM-4241, and predate the displacement of the alluvial fan and the shift of the active depositional lobe towards the east. Sample LUM-4242 has yielded an age of 4.1 ± 0.7 ka for the sediments that postdate the transpressional displacement by active faulting along the KBF at Burikhel.

5.5 Discussion

Luminescence ages determined from the 13 samples are classified into two groups. The first group corresponds to well-bleached sediments that yield middle-late Pleistocene ages, between ~212 ± 11 and 122 ± 7 ka. Well-bleached sediments of LUM-4231, LUM-4232, LUM-4236, LUM-4239 and LUM-4240 indicate that these samples belong to the deposits that have undergone transportation and sufficient bleaching prior to deposition. Such transportation and solar bleaching were possible for the far derived river sediments as compared with the locally originated sediments at the mountain front. The second group represents partially-bleached sediments that were deposited during the Holocene and before the seismic deformations. The partially-bleached samples represent the sediments from the foreland and piggyback basin along the KBF (Fig. 5.2). These sediments were deposited in the proximal vicinity from their provenance and did not bleach well-before deposition. Geological evidences suggest these sediments should be younger than the well-bleached samples, as partially-bleached samples are reworked and deposited in the immediate vicinity of the tectonically uplifted sedimentary units of the push-up block.

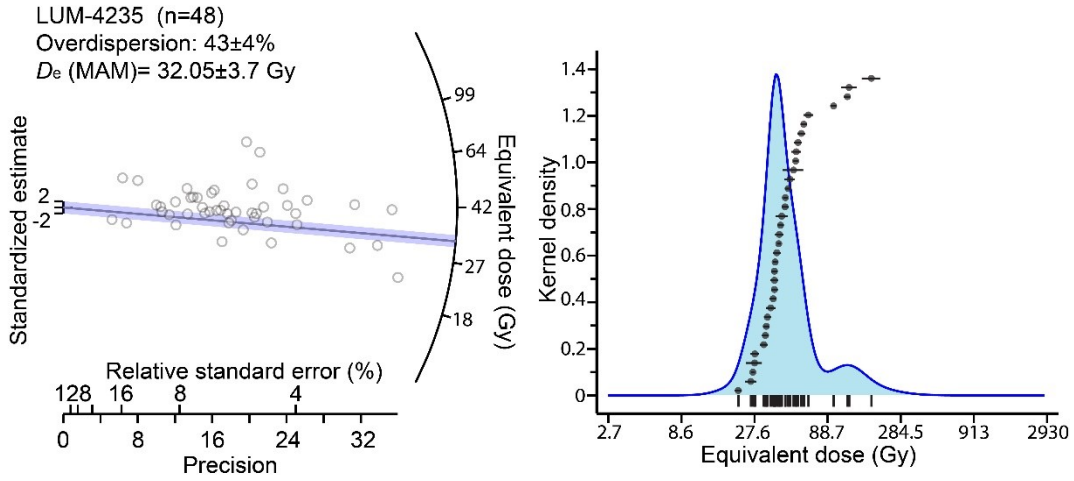

Fig. 5.15 Radial and Kernel density plots of quartz OSL from LUM-4235. Minimum age model was applied for the partially-bleached sediments.

Table 5.4 D_e, dose rate and ages of the samples. In this study CAM was applied for K-feldspar $pIRIR_{225}$ and MAM was used for quartz OSL.

Sample	Dose rate (Gy/ka)	Signal	g_{2days} (%/decade)	ρ' (x10^{-6}) [a]	I_n/I_{field} [b]	$(n/N)_{ss}$ [c]	$(D0)_{ss}$ [d] (Gy)	D_e [e] (Gy)	Fading corrected D_e (Gy)	Apparent age (ka)	Age (ka)
LUM-4230	2.86 ± 0.07	OSL						6.1 ± 0.7			2.2 ± 0.3
LUM-4231	3.90 ± 0.14	$pIRIR_{225}$	2.09 ± 0.09	1.36 ± 0.29	0.59 ± 0.13	0.69 ± 0.15	537 ± 2	330 ± 15	484 ± 23	85 ± 5	122 ± 7
LUM-4232	3.67 ± 0.2	$pIRIR_{225}$	1.42 ± 0.08	1.07 ± 0.32	0.68 ± 0.22	0.75 ± 0.24	522 ± 2	462 ± 22	603 ± 34	127 ± 9	162 ± 13
LUM-4233	2.88 ± 0.13	OSL						36.2 ± 3.7			12.6 ± 1.4
LUM-4234	3.07 ± 0.11	OSL						27.3 ± 1.7			8.9 ± 0.6
LUM-4235	2.90 ± 0.11	OSL						32.1 ± 3.7			11.1 ± 1.3
LUM-4236	3.32 ± 0.13	$pIRIR_{225}$	1.64 ± 0.07	1.03 ± 0.29	0.66 ± 0.18	0.74 ± 0.2	574 ± 2	479 ± 26	638 ± 33	145 ± 10	190 ± 12
LUM-4237	2.81 ± 0.1	OSL						25.1 ± 3.2			8.9 ± 1.2
LUM-4238	2.51 ± 0.1	OSL						28.3 ± 2.04			11.3 ± 0.9
LUM-4239	4.22 ± 0.15	$pIRIR_{225}$	2.14 ± 0.09	1.39 ± 0.28	0.77 ± 0.17	0.69 ± 0.15	612 ± 2	608 ± 16.7	903 ± 31	144 ± 6	212 ± 11
LUM-4240	2.96 ± 0.12	$pIRIR_{225}$	2.00 ± 0.07	1.43 ± 0.26	0.57 ± 0.11	0.68 ± 0.13	521 ± 2	300 ± 17.0	439 ± 17	106 ± 6	146 ± 8
LUM-4241	2.96 ± 0.08	OSL						3.1 ± 0.6			1.1 ± 0.2
LUM-4242	2.88 ± 0.08	OSL						11.7 ± 1.9			4.1 ± 0.7

[a] Density of recombination centers (*ρ'*)

[b] Level of saturation

[c] Field saturation i.e. athermal steady state

[d] Characteristic saturation dose for the stimulated natural DRC

[e] Measured D_e for K-feldspar (Fading uncorrected) or MAM D_e for quartz

The first group is utilized to illustrate the deformation and uplift history of the frontal part of the push-up block (Fig. 5.1c), along with the diversion history of the Indus River. The second group gives timing of the earthquakes that had caused surface ruptures and deformations on the earth surface during the Holocene. Luminescence ages from the pIRIR and OSL dating validate the chronological order of deposition and deformation of the sediments discussed in the following text. Reliability in the MAM results is observed to be quite high as confirmed by the age similarity of LUM-4234 with LUM-4237 and LUM-4235 with LUM-4238. These samples belong to the same sedimentary layers extending laterally along the fault that has ruptured the R1 (Fig. 5.3).

5.5.1 Pleistocene deformation history

5.5.1.1 Khairabad section

Luminescence ages of the samples LUM-4231, LUM-4232 and LUM-4236 represent the timing of deposition along the KBF at Khairabad before they were seismically uplifted up to the present-day elevation (Figs. 5.3 and 5.4). The sand intercalations in diorite bearing conglomerates belong to the paleo Indus River deposits as observed in the Chisal Algad stream. The ages of these sedimentary units therefore, imply that the Indus River was flowing from north to south through Khairabad during ~190 ± 12 to 122 ± 7 ka (Table 5.4). Moreover, the lake sediments of the piggyback basin (Fig. 5.2) overlain by these fluvial deposits imply that the initial expression of the KBF at Khairabad appeared before ~190 ka, forming this piggyback basin behind the drainage divide that was formed along the KBF. As LUM-4231 predates the tectonic uplift at Khairabad, the Indus River had been flowing through Khairabad until ~120 ka and repeated seismic activity along the KBF had uplifted these fluvial deposits afterwards. Considering 12 ± 4 paleoseismic events after Abbas et al. (2022), and accommodation of stress by the aseismic KBF, a long earthquake recurrence interval for the KBF is suggested at Khairabad during the last ~120 ka, that is, 10 ± 2 ka on average.

5.5.1.2 Larkakki section

The sample LUM-4239 represents sediments at the apex of the Larkakki alluvial fan that were deposited at 212 ± 11 ka (Fig. 5.7, Table 5.4). An initial bulge was formed along the KBF at this location that caused inception of the alluvial fan. Further uplift along the KBF had uplifted the sediments on the alluvial fan apex. This implies that uplift of the push-up block at Larkakki started at ~220 ka, i.e., before the deposition of these sediments on the alluvial fan (Fig. 5.7b).

Abbas et al. (2022) have established that the inception of the KBF stepover was synchronous with the termination of the TSK deposition that is around 0.5 Ma. Whereas, the ~190 and ~220 ka timing of the first surface expression of the KBF at Khairabad and Larkakki indicates the timing of the strain

development in the north and the south of the restraining faults of the stepover zone. These evidences suggest the rise of the push-up block in two phases: (i) ~500 to ~220 ka between the restraining faults (ii) ~220 ka to the present in the north and the south of the restraining faults (Fig. 5.16).

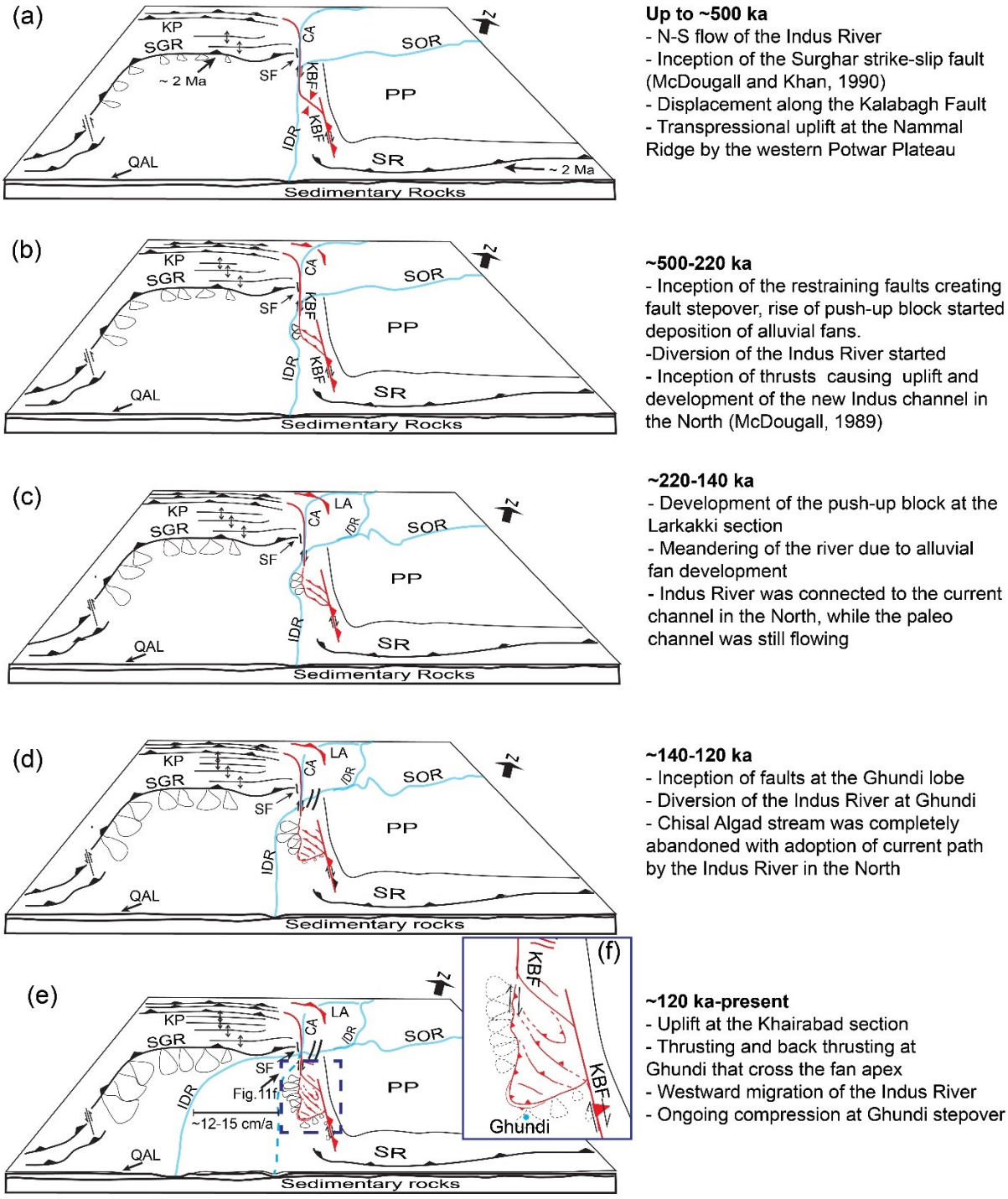

Up to ~500 ka
- N-S flow of the Indus River
- Inception of the Surghar strike-slip fault (McDougall and Khan, 1990)
- Displacement along the Kalabagh Fault
- Transpressional uplift at the Nammal Ridge by the western Potwar Plateau

~500-220 ka
- Inception of the restraining faults creating fault stepover, rise of push-up block started deposition of alluvial fans.
-Diversion of the Indus River started
- Inception of thrusts causing uplift and development of the new Indus channel in the North (McDougall, 1989)

~220-140 ka
- Development of the push-up block at the Larkakki section
- Meandering of the river due to alluvial fan development
- Indus River was connected to the current channel in the North, while the paleo channel was still flowing

~140-120 ka
- Inception of faults at the Ghundi lobe
- Diversion of the Indus River at Ghundi
- Chisal Algad stream was completely abandoned with adoption of current path by the Indus River in the North

~120 ka-present
- Uplift at the Khairabad section
- Thrusting and back thrusting at Ghundi that cross the fan apex
- Westward migration of the Indus River
- Ongoing compression at Ghundi stepover

Fig. 5.16 Schematic model showing chronology of development of the push-up block in the Kalabagh Fault stepover zone, along with the eastward diversion of the Indus River (McDougall, 1989) and westward migration as inferred from the Luminescence dating, modified after Abbas et al. (2022). Remaining tectonic features are presented according to the present stage and alluvial fans are symbolic. Fig. 5.16f shows zoomed in segment at present level. Model is without scale and alluvial fans are symbolic. CA=Chisal Algad, IDR=Indus River, KBF=Kalabagh Fault, KP=Kohat Plateau, LA=Lagorai Algad, PP=Potwar Plateau, QAL=Quaternary Alluvium, SF= Surghar Fault, SGR=Surghar Range, SOR=Soan River, SR=Salt Range

5.5.1.3 Diversion of the Indus River

Fig. 5.16 illustrates different stages of evolution and chronology of the stepover development and uplifting of the push-up block along with the Indus River diversion. The sample LUM-4240 belongs to the foreland ridges at the Ghundi section that consist of the QKC sediments on the earth surface, underlain by the sands (Fig. 5.8). Abbas et al. (2022) have suggested that these sands form a time-equivalent to the sand deposits below the lake sediments at Khairabad (Fig. 5.4). The possibility of these sands to be deposited by the Wahi stream in the south of the KBF stepover is not convincing, as the Wahi stream is flowing through the Nammal Ridge and has deposited the Nammal alluvial fan (Fig. 5.1c). The Wahi stream is diverted northwards due to the development of the Nammal alluvial fan and therefore it has not deposited these sand sediments. The sands were deposited by the same sediment source as that of the sands at the Khairabad section, i.e., Indus River. the Indus River was flowing through Ghundi until uplift of the push-up block along the KBF started westward diversion of the Indus River, whereas sediments from the uplifting sedimentary rocks were reworked and deposited as the QKC above the Indus River sands. The pIRIR age of LUM-4240 is 146 ± 8 ka and implies two conclusions: (i) it determines the age for the base of the QKC at Ghundi that marks the onset of the uplift along the KBF, (ii) as it predates the uplift of the push-up block at Ghundi that has diverted the course of the Indus River, the inception of the push-up block and diversion of the Indus River at Ghundi occurred at ~140 ka. Moreover, the fluvial sediments represented by the samples LUM-4231, LUM-4232 and LUM-4236 from Khairabad indicates the Indus River was flowing along the KBF until ~120 ka. Based on our dating results, we infer that the inception of the stepover zone between the restraining faults, uplift of the push-up block and deposition of the alluvial fans has started the divergence of the Indus River during past ~500 to ~220 ka (Fig. 5.16). The diversion was followed by the westward migration of the Indus River channel since ~140 ka at Ghundi and ~120 ka at Khairabad. Our evidences cumulatively imply a ~12-15 cm/a westward diversion rate of the Indus River to migrate it ~15-18 km away from the KBF, bringing the river channel up to its present-day location.

5.5.2 Holocene seismicity

The MAM ages from the quartz OSL are given in Table 5.4, exhibiting the timing of deposition of these sediments during the Holocene. Sample LUM-4230 represents the youngest sediments on the alluvial fan. As the deeply incised streams in the push-up block have reduced the sediment influx and stopped the development of the alluvial fans in the south of Thathi (Fig. 5.2), this episode was followed by the incision of the alluvial fans. The OSL dating of these sediments exhibit an age of 2.2 ± 0.3 ka (Tables 5.1 and 5.4). This implies the development of the alluvial fans was stopped at ~2.2 ± 0.3 ka in the central part of the KG section. Lack of paleoseismic evidences suggest that the central part of the KG

section, that is also acting as a restraining bend, is tectonically mature as compared with the Khairabad and the Ghundi sections.

The samples from the Khairabad section represent the sediments that have a cross-cutting relation with the faults and predate or postdate the seismic displacements along these faults (Fig. 5.5 and 5.6). The quartz OSL dates of LUM-4234, 4235, 4237, 4238 imply that displacement along the R1 occurred due to an earthquake at ~9 ka ago (Figs. 5.3 and 5.6). Undisturbed travertine deposits overlying the fault trace indicate that the R1 has not been displaced afterwards. Moreover, the sample LUM-4233 was collected from the sediments that are crosscut by the R2 (Fig. 5.5) and yields an age of 12.6 ± 1.4 ka, indicating an earthquake younger than 12.6 ± 1.4 ka. As the ages only predate or postdate the earthquakes, the R1 and R2 are either formed by the concurrent events or there was a recurrence interval of 2-3 ka between these two earthquakes. In both cases, the latest earthquake at Khairabad occurred along the R1 at ~9 ka ago. Furthermore, considering the estimated earthquake recurrence interval of ~10 ± 2 ka during the past ~120 ka at Khairabad, along with the latest earthquake at ~9 ka and ongoing displacements that are decreasing southward from the Ainwan and Dinghot splay faults (Chen and Khan, 2010), it can be inferred that the stress accumulation at Khairabad is reaching the inflection point of deformation that can lead to release of stress in the form of earthquakes.

OSL dating of LUM-4241 reveals that the youngest sediments at the Ghundi alluvial fan were deposited 1.1 ± 0.2 ka ago (Table 5.4), until an earthquake has disrupted the antithetic fault across the fan apex (Figs. 5.8 and 5.16f). The displacement of the alluvial fan was followed by morphological degradation. This defines the latest seismic displacement that occurred at the stepover at Ghundi happened during past ~1 ka. A recent M_w=4.6 earthquake observed in the south of this area indicates the active foreland seismicity. The deposition of sample LUM-4242 dates to 4.1 ± 0.7 ka (Fig. 5.9) which reflects an earthquake causing an uplift along the range front at ~5 ka at Burikhel, forming a piggyback basin. The foreland of the Nammal Ridge has also lower aseismic displacements as compared with other segments of the KBF (Chen and Khan, 2010). Relatively younger paleoseismic events at Ghundi and Burikhel along with lower displacement rates indicate more stress accumulation in this part of the KBFZ that can produce more earthquakes with shorter earthquake intervals.

5.6 Conclusions

With the chronology of the paleoseismic features presented here, we have established a framework for the timing and recurrence intervals of surface rupturing earthquakes in the fault zone that is regarded as an aseismically active part of the KBFZ. The pIRIR ages of the deformed middle-late Pleistocene sediments and sedimentary correlations are used to decipher the deformation history of

the KBFZ. The KBFZ has undergone major tectonic deformations during the past ~0.5 Ma. The Indus River has been flowing from north to south along the KBF until ~0.5 Ma. The tectonic uplift of the push-up block has gradually diverted the course of the Indus River towards the west with a major diversion that occurred during the last ~140 ka. The MAM of correlated sediments proves it as a reliable statistical approach for age estimations of partially-bleached alluvial fan sediments with a nearby provenance. Apart from the aseismic displacements and dissipation of stress in the KBFZ, the KBFZ is still able to produce surface rupturing earthquakes. However, the earthquake recurrence interval along the KBF is long. The Khairabad, Ghundi and Burikhel are the most likely sections that can produce earthquakes. The foreland in the south of the stepover is seismically more active with shorter earthquake recurrence intervals. In contrast, ongoing stress accumulation at the Khairabad section during the past ~9 ka might point to an increased seismic hazard.

Acknowledgments

We would like to thank the “Higher Education Commission, Pakistan” and the “German Academic Exchange Service (DAAD), Germany” for the financial and management support for this research. The experiments were conducted at the Leibniz Institute for Applied Geophysics, Hannover. Technical help by Petra Posimowski, Sabine Mogwitz and Sonja Riemenschneider was important during the lab experiments. We are also grateful for the field work cooperation by Farooq Sultan from the Mines and Minerals department, Punjab, Pakistan.

6. Conclusions and outlook

6.1 Conclusions

Morphotectonic parameters were analyzed in the Sub-Himalayas to assess the active tectonics of the area. Whereas paleoseismic investigations along the Kalabagh Fault were carried out to describe the late Quaternary deformations and seismic history. The analysis reveals that a morphometric indicator in the study area cannot be applied alone, rather a tectonic activity Index (I_{at}) that is calculated from multiple morphometric indices can yield results that are comparable with the instrumental data. This is because of lithological controls and geological context of the study area.

Tectonic geomorphology and paleoseismology are helpful tools to investigate the deformation and seismic history for aseismically moving active faults with long earthquake recurrence intervals. Luminescence dating techniques were applied to determine the ages of the deformed sediments, that convincingly describe the paleoseismic history of the Kalabagh Fault. The deformation history of the stepover zone of the Kalabagh Fault during past ~ 0.5 Ma is described by luminescence dating of the tectonically deformed sediments. This study establishes that a fault stepover between the Khairabad-Ghundi section and the Nammal Ridge got the first surface expression ~0.5 Ma ago. This stepover developed push-up structure, in the first phase, between the Thathi and Zaluch up to ~220 ka. In the second phase, the landform was developed at Larkakki, Khairabad and Ghundi during the last ~220 ka, ~190 ka and ~140 ka, respectively. The deformation during past ~0.5 Ma is synchronous with the major distortions along the Chisal Algad stream, as suggested by McDougall (1989b).

The Indus River in the Mianwali Reentrant was flowing along the strike of the Kalabagh Fault until ~0.5 Ma. At the start of the tectonic uplift of the push-up block and deposition of alluvial fans, a meander was formed in the Indus River. At later stage, the landform was further developed, and reworked sediments were deposited and formed more alluvial fans at the foothills. This was coincided by a diversion of the Indus River towards the West. The Indus River was flowing along the Kalabagh Fault until ~ 0.5 Ma at Zaluch and Thathi, ~220 ka at Larkakki, ~140 ka at Ghundi and ~120 ka at Khairabad (Table 5.4, Figs. 5.2 and 5.16). This tectonic diversion was synchronous with the eastward diversion of the Indus River in the North.

Stream deflections in the late Quaternary sediments confirm the ongoing dextral movement in the fault zone. The Kalabagh Fault and its offshoots in the Khairabad section reveal surface rupturing earthquakes that have occurred in the early Holocene at Khairabad (~ 9 ka), mid-Holocene at Burikhel (~ 5 ka), and late Holocene (~ 1 ka) at Ghundi. This diachronous activity denotes the caterpillar type of movement along the Kalabagh Fault, where displacement and seismicity are temporally and

geographically distributed. The Khairabad section exhibits an earthquake recurrence interval of ~10±2 ka on average. The ~ 9 ka earthquake is the youngest seismic event as shown by undisturbed travertine deposits covering the fault trace. This indicates the Khairabad section is close to the inflection point of stress accumulation and may pose a seismic risk. Whereas, small magnitude earthquakes, in the foreland of the Ghundi stepover and ~ 1 ka old seismic event displacing the fan apex shows seismically active behavior of the faut stepover.

6.2 Outlook

The tectonic history of the Sub-Himalayas in Pakistan was investigated by various authors using sedimentary chronology older than late Pleistocene. Whereas instrumental data such as seismic catalogs, GPS and InSAR data were utilized to evaluate the active tectonics. This leaves a research gap to illustrate the active faults with higher earthquake recurrence interval, that span beyond human civilization archives. Moreover, after the M_w=5.4 earthquake of 2019 nearby Mangla dam reservoir, the paleoseismic investigations gain more importance to draw the level of seismic risks. Therefore, the morphotectonics and paleoseismology combined with chronology of the late Quaternary sediments are the best sources of information in this situation. The methods may be applied to the mountain fronts along the Jhelum Fault, Salt Range, Surghar Range, Bannu Basin, Khisor Range, Marwat Range and the Kurram Fault. These faults and mountain ranges in the absence of the seismic catalogs can present fruitful information, if the paleoearthquakes and their recurrence intervals are estimated.

The base of the Kalabagh Conglomerates marks the onset of the landform development. The timing of the formation of surface expressions varies among different faults. The chronology for the base of the Kalabagh Conglomerates can thus be determined using modern dating methods. This may lead to further elaborate the evolution and deformation of the faults and mountain ranges, where morphotectonic features are not evident.

References

Abbas, W., Ali, S., Reicherter, K., 2022. Seismicity and landform development of the dextral Kalabagh Fault Zone, Pakistan: Implications from morphotectonics and paleoseismology. Tectonophysics 822, 229182. https://doi.org/10.1016/j.tecto.2021.229182

Abbasi, I.A., 1991. Large scale vertical aggradation of sandstones in the Kamlial Formation of the Kohat Basin, Pakistan. Geol. Bull. Univ. Peshawar 24, 33–44.

Abbasi, I.A., Haneef, M., Obaid, S., Daud, F., Qureshi, A.W., 2011. Mesozoic deltaic system along the western margin of the Indian plate : lithofacies and depositional setting of Datta Formation , North Pakistan. Arab. J. Geosci. 5, 471–480. https://doi.org/10.1007/s12517-010-0276-1

Abbasi, I.A., Khan, M.A., 1990. Heavy mineral analysis of the Molasse sediments, Trans Indus ranges, Kohat, Pakistan. Geol. Bull. Univ. Peshawar 23, 215–229.

Abbasi, I.A., McElroy, R., 1991. Thrust kinematics in the Kohat Plateau, Trans Indus Range, Pakistan. J. Struct. Geol. 13, 319–327.

Abbasi, N., Khan, M.S., Mughal, M.S., Yasin, M., 2017. Sedimentary facies analysis of Nagri Formation, Kashmir Basin, Sub-Himalayas, Pakistan. Pakistan J. Geol. 1, 3–6.

Abir, I.A., Khan, S.D., Aziz, G.M., Tariq, S., 2017. Bannu Basin, fold-and-thrust belt of northern Pakistan: Subsurface imaging and its implications for hydrocarbon exploration. Mar. Pet. Geol. 85, 242–258. https://doi.org/10.1016/j.marpetgeo.2017.05.023

Abir, I.A., Khan, S.D., Ghulam, A., Tariq, S., Shah, M.T., 2015. Active tectonics of western Potwar Plateau–Salt Range, northern Pakistan from InSAR observations and seismic imaging. Remote Sens. Environ. 168, 265–275. https://doi.org/10.1016/j.rse.2015.07.011

Ahmad Abir, I., 2012. Application of InSAR and 2D seismic interpretation for salt tectonic studies in the Salt Range and Potwar Plateau region, northern Pakistan. University of Houston.

Ahmad, I., Ahmad, Z., Munir, S., Ali, S.R., Shabbir, Y., 2018. Characterization of Upper Indus Basin based on DEM Hypsometric Analysis. Nucl. 55, 8–16.

Ahmad, S., 2009. Seismicity in Pakistan during 2008 and Local Site Response in Muzaffarabad and Islamabad , Pakistan.

Ahmad, S., Ali, F., Sayab, M., Ahmad, I., Hamidullah, S., 1999. Structural geometry of the Himalayan Frontal Thrust Zone: Surghar Range, Pakistan. Geol. Bull. Univ. Peshawar 32, 13–23.

Ahmad, S., Rigby, Su., Kroon, D., Khan, S., Haneef, M., Ahamd, S., 2011. Integrated Paleogene Sequence Stratigraphy of the Kohat Basin , Northwest Pakistan. Pakistan J. Hydrocarb. Res. 21, 41–47.

Ahmad, S., Wadood, B., Khan, S., Ahmed, S., Ali, F., Saboor, A., 2020. Integrating the palynostratigraphy , petrography , X - ray diffraction and scanning electron microscopy data for evaluating hydrocarbon reservoir potential of Jurassic rocks in the Kala Chitta Range , Northwest Pakistan. J. Pet. Explor. Prod. Technol. https://doi.org/10.1007/s13202-020-00957-7

Ahmad, S., Waqas, M., Khan, S.S., Swati, M.A.F., Jan, I.U., Ali, F., Yaqoob, M., Sadiq, A., Khan, S., Rehman, I. ur, 2015. Facies analysis and dynamic depositional modelling of the Upper Permian Chhidru Formation , Salt Range , Upper Indus Basin , Pakistan. J. Himal. Earth Sci. 48, 64–80.

Ahmed, S., Mertmann, D., Manoutsoglou, E., 1997. Jurassic shelf sedimentation and sequence stratigraphy of the Surghar Range, Pakistan. J. Nepal Geol. Soc. 15, 15–22.

Ahsan, N., Chaudhry, M.N., 2008. Geology of the Hettangian to middle Eocene rocks of Hazara and Kashmir basins, Northwest Lesser Himalayas, Pakistan.

Alam, I., 2008. Structural and stratigraphic framework of the Marwat-Khisor ranges, N-W.F.P., Pakistan. University of Peshawar.

Ali, A., 2010. Structural Analysis of the Trans-Indus Ranges: Implications for the Hydrocarbon Potential of the NW Himalayas, Pakistan. University of Peshawar, Pakistan.

Ali, F., Khan, M.I., Ahmad, S., Rehman, G., Rehman, I., Ali, T.H., 2014. Range front structural style: An example from Surghar Range, North Pakistan. J. Himal. Earth Sci. 47, 193–204.

Ali, F., Qiang, J., Ahmad, S., Khan, S., Hanif, M., Jan, I.U., 2019. Sedimentological and Geochemical Analysis of the Middle Jurassic Shinawari Formation , Upper Indus Basin , Pakistan : Implications for Palaeoenvironmental and Hydrocarbon Assessment. Arab. J. Sci. Eng. 44, 6465–6487. https://doi.org/10.1007/s13369-019-03778-x

Ali, S., Biermanns, P., Haider, R., Reicherter, K., 2018. Landslide susceptibility mapping by using GIS along the China–Pakistan economic corridor (Karakoram Highway), Pakistan. Nat. Hazards Earth Syst. Sci. Discuss. 1–28. https://doi.org/10.5194/nhess-2018-39

Asrarullah, 1967. Geology of the Khewra Dome.

Auclair, M., Lamothe, M., Huot, S., 2003. Measurement of anomalous fading for feldspar IRSL using SAR. Radiat. Meas. 37, 487–492. https://doi.org/10.1016/S1350-4487(03)00018-0

Awais, M., Hanif, M., Jan, I.U., Ishaq, M., Khan, M.Y., 2020. Eocene carbonate microfacies distribution of the Chorgali Formation, Gali Jagir, Khair-e-Murat Range, Potwar Plateau, Pakistan: approach of reservoir potential using outcrop analogue 13.

Awais, M., Ullah, F., Khan, N., Ghani, M., Siyar, S.M., Wadood, B., Mukhtiar, A., 2019. Investigation of reservoir characteristics , depositional setting and T – R sequences of the Lockhart Limestone of Meyal Oil Field , Pakistan : a petrophysical approach. J. Pet. Explor. Prod. Technol. 9, 2511–2530. https://doi.org/10.1007/s13202-019-0730-x

Baig, M.S., Yeats, R.S., Pervez, S., Jadoon, I.A.K., Khan, M.R., Sidiqui, I., Saleem, M., 2010. Active tectonics , October 8 , 2005 earthquake deformation , active uplift , scarp morphology and seismic geohazards microzonation , Hazara-Kashmir Syntaxis , Northwest Himalayas , Pakistan 43, 17–21.

Baker, D.M., Lillie, R.J., Yeats, R.S., Johnson, G.D., Yousuf, M., Zamin, A.S.H., 1988. Development of the Himalayan frontal thrust zone: Salt Range, Pakistan. Geology 16, 3–7. https://doi.org/10.1130/0091-7613(1988)016<0003:DOTHFT>2.3.CO;2

Bakr, M.A., Jackson, R.O., 1964. Geological map of Pakistan.

Barndt, J., Johnson, N.M., Johnson, G.D., Opdyke, N.D., Lindsay, E.H., Pilbeam, D., Tahirkheli, R.A.K., 1978. The magnetic polarity stratigraphy and age of the Siwalik group near Dhok Pathan village, Potwar plateau, Pakistan. Earth Planet. Sci. Lett. 41, 355–364.

Barnhart, W.D., 2017. Fault creep rates of the Chaman fault (Afghanistan and Pakistan) inferred from InSAR. J. Geophys. Res. Solid Earth 122, 372–386. https://doi.org/10.1002/2016JB013656

Bilal, A., Yasin, M., Ali, A., 2017. The geology and structure of Neogene rocks in Dadyal and adjacent areas, in the Sub-Himalayas, Azad Jammu and Kashmir, Pakistan. Earth Sci. Malaysia 1, 15–20.

Biswas, A., Majumdar, D. Das, Banerjee, S., 2014. Morphometry Governs the Dynamics of a Drainage Basin : Analysis and Implications 2014.

Bossart, P., Ottiger, R., 1989. Rocks of the Murree formation in Northern Pakistan : indicators of a descending foreland basin of late Paleocene to middle Eocene age. Eclogae geol. Helv.1 82, 133–165.

Brennan, B.J., Lyons, R.G., Phillips, S.W., 1991. Attenuation of alpha particle track dose for spherical grains. Int. J. Radiat. Appl. Instrumentation. Part D. Nucl. Tracks Radiat. Meas. 18, 249–253. https://doi.org/10.1016/1359-0189(91)90119-3

Bull, W., 2007. Tectonic Geomorphology of Mountains, 1st ed. Blackwell Publishing Ltd.

Bull, W.B., 2007. Tectonic Geomorphology of Mountains. Blackwell Publishing Ltd, Oxford, UK. https://doi.org/10.1002/9780470692318

Bull, W.B., Mcfadden, L.D., 1977. Tectonic Geomorphology North and South of the Garlock Fault, California.

Burbank, D.W., Anderson, R.S., 2001. Tectonic geomorphology. Blackwell SCience Ltd. https://doi.org/10.5408/0022-1368-32.5.310

Butler, R.W.H., Coward, M.P., Harwood, G.M., Knipe, R.J., 1987. Salt Control on Thrust Geometry, Structural Style and Gravitational Collapse Along the Himalayan Mountain Front in the Salt Range of Northern Pakistan, Dynamical Geology of Salt and Related Structures. https://doi.org/10.1016/b978-0-12-444170-5.50013-0

Buylaert, J.-P., Jain, M., Murray, A.S., Thomsen, K.J., Thiel, C., Sohbati, R., 2012. A robust feldspar luminescence dating method for Middle and Late Pleistocene sediments. Boreas 41, 435–451. https://doi.org/10.1111/j.1502-3885.2012.00248.x

Buylaert, J.-P., Thiel, C., Murray, A., Vandenberghe, D., Yi, S., Lu, H., 2011. IRSL and post-IR IRSL residual doses recorded in modern dust samples from the Chinese Loess Plateau. Geochronometria 38, 432–440. https://doi.org/10.2478/s13386-011-0047-0

Buylaert, J.P., Murray, A.S., Thomsen, K.J., Jain, M., 2009. Testing the potential of an elevated temperature IRSL signal from K-feldspar. Radiat. Meas. 44, 560–565. https://doi.org/10.1016/j.radmeas.2009.02.007

Calkins, J.A., Offield, T.W., Abdullah, S.K.M., Ali, S.T., 1975. Geology of the southern Himalaya in Hazara , Pakistan , and adjacent areas. United States Geol. Surv. Prof. Pap. VOL 716-C, Page 15-20.

Campagna, D.J., Levandowski, D.W., 1991. The recognition of strike-slip fault systems using imagery, gravity, and topographic data sets. Photogramm. Eng. Remote Sens. 57, 1195–1201.

Chaudhry, M.N., Ghazanfar, M., 1990. Position of the Main Central Thrust in the tectonic framework of Western Himalaya. Tectonopgysics.

Chaudhry, M.N., Mahmood, T., Ahmed, R., Ghazanfar, M., 1992. A Reconnaissance Microfacies Study of Kawagarh Formation Near Giah, Abbottabad-Nathiagali Road, Hazara, Pakistan. Pakistan J. Hydrocarb. Res. 4, 19–32.

Cheema, M.R., Raza, S.M., Ahmad, H., 1977. Cenozoic, in: Shah, S.M.I. (Ed.), Memoirs of the Geological

Survey of Pakistan, Startigraphy of Pakistan. Geological Suvrey of Pakistan, Quetta, pp. 56–98.

Chen, L., Khan, S.D., 2010. InSAR observation of the strike-slip faults in the northwest Himalayan frontal thrust system. Geosphere 6, 731–736. https://doi.org/10.1130/GES00518.1

Colarossi, D., Duller, G.A.T., Roberts, H.M., 2018. Exploring the behaviour of luminescence signals from feldspars: Implications for the single aliquot regenerative dose protocol. Radiat. Meas. 109, 35–44. https://doi.org/10.1016/j.radmeas.2017.07.005

Cortés-Aranda, J., Mugnier, J.-L., Jouanne, F., Vassallo, R., Carcaillet, J., Alam Awan, A., 2017. Holocene shortening rates and seismic hazard assessment for the frontal Potwar Plateau, NW Himalaya of Pakistan: Insights from 10 Be concentrations on fluvial terraces of the Mahesian Anticline. Quat. Int. 462, 75–89. https://doi.org/10.1016/j.quaint.2017.02.032

Crawford, A.R., 1974. The Salt Range, the Kashmir Syntaxis and the Pamir Arc. Earth Planet. Sci. Lett. 22, 371–379. https://doi.org/10.1016/0012-821X(74)90147-2

Dar, R.A., Romshoo, S.A., Chandra, R., Ahmad, I., 2014. Tectono-geomorphic study of the Karewa Basin of Kashmir Valley Tectono-geomorphic study of the Karewa Basin of Kashmir Valley. J. ASIAN EARTH Sci. 92, 143–156. https://doi.org/10.1016/j.jseaes.2014.06.018

Dawar, M.A.K., Khan, A., Rehman, F., Husain, A., Afridi, A.G.K., 2009. Geological map of the Sabirabad quadrangle, Karak district, NWFP and parts of Mianwali district, Punjab, Pakistan.

Demanet, D., Evers, L.G., Teerlynck, H., Dost, B., Jongmans, D., 2001. Geophysical investigation across the Peel boundary fault (The Netherlands) for a paleoseismological study. Netherlands J. Geosci. 80, 119–127. https://doi.org/10.1017/S0016774600023787

Dipietro, J.A., Pogue, K.R., 2004. Tectonostratigraphic subdivisions of the Himalaya : A view from the west. Tectonics 23. https://doi.org/10.1029/2003TC001554

Doornkamp, J.C., 1986. Geomorphological approaches to the study of neotectonics. J. Geol. Soc. London. 143, 335–342. https://doi.org/10.1144/gsjgs.143.2.0335

Duller, G.A.., Bøtter-Jensen, L., Murray, A.., 2000. Optical dating of single sand-sized grains of quartz: sources of variability. Radiat. Meas. 32, 453–457. https://doi.org/10.1016/S1350-4487(00)00055-X

El Hamdouni, R., Irigaray, C., Fernández, T., Chacón, J., Keller, E.A., 2008. Assessment of relative active tectonics, southwest border of the Sierra Nevada (southern Spain). Geomorphology 96, 150–173. https://doi.org/10.1016/j.geomorph.2007.08.004

Fatmi, A.N., 1977. Mesozoic, in: Shah, S.M.I. (Ed.), Memoirs of the Geological Survey of Pakistan, Startigraphy of Pakistan. Geological Suvrey of Pakistan, Quetta, pp. 29–56.

Fatmi, A.N., Hölder, H., 1975. A new Lower Jurassic ammonite genus Kohaticeras from the Shinawari Formation , Kohat Tribal Belt , Pakistan. Paläont.Z 49, 35–43.

Fattahi, M., Walker, R., Hollingsworth, J., Bahroudi, A., Nazari, H., Talebian, M., Armitage, S., Stokes, S., 2006. Holocene slip-rate on the Sabzevar thrust fault, NE Iran, determined using optically stimulated luminescence (OSL). Earth Planet. Sci. Lett. 245, 673–684. https://doi.org/10.1016/j.epsl.2006.03.027

Fu, X., Li, S.H., Li, B., 2015. Optical dating of aeolian and fluvial sediments in north Tian Shan range, China: Luminescence characteristics and methodological aspects. Quat. Geochronol. 30, 161–167. https://doi.org/10.1016/j.quageo.2015.03.001

Gaetani, M., Garzanti, E., 1991. Multicyclic History of the Northern India Continental Margin (Northwestern Himalaya) (1). Am. Assoc. Pet. Geol. Bull. 75, 1427–1446. https://doi.org/10.1306/0C9B2957-1710-11D7-8645000102C1865D

Gaidzik, K., Ramírez-Herrera, M.T., 2017. Geomorphic indices and relative tectonic uplift in the Guerrero sector of the Mexican forearc. Geosci. Front. 8, 885–902. https://doi.org/10.1016/j.gsf.2016.07.006

Galbraith, R.F., Roberts, R.G., Laslett, G.M., Yoshida, H., Olley, J.M., 1999. Optical dating of single and multiple grains of quartz from Jinmium rock shelter, northern Australia: Part I, experimental design and statistical models. Archaeometry 41, 339–364. https://doi.org/10.1111/j.1475-4754.1999.tb00987.x

Gansser, A., 1964. Geology of the Himalayas. A Vol. Reg. Geol. Ser. 39–79.

Gao, M., Zeilinger, G., Xu, X., Tan, X., Wang, Q., Hao, M., 2016. Active tectonics evaluation from geomorphic indices for the central and the southern Longmenshan range on the Eastern Tibetan Plateau, China. Tectonics 35, 1812–1826. https://doi.org/10.1002/2015TC004080

Gee, E.R., 1980. Salt Range Series Geological Maps: Directorate of Overseas Surveys, United Kingdom, Government of Pakistan and Pakistan Geological Survey, Scale 1:50,000, 6 Sheets.

Ghani, H., 2019. Structural Evolution of the Kohat and Potwar Fold and Thrust Belts of Pakistan. Universität Potsdam.

Ghani, H., Zeilinger, G., Sobel, E.R., Heidarzadeh, G., 2018. Structural variation within the Himalayan

fold and thrust belt : A case study from the Kohat-Potwar Fold Thrust Belt of Pakistan Structural variation within the Himalayan fold and thrust belt : A case study from the Kohat-Potwar Fold Thrust Belt of Pakis. J. Struct. Geol. 116, 34–46. https://doi.org/10.1016/j.jsg.2018.07.022

Ghauri, A.A.K., Anwar, M., Kamel, K.S., Issa, I.M., 1977. The Study of Nature and origin of the Tobra Formation in the Eastern part of the Punjab Salt Range. Geol. Bull. Univ. Peshawar 9–10, 67–81.

Ghazi, S., Mountney, N.P., 2009. Facies and architectural element analysis of a meandering fl uvial succession : The Permian Warchha Sandstone , Salt Range , Pakistan. Sediment. Geol. 221, 99–126. https://doi.org/10.1016/j.sedgeo.2009.08.002

Ghazi, S., Mountney, N.P., Butt, A.A., Sharif, S., 2012. Stratigraphic and palaeoenvironmental framework of the Early Permian sequence in the Salt Range , Pakistan IS. J. Earth Syst. Sci. 121, 1239–1255.

Gourabi, A., Yamani, M., 2011. Active Faulting and Quaternary Landforms Deformation Related to the Nain Fault. Am. J. Environ. Sci. 7, 441–447. https://doi.org/10.3844/ajessp.2011.441.447

Grützner, C., Reicherter, K., Hübscher, C., Silva, P.G., 2012. Active faulting and neotectonics in the Baelo Claudia area, Campo de Gibraltar (southern Spain). Tectonophysics 554–557, 127–142. https://doi.org/10.1016/j.tecto.2012.05.025

Guérin, G., Jain, M., Thomsen, K.J., Murray, A.S., Mercier, N., 2015. Modelling dose rate to single grains of quartz in well-sorted sand samples: The dispersion arising from the presence of potassium feldspars and implications for single grain OSL dating. Quat. Geochronol. 27, 52–65. https://doi.org/https://doi.org/10.1016/j.quageo.2014.12.006

Guérin, G., Mercier, N., Nathan, R., Adamiec, G., Lefrais, Y., 2012. On the use of the infinite matrix assumption and associated concepts: A critical review. Radiat. Meas. 47, 778–785. https://doi.org/10.1016/j.radmeas.2012.04.004

Hack, J.T., 1973. Stream-profile analysis and stream-gradient index. J. Res. U.S. Geol. Surv. 1, 421–429.

Hallam, A., Maynard, J.B., 1987. The iron ores and associated sediments of the Chichali formation (Oxfordian to Valanginian) of the Trans-Indus Salt Range , Pakistan. J. Geol. Soc. London 144, 107–114.

Henderson, A.L., Najman, Y., Parrish, R., Mark, D.F., Foster, G.L., 2011. Constraints to the timing of India–Eurasia collision; a re-evaluation of evidence from the Indus Basin sedimentary rocks of the Indus–Tsangpo Suture Zone, Ladakh, India. Earth-Science Rev. 106, 265–292. https://doi.org/10.1016/j.earscirev.2011.02.006

Honegger, K., Dietrich, V., Frank, W., Gansser, A., Thrni, M., Trommsdorff, V., 1982. Magmatism and metamorphism in the Ladakh Himalayas (the Indus-Tsangpho suture zone). Earth Planetry Sci. Lett. 60, 253–292.

Huntley, D., Baril, M., 1997. The K content of the K-feldspars being measured in optical dating or in thermoluminescence dating. Anc. TL 15, 11–13.

Huntley, D.J., Hancock, R., 2001. The Rb contents of the K-feldspar grains being measured in optical dating. Anc. TL 19, 43–46.

Iqbal, S., Jan, I.U., Akhter, M.G., Bibi, M., 2015. Palaeoenvironmental and sequence stratigraphic analyses of the Jurassic Datta Formation , Salt Range , Pakistan. J. Earth Syst. Sci. 124, 747–766.

Iqbal, S., Jan, I.U., Hanif, M., 2013. The Mianwali and Tredian Formations : An Example of the Triassic The Mianwali and Tredian Formations : An Example of the Triassic Progradational Deltaic System in the Low-Latitude Western Salt Range , Pakistan. Arab. J. Sci. Eng. https://doi.org/10.1007/s13369-013-0836-2

Ivo, S., Maschio, L., Alessio, M., Ferranti, L., Improta, S., Schiattarella, M., 2000. Radiocarbon dating of active faulting in the Agri high. J. Geodyn. 29, 371–386.

Jan, I.U., Shah, A., Stephenson, M.H., Iqbal, S., Hanif, M., Wagreich, M., Hussain, H.S., 2016. The sedimentology of the Lower Permian Dandot Formation: a component of the Gondwana deglaciation sequence of the Salt Range, Pakistan. Riv. It. Paleont. Strat. 122(1) 122, 75–90.

Jan, I.U., Stephenson, M.H., 2011. Palynology and Correlation of the Upper Pennsylvanian Tobra Formation from Palynology and correlation of the Upper Pennsylvanian Tobra Formation from Zaluch Nala , Salt Range , Pakistan. Palynology 35, 212–225. https://doi.org/10.1080/01916122.2011.573964

Jan, I.U., Stephenson, M.H., Khan, F.R., 2009. Review of Palaeobotany and Palynology Palynostratigraphic correlation of the Sardhai Formation (Permian) of Pakistan. Rev. Palaeobot. Palynol. 158, 72–82. https://doi.org/10.1016/j.revpalbo.2009.08.002

Jaumé, S.C., Lillie, R.J., 1988. Mechanics of the Salt Range-Potwar Plateau, Pakistan: A fold-and-thrust belt underlain by evaporites. Tectonics 7, 57–71. https://doi.org/10.1029/TC007i001p00057

Johnson, G.D., Burbank, D.W., Raynolds, R.G.H., 1986a. Late Cenozoic Tectonics and Sedimentation in the North-Western Himalayan Foredeep: II. Eastern Limb of the Northwest Syntaxis and Regional Synthesis, in: Foreland Basins. Blackwell Publishing Ltd., Oxford, UK, pp. 293–306. https://doi.org/10.1002/9781444303810.ch16

Johnson, G.D., Johnson, N.M., Opdyke, N.D., Tahirkheli, R.A.K., 1979. Magnetic reversal stratigraphy and sedimentary tectonic history of the upper Siwalik Group, eastern Salt Range and southwestern Kashmir, in: Farah. A., De Jong, K.A. (Eds.), Geodynamics of Pakistan. Geological survey of Pakistan, pp. 149–165.

Johnson, G.D., Raynolds, R.G.H.H., Burbank, D.W., 1986b. Late Cenozoic Tectonics and Sedimentation in the North-Western Himalayan Foredeep: I. Thrust Ramping and Associated Deformation in the Potwar Region, in: Foreland Basins. Blackwell Publishing Ltd., Oxford, UK, pp. 273–291. https://doi.org/10.1002/9781444303810.ch15

Jouanne, F., Awan, A., Pêcher, A., Kausar, A., Mugnier, J.L., Khan, I., Khan, N.A., Van Melle, J., 2014. Present-day deformation of northern Pakistan from Salt Ranges to Karakorum Ranges. J. Geophys. Res. Solid Earth 119, 2487–2503. https://doi.org/10.1002/2013JB010776

Kadri, I. b, 1995. Petroleum_Geology_of_Pakistan. Pakistan Petroleum Limited, Karachi.

Kagan, E., Stein, M., Marco, S., 2018. Integrated Paleoseismic Chronology of the Last Glacial Lake Lisan: From Lake Margin Seismites to Deep-Lake Mass Transport Deposits. J. Geophys. Res. Solid Earth 123, 2806–2824. https://doi.org/10.1002/2017JB014117

Kars, R.H., Reimann, T., Ankjaergaard, C., Wallinga, J., 2014. Bleaching of the post-IR IRSL signal: new insights for feldspar luminescence dating. Boreas 43, 780–791. https://doi.org/10.1111/bor.12082

Kars, R.H., Wallinga, J., Cohen, K.M., 2008. A new approach towards anomalous fading correction for feldspar IRSL dating — tests on samples in field saturation. Radiat. Meas. 43, 786–790. https://doi.org/10.1016/j.radmeas.2008.01.021

Kazmi, A.H., Abbasi, I.A., 2008a. Stratigraphy and historical Geology of Pakistan. National centre of excellance in Geology, Peshawar.

Kazmi, A.H., Abbasi, I.A., 2008b. Stratigraphy & Historical Geology of Pakistan. National centre of excellance in Geology, Peshawar.

Kazmi, A.H., Jan, M.Q., 1997. Gology and Tectonics of Pakistan. Graphic Publishers, Karachi, Karachi.

Kazmi, A.H., Rana, R.A., 1982. Tectonic map of north Pakistan.

Keller, E.A., Pinter, N., 2002. Active Tectonics, Earthquakes, Uplift and Landscape.

Keller, E.A., Rockwell, T.K., 1984. Tectonic geomorphology, Quaternary chronology, and paleoseismicity. Dev. Appl. Geomorphol. 203–239. https://doi.org/10.1007/978-3-642-69759-

3_7

Keller, H.M., Tahirkheli, R.A.K., Mirza, M.A., Johnson, G.D., Johnson, N.M., Opdyke, N.D., 1977. Magnetic polarity stratigraphy of the Upper Siwalik deposits, Pabbi Hills, Pakistan. Earth Planet. Sci. Lett. 36, 187–201. https://doi.org/10.1016/0012-821X(77)90198-4

Khan, M., Khan, M.A., Shami, B.A., Awais, M., 2018. Microfacies analysis and diagenetic fabric of the Lockhart Limestone expoosed near Taxila, Margalla Hill Range, Punjab, Pakistan. Arab. J. Geosci. 11.

Khan, M.A., Khan, M.J., 1979. Stratigraphy of the Baghanwala Formation, Khewra Gorge, Khewra, Jhelum District; Punjab: Pakistan. Geol. Bull. Univ. Pesh. 12, 21–32.

Khan, M.A., Khan, M.J., Alizai, A.A.K., 1977. Stratigraphy and Petrography of the Jutana Dolomite, Khewra Gorge, Khewra, Jhelum District; Punjab: Pakistan. Geol. Bull. Univ. Pesh. 9–10, 43–66.

Khan, M.J., 1983. Magnetostratigraphy of the Neogene and Quaternary Siwalik Group sediments of the Trans-Indus Salt Range, northwestern Pakistan, , Ph.D. thesis, 217 pp., Columbia Univ., New York. Columbia University, New York.

Khan, S., Shah, M.M., 2019. Multiphase dolomitization in the Jutana formation (Cambrian), salt range (Pakistan): Evidences from field observations, microscopic studies and isotopic analysis. Geol. Acta 17, 1–18. https://doi.org/10.1344/GeologicaActa2019.17.2

Khan, S.D., Chen, L., Ahmad, S., Ahmad, I., Ali, F., 2012. Lateral structural variation along the Kalabagh Fault Zone, NW Himalayan foreland fold-and-thrust belt, Pakistan. J. Asian Earth Sci. 50, 79–87. https://doi.org/10.1016/j.jseaes.2012.01.009

Koster, B., Reicherter, K., Vött, A., Grützner, C., 2011. Identifying sedimentary structures and spatial distribution of tsunami deposits with GPR - examples from Spain and Greece, in: 2011 6th International Workshop on Advanced Ground Penetrating Radar (IWAGPR). IEEE, pp. 1–6. https://doi.org/10.1109/IWAGPR.2011.5963850

Kreutzer, S., Schmidt, C., DeWitt, R., Fuchs, M., 2014. The a-value of polymineral fine grain samples measured with the post-IR IRSL protocol. Radiat. Meas. 69, 18–29. https://doi.org/10.1016/j.radmeas.2014.04.027

Kreutzer, S., Schmidt, C., Fuchs, Margret, Dietze, M., Fischer, M., Fuchs, Markus, 2012. Introducing an R package for luminescence dating analysis. Anc. TL 30, 1–8.

Le Fort, P., 1975. Himalayas: The Collided Range. Present Knowledge of the Continental Arc. Am. J. Sci.

275-A, 1–44.

Lettis, W.R., Wells, D.L., Baldwin, J.N., 1997. Empirical observations regarding reverse earthquakes, blind thrust faults, and quaternary deformation: Are blind thrust faults truly blind? Bull. Seismol. Soc. Am. 87, 1171–1198.

Li, B., Jacobs, Z., Roberts, R.G., 2016. Investigation of the applicability of standardised growth curves for OSL dating of quartz from Haua Fteah cave, Libya. Quat. Geochronol. 35, 1–15. https://doi.org/10.1016/j.quageo.2016.05.001

Li, G., Yang, H., Stevens, T., Zhang, X., Zhang, H., Wei, H., Zheng, W., Li, L., Liu, X., Chen, J., Xia, D., Oldknow, C., Ye, W., Chen, F., 2020. Differential ice volume and orbital modulation of Quaternary moisture patterns between Central and East Asia. Earth Planet. Sci. Lett. 530, 115901. https://doi.org/10.1016/j.epsl.2019.115901

Li, Y., Tsukamoto, S., Frechen, M., Gabriel, G., 2018. Timing of fluvial sedimentation in the Upper Rhine Graben since the Middle Pleistocene: constraints from quartz and feldspar luminescence dating. Boreas 47, 256–270. https://doi.org/10.1111/bor.12266

Li, Y., Tsukamoto, S., Shang, Z., Tamura, T., Wang, H., Frechen, M., 2019. Constraining the transgression history in the Bohai Coast China since the Middle Pleistocene by luminescence dating. Mar. Geol. 416, 105980. https://doi.org/10.1016/j.margeo.2019.105980

Liang, P., Forman, S.L., 2019. LDAC: An Excel-based program for luminescence equivalent dose and burial age calculations. Anc. TL 37, 21–40. https://doi.org/http://ancienttl.org/ATL_37-2_2019/ATL_37-2_Liang_p21-40.pdf

Liritzis, I., Singhvi, A.K., Feathers, J.K., Wagner, G.A., Kadereit, A., Zacharias, N., Li, S.-H., 2013. Luminescence Dating in Archaeology, Anthropology, and Geoarchaeology, SpringerBriefs in Earth System Sciences. Springer International Publishing, Heidelberg. https://doi.org/10.1007/978-3-319-00170-8

Lisa, M., Khwaja, A.A., Jan, M.Q., 2007. Seismic hazard assessment of the NW Himalayan fold-and-thrust belt, Pakistan, using probabilistic approach. J. Earthq. Eng. 11, 257–301. https://doi.org/10.1080/13632460601031243

Luo, M., Xu, Y., Mu, K., Wang, R., Pu, Y., 2018. Spatial variation of the hypsometric integral and the implications for local base levels in the Yanhe River, China. Arab. J. Geosci. 11. https://doi.org/10.1007/s12517-018-3711-3

Mahmood, S. a, Yameen, M., Sheikh, R. a, Rafique, H.M., Almas, a S., 2012. DEM and GIS based

Hypsometric Analysis to Investigate Neotectonic influence on Hazara Kashmir Syntaxis. Pak. J. Sci. 64, 5.

Mahmood, S.A., Gloaguen, R., 2012. Appraisal of active tectonics in Hindu Kush: Insights from DEM derived geomorphic indices and drainage analysis. Geosci. Front. 3, 407–428. https://doi.org/10.1016/j.gsf.2011.12.002

Mason, J., Reicherter, K., 2017. The palaeoseismological study of capable faults on crete, in: Degryse, P., Freestone, I., Knappett, C., Shortland, A., Sintubin, M., Waelkens, M. (Eds.), Studies Is Archaeological Sciences, Minoan Earthquakes Breaking the Myth through Interdisciplinarity. Leuven University Press, pp. 191–219. https://doi.org/10.2307/j.ctt1whm9cf.14

Mayya, Y.S., Morthekai, P., Murari, M.K., Singhvi, A.K., 2006. Towards quantifying beta microdosimetric effects in single-grain quartz dose distribution. Radiat. Meas. 41, 1032–1039. https://doi.org/https://doi.org/10.1016/j.radmeas.2006.08.004

McCalpin, James P., 2009. Field techniques in paleoseismology-terrestrial environments. Int. Geophys. 95, 29–118. https://doi.org/10.1016/S0074-6142(09)95002-1

McCalpin, J.P., 2009. Paleoseismology. Academic, London.

McCalpin, J.P., Nelson, A.R., 2009. Introduction to Paleoseismology, in: International Geophysics. pp. 1–27. https://doi.org/10.1016/S0074-6142(09)95001-X

McCalpin, J.P., Rockwell, T.K., Weldon, R.J., 2009. Paleoseismology of strike-slip tectonic environments, International Geophysics. https://doi.org/10.1016/S0074-6142(09)95006-9

McDougall, J.W., 1989a. Geology and Geophysics of the Foreland Fold and Thrust Belt of Northwestern Pakistan.

McDougall, J.W., 1989b. Tectonically-induced diversion of the Indus River west of the Salt Range, Pakistan. Palaeogeogr. Palaeoclimatol. Palaeoecol. 71, 301–307. https://doi.org/10.1016/0031-0182(89)90057-6

McDougall, J.W., Khan, S.H., 1990. Strike-slip faulting in a foreland fold-thrust belt: The Kalabagh Fault and Western Salt Range, Pakistan. Tectonics 9, 1061–1075. https://doi.org/10.1029/TC009i005p01061

Meissner, C.R., Master, J.M., Rashid, M.A., Hussain, M., 1974. Stratigraphy of the Kohat Quadrangle , Pakistan. U.S. govt printing office Washington.

Mertmann, D., 2003. Evolution of the marine Permian carbonate platform in the Salt Range (Pakistan).

Palaeogeogr. Palaeoclimatol. Palaeoecol. 191, 373–384. https://doi.org/10.1016/S0031-0182(02)00672-7

Michetti, A.M., Ferreli, L., Esposito, E., Porfido, S., Blumetti, A.M., Vittori, E., Serva, L., Roberts, G.P., 2000. Ground effects during the 9 September 1998, MW = 5.6, Lauria earthquake and the seismic potential of the "aseismic" Pollino region in Southern Italy. Seismol. Res. Lett. 71, 31–46. https://doi.org/10.1785/gssrl.71.1.31

Mirza, M.A., 1980. Magnetic polarity stratigraphy of Soan Formation (Plio- Pleistocene). Mujahad village, Rawalpindi district, Punjab, Pakistan, in: Pakistan Geological Survey Records 45. Geological survey of Pakistan, pp. 1–5.

Mohser, M.S., 2017. The Achitecture of Mohenjo-Daro as Evidences for the Organization of the Indus Civilization Urban Neighbourhoods. University of Toronto.

Mozafari, N., Tikhomirov, D., Sumer, Ö., Özkaymak, Ç., Uzel, B., Yeşilyurt, S., Ivy-Ochs, S., Vockenhuber, C., Sözbilir, H., Akçar, N., 2019. Dating of active normal fault scarps in the Büyük Menderes Graben (western Anatolia) and its implications for seismic history. Quat. Sci. Rev. 220, 111–123. https://doi.org/10.1016/j.quascirev.2019.07.002

Muhammad, S., Ullah, R., Turab, S.A., Khan, M.Y., Khattak, N.U., Khan, M.A., 2020. Radon concentration in drinking water and soil after the September 24, 2019, Mw 5.8 earthquake, Mirpur, Azad Jammu, and Kashmir: an evaluation for potential risk. Environ. Sci. Pollut. Res. 27, 32628–32636. https://doi.org/10.1007/s11356-020-09589-0

Murray, A.S., Schmidt, E.D., Stevens, T., Buylaert, J.-P., Marković, S.B., Tsukamoto, S., Frechen, M., 2014. Dating Middle Pleistocene loess from Stari Slankamen (Vojvodina, Serbia) — Limitations imposed by the saturation behaviour of an elevated temperature IRSL signal. CATENA 117, 34–42. https://doi.org/10.1016/j.catena.2013.06.029

Murray, A.S., Wintle, A.G., 2000. Luminescence dating of quartz using an improved single-aliquot regenerative-dose protocol. Radiat. Meas. 32, 57–73. https://doi.org/10.1016/S1350-4487(99)00253-X

Nian, X., Li, F., Chen, F., Zhang, W., Zhao, Y., Zhou, J., Gao, X., 2016. Optically stimulated luminescence ages for human occupation during the penultimate glaciation in the western Loess Plateau of China. J. Quat. Sci. 31, e2917. https://doi.org/10.1002/jqs.2917

Nizami, A.R., Sheikh, R.A., 2009. Mocrofacies analysis and diagenetic settings of the middle Jurassic Samana Suk Formation, Sheikh Badin hill section, Trans Indus Ranges-Pakistan. Geol. Bull. Punjab

Uni. 44, 69–84.

Ntokos, D., Lykoudi, E., Rondoyanni, T., 2016. Geomorphic analysis in areas of low-rate neotectonic deformation: South Epirus (Greece) as a case study. Geomorphology 263, 156–169. https://doi.org/10.1016/j.geomorph.2016.04.005

Olley, J.M., Roberts, R.G., Murray, A.S., 1997. Disequilibria in the uranium decay series in sedimentary deposits at Allen's cave, nullarbor plain, Australia: Implications for dose rate determinations. Radiat. Meas. 27, 433–443. https://doi.org/10.1016/S1350-4487(96)00114-X

Opdyke, N.D., Johnson, N.M., Johnson, G.D., Lindsay, E.H., Tahirkheli, R.A.K., 1982. Paleomagnetism of the middle Siwalik Formations of northern Pakistan and rotation of the Salt Range decollement. Paleogeography, Paleoclimatology, Paleoecol. 37, 1–15.

Peng, J., Dong, Z., Han, F., Long, H., Liu, X., 2013. R package numOSL : numeric routines for optically stimulated luminescence dating. Anc. TL 31, 41–48.

Peng, J., Li, B., 2017. Single-aliquot regenerative-dose (SAR) and standardised growth curve (SGC) equivalent dose determination in a batch model using the R package 'numOSL.' Anc. TL 35, 32–53.

Pervaiz, R., Umar, M., Wajid, A.A., Khan, J.K., Israr, A., Rehman, S.U., Pervaiz, A., 2017. The Nucleus Provenance Analysis and Diagenetic Control of Early Cambrian Kussak Formation, Upper Indus Basin, Pakistan. Nucl. 54, 52–65.

Petterson, M.G., 2010. A Review of the geology and tectonics of the Kohistan island arc , north Pakistan. Geol. Soc. London, Spec. Publ. 287–327.

Prescott, J.R., Hutton, J.T., 1994. Cosmic ray contributions to dose rates for luminescence and ESR dating: Large depths and long-term time variations. Radiat. Meas. 23, 497–500. https://doi.org/10.1016/1350-4487(94)90086-8

Qin, J.T., Zhou, L.P., 2012. Effects of thermally transferred signals in the post-IR IRSL SAR protocol. Radiat. Meas. 47, 710–715. https://doi.org/10.1016/j.radmeas.2011.12.011

Quittmeyer, R., Jacob, K.H., 1979. Historical and modern seismicity of Pakistan , Afghanistan , northwestern India , and southeastern Iran.

Qureshi, A.W., Tanoli, S.K., 1992. Early molasse sediments (Murree Formation) in Pathan Algad, Southern Kohat. Geol. Bull. Univ. Peshawar1 25, 85–93.

Qureshi, K.A., Khan, S.D., 2020. Active Tectonics of the Frontal Himalayas: An Example from the Manzai

Ranges in the Recess Setting, Western Pakistan. Remote Sens. 12, 3362. https://doi.org/10.3390/rs12203362

Sadiq, I., Ahmad, S., Hanif, M., Ali, Fahad, Jan, I.U., Ali, Fayaz, Khan, N., Khan, S., Farhan, M., 2016. Depositional system and sequence stratigraphy of Permian Amb Formation, Salt Ranges, Northwest Pakistan. J. Himal. Earth Sci. 49, 26–39.

Sameeni, S.J., Haneef, M., Shabbir, F., Ahsan, N., Ahmad, N., 2013. Biostratigraphic studies of the Lockhart Limestone, Changlwagali area, Nathiagali-Murree road, Hazara, Northern Pakistan. Sci. Int. 25, 543–550.

Sana, H., Kumar Nath, S., 2016. In and Around the Hazara-Kashmir Syntaxis: a Seismotectonic and Seismic Hazard perspective. J. Indian Geophys. Union 20, 496–505.

Sandmeier, K.J., 2012. ReflexW Version 7.0 Radar processing and interpretation software package. Sandmeier Scientific Software, Karlsruhe, Germany.

Saqib, M.M., Murtaza, G., Khan, M.A., Ahmad, T., Rahim, H., 2009. Sedimentology and Reservoir Potential of the Early Cambrian Khewra Sandstone , Khewra Gorge , Eastern Salt Range , Pakistan.

Satyabala, S.P., Yang, Z., Bilham, R., 2012. Stick–slip advance of the Kohat Plateau in Pakistan. Nat. Geosci. 5, 147–150. https://doi.org/10.1038/ngeo1373

Schmidt, E.D., Tsukamoto, S., Frechen, M., Murray, A.S., 2014. Elevated temperature IRSL dating of loess sections in the East Eifel region of Germany. Quat. Int. 334–335, 141–154. https://doi.org/10.1016/j.quaint.2014.03.006

Schneiderwind, S., Mason, J., Wiatr, T., Papanikolaou, I., Reicherter, K., 2016. 3-D visualisation of palaeoseismic trench stratigraphy and trench logging using terrestrial remote sensing and GPR – a multiparametric interpretation. Solid Earth 7, 323–340. https://doi.org/10.5194/se-7-323-2016

Schumm, S.A., 1956. Evolution of drainage system and slopes in badlands at Perth Amboy, New Jersey. GSA Bull. 67, 597–646. https://doi.org/10.1130/0016-7606(1956)67[597:EODSAS]2.0.CO;2

Searle, M.P., Khan, M.A., Fraser, J.E., J, G.S., Jan, M.Q., 1999. The tectonic evolution of the Kohistan-Karakoram collision belt along the Karakoram Highway transect, north Pakistan. Tectonics 18, 929–949.

Searle, M.P., Treloar, P.J., 2019. Introduction to Himalayan tectonics: a modern synthesis. Geol. Soc. London, Spec. Publ. 483, 1–17. https://doi.org/10.1144/SP483-2019-20

Shah, S.M.I., 2009. memoir 22.pdf, 22nd ed, Stratigraphy of Pakistan, Geological Survey of Pakistan, Memoirs. Geological Suvrey of Pakistan.

Shah, S.M.I., 1977a. Paleozoic, in: Shah, S.M.I. (Ed.), Memoirs of the Geological Survey of Pakistan, Startigraphy of Pakistan. Geological Suvrey of Pakistan, Quetta, pp. 5–29.

Shah, S.M.I., 1977b. Precambrian, in: Shah, S.M.I. (Ed.), Memoirs of the Geological Survey of Pakistan, Startigraphy of Pakistan. Geological Suvrey of Pakistan, Quetta, pp. 1–5.

Sharma, G., Ray, P.K.C., Mohanty, S.P., 2018. Morphotectonic analysis and GNSS observations for assessment of relative tectonic activity in Alaknanda basin of Garhwal Himalaya, India. Geomorphology 301, 108–120. https://doi.org/10.1016/j.geomorph.2017.11.002

Shehzad, S., Iqbal, A., Rahim, H. ur, Ahmad, T., Ahmad, W., 2018. Microfacies Analysis and Source Rock Potential of Nammal Formation , Western Salt Range Pakistan. Int. J. Econ. Environ. Geol. 9.

Sohbati, R., Murray, A.S., Buylaert, J.-P., Ortuño, M., Cunha, P.P., Masana, E., 2012. Luminescence dating of Pleistocene alluvial sediments affected by the Alhama de Murcia fault (eastern Betics, Spain) - a comparison between OSL, IRSL and post-IRIRSL ages. Boreas 41, 250–262. https://doi.org/10.1111/j.1502-3885.2011.00230.x

Stevens, T., Buylaert, J.-P., Thiel, C., Újvári, G., Yi, S., Murray, A.S., Frechen, M., Lu, H., 2018. Ice-volume-forced erosion of the Chinese Loess Plateau global Quaternary stratotype site. Nat. Commun. 9, 983. https://doi.org/10.1038/s41467-018-03329-2

Strahler, A.N., 1964. Handbook of Applied Hydrology, edited by: Chow, VT, 4–39, 4–76.

Strahler, A.N., 1952. Hypsometric (area-altitude) analysis of erosional topography. GSA Bull. 63, 1117–1142. https://doi.org/10.1130/0016-7606(1952)63[1117:HAAOET]2.0.CO;2

Tahirkheli, R.A.K., 2005. Pre and post earthquakes seismo-tectonic scenario of Hazara-Kashmir Terrain of Pakistan. Int. J. Econ. Environ. Geol. 1, 1–5.

Thomas, J., Biermanns, P., Hürtgen, J., Reicherter, K., Baize, S., 2017. Characterization of potentially active faults in the southern Upper Rhine Graben using GPR, in: 2017 9th International Workshop on Advanced Ground Penetrating Radar (IWAGPR). IEEE, pp. 1–6. https://doi.org/10.1109/IWAGPR.2017.7996047

Thomsen, K.J., Murray, A.S., Jain, M., Bøtter-Jensen, L., 2008. Laboratory fading rates of various luminescence signals from feldspar-rich sediment extracts. Radiat. Meas. 43, 1474–1486. https://doi.org/10.1016/j.radmeas.2008.06.002

Troiani, F., Galve, J.P., Piacentini, D., Della Seta, M., Guerrero, J., 2014. Spatial analysis of stream length-gradient (SL) index for detecting hillslope processes: A case of the Gállego River headwaters (Central Pyrenees, Spain). Geomorphology 214, 183–197. https://doi.org/10.1016/j.geomorph.2014.02.004

Ullah, K., Arif, M., Shah, M.T., 2006. Petrography of Sandstones from the Kamlial and Chinji Formations , Southwestern Kohat Plateau , NW Pakistan : Implications for Source Lithology and Paleoclimate. J. Himal. Earth Sci. 39, 1–13.

USGS earthquake catalogue, 2019. available online at https://earthquake.usgs.gov/earthquakes/search/, last accessed on Nov. 06, 2019.

Van Balen, R.T., Bakker, M.A.J., Kasse, C., Wallinga, J., Woolderink, H.A.G., 2019. A Late Glacial surface rupturing earthquake at the Peel Boundary fault zone, Roer Valley Rift System, the Netherlands. Quat. Sci. Rev. 218, 254–266. https://doi.org/10.1016/j.quascirev.2019.06.033

Vittori, E., Deiana, G., Esposito, E., Ferreli, L., Marchegiani, L., Mastrolorenzo, G., Michetti, A.M., Porfido, S., Serva, L., Simonelli, A.L., Tondi, E., 2000. Ground effects and surface faulting in the September-October 1997 Umbria-Marche (Central Italy) seismic sequence. J. Geodyn. 29, 535–564. https://doi.org/10.1016/S0264-3707(99)00056-3

Wallinga, J., Murray, A., Wintle, A., 2000. The single-aliquot regenerative-dose (SAR) protocol applied to coarse-grain feldspar. Radiat. Meas. 32, 529–533. https://doi.org/10.1016/S1350-4487(00)00091-3

Wang, J., He, Z., 2020. Responses of Stream Geomorphic Indices to Piedmont Fault Activity in the Daqingshan Area of China. J. Earth Sci. 31, 978–987. https://doi.org/10.1007/s12583-020-1321-y

Wardlaw, B.R., Martin, W.E., Haydri, I.H., 2007. Stratigraphic Analysis of Paleocene and Lower Eocene Rocks Adjacent to the Potwar Plateau, Northern Pakistan, in: Warwick, P.D., Wardlaw, B.R. (Eds.), Regional Studies of the Potwar Plateau Area, Northern Pakistan. U.S. Geological Survey, p. 18.

Warwick, P.D., Wardlaw, B.R., 2007. Regional Studies of the Potwar Plateau Area , Northern Pakistan, in: Regional Studies of the Potwar Plateau Area, Northern Pakistan. p. 9.

Wells, D.L., Coppersmith, K.J., 1994. New empirical relationships among magnitude, rupture length, rupture width, rupture area, and surface displacement. Bull. - Seismol. Soc. Am. 84, 974–1002.

Wilson, J.S.J., Chandrasekar, N., Magesh, N.S., 2012. Morphometric Analysis of Major Sub-Watersheds in Aiyar & Karai Pottanar Basin, Central Tamil Nadu, India Using Remote Sensing & GIS

Techniques. Bonfring Int. J. Ind. Eng. Manag. Sci. 2, 8–15.

Wintle, A.G., Murray, A.S., 2006. A review of quartz optically stimulated luminescence characteristics and their relevance in single-aliquot regeneration dating protocols. Radiat. Meas. 41, 369–391. https://doi.org/10.1016/j.radmeas.2005.11.001

Yaseen, A., Munir, M., 2007. Microfacies analysis of the Middle Eocene Kohat Formation , Shekhan Nala , Kohat Basin, Pakistan. Geol. Bull. Punjab Uni. 42, 15–24.

Yeats, R.S., Khan, S.H., Akhtar, M., 1984. Late Quaternary deformation of the Salt Range of Pakistan. Geol. Soc. Am. Bull. 95, 958. https://doi.org/10.1130/0016-7606(1984)95<958:LQDOTS>2.0.CO;2

Yi, S., Buylaert, J.-P., Murray, A.S., Lu, H., Thiel, C., Zeng, L., 2016. A detailed post-IR IRSL dating study of the Niuyangzigou loess site in northeastern China. Boreas 45, 644–657. https://doi.org/10.1111/bor.12185

Zaidi, S.N.A., Brohi, I.A., Ramzan, K., Ahmed, N., Mehmood, F., Brohi, A.U., 2013. Distribution and Hydrocarbon Potential of Datta Sands in Upper Indus Basin, Pakistan. Sindh Univ. Res. Jour. (Sci. Ser.) 45, 325–332.

Zhao, H., Li, S.-H., 2005. Internal dose rate to K-feldspar grains from radioactive elements other than potassium. Radiat. Meas. 40, 84–93. https://doi.org/10.1016/j.radmeas.2004.11.004

Zia, S., Rahim, H. ur, Fida, M.H., Ahmad, T., Ahmad, W., Khan, S., 2018. Provenance studies of Miocene-Pliocene Nagri Formation exposed at Kanati area, District Khushab, Punjab, Pakistan. Pakistan J. Geol. 02, 27–30.

Appendices

Sample Preparation (150-200µm)													
Sample no.	LUM-4230	LUM-4231	LUM-4232	LUM-4233	LUM-4234	LUM-4235	LUM-4236	LUM-4237	LUM-4238	LUM-4239	LUM-4240	LUM-4141	LUM-4242
Field Sample no.	KBF-01	KBF-02	KBF-03	KBF-04	KBF-05	KBF-06	KBF-07	KBF-08	KBF-09	KBF-10	KBF-11	KBF-12	KBF-13
Dry/ Wet sieving	Dry	Dry	Dry	Wet	Wet	Wet	Dry	Wet	Wet	Wet	Dry	Dry	Wet
Grain Size fractions (gram)													
<63 µm	77.5	31.6	46.1	151.9	27	152.9	17.4	90.5	217.1	25.6	68.0	17.8	165
63-100 µm	61.1	24.7	17.6	45.6	27.8	36.4	8.4	52.3	55.1	38.0	35.2	11.5	88.9
100-150 µm	91.8	73.5	26.5	34.4	31.5	27.9	8.3	73.7	67.1	35.5	82.4	18.3	98
150-200 µm	81.6	147.4	19.6	19.5	24.8	16.0	8.6	66.8	61.3	35.7	92.0	20.4	76.1
200-250 µm	40.6	165.3	23.6	12.9	17.7	9.3	14.3	48.2	37.2	32.7	142.6	22.4	49.7
>250 µm	63.5	205.4	305.1	46.4	92.3	43.8	330.4	173.5	154.4	167.4	241.7	589.1	100.7
Fraction preparation (150-200 µm)													
Employed material (g)	41.0	44.4	19.6	19.5	24.8	16	8.6	40.4	41.1	35.7	41.4	20.4	40.5
HCL reaction	Mild	Mild	Mild	Mild	Mild	Mild	Mild	Mild	Strong	Strong	Mild	Low	v. Low
$N_2C_2O_4$ reaction	No	No	No	No	No	No	No	No	No	No	No	No	No
H_2O_2 reaction	Mild	Mild	No	no	No	No	No	No	No	No	No	No	No
Remaining weight (g)	27.07	36.61	10.94	12.08	15.55	9.46	5.45	28.46	30.0	30.89	31.6	12.73	35.4
Heavy liquid separation													
Feldspar+Plagioclase <2.62 g/cm^3 (g)	1.02	3.5	1.07	0.43	1.09	0.45	0.43	1.93	3.0	2.5	3.5	2.8	9.3
Quartz+Heavy minerals >2.62 g/cm^3 (g)	25.7	32.9	9.67	11.52	14.27	8.83	4.90	26.31	26.65	28.0	27.9	9.8	25.26
Feldspar <2.58 g/cm^3 (g)	0.51	2.23	0.66	0.26	0.50	0.19	0.21	0.88	1.067	1.66	1.86	1.4	4.0
Quartz <2.70 g/cm^3 (g)	23.9			10.1	12.5	7.54		13.1	22.8			8.66	23.6
Heavy minerals >2.70 g/cm^3 (g)	1.14			1.14	1.25	0.857		12.91	3.39			0.88	1.25
Quartz etching (40% HF, 20% HCL)													
Weight employed (g)	10.04			10.06	10.07	7.53		10.08	10.06			8.66	10.11
Weight after etching (g)	7.03			7.0	6.78	4.995		6.8	6.8			4.43	5.45
Weight after sieving	2.57			5.4	5.01			4.62	4.33			2.71	3.67
Feldspar considered		✓	✓				✓			✓	✓		
Quartz measured	✓			✓	✓	✓		✓	✓			✓	✓

Appendix 5.1 Measured weights of different grain size fractions during sample preparation for luminescence dating

Elemental Concentrations from Gamma Spectrometry																				
Sample no.	U (ppm)	S.E. U (ppm)	Th (ppm)	S.E. Th (ppm)	K (%)	S.E. K (%)	228 Ac	S.E. 228 Ac	208 Tl	S.E. 208 Tl	212 Pb	S.E. 212 Pb	234 Th	S.E. 234 Th	214 Bi	S.E. 214 Bi	214 Pb	S.E. 214 Pb	210 Pb	S.E. 210 Pb
LUM-4230	3.2	0.03	19.7	0.08	0.7	0.01	81.0	0.6	78.6	0.9	79.6	0.4	38.0	1.7	40.4	0.5	38.8	0.5	35.6	1.4
LUM-4231	2.3	0.04	12.3	0.09	1.5	0.02	51.4	0.9	50.2	1.0	49.3	0.4	26.3	2.0	29.5	0.7	28.6	0.5	24.4	1.8
LUM-4232	2.4	0.04	13.3	0.09	1.5	0.02	55.6	0.9	53.1	1.2	53.5	0.5	28.0	2.1	31.2	0.7	28.9	0.5	25.1	1.8
LUM-4233	3.3	0.04	14.7	0.10	1.3	0.02	62.5	1.0	59.4	1.2	58.8	0.5	35.1	2.2	41.5	0.8	40.7	0.6	33.6	1.7
LUM-4234	1.7	0.03	7.8	0.08	2.1	0.02	35.4	1.0	31.1	1.0	31.3	0.4	20.7	1.9	22.4	0.7	21.2	0.5	19.0	1.8
LUM-4235	2.3	0.04	12.3	0.09	1.5	0.02	51.4	0.9	50.2	1.0	49.3	0.4	26.3	2.0	29.5	0.7	28.6	0.5	24.4	1.8
LUM-4236	1.7	0.03	8.4	0.08	1.4	0.02	36.5	0.9	32.6	1.0	33.8	0.4	20.0	1.8	20.3	0.6	20.6	0.5	18.7	1.7
LUM-4237	3.2	0.04	13.4	0.09	1.2	0.02	58.0	1.1	54.2	1.1	53.5	0.4	32.5	2.1	40.3	0.7	39.0	0.6	34.2	2.0
LUM-4238	3.0	0.03	11.9	0.07	1.1	0.01	50.7	0.7	47.7	0.9	48.0	0.3	32.0	1.7	38.4	0.6	36.0	0.5	32.3	1.4
LUM-4239	2.8	0.03	16.4	0.08	1.5	0.02	69.0	0.7	66.5	1.0	65.7	0.4	34.5	1.8	36.7	0.6	33.8	0.4	30.3	1.7
LUM-4240	1.5	0.03	7.4	0.08	1.2	0.02	31.5	0.7	29.8	1.0	29.6	0.4	16.9	1.6	20.0	0.7	18.2	0.5	15.3	1.6
LUM-4141	1.8	0.02	9.0	0.05	1.8	0.01	38.9	0.6	34.9	0.7	36.3	0.3	25.2	1.2	23.5	0.5	22.4	0.3	19.8	1.1
LUM-4242	3.2	0.03	13.7	0.06	1.3	0.01	56.7	0.5	54.0	0.8	55.4	0.3	35.6	1.3	41.3	0.5	38.8	0.4	33.0	1.2

Appendix 5.2 Elemental concentrations of the samples measured during gamma spectrometry

Dose rate parameters (Gy/ka) for coarse grained quartz (150-200µm)								
Sample no.	Cosmic Ray	Cosmic ray error	Beta dose	Beta dose error	Gamma dose	Gamma dose error	Dose rate	Dose rate error
4230	0.2	0.02	1.3	0.04	1.4	0.05	2.9	0.1
4231	0.2	0.02	1.6	0.07	1.2	0.04	3.0	0.1
4232	0.2	0.02	1.5	0.10	1.1	0.07	2.8	0.1
4233	0.2	0.02	1.5	0.10	1.2	0.08	2.9	0.1
4234	0.2	0.02	1.9	0.10	1.0	0.04	3.1	0.1
4235	0.2	0.02	1.6	0.09	1.1	0.06	2.9	0.1
4236	0.2	0.02	1.4	0.06	0.9	0.03	2.5	0.1
4237	0.2	0.02	1.5	0.08	1.2	0.06	2.8	0.1
4238	0.2	0.02	1.3	0.08	1.1	0.06	2.5	0.1
4239	0.2	0.02	1.7	0.07	1.4	0.05	3.3	0.1
4240	0.1	0.01	1.2	0.05	0.8	0.03	2.1	0.1
4241	0.2	0.02	1.7	0.07	1.0	0.04	3.0	0.1
4242	0.2	0.02	1.5	0.06	1.2	0.05	2.9	0.1

Appendix 5.3 Dose rate parameters used for dose rate calculation for coarse grained quartz in Table 5.2

Dose rate parameters (Gy/ka) for coarse grained K-feldspar (150-200µm)														
Sample no.	Cosmic ray	Cosmic error	Internal dose	Internal dose error	External alpha dose	External alpha dose error	External beta dose	External beta dose error	External gamma dose	External gamma dose error	Total external dose	Total external dose error	Dose rate	Dose rate error
4230	0.2	0.02					1.3	0.04	1.4	0.05	2.9	0.1	3.8	0.1
4231	0.2	0.02	0.7	0.1	0.1	0.03	1.7	0.07	1.2	0.04	3.0	0.1	3.9	0.1
4232	0.2	0.02	0.7	0.1	0.1	0.03	1.5	0.14	1.1	0.09	2.8	0.2	3.7	0.2
4233	0.2	0.02					1.5	0.14	1.2	0.10	2.9	0.2	3.8	0.2
4234	0.2	0.02					1.9	0.10	1.0	0.04	3.0	0.1	3.9	0.2
4235	0.2	0.02					1.6	0.09	1.1	0.06	2.9	0.1	3.8	0.2
4236	0.2	0.02	0.7	0.1	0.1	0.02	1.4	0.06	0.9	0.03	2.4	0.1	3.3	0.1
4237	0.2	0.02					1.5	0.08	1.2	0.06	2.8	0.1	3.7	0.1
4238	0.2	0.02					1.3	0.08	1.1	0.06	2.5	0.1	3.4	0.2
4239	0.2	0.02	0.7	0.1	0.2	0.03	1.8	0.07	1.4	0.05	3.3	0.1	4.2	0.1
4240	0.1	0.01	0.7	0.1	0.1	0.02	1.2	0.05	0.8	0.03	2.1	0.1	3.0	0.1
4241	0.2	0.02					1.8	0.08	1.0	0.04	2.9	0.1	3.8	0.1
4242	0.2	0.02					1.5	0.06	1.2	0.05	2.9	0.1	3.8	0.1

Appendix 5.4 Dose rate parameters used for dose rate calculations in Table 5.2.

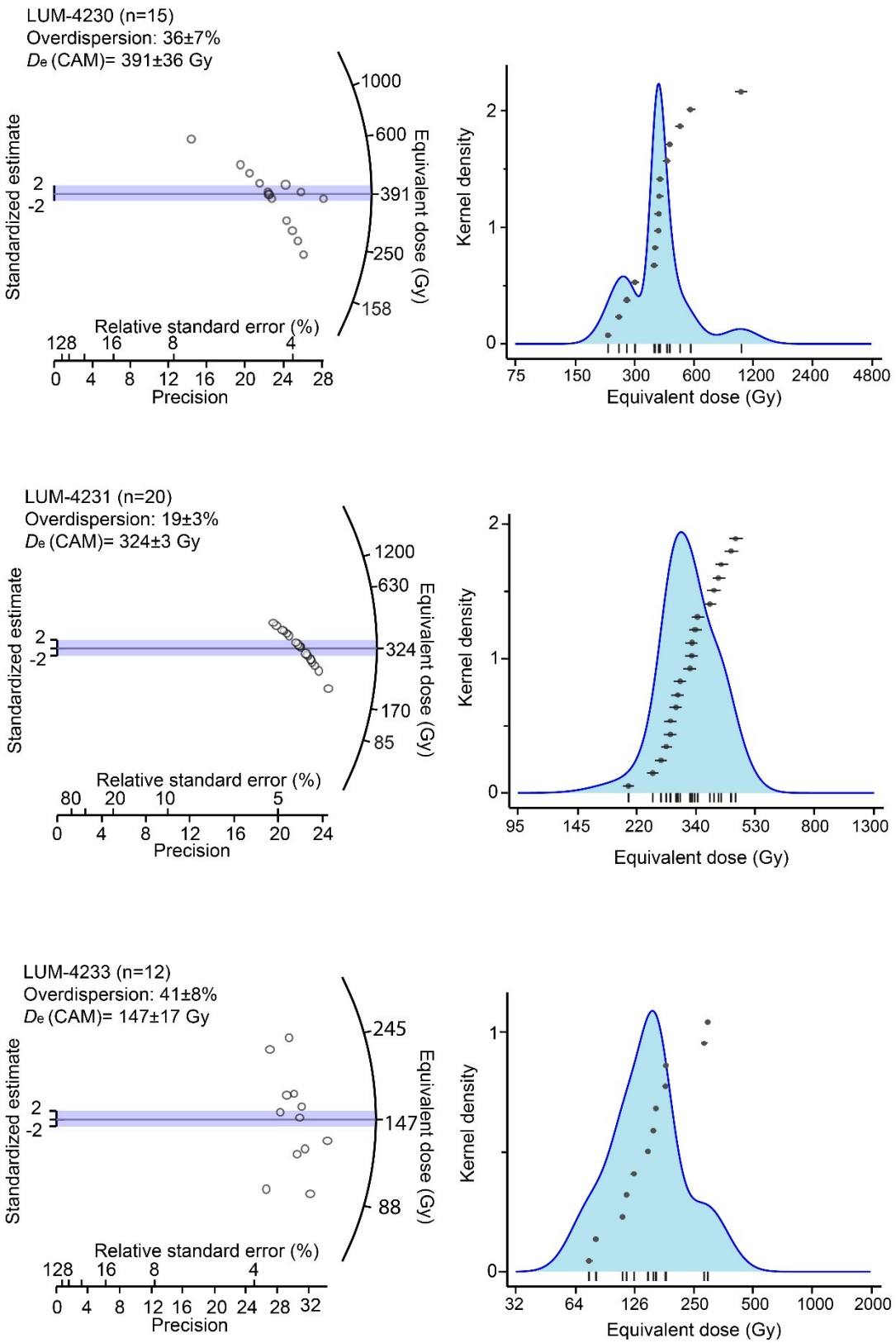

Appendix 5.5 Radial and kernel density plots for samples LUM-4230, LUM-4231 and LUM-4233, showing data from pIRIR D_e measurements of k-feldspar.

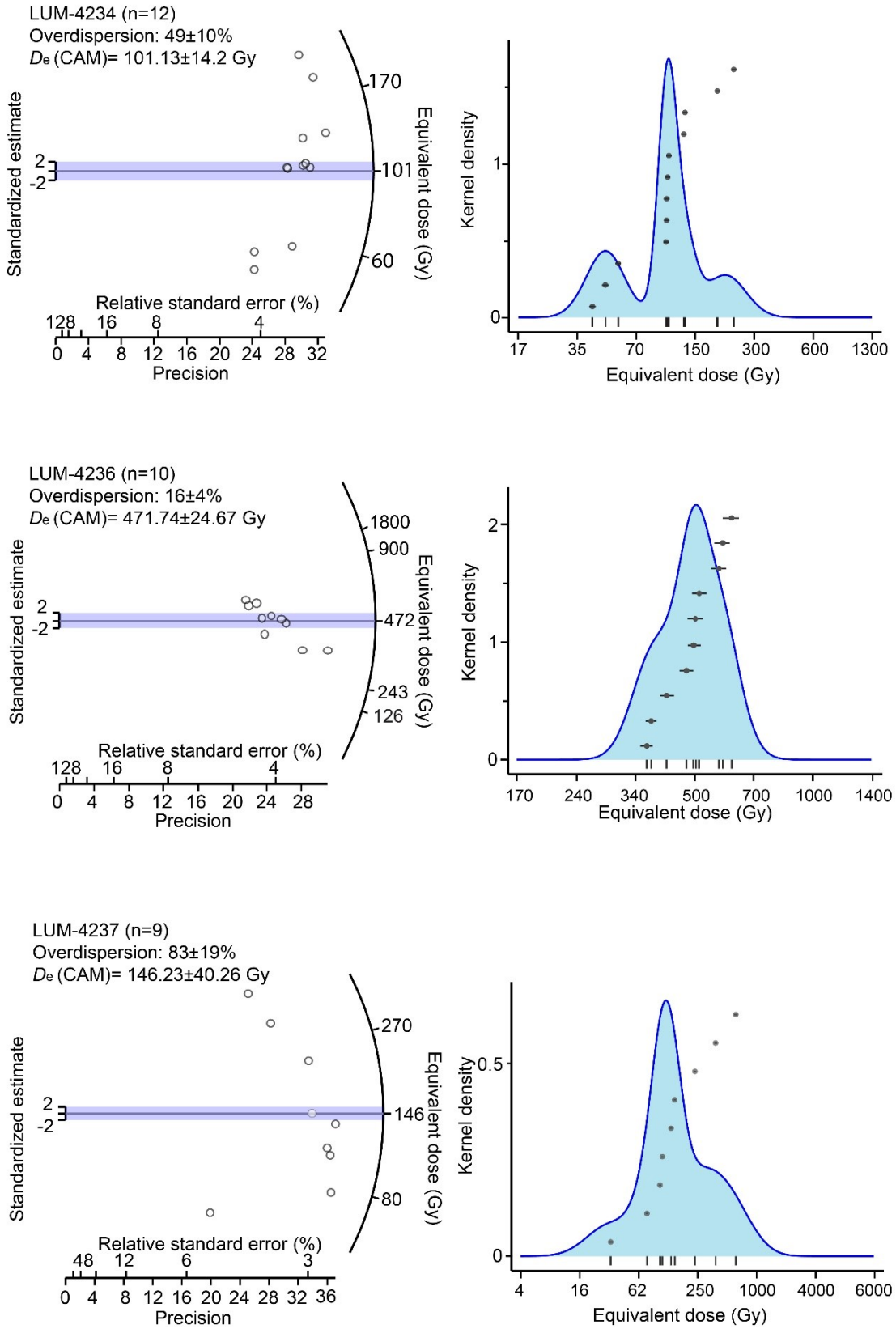

Appendix 5.6 Radial and kernel density plots for samples LUM-4234, LUM-4236 and LUM-4237, showing data from pIRIR D_e measurements of k-feldspar.

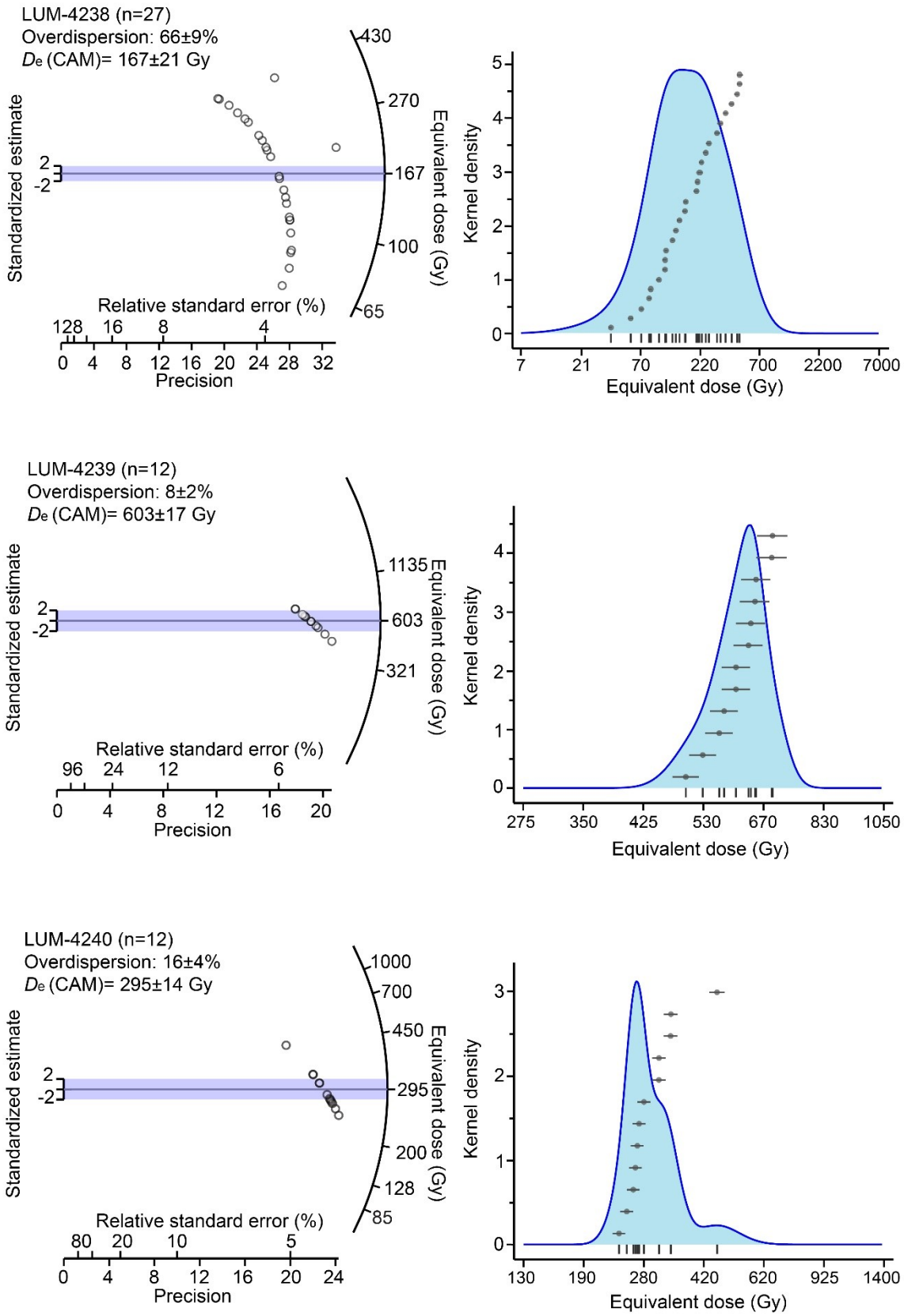

Appendix 5.7 Radial and kernel density plots for samples LUM-4238, LUM-4239 and LUM-4240, showing data from pIRIR D_e measurements of k-feldspar.

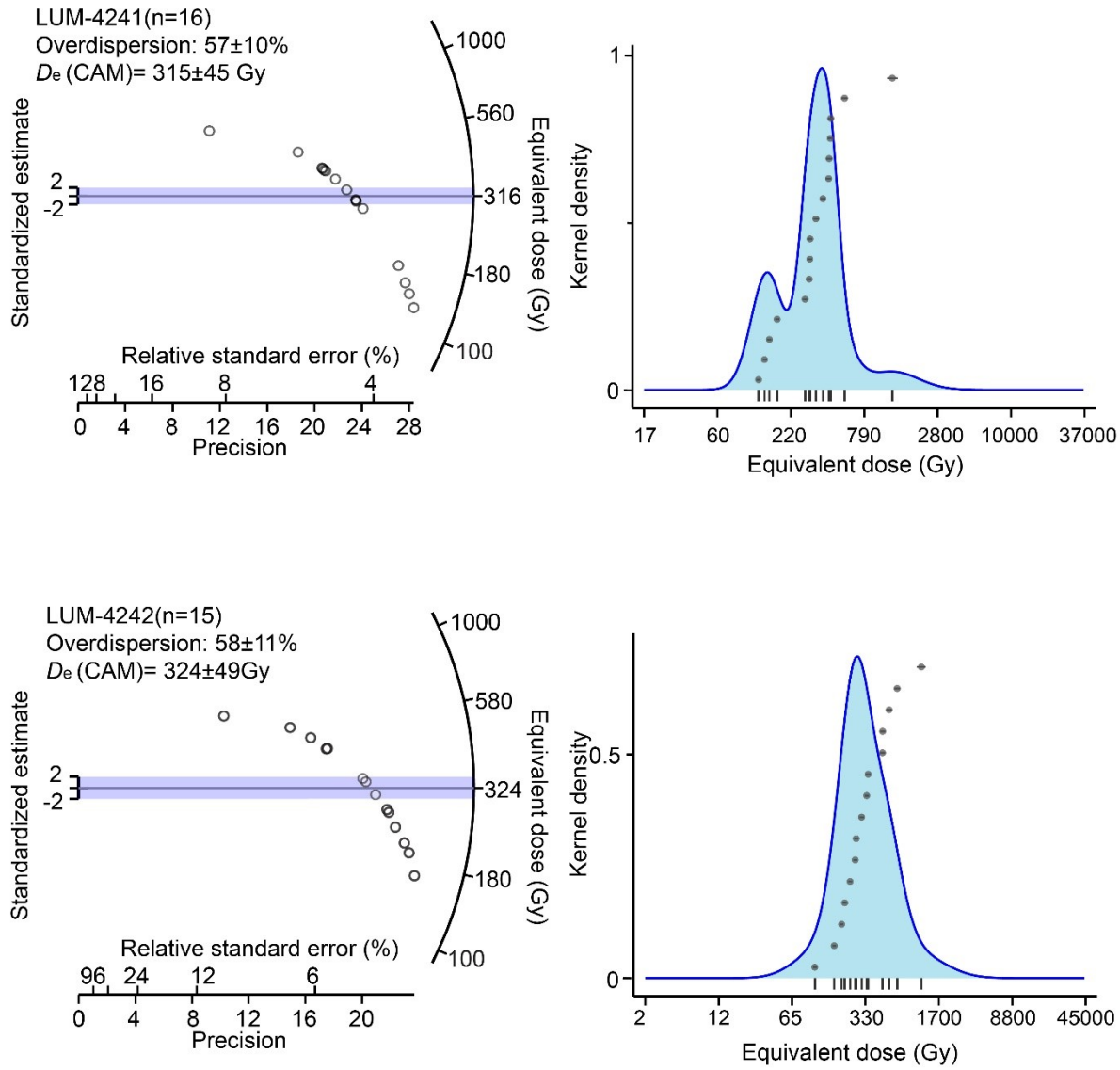

Appendix 5. 8 Radial and kernel density plots for samples LUM-4241 and LUM-4242, showing data from pIRIR D_e measurements of k-feldspar.

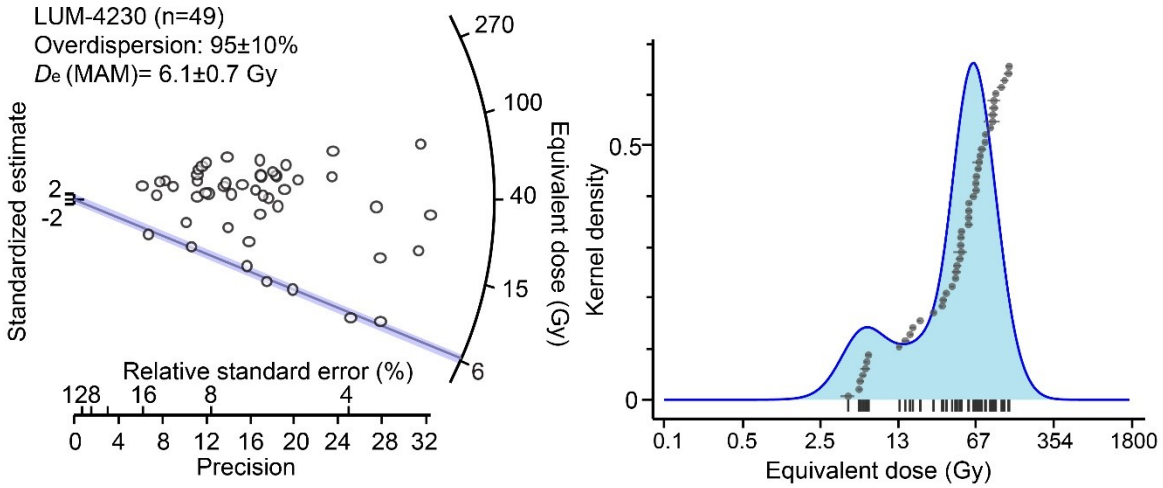

Appendix 5.9 Radial and kernel density plot for sample LUM-4230, showing data from quartz OSL D_e measurements.

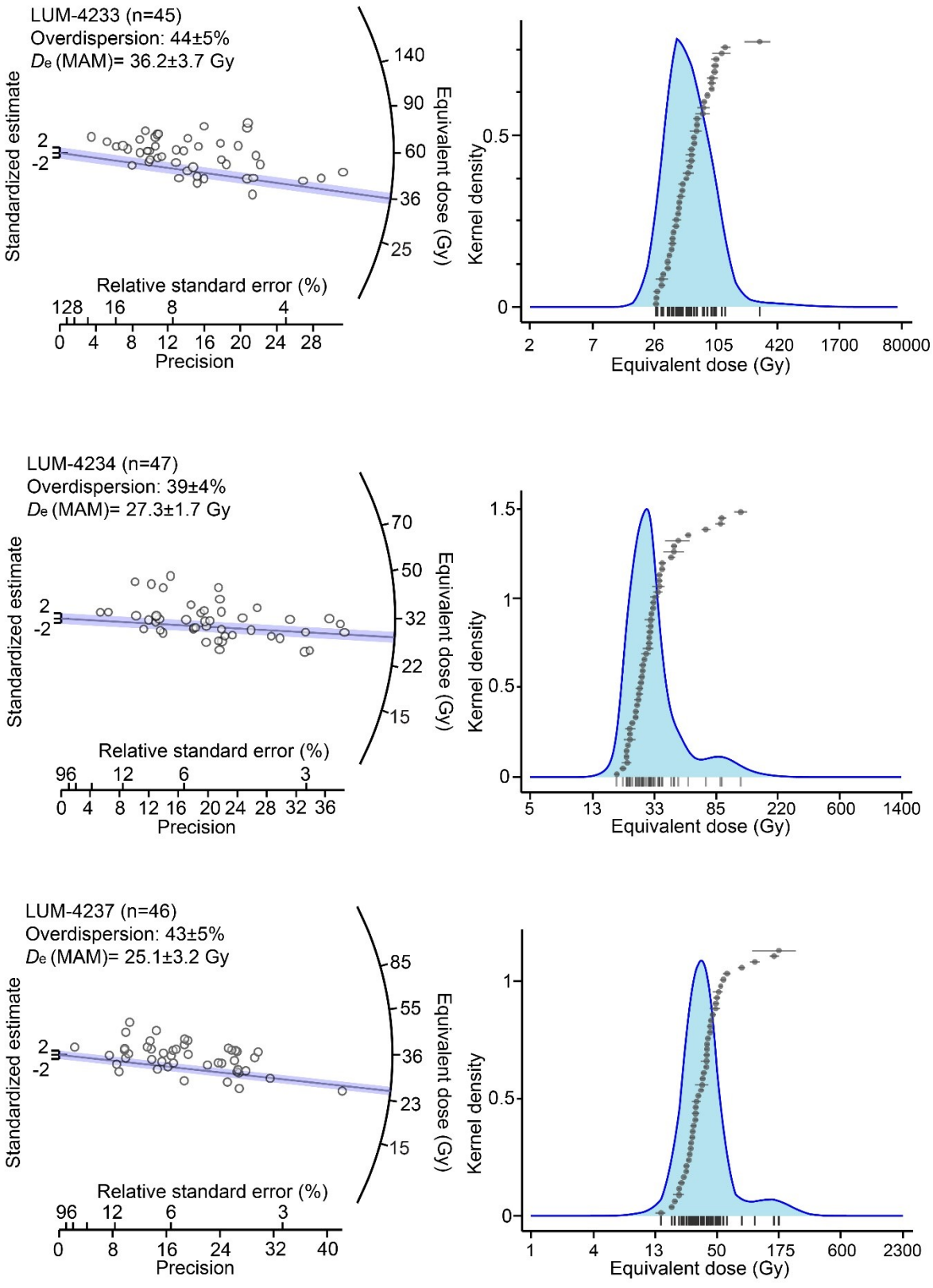

Appendix 5.10 Radial and kernel density plots for samples LUM-4233, LUM-4234 and LUM-4237, showing data from quartz OSL D_e measurements.

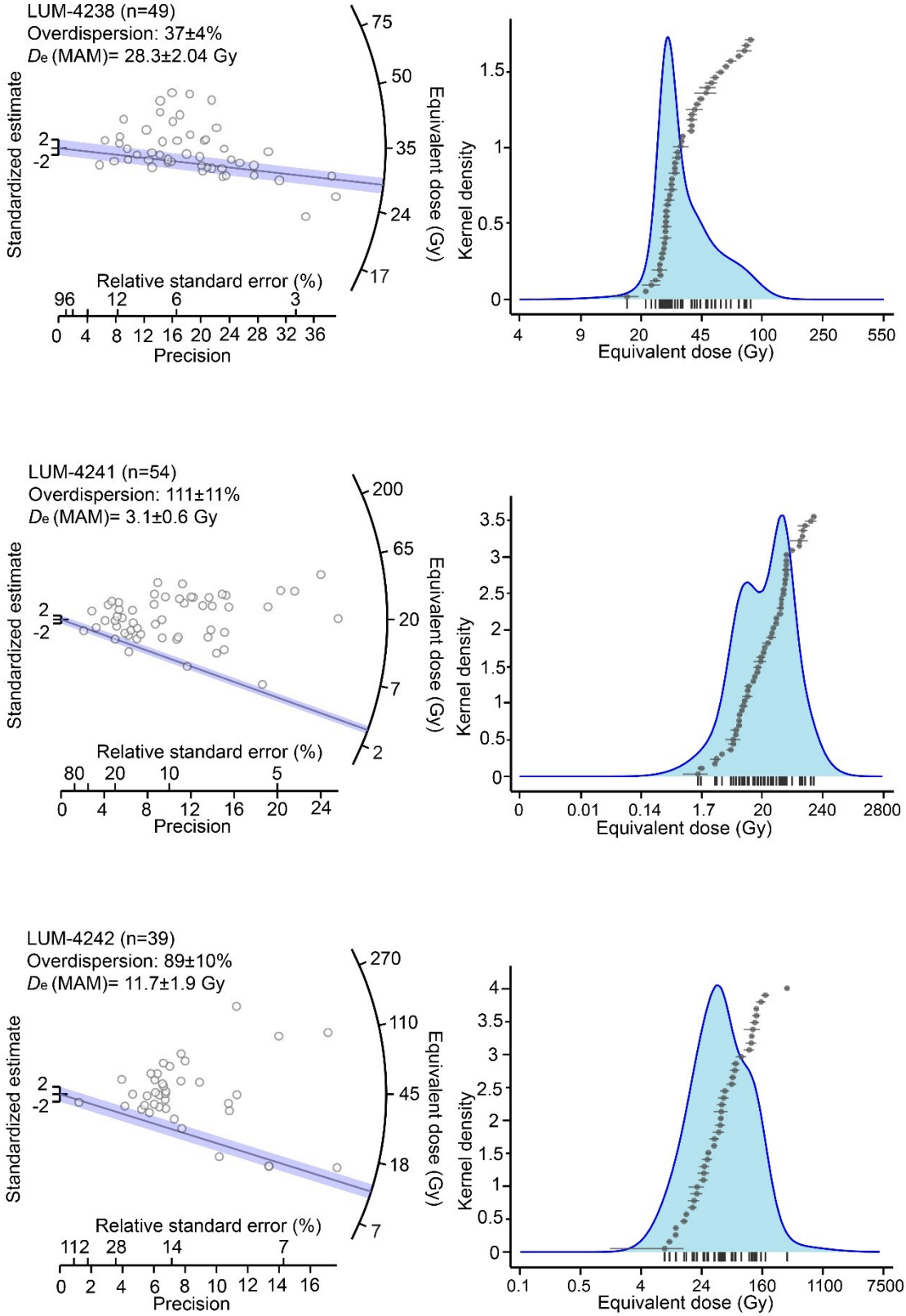

Appendix 5.11 Radial and kernel density plots for samples LUM-4238, LUM-4241 and LUM-4242, showing data from quartz OSL D_e measurements.

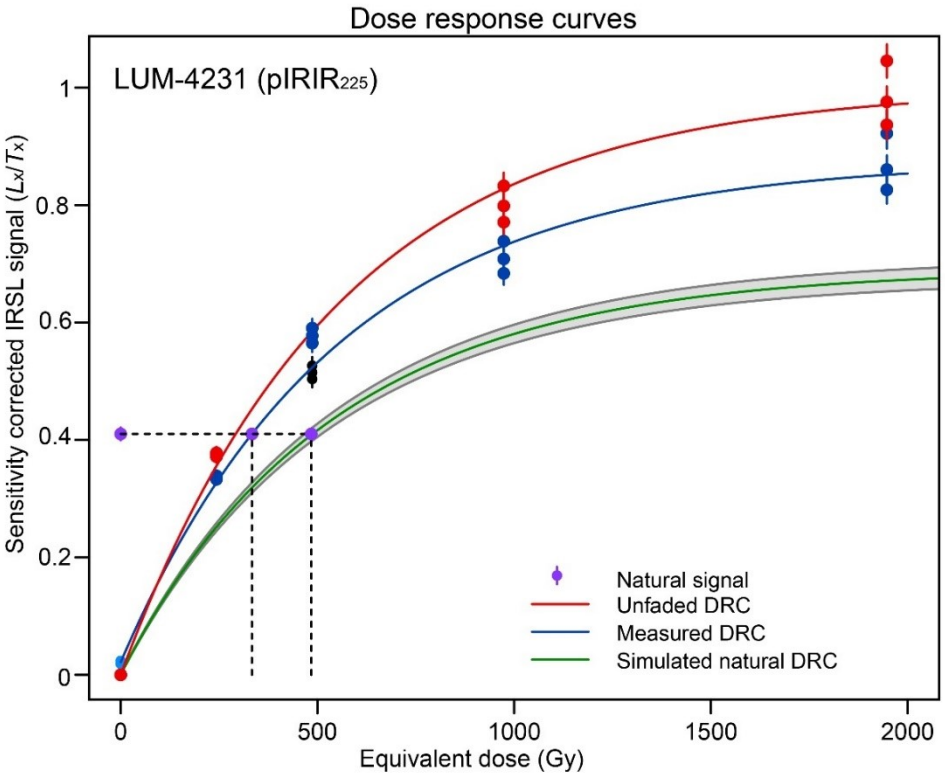

Appendix 5.12 Standard growth curve from LUM-4231 measured in Lab, Dose response curve of unfaded signal and simulated natural DRC of faded signal. Sensitivity corrected natural signal is projected up to the curves for De estimation.

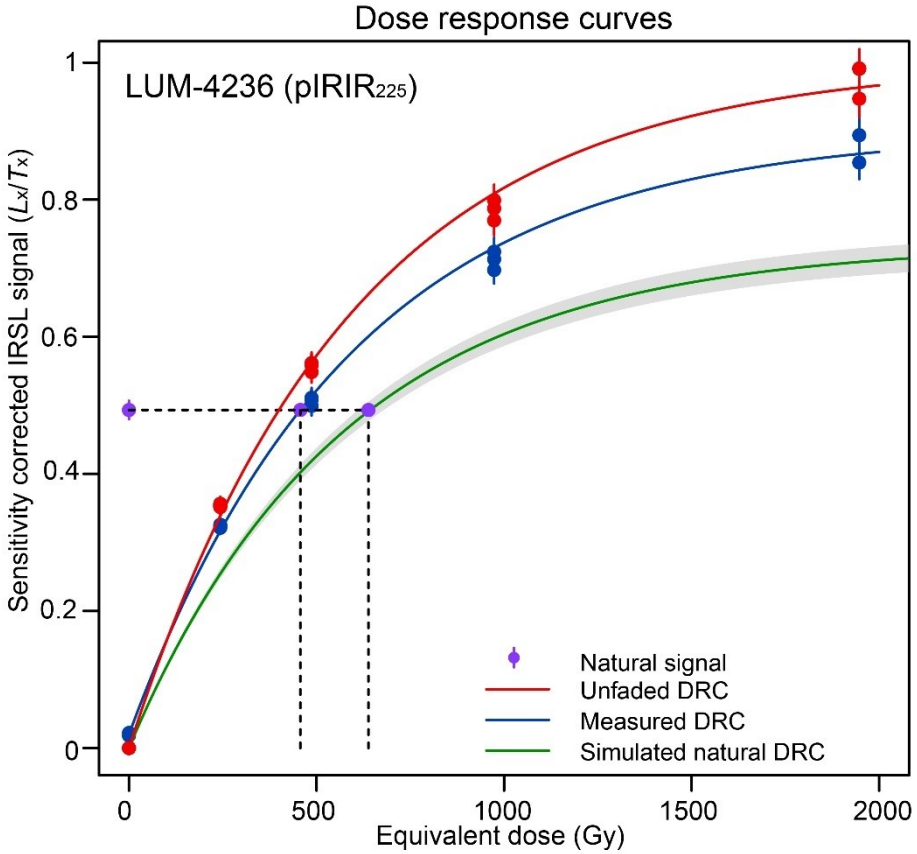

Appendix 5.13 Standard growth curve from LUM-4236 measured in Lab, Dose response curve of unfaded signal and simulated natural DRC of faded signal. Sensitivity corrected natural signal is projected up to the curves for D_e estimation.

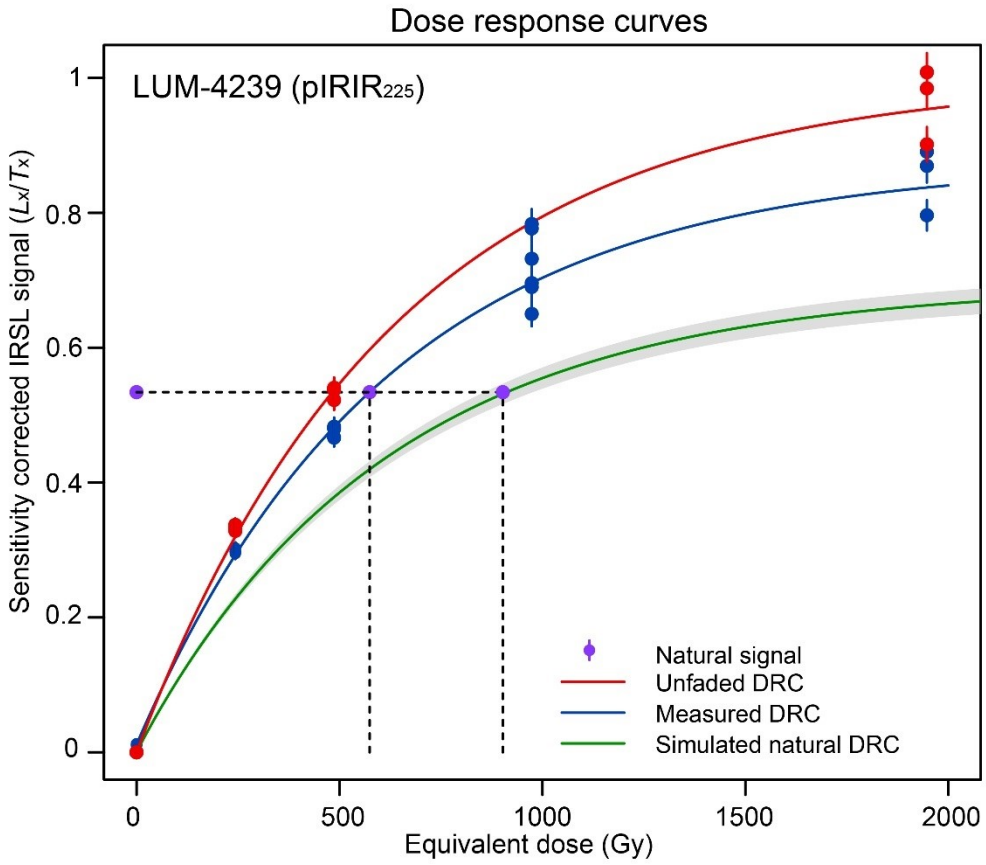

Appendix 5.14 Standard growth curve from LUM-4239 measured in Lab, Dose response curve of unfaded signal and simulated natural DRC of faded signal. Sensitivity corrected natural signal is projected up to the curves for D_e estimation.

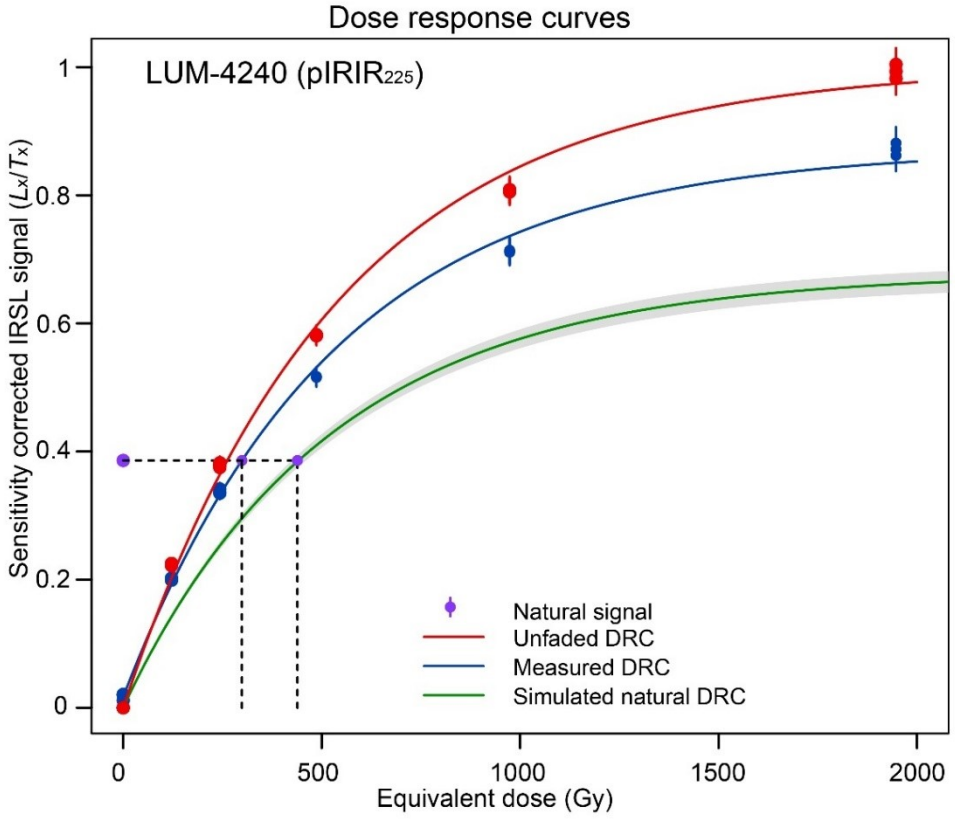

Appendix 5.15 Standard growth curve from LUM-4240 measured in Lab, Dose response curve of unfaded signal and simulated natural DRC of faded signal. Sensitivity corrected natural signal is projected up to the curves for D_e estimation.